REPUBLIQUE ALGERIENNE DEMOCRATIQUE ET POPULAIR
MINISTERE DE L'ENSEIGNEMENT SUPERIEUR ET DE LA RECHERCHE SCIENTIFIQUE

UNIVERSITE ABBES LAGROUR KHENCHELA

FACULTE DES SCIENCES ET DE LA TECHNOLOGIE

DEPARTEMENT DES SCIENCES DE LA MATIERE

N° d'ordre: N°
N° de Serie

THESE

Présentés par :

Faiza SALHI

En vue de l'obtention du diplôme de doctorat LMD

Spécialité: Chimie

OPTION: Chimie et physique de la matière condensée

TITRE

Elaboration et caractérisation de revêtements à base de nitrure de titane et de zirconium par pulvérisation magnétron

Soutenue le : / /

Devant le jury

Amel MASSAI	Université Abbes LAGHROUR Khenchela	Professeur	**Président**
Linda AISSANI	Université Abbes LAGHROUR-Khenchela	M.C.A	**Rapporteur**
Mamoun FELLAH	Université Abbes LAGHROUR-Khenchela	Professeur	**Co-Rapporteur**
Brahim CHERMIME	Université Abbes LAGHROUR-Khenchela	M.C.A	**Examinateur**
Mourad ZAABAT	Université Larbi Ben M'hidi-OEB	Professeur	**Examinateur**
Abdelhak AYAD	Université Salah BOUBNIDER-Constantine 3	M.C.A	**Examinateur**

PEOPLE'S DEMOCRATIC REPUBLIC OF ALGERIA

MINISTRY OF HIGHER EDUCATION AND SCIENTIFIC RESEARCH

UNIVERSITY OF ABBES LAGROUR KHENCHELA

FACULTY OF TECHNOLOGY SCIENCES

DEPARTMENT OF MATER SCIENCES

Order N°:

Serial N°:

THESIS

SUBMITTED BY:

Faiza SALHI

WITH A VIEW TO OBTAINING THE LMD DOCTORATE DEGREE

SPECIALITY: CHEMISTRY

OPTION: CHEMISTRY AND PHYSICS OF CONDENSED MATTER

TITLE

Elaboration and characterization of based titanium and zirconium nitrides coatings deposited by magnetron sputtering

Defended: / /

In front of the jury

Amel MASSAI	Abbas Laghrour University - Khenchela	Professor	**President**
Linda AISSANI	Abas Laghrour University - Khenchela	M.C.A	**Supervisor**
Mamoun FELLAH	Abas Laghrour University - Khenchela	Professor	**Co- Supervisor**
Brahim CHERMIME	Abbas Laghrour University - Khenchela	M.C.A	**Reviewer**
Mourad ZAABAT	Larbi Ben M'hidi University-OEB	Professor	**Reviewer**
Abdelhak AYAD	Salah BOUBNIDER University-Constantine 3	M.C.A	**Reviewer**

Dedication

Above all I must say"اللهم لك الحمد والشكر", thank you ALLAH.

Because he was the one who told us: " أن اشْكُرْ لِي وَلِوَالِدَيْكَ ",

My life's sunshine, mom, my dear father, receive my words of thanks and gratitude for everything you did to make me happy.

Thanks for your support and patience.

Mom, dad ! this is for you

To my dear husband BELHADI Abdellah,

and my little secret Yahya Sedjid.

To my very dear brothers and sisters:

Khedidja, and her husband,

Yacine,

Mariama, and her husband, and

Youcef.

To all my friends.

Salhi Faiza

Acknowledgment

This doctoral thesis is the result of a productive and stimulating process where I could share experiences, discussions, and moments with many different people. The very first person I would like to thank is my supervisor ***Dr. AISSANI Linda****, University of Abbas LAGHROUR –Khenchela, for her, advice and guidance from the early stage of this research as well as for giving me extraordinary experiences throughout the work, for her time, good spirits, support, and knowledge. It has been a great privilege for me to work with one of the most distinguished names in our university and, moreover, to be her first doctoral student. The second person I would like to thank is my co-supervisor, Pr.* ***FALLEH Mamoun*** *at Abbes Laghrour - Khenchela University, I am very thankful for his help as co-supervisor.*

Then I would like to express my heartfelt to ***Dr. Alhussein Akramin*** *and the* ***Ph.D. BELAGROUNE Ahlem****, LASMIS laboratory, University of Technology of Troyes-France, who played a very important role in allowing me to realize the experimental part of this doctoral thesis in France during the confinement period of COVID 19.*

A very special thanks to the members of the jury, composed of Dr. ***CHERMIME Brahim****, University of Abbas LAGHROUR-Khenchela.* ***Pr. ZAABAT Mourad****, University Larbi Ben M'hidi OEB,* ***Dr. AYAD Abdelhak,*** *University of Salah BOUBNIDER Constantine 3 as an examiners for their time, interest, and helpful comments, and thank warmly* ***Pr. MASSAI Amel,*** *University of Abbas LAGHROUR–Khenchela, for having agreed to be the President of my thesis committee, and for having supervised me in my master's graduation in 2015.*

My sincere thanks and gratitude also go to ***Pr. DJALLOUL Abdelkader*** *and* ***Dr. ABOUDI Abdelazize,*** *University of Khenchela, for their support and help. Also all my thanks to* ***Dr. CHERIET Abderahmane****, University of Laghouat, and* ***Ph.D. Fares Sara****, University of Constantine 1, for all Numerical calculation, which was a great contribution in the thesis.*

I especially rend thanks to my family members and all my friends for supporting and encouraging me in the execution of this project, as well as express my apology that I could not mention personally one by one. Finally, my thanks go to everyone who contributed in any way to the development of this work.

Salhi Faiza

Table of contents

Chapter II. Elaboration and Caracterization techniques

Chapter III. Structure, surface topography and tribo-mechanical behavior of TiN thin films

Chapter IV.Effects of zirconium sputtering current on the structure, mechanical and tribological properties of TiN Films

Table list

Chapter I

Chapter II

Chapter III

Chapter IV

Figure list

Chapter I

Chapter II

Chapter III

Chapter IV

Glossary

A

AFM Atomic force microscope

a- Amorphous

Ar Argon

at.% Atomic percentage

C

CrZrN Chromium Zirconium Nitride

CVD Chemical Vapor Deposition

°C Degree Celsius

D

DLC Diamond Carbon (Diamond-Like-Carbon)

D.C Direct Current

DFT Density functional theory

d_{hkl} (nm) Distance between two consecutive reticular planes of Miller index h,k,l

E

EDS Energy Dispersive Spectroscopy

E (GPa) Young's modulus of the film

eV Electron-volt

H

hkl Miller index

H (GPa) Hardness

H_V Hardness Vickers

L

LaBoMaP Burgundy Laboratory of Materials and Processes

M

mTorr Millitorrs

mm Millimeters

MeN Nitride of a metallic element

min Minutes

MOCVD Metal Organochemical Vapor Deposition

MZS Structure Zone Model

N

N Nitrogen

P

PVD Physical Vapor Deposition

PEPVD Plasma Enhanced Physical Vapor Deposition

PACVD Plasma Enhanced Chemical Vapor Deposition

SEM Scanning Electron Microscope

S

Si Silicium

T

Ti Titanium

TiN Titanium Nitride

TiN Titanium nitride, cubic phase

Ti_2N Titanium nitride, hexagonal phase

TiZN Titanium-Zirconium-Nitrogen

V

V Volts

W

WDS Wavelength Dispersive Spectroscopy

X

XPS Xray Photoelectron Spectroscopy

XRD X-ray diffraction

XC100

Z

ZrN Zirconium Nitride

θ (°) Angle formed by the incident or diffracted X-rays with the planereticular

σ(GPa) Residual stress measured

GENERAL INTRODUCTION

Introduction

The growing technological evolution we are witnessing today has generated the loss of a considerable amount of energy as a result of the behavior of mechanical parts and steel instruments exposed to harsh environments from elevated temperatures to friction. This has a negative impact on both the economic and environmental scales. Solving the problem requires the improvement in surfaces performance of mechanical parts subjected to the aggressive tensions of friction, which received great interest by researchers for many years. The field of thin films in particular hard coatings offered the bright economical solution for enhanced mechanical and tribological proprieties with prolonged service life, these latest constitute the surface treatments by applying coatings in thin layers (< 10 μm thick).This technology makes it possible to deposit a superficial coating which brings remarkable improvements in the service life of mechanical parts, especially cutting tools. The specific properties targeted by a coating require obtaining a particular structure that determines the quality of the films. This particular structure depends closely on the operating conditions associated with the processes of deposition [1].

Thin films could be produced with different common methods. Physical vapor deposition in special represents a variety of vacuum deposition techniques that can be employed to grow thin films and coatings. The most common physical vapor deposition processes are sputtering and evaporation. PVD is characterized by a procedure in which the material ranges from a condensed phase to a vapor phase and then back to a thin film condensed phase on the surface of the desired substrate [2].

Magnetron sputtering coating is a vacuum coating process that falls under the category of physical vapor deposition (PVD), this technique does not demand melting and evaporation of the source material, leading to considerable advantages over different PVD technologies; where almost all materials can be deposited by magnetron sputtering anyway of their melting temperature; sources can be mounted and set anywhere in the chamber established on the needs of the substrate and the coating, and films of alloys and compounds can be deposited while keeping similar composition to that of the original material.

The protective Transition Metal Nitride (TMN) coatings are used for cutting tools and wear resistant parts thanks to their high abrasion resistance, thermal stability and corrosion

resistance at high temperature [3]. Among these coatings, titanium nitrides has been extensively studied in the last few years because of its special properties such as good electrical and thermal conductivity, and corrosion resistance [4] high hardness [5], preferred (111)-oriented texture [6], high strength and rigidity [7], excellent thermal stability and wear resistance [8]. These appreciable properties make it an attractive candidate for different technologic applications as well as for the development of decorative purpose, due to its golden color [9]. TiN coatings are used in large applications mainly in the modern industrial systems and for products having excellent tribological and mechanical performance and high corrosion resistance [10]. Over the years, several deposition techniques have been developed to reduce the defects in the binary TiN coating.

The effect of nitrogen content in titanium nitride was widely studied in many applications. Tests of hardness, tribological behavior, corrosion and heat resistance showed that titanium nitride coatings with predominate (111) crystalline plane have a great potential to be used for protection of steels and tools [11]. In addition, nitrogen is a lubricated solid element with low friction coefficient and wear rate that has also been used in severe industrial applications [12]. However, in the literature there have been insufficient investigation on the combination of the mechanical, tribological and hydrophobic properties of sputtered TiN films (hardness, adhesion and wear resistance) and the texture (predominate plane and preferential orientation) [13]. They discussed either the microstructure and mechanical properties with different nitrogen content, or the influence of nitrogen content on the mechanical and tribological behavior without understanding the chemical bonding structure and the preferential orientation [14].

Recently, TiMN (M=B, Al, C, Si, Zr) nanocomposite coatings with higher hardness, excellent tribo-mechanical properties, improved stabilization and higher oxidation resistance have been developed and investigated. Many researchers reported that the addition of specific elementsto TiN matrix could enhance the system properties. The TiZrN coating can be manufactured using different methods and techniques [15, 16]. Furthermore, The TiZrN coatings show specific properties, such as excellent toughness, high melting point, biocompatibility with the human body, and good oxidation resistance [17]. When the film is mechanically damaged, it regenerates itself because of the formation of zirconium oxide on the surface [18]. However, the effect of zirconium (Zr) on the structural, mechanical, and tribological properties of TiN coatings is less investigated in comparison to other elements.

Consequently, the wear mechanisms of TiZrN coatings while protecting alloy surfaces remain largely unknown. Nevertheless, there have been few works on the tribological performance of TiZrN coatings. The aim of this thesis was to improve the coating wear resistance and wettability by creating a dense structure of TiN and TiZrN thin coatings prepared by reactive R.F. magnetron sputtering. The effect of N_2 and Zr contents on the mechanical and tribological performance of TiZrN coatings in atmospheric environment was then examined in detail.

The thesis is divided into four chapters:

***The first chapter*:** present the state-of-the-art of this thesis; presenting some concepts necessary to understand, thin films description, hard coatings, in particular, have been highlighted owing to their importance, and finely a bibliographical synthesis on TiN, ZrN and TiZrN thin films.

***The second chapter*:** present the used experimental techniques, namely, production systems and physico-chemical, mechanical and tribological characterization techniques.

The third chapter: structure, surface topography, and tribo-mechanical behavior of Ti-N thin films deposited by reactive magnetron sputtering on Si (100) wafers, glass, and XC100 steel substrates, in a mixture of Ar and N_2 with varying nitrogen content from 0 and 30 % of the total gas mixture, were investigated.

Finally, ***the fourth chapter***: the deposition of TiZrN thin films on Si (100) wafers and XC100 steel substrates by reactive R.F. magnetron sputtering to estimate the effect of changing Zr content on the film structure, surface wettability, hardness and wear resistance.

The thesis is ended with a ***general conclusion*** and ***perspectives*** of our future works.

Finally, we had presented a list of our articles and the communications.

References

[1] J.A. Thornton, The microstructure of sputter-deposited coatings, Journal of Vacuum Science & Technology A: Vacuum, Surfaces, and Films, 4 (1986) 3059-3065.

[2] A.V. Rane, K. Kanny, V. Abitha, S. Thomas, Methods for synthesis of nanoparticles and fabrication of nanocomposites, Synthesis of inorganic nanomaterials, Elsevier(2018) 121-139.

[3] C. Hu, Y. Tian, W. Zheng, A Review of Corrosion-Protective Transition Metal Nitride Coatings, Innovations in Corrosion and Materials Science (Formerly Recent Patents on Corrosion Science), 5 (2015) 2-9.

[4] M. Omrani, M. Habibi, R. Amrollahi, A. Khosravi, Improvement of corrosion and electrical conductivity of 316L stainless steel as bipolar plate by TiN nanoparticle implantation using plasma focus, International journal of hydrogen energy, 37 (2012) 14676-14686.

[5] S. Zhang, W. Zhu, TiN coating of tool steels: a review, Journal of Materials Processing Technology, 39 (1993) 165-177.

[6] T.-S. Yeh, J.-M. Wu, L.-J. Hu, The properties of TiN thin films deposited by pulsed direct current magnetron sputtering, Thin Solid Films, 516 (2008) 7294-7298.

[7] D. Ozkan, P. Panjan, M.S. Gok, A.C. Karaoglanli, Investigation of machining parameters that affects surface roughness and cutting forces in milling of CFRPs with TiAlN and TiN coated carbide cutting tools, Materials Research Express, 6 (2019) 095616.

[8] C.-C. Kuo, Y.-T. Lin, A. Chan, J.-T. Chang, High temperature wear behavior of titanium nitride coating deposited using high power impulse magnetron sputtering, Coatings, 9 (2019) 555.

[9] N. Mustapha, Z. Fekkai, Impact of nitrogen reactive gas and substrate temperature on the optical, electrical and structural properties of sputtered TiN thin films, Journal of Materials Science: Materials in Electronics, 31 (2020) 20009-20021.

[10] M. Ghufran, G.M. Uddin, S.M. Arafat, M. Jawad, A. Rehman, Development and tribo-mechanical properties of functional ternary nitride coatings: applications-based comprehensive review, Proceedings of the Institution of Mechanical Engineers, Part J: Journal of Engineering Tribology, 235 (2021) 196-232.

[11] P. Pedrosa, E. Alves, N.P. Barradas, N. Martin, P. Fiedler, J. Haueisen, F. Vaz, C. Fonseca, Electrochemical behaviour of nanocomposite Agx: TiN thin films for dry biopotential electrodes, Electrochimica Acta, 125 (2014) 48-57.

[12] S. Schiller, U. Heisig, G. Beister, K. Steinfelder, J. Strümpfel, C. Korndörfer, W. Sieber, Deposition of hard wear-resistant coatings by reactive dc plasmatron sputtering, Thin Solid Films, 118 (1984) 255-270.
[13] A. Obrosov, R. Gulyaev, M. Ratzke, A.A. Volinsky, S. Bolz, M. Naveed, S. Weiß, XPS and AFM investigations of Ti-Al-N coatings fabricated using DC magnetron sputtering at various nitrogen flow rates and deposition temperatures, Metals, 7 (2017) 52.
[14] S. Zhang, F. Yan, Y. Yang, M. Yan, Y. Zhang, J. Guo, H. Li, Effects of sputtering gas on microstructure and tribological properties of titanium nitride films, Applied Surface Science, 488 (2019) 61-69.
[15] S. Jeon, B. Kim, Y. Choi, I. Jo, H.J.C.I. Lee, Thermal shock behaviors of Ti1− xZrxN coatings by accelerated test based on pulsed laser ablation, Ceramics International, 42 (2016) 2241-2249.

[16] E. Hong, H.J.S. Lee, C. Technology, Microstructure, bonding state and phase formation behavior of carbon-doped TiZrN coating by laser carburization, Surface and Coatings Technology, 385 (2020) 125373.
[17] L. Chen, D. Holec, Y. Du, P.H. Mayrhofer, Influence of Zr on structure, mechanical and thermal properties of Ti-Al-N, Thin Solid Films, 519 (2011) 5503-5510.
[18] T.L. Yau, V.E. Annamalai, Corrosion of Zirconium and its Alloys, 2016.

Chapter I.

State of the art

I.1. Introduction

To enhance surfaces properties, extend the service life, and improve the appearance of materials, thin films are frequently used, whether in electronics fields, optics, or in mechanics, the development of different deposition techniques and the control of operating parameters have made it possible to obtain coatings with good wear resistance, very high hardness and, good thermal and chemical stability.

The hard materials are generally applied for protecting the cutting tool and given an economical advance in the industry. However, they are inadequate to support severs mechanical applications (turning, milling, stamping, etc.). Surface treatments remain the adequate solution to improve the performance of a metal surface. These treatments consist of structural transformations, thermo-chemical diffusion treatments, and conversion, which improve the performance of new materials obtained.

Thin films are subject to new searches due to the great interest concerning lifetime prolongation in the industrial fields, thus the ability to obtain coated tools with prolonged life in a way significant from 2 to 4 times compared to uncoated.In this chapter, we present generalities on thin films,and their applications, then we presented the hard coatings and their categories, generalities about transition metal nitrides, also literature reviews of titanium and titanium nitride, zirconium, and zirconium nitride, and finally, the interesting ternary TiZrN system.

I.2. Thin films

The thin film appears as a thin layer of material, ranging in thickness from a few nanometers to a few micrometers. As with all materials, the structure of thin films is divided into amorphous and polycrystalline structures depending on the fabrication conditions and the properties of the material. A thin film consists of two regions: the layer where the thin film is deposited and the substrate [1], as shown in *Figure I.1*

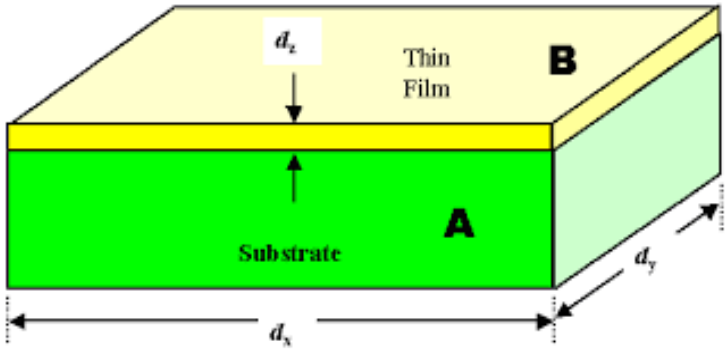

Figure I.1. Schematic of thin film deposited on a substrate.

The "Substrate /coating" (*Fig. I.2*) system should achieve the followingcharacteristics:

- ✓ *High toughness,*
- ✓ *Perfect adhesion to the substrate,*
- ✓ *High resistance to the formation and progression of cracks,*
- ✓ *Low thermal conductivity and diffusivity,*
- ✓ *High resistance to oxidation,*
- ✓ *Sufficientthickness,*
- ✓ *A diffusion barrierfunction* [2].

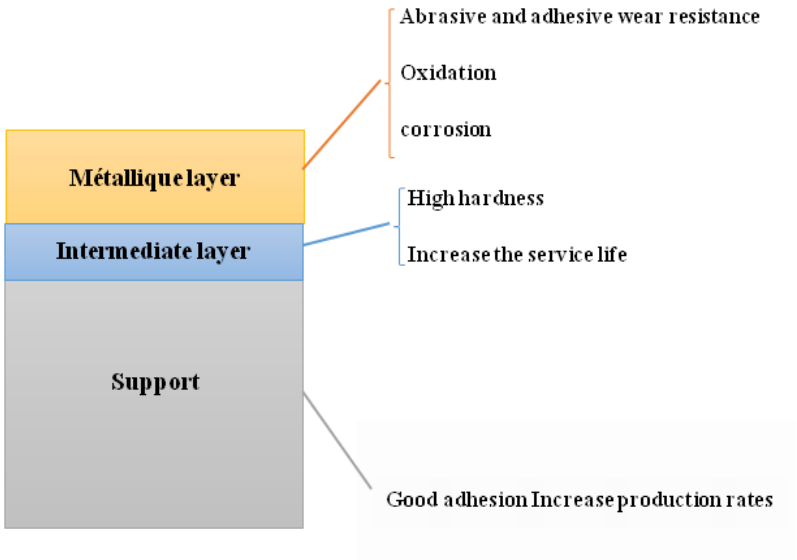

Figure I.2. Support (substrate)/thin film (coating) system.

Thin films are a large subset of surface engineering that is used to change the physical, chemical, and morphological properties of a chosen surface or substrate. A thin film can have a single homogenous composition, crystalline phase composition, and microstructure, or a multilayer or composite structure that is inhomogeneous. The multilayer structure might be regular, follow a pattern, or be completely random. Optical multilayer coatings, rugate filters, superlattices, and nanolaminates are examples of periodic structures. Random or periodic nanocomposites are possible. *Figure 1.3* shows the progression of the dimensionality of thin films from zero dimensions (quantum dots) to three-dimensional (**3D**) film.

The quantum dot is a **0 D** quantum well with width and thickness between 1 and 3 nm. *X. Shi et al.* [3] developed a new **0D** ternary nanocomposite–based strain sensor with heightened sensitivity in broad functional strain range, down hysteresis, good linearity, and long-term durability. The 0D fullerene offering lubricity fabricated through one-step screen-printing.

The quantum wire is a **1D** structure with arbitrary length and thickness between 1 and 10 nm. Nanotubes fall into this category could find potential applications in tumor targeting, photocatalysis and metamaterials. *S. Farsinezhad et al.* [4] used the atomic layer deposition to produce TiN on to self-organized TiO_2 nanotube arrays grown by electrochemical anodization with thikness of 10 nm. The core-shell TiO_2−TiN nanotube arrays were found to demonstrate broad near-infrared extinction peaks that possibly will hit upon potential applications in tumor targeting, photocatalysis and metamaterials.

Superlattices, quantum wells, and nanolaminates are **2D** films consisting of hundreds to thousands of periodic compositions with the thickness of each layer in the range of 1–10 nm. The total thickness of this structure can be as large as 20 mm. *P. M Martin et al*. [5] were deposited AlN/Si_3N_4 optical Superlattice by D.C and R.F reactive magnetron sputtering thicknesses of 2 nm for abrasion protection of ZnS IR windows and exhibited a nanohardness of 35 GPa.

The three-dimensional (**3D**) film is homogeneous in composition and crystalline structure, with thickness greater than 20 nm. *M. D. Fleischaueret al*. [6] fabricated 500 nm thick Si films deposited on a Si(100) wafer, using the physical vapor deposition, in order to reduce the amount of substrate area device “footprint” for a provided capacity/volume of electrode material by shifting from al 2D to a three-dimensional 3D electrode.

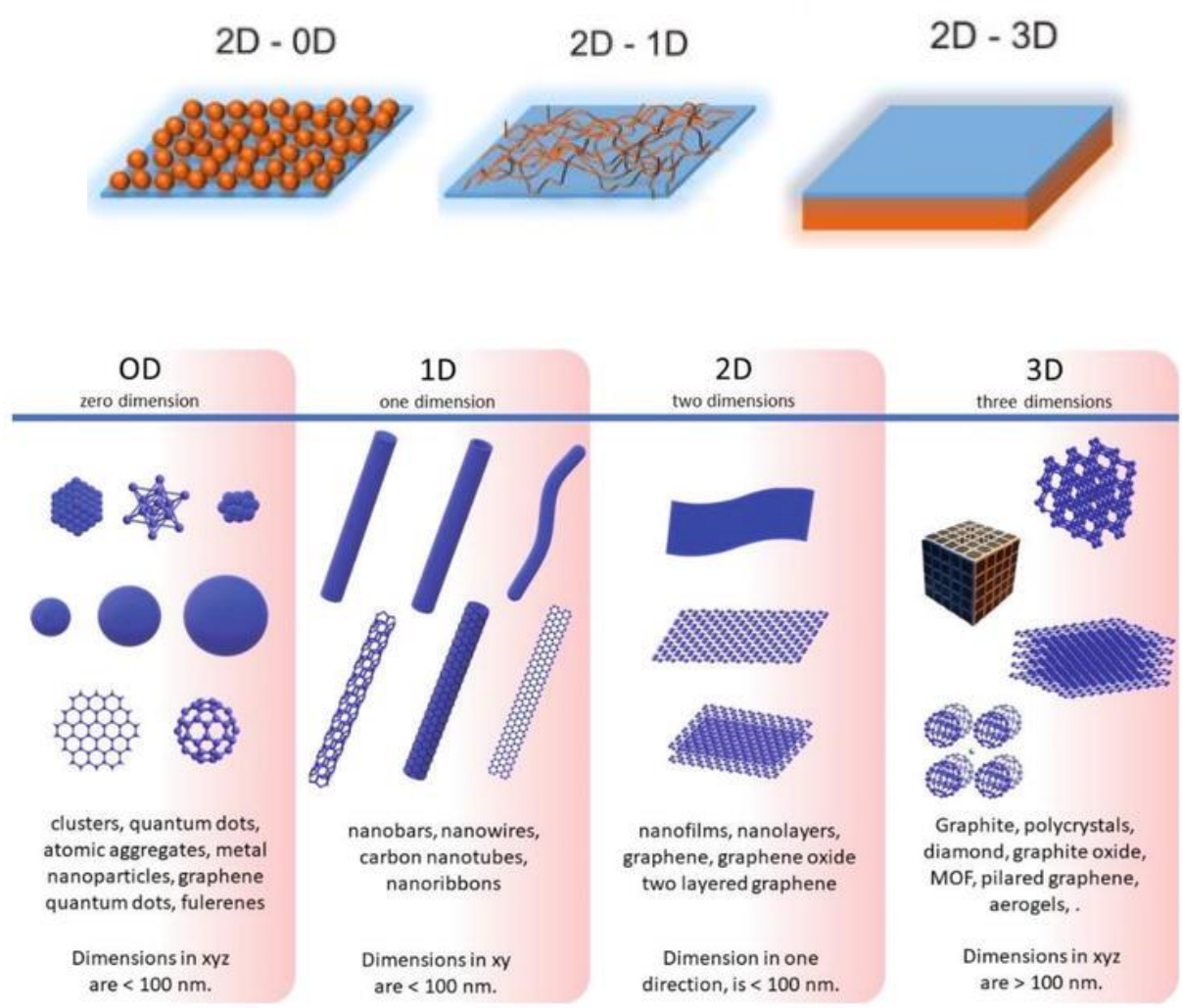

Figure I.3. Progression of the dimensionality of thin film structures [7].

I.3. Enhancing surface resistance via coatings

To improve the performance as well as the behavior of a surface, we are led to seek to modify either its surface hardness, surface energy, or its corrosion resistance. One of the fundamental techniques to attain this objective is coating. The choice of a type of coating must be made in such a way as to satisfy the conditions of service of the system and to best meet the technical requirements (resistance to friction, wear, corrosion, and properties specific to the system). Transition metals seem to offer a good alternative. The choice of the performance process is dictated by operating conditions (mainly cost and productivity) [8]. Effectively the economic factor is essential, and the gain generated by the coating in terms of the wear must be sufficient to justify its use compared to the uncoated part. In this sense, the physical vapor deposition (PVD) techniques have developed in a way significant, and they represent a strong potential for improving the tribological performance.

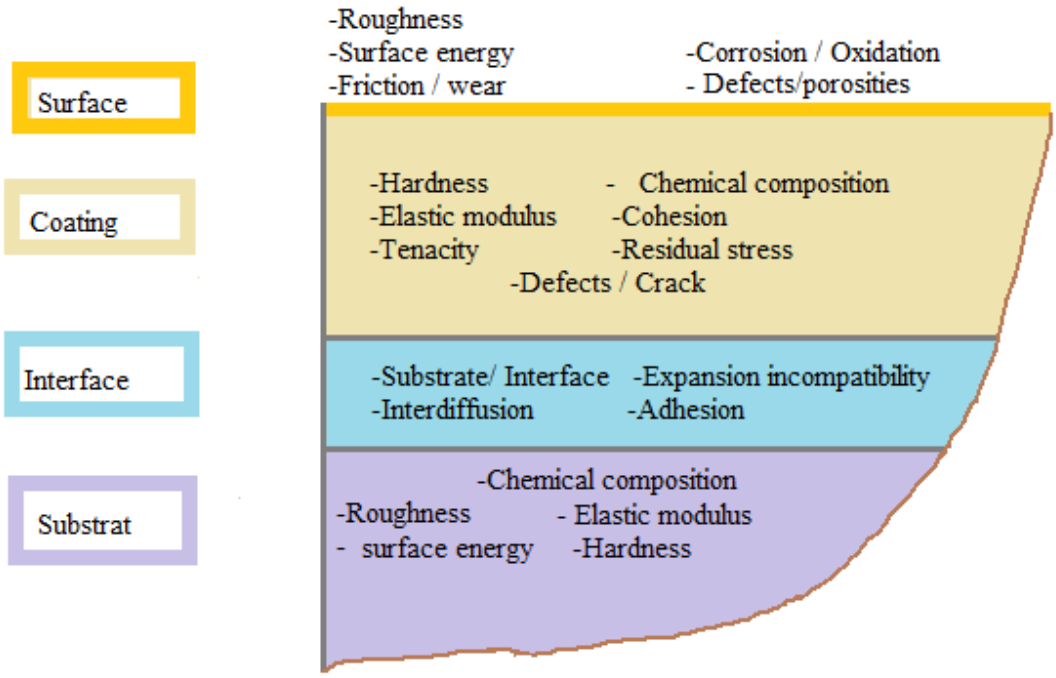

Figure I.4. Properties of the coating/substrate system, necessary for the determination of its performance in technological applications.

The following are some surface features that play an important role in tribology.

I.3.1. Surface hardness

In metallurgy, hardness (H) is defined as the resistance to plastic deformation of a body. It characterizes the ability of a material (and therefore its surface) to resist penetration. It is generally measured by applying a force utilizing an indenter (harder than the material to be tested) to leave an imprint on the surface (see *Fig. I.4*). Hardness is determined from the depth or width of the indentation left by an indenter, two characteristic quantities of the surface of the indentation. The size of the imprint left is inversely proportional to the hardness. The standardized techniques differ according to the shape of the indenter and the method of measurement. For thin films, the hardness test is at the micrometric, even nanometric, scale. The general criterion for measuring the hardness of a coating, so that the influence of the substrate is negligible, is that the depth of penetration is not greater than 10% (*Buckel's rule* [9]) the thickness of the thin layer that is desired characterize. In our study, we chose to define a zone of depth of indentation between 7 and 9% of the thickness of the coating, to overcome the effect of the substrate and that of the asperity. A second mechanical property, the modulus of elasticity (E), essential to the analysis of the behavior of the coatings is systematically calculated at the outcome of the nanoindentation tests.

I.3.2. Adhesion

The mechanical bonding of the coating to the substrate will vary according to the structure and the intrinsic mechanical properties of the film obtained [10, 11]. This is where the concept of film adhesion comes into play. While the contact resistance weakens, the coating is more subject to cracking when under stress. Adhesion is a major issue in PVD, and it is largely influenced by residual stresses: defects in the coatings and ion bombardment during deposition cause intrinsic stresses. As a result, adhesion may be affected by the coating's stress condition. In our study, a metallic layer of titanium has been deposited beforehand, as an underlayer, to ensure a mechanical gradient, and thus aims to reduce the localized stress at the interface substrate/coating. It is common to start the treatment with a first layer metal that promotes good adhesion to the substrate [9]. Trials of scratching, commonly called Scratch-test, have been used to assess the adhesion of deposits made.

I.4. Thin film applications

Coatings are currently used in a wide range of applications, including optical coatings, energy-related electrical devices, instrument hard coatings, ornamental, and biological components, as we menshed in *Table I.1:*

Table I.1. Application field of metal thin films

Thin films Application field	***Examples***
Optically functiona [12]	laser optics (reflective, semi-transmitting and transmitting),phase separation, telecommunication filters, architectural glazing,residential mirrors, automotive rear-view mirrors and headlamps, reflective andantireflection coatings, optically absorbing materials, lowcoatings, solar selectivecoatings, free-standing reflectors, transparent conductive films. 
Energy related [13]	Thin films battery, fuel cell, solar cell, thermoelectric thin films, superlattice, electrochromic coatings, low-e coatings, solar absorbers, barrier coatings (oxygen and water permeation barriers), transparent solar cells, organic solar cells, photocatalytic coatings. 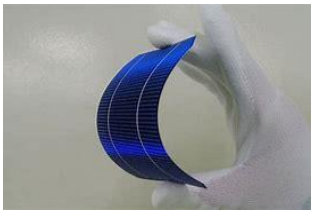
Electrically functionl [14]	Electrical conductors, electrical contacts, semiconductor films, active solid state devices, electrical insulators, photovoltaics, transparent electricalcontacts. 
Mechanically functional [15]	Tribological coatings, lubrication films, nanocomposites, diffusion barriers, hard coatings for dies, and cutting tools, wear- and erosion-resistantcoatings, biomedical coatings. 
Chemically functional [16]	Corrosion-resistant coatings, catalytic coatings, biomedicalcoatings, photocatalytic coatings, thin film electrolytes, organic materials. 

I.5. Hard coatings

The use of hard coating techniques dates back to 1643, when Evangelista Torricelli used an upturned glass tube filled with mercury in vacuum to create his famous essay. Following that, in 1838, Michel Faraday established the deposition technique in the industrial applications for enhancing the qualities of cutting tools by depositioning TiN films for the first time in the United States [17]. Hard coatings are applied to tool substrates (such as cutting or forming tools) and machine components (such as gears and bearings) to increase desirable attributes including hardness, friction, wear, and corrosion resistance while preserving the bulk substance's properties. The goals are to extend their life, minimize lubricant use, boost productivity, and/or develop new material machining. As a result, hard coatings have become an important aspect of modern tool technology, and a lot of research has gone into finding better coating materials and novel deposition procedures. The wear resistance of coatings is determined by the contact between the cutting tool and the workpiece [18].

The concept of hard thin films may be expanded beyond its typical tribological meaning to encompass the ability to resist harsh operating conditions such as high temperature, pressure, or radiation [19]. Optimal coating thickness, fine microstructure, and compressive residual stresses can all significantly improve the coating products. These ftures can essentially be attained exclusively through ceramic. In practice, the choice is limited to based transition metal are the only materials that can be consistently produced in a thin film pattern using CVD or PVD processes.

I.5.1. Hard coatings classifications

Hard coatings exist in a variety of forms, including complex and less complex compounds made of transition metal nitrides, carbides, oxides, and borides, carbon-based coatings, and so on. Hard coatings class consists of monolayer coatings with a simple structure to the complex coatings that have additionally subdivided into multi-component coatings, multi-phase coatings, composite coatings, multi-layer coatings, and gradient coatings multilayers (see *Fig. I.5*) [20].

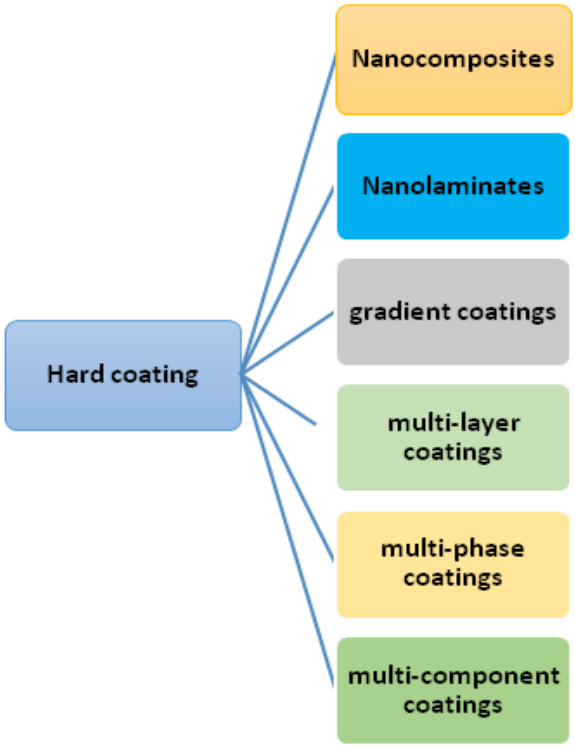

Figure I.5. Hard coating classifications [20].

I.5.1.1. Single component coatings

Single-component coatings are the most basic, most commercial PVD and CVD coatings, for example, are composed of a single layer of TiC, TiN, CrN, CrC, Al_2O_3, TiAlN, TiCN, DLC, W_2C, MoS_2, , soft metals, or polymers. An adhesion interlayer is sometimes applied before the used films to enhance the bonding strength with substrates. However, in some applications when a compound with low friction, good wear resistance, and extra functionalities is required, single-component coatings are ineffective, necessitating the application of coatings with complex structures [21].

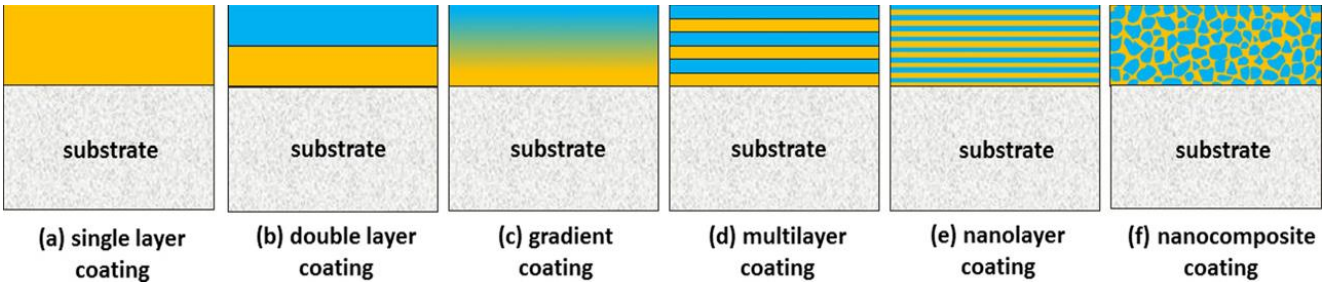

Figure I.6. Hard coatings Design [20].

I.5.1.2. Gradient coatings

The functionally gradient coating concept is a natural progression of the multilayer principle for tailoring coating microstructure. High residual stresses at the interfaces might result from a distinct shift in mechanical, physical, and chemical characteristics between layers and the substrate, leading to crack development, and film detachment. As a result, a gradient transition between the substrate and the layers is provided. To improve the load-carrying ability of low friction DLC coatings on low-cost steel substrates under a high normal load, for example, *A.A. Voevodin et al*. [22] produced the functionally gradient metal-ceramic Ti-TiN-TiCN supporting interlayers, as shown in *Figure I.7*. Low friction coefficients in combination with low wear rate were obtained in ball-on-disk experiments against steel and cemented tungsten carbide balls.

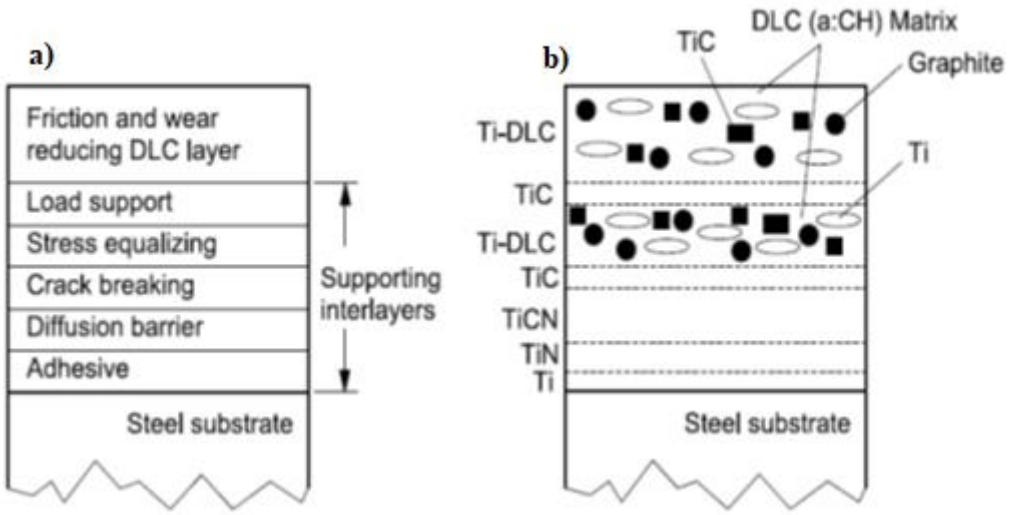

Figure I.7. Gradient multilayer coating with an upper DLC layer on a steel substrate**: a)** theoreticalconstitution of supporting interlayer, **b)** coating developed for sliding wear applications [22].

I.5.1.3. Multilayer coatings

Multilayer coatings involve two types: several successive layers of many compositions (sandwich coatings), and regularly repetitive structure of lamellae of two or more materials. In sandwich structure, the interlayers can conquer the mismatch in mechanical or chemical properties between coatings and substrates, and enhanced the adhesion of the coating. For exemple: *Z. Wan et al.* [23] found that the dense Al_2O_3 interlayer acts as a great sealing layer that inhibits charge transfer, diffusion of corrosive substances, and dislocation motion; where

the addition of a dense atomic layer of Al_2O_3 interlayer led to a significant reduction in the average grain size and surface roughness and amazing improved corrosion resistance and corrosion durability of CrN coatings while maintaining their mechanical properties.

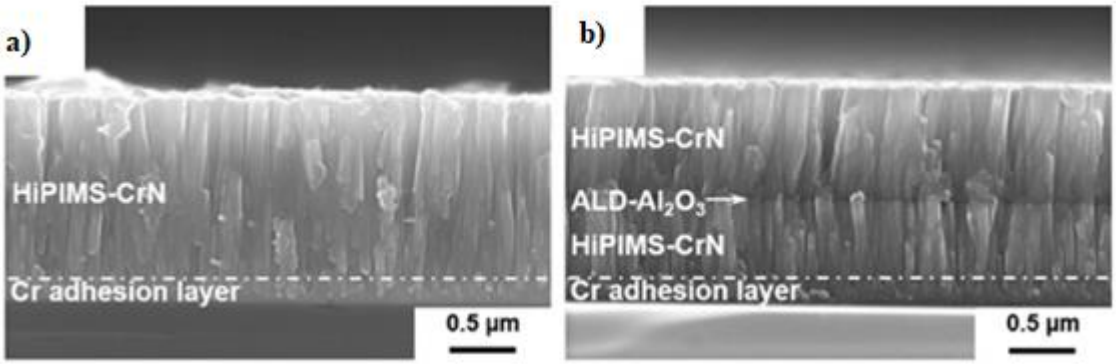

Figure I.8. Improving the corrosion resistance of CrN hard coatings by inserting a Al_2O_3 layer through atomic layer deposition :**a)** pure CrN coating, **b)** CrN coating with Al_2O_3 layer [23].

In the periodically repeated structure, alternating layers can perform as crack-stoppers either by introducing layer boundaries to arrest cracks or fitting a tough medium through which spread is moderated [20]. Via magnetron sputtering *M. Kot et al*. [24] examined the influences of bilayer period of ceramic and carbon layers (TiN/a-C: H multilayer coating) on the hardness, resistance to scratching, fracture, wear, and coefficient of friction, which were compared with the properties of both single TiN and a-C: H coatings. The results of mechanical and tribological tests showed very good properties of ceramic/carbon, and the multilayers bilayer with 32 nm in 32xTiN/a-C: H resulted in better resistance to scratching.

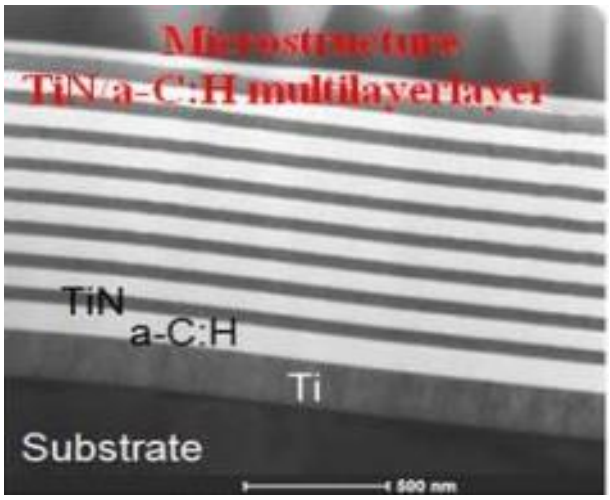

Figure I.9. TiN/a-C:H multilayers architecture [24].

X. Xu et al. [25] used PVD technique to produce TiAlN/W_2N multilayer coating, starting depositing TiAlN layers via multi-arc ion plating, while the W_2N layers deposited with D.C magnetron sputtering on substrates of mirror-polished AISI 304L SS with TiN interlayer that was firstly deposited by multi-arc ion plating for the improvement of the adhesion strength between the multilayer coating and the substrate. Multilayered coating with a modulation period of 373 nm presented the highest hardness of 1757 kgf·mm^{-2} and the lowest wear rate of 2.52×10^{-6}mm^3 (Nm)$^{-1}$ among all samples. In addition, the TiAlN/W_2N multilayer coating presented better tribological properties under high temperature.

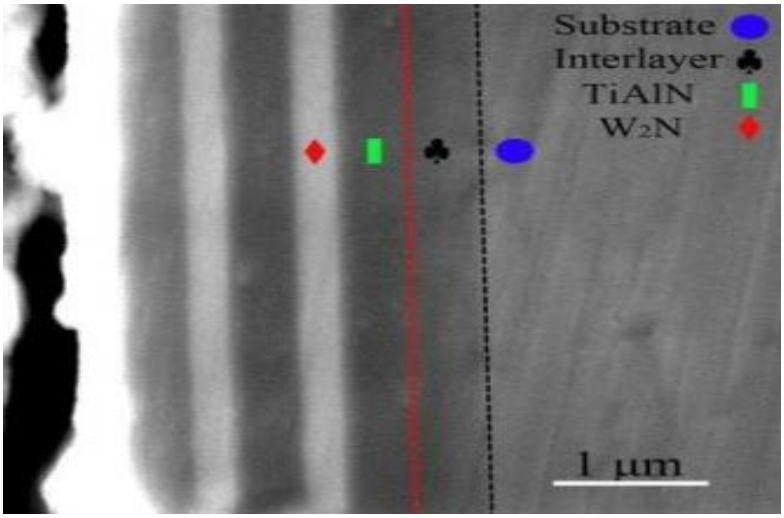

Figure I.10. Cross-sectional SEM images of as-deposited TiAlN/W_2N multilayer coatings [25].

I.5.1.4. Nanostructure coatings

Nanostructure coatings are nanocrystallized films with grain sizes in the nanometer range [21]. According to the well-known *Hall–Petch relation*, the yield strength, hardness, and toughness of polycrystalline materials are usually increased with reducing grain size, which is also proper for nanostructure coatings [21]. *S. YChun et al.* [26] investigated the effect of grain size on the hardness (H) and Young's modulus of TiN films, where H and Yong's modulus was found to increase from about (18.7 to 21.4) GPa and from (26.1 to 54.4)GPa and from (234.1 to 267.2) GPa then from (435.7 to 596.7) GPa respectively when grain size decreases from (13.4 to 10.9) nm then from (8.1 to 6.2) nm respectively.

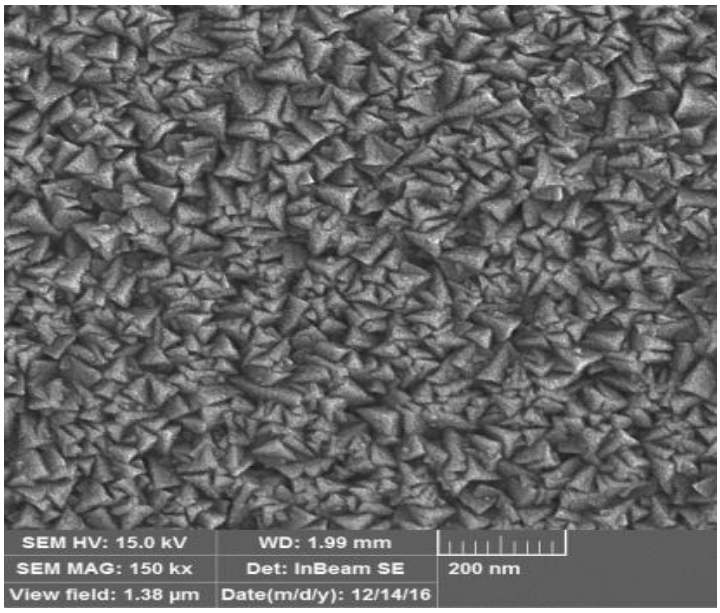

Figure I.11. Surface morphology of the TiN nanostructure coating [27].

I.5.1.5. Nanocomposite hard coatings

Nanocomposite coatings are a new class of materials that are comprised up of at least two phases: a nanocrystalline phase as well as an amorphous phase, or two nanocrystalline phases. Nanocomposite materials provide improved properties than traditional materials because their grain sizes are smaller (D = 10 nm). The main aspect of nanocomposite coatings is their enhanced hardness; a nanocomposite coating can have a hardness that is more than two times that of its harder component. Dislocation-induced plastic deformation, material nanostructure, and cohesive forces between atoms of adjacent grains are the major causes of increased hardness. The nanocomposite coatings may be divided into three classes based on their hardness ratings [19, 20]:

C_1: The hard coatings with hardness *of about* 40 GPa; for exemple $Ti_{0.49}Al_{0.44}Zr_{0.07}N$, single-phase cubic exhibited a hardness value of about 35 GPa [28].

C_2: The superhard coatings with *H ranged etween 40 and 80* GPa; in 1998, *M. L Wu et al.* [29] succeeded in producing TiB_2 coatings and CNx/ZrN multilayers, respectively, utilizing Single- and dual-cathode DC magnetron sputtering, CNx/ZrN multilayers achieved hardness passing40 GPa, where TiB_2 coatings accomplish hardness surrounding 50 GPa, also ZrYN nanocomposite films produced by *J. Musil et al.* [30] showed hardness value up to 47 GPa.

C_3: The ultrahard coatings with *hardness up than* 80 GPa; the hardness of about 105 GPawas reported for the nc-TN/a- and nc-TiSi nanocomposites coating fabricated by *S. Vepřiek et al*. [31].

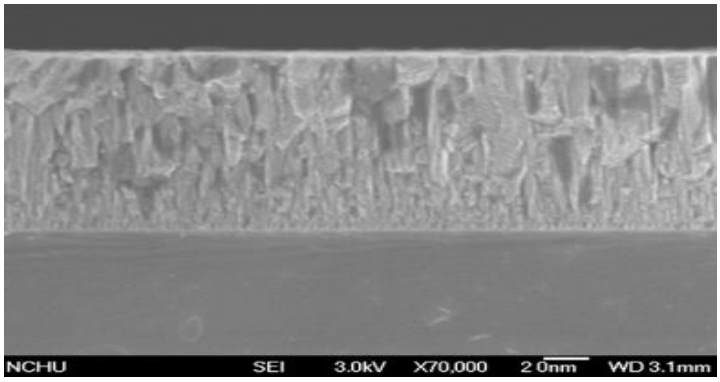

Figure I.12. The cross-sectional view SEM pictures of the nanocomposites (Ti,Zr)N films [32].

I.5.1.6. Nano layer hard coating

The great number of interfaces between layers in nanolayer coating increase hardness and strength. TiN/TiAlNnanolayer coatings were deposited on 100C6 steel (AISI 52100) substrates applying a commercial unbalanced magnetron sputtering system by *K. Khlifi et al*. [33] compared to the TiN single-layer thin films, the grain sizes are finer in the TiN/TiAlNnanolayer thin film, with high values of hardness and elastic modulus of about 55, and 450 GPa, respectively, with better adhesion on the substrate. The improvement of mechanical properties of TiN/TiAlN nanolayer coating could be attributed to a small grain-sized microstructure explained by *Hall Petch*effect.

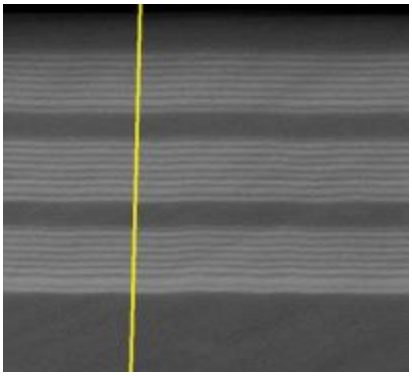

Figure I.13. EDS analysis of ZrN/Cr Nnano-multilayers [34].

I.5.1.6. Superlattice

Superlattice coatings are regularly repetitive multilayer coatings with a thickness of singular layers in the range of 5~50 nm. Some researchers found that the superlattice coatings especially TiN-based superlattice coatings (such as TiN/WN, TiN/CrN, TiN/TaN, TiN/MoN, and TiN/AlN), can improve hardness, toughness, and thermal stability in comparison to single layers [21]. *X.T. Zenget et al.* [35] deposited TiN/NbN superlattice hard coatings on high-speed steel substrates using unbalanced magnetron sputtering. The coatings exhibited a high toughness, a great elasticity, a super hardness (48 GPa), and an optimized superlattice wavelength of about 7 nm.

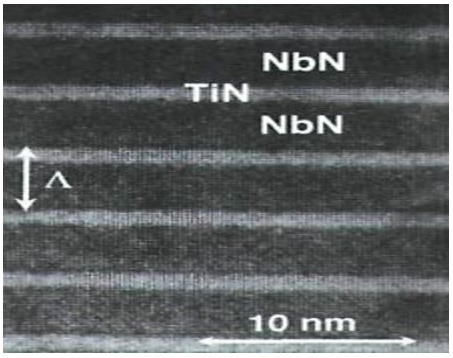

Figure I.14. Superlattice structures TiN/ NbN [36].

I.5.2. Hard coating materials categories

Hard coatings such as nitrides, diamond, and cBN are being employed in a variety of industrial applications. Over the last 30 years, several different types of coatings have been produced, ranging from metal nitrides like TiN, TiAlN, or CrN to carbon-based films. Hard coatings can be applied to a variety of alloy materials as well as all major stainless steel variants, including austenitic, ferritic, martensitic, precipitation-hardening, duplex, and super duplex. Increased corrosion or erosion resistance, as well as heat protection, are all difficult settings for hard coatings. Depending on the chemical bonding nature of the compounds, hard coating materials can be divided into three categories, with all the compounds standing out for their high hardness andelevated melting points [37].

The first group contains ***ionic hard oxides*** (ceramic) of Al, Zr, Ti, Be, Si, and others, which have a lower modulus of elasticity and are particularly ideal for surfaces due to their excellent stability and low inter-action tendency [37].

Next are the ***covalent hard materials*** exemplified by the borides, carbides, and nitrides of Al, Si, and B, as well as diamond materials such as diamond, c-BN, SiC, Si_3 N_4 are predominantly covalently bonded with attractive characteristics such as high hardness, high E-modulus, and high chemical stability. The adhesion of covalent thin films on metallic substrates is poor so that high compressive stresses lead to early delamination of the films if the system is used for machining. At typical PVD deposition parameter (T<400°C) most covalent components are deposited in an amorphous state; growth behaviour can be influenced by the deposition parameters (temperature, bias voltage, reactive gas flowgrowth rate) as well as the amount of interfaces and surface for the nucleation of the film [38].

Finally, the ***metallic hard compounds*** of the transition metal borides, carbides, and nitrides. From covalent to metallic and ionic hard materials, the linear thermal expansion coefficient increases.

In this chapter, we discussed the properties of transition metal nitrides, carbides, borides, and oxides *Table I.2.*

Table I.2. Some properties of binary transition metal thin films (TM).

	System	Conditions	Preferred orientation	Hardness (GPa)	Young's Modulus (GPa)	Ra (nm)	COF	Technique	Ref.
TMN	TiN	Ar/N_2 1:1	(111)	-	-	7.9	0.12	DC magnetronsputtering	[39]
		Ar+ N 6 cm^3 /min	-	up to 30	up to 300	1.3	-	DC reactive sputtering of a hot target	[39]
		20 min bias -90 V	(200)	19.06	134.78	0.413	-	DC reactivemagnetronsputtering	[40]
	ZrN	0.7 Pa	(111)	16.022	-	11.20	-	RF magnetron sputtering in	[41]
		50 V	(111)	23.5	-		-	DC magnetron sputtering system	[42]
		N_2parcielpressur1× 10^{-4} and 10× 10^{-4} Torr	(320)	25 to 27	360 and 280 at 1× 10^{-4} and 10× 10^{-4}Torr	29	0.7	DC reactivemagnetronsputtering	[43]
	CrN	300 °C and 290 V	(200)	21.2	-	-	4.97	pulsed DC reactive magnetron sputtering	[44]
		N_2flow rates 2–25 sccm substrate T° 303–973 K	(100)	12 ± 1.81	250 ± 51.28	2	0.16	pulsed DC magnetronsputtering	[45]
		Substrate bias 0 -628 V	(110)	21 GPa	-	2.39	-	pulsed DC magnetronsputtering	[46]
TMO	TiO	DC power (350W) Substrate T° (120 °C)	(101)	3.426		-	-	Magnetronsputtering (PVDMS)	[47]
		TiO_2 deposited on amorphous $SiO_2$with magnetron sputtering processes	(101)	4.8	-	-	-	Conventionalmagnetronsputtering	[48]
		TiO_2deposited on Si substrates with modulated plasma magnetron sputtering	(110)	16.1	-	-	-	plasma modulatedmagnetronsputtering	[48]
	ZrO	O_2flow rate 7.0–20.0 cm^3 min^{-1} P(Ar) 0.30–1.0 Pa P(O_2) 0.04–0.15 Pa	(200)	17.8	220	2.9	-	D.C. reactive magnetron sputtering	[49]
	CrO	O_2flow rate 2.0 - 3.2 sccm with 0.3 sccm increments	(300)	11–21		-		reactivemagnetronsputtering	[50]
TMB	TiB_x	Bias −120 V and −50 V	(002)	35.7	401.3	0.0158 µ m	-	unbalanced magnetron sputtering (PVD)	[51]
	ZrB_2	deposition times were 5 min and 15 min	(001)	45	350-400	-	-	DCmagnetronsputtering	[52]
	CrB_2	DefferentB/Cr ratios	(101)	25	-	-	0.52–0.78	non-reactive DC-magnetron sputtering	[53]
TMC	TiC	substrate bias −20 to −200 V	(111)	28.8	302.5	-	-	E303A magnetronsputtering	[54]
	ZrC	Ts 25 – 290°C	(111)	30. 2	-	-	-	DCmagnetronsputtering	[55]
	CrC	as a function of the a-C:H phase content	(200)	13	-	-	0.13	DC magnetron sputtering	[56]

I.6. Transition metal nitrides (TMN) thin films

Transition metal nitrides have attracted a lot of attention in the last decade, since of their fascinating and useful refractory properties; nitrides of various elements play a major role in industry, research, and technology. Because of their extreme hardness, wear and corrosion resistance, and thermal and electrical properties, numerous transition metal nitrides based on titanium, boron, and nitrogen have attracted commercial interest (*Table I.3*). The associated structures, as well as the high covalency of the transition metal-nitride bonds, increase all of these characteristics. Coatings of these materials are extensively implemented in industry to protect cutting tools or engine components [57]. TMN could be deposited by both PVD and CVD depositions methodes. Most transition metal nitrides (TMN) crystalize in the NaCl cubic structure, which consists of two interpenetrated metals and nitrogen. The (metal) atom is octahedrally adjusted to 6 nearest neighbor metal [58].

Table I.3. Nitride formation in transition metal series[57].

III	IV	V	VI	VII	VIII
ScN	TiN	VN	CrN	Mn_4N	FeN Co_2N Ni_3N
YN	ZrN	NbN	MoN	TcN	x x x
LaN	HfN	TaN	WN	Re_2N	x xx
		Ta_2N			

High interest was given to transition metal nitride owing to numerous researches available.

The binary transition metal nitrides as ScN, TiN, VN, YN, ZrN, NbN, LaN, HfN, TaN and AlN [59] were vastly studied; in earlier *H.A. Jehn, et al.* [60] realized a compression between three transition metal nitride thin films ZrN_x,NbN_x, MoN_x deposited by reactive dc magnetron sputtering.ZrN was found in the cubic nitride forms even for the lower nitrogen concentration, with hardness value in the range of 2000-2250 HV. Niobium exhibits the subnitride Nb_2N for lower N_2 pressures and the cubic nitride NbN for higher N_2 pressures, but NbN_X shows the lowest hardness 1200-1400 HV. Finally, molybdenum sputtering yields a metastable MoN solid solution with Mo_2N for lower and higher N_2 pressures respectively, with hardnesses between 1550 and 1900 HV.

L. Aissani et al. [61] reported that CrN thin films reactively magnetron sputtered at 650 Won XC100 steel substrates exhibited NaCl cubic structure, hardness of 19.53 GPa, and a friction coefficient of 0.55. Extremely oriented and dense columnar VN coatings with elevated harness value (25–30)GPa, and very low wear rates (5×10^{-17} m^3/N m) were obtained by *F. Ge et al*. [62].

In order to enhance the binary components proprieties, ternary transition metal nitrides were designed, and from earlier investigations, it was so clear that the ternary systems offered great enhancements in mechanical and tribological properties like low friction and high wear resistance that are the main characteristics of hard coatings continually employed for the protection of tool surfaces, as examples for ternary transition metal nitrides in literatures we site $Ti_xMe_{1-x}N$, $Ta_xMe_{1-x}N$ (Me = Ti, Zr, Hf, Nb, Ta, Mo, W) [63], CrFeN [64], CrVN [61], LiMN (M = Co, Ni, Cu), $SrTiN_2$, SrZrN, SrHfN, BaZrN, and BaHfN [65], etc...

L. Aissani et al. [66] deposited Cr–Zr–N thin films utilizing R.F reactive magnetron sputtering technique on Si (100) wafer and XC100 steel substrate without heating. The films comprised a (Cr, Zr) N solid solution where Zr atoms replace Cr atoms. CrN lattice parameter rose from 4.17 to 4.32 Å with crystallite size refinement. The mechanical parameters (H, σ, E, H/E, *and* H^3/E^2) were greatly enhanced in comparison to binary films, specifically at 29 at. % Zr. The friction and wear behavior of the CrZr (29 at.% Zr)–N coating also demonstrated a notable improvement. *Q. Yang et al.* [67] deposited TiAlN on Ti6Al4V substrate by reactive magnetron sputtering, the produced coatings with different Al content illustrated significant enhancement in erosion performance with the best erosion resistance several times higher than TiN coating. The outstanding erosion performance results from a good combination of increased hardness and toughness.

I.6.1. Titanium nitride

- ***Titanium (Ti)***

Titanium is one of the most prevalent metals in the Earth's crust. It was discovered by English chemist *William Gregor* in 1791, but it was only in 1910 that American chemist *M. A. Hunter* produced the first pure titanium. Titanium is a lustrous transition metal with a silvery grey color, low density, and high strengthand, light metal of high melting point and excellent corrosion resistance positioned in forth group, located after Scandium with the atomic number

22. In the nature, titanium is found in the composition of minerals such as $CaTiSiO_5$titanite and rutile TiO_2 characterizd by:

- *Water insoluble, while soluble in concentrated acids,*
- *Titanium metal burns at high temperatures in the air and also in pure nitrogen,*
- *Excellent corrosion resistance,*
- *Pure titanium is a light, silvery-gray, solid, bright metal with a high strength-to-weight ratio.*

Titanium is wedliy used in several applications:

- *Industry (Chemical, Electrical, Electronic),*
- *A fundamental of the medical field (Titanium surgical instruments, Hip and knee joints, Wheelchairs, Dental implants,*
- *Titanium alloys are used in the Aerospace and war industries.*

Figure I.15.a) Titanium in minerals stones [68], **b)** pure titanium [69].

Titanium alloys can maintain the α-Ti hexagonal-close-packed (**hcp**) crystal structure and the β-Ti which is called body-centered cubic (**bcc**) structureat room temperature.

At 882 °C, pure titanium undegroes an allotrope phase transition, from a body-centered cubic (**bcc**) crystal structure (**β** phase) to a hexagonal close-packed (**hcp**) crystal structure (**α**) at a low temperature. The transition temperature relies on the titanium purity, which is influenced by alternating and interstitial elements. The room temperature values of the lattice parameters a = 0.295 nm, c = 0.468 nm, since the ideal ratio of the hexagonal-packed crystal structure is superior to that of pure alpha titanium 1.633 > 1.587.

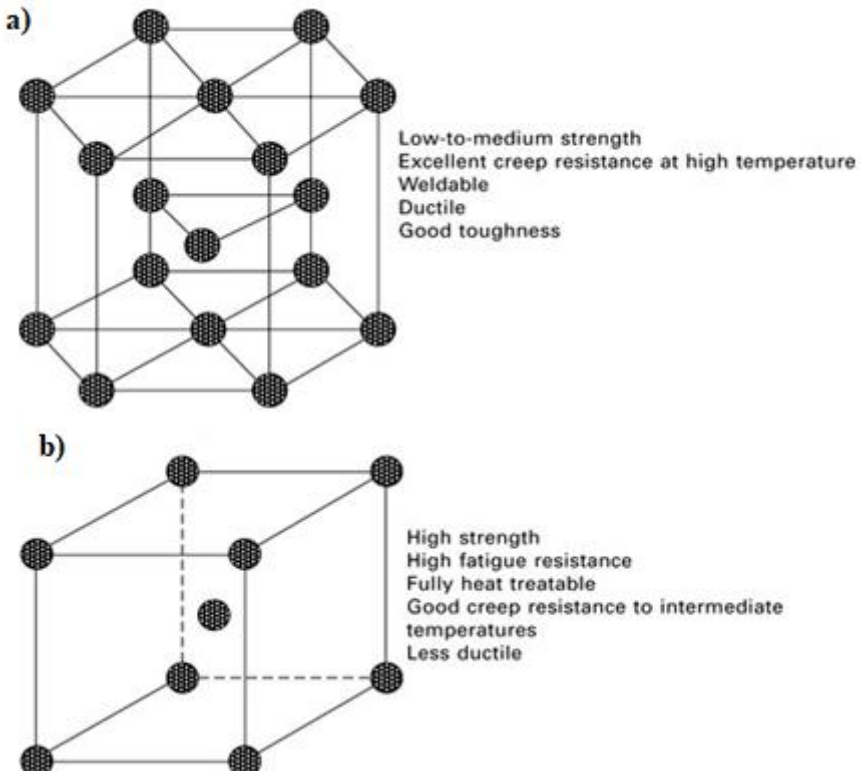

Figure I.16. Crystal structure and properties of**: a)** α-titanium, and **b)** β-titanium [70].

Titanium nitrides

Titanium nitride (TiN) is a rock-salt structure (NaCl-structure) compound made up of titanium atoms in a face-centered cubic (**fcc**) based lattice with nitrogen atoms filling all octahedral positions. Ti-N coatings have been used in a wide range of applications due to their unique properties, such as high chemical stability, high hardness, excellent wear and corrosion resistance, high melting temperatures, and chemical inertness, not only as hard coatings in industrial applications, but also as decorative coatings, wear-resistant coatings, diffusion barriers in the microelectronics industry, and in biomedical applications [71].

Titanium nitride has two known intermediate phases ε-Ti_2N and δ-Ti_2N formed at approximately 900 °C, The ε-$\boldsymbol{Ti_2N}$ phase crystallizes in an "anti-rutile" structure consists of a bcc-Ti lattice, as N atoms do not occupy all of the octahedral sites, but they occupy half of

theoctahedral sites, as opposed to (TiN). (TiN occupies all of the sites octahedral). The unit cell is tetragonal, with (a = 4.945 Å) (c = 3.034 Å) [72, 73].

The **δ−Ti_2N** phase, an unoccupied ordered form of the rock salt structure with few tetragonal deformations has output symmetry 141/amd and nitrogen breaking of ~38 $at.\%$. adding N to Ti cause it to transition from the **hcp** α-Ti phase to the **bcc** ε−Ti_2N phase and at the end to fcc-δ-Ti_2N and δ-TiN phases, as expected by the Engel-Brewer theory, The number of valence electrons increases with increasing N fraction. It has been indicated that Ti_2N phases have a bright yellow color, in contrast to the golden yellow color of TiN [73].

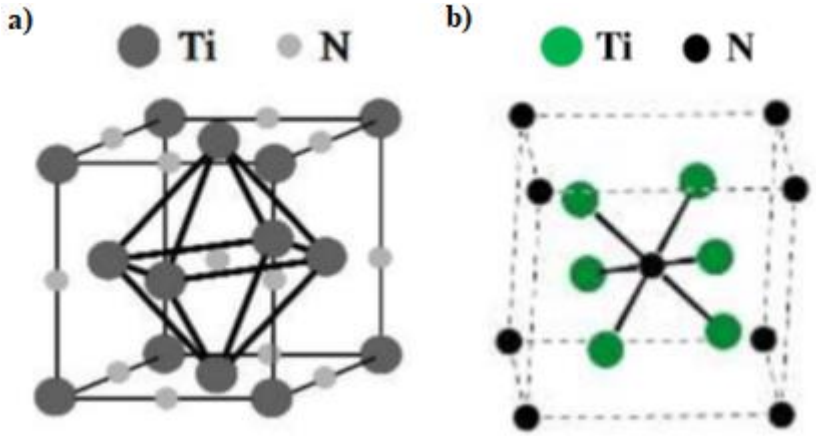

Figure I.17. Illustration of lattice structure of**: a)** TiN, and **b)** Ti_2N [74].

Table I.4. Characteristics of titanium and the both phaases of titanium nitride [72, 75, 76].

Caracteristiques and proprietes	**Ti**	**TiN**	**Ti_2N**
Cristalline Structure and machparameter(nm)	Lattice constants of α-Ti at room temperature, nmc=0.4679 a=0.2951 0.3306	cfcNaCl type a = 0.4144, c = 0.8781	tetragonal structure a = 0.4144, c = 0.8781
Spatial Groupe	p_6/mmc α-Ti Im3m β-Ti	$F_m3_mF_m3_m$	$P4_2$ /mnm
Composition	-	$TiN_{0.6}$ à $TiN_{1.1}$	33 %N_2
Molare Masse (g/mol)	47.867	64.95	
Atomicradus	0.145	-	-
BindingenergyE$_o$ (eV)		13.24	Formation Energy / Atom -1.446
Elasticmodulus (GPa)	116	505	344
Poisson's Ratio	0.3	0.235	0.277
Yong's modulus	105	466	287
Hardness (GPa)	700~2700 MPa	22.55	11.87
Electricalresistivity (μΩ•cm)		20 ± 10	
Superconductivity transition temperature (K)		5.6	
OxidationresistanceSlightoxidation		starts from 800 ° C in air	

I.6.1.1.Equilibrium phase diagram of TiN binary system

The equilibrium phase diagram of Ti-N binary system (*Fig. I.18*) demonstratesthat if some nitrogen is dissolved in titanium, the Ti(α) can be stable up to the melting point, which subsequently elevated to around 2350 ^oC and the maximum N containing is attained at approximately 25 at.%. When more nitrogen is added to the binary systemanε-phase occurs until the content of N increases to 33.7 at. % and the stoichiometric formula Ti_2N is created, which has a tetragonal structure. Adding additional nitrogen to the system, a δ-phase appears which has a Tiriched composition (TiNx, x≤1) with a NaCl type structure. In conventional TiN films, titanium nitride crystallizes mainly in the B1 NaCl structure comprising nitrogen in

the range (33.7-50) at. % (*Fig. I.18*) and also contains mixture of Ti_2N and Ti phases in some cases. *Figure I.17* illustrates the lattice structure of a NaCl type TiN crystal, with Ti atoms forming the center of the fcc lattice and N atoms representing the point of the **fcc** lattice. (1/2, 0, 0) [73, 74].

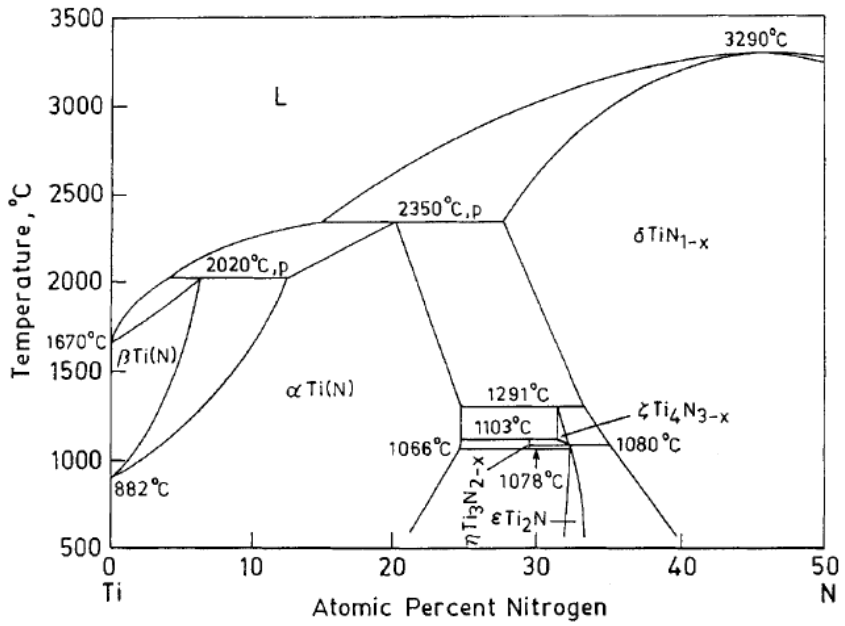

Figure I.18. Equilibrium phase diagram of Ti-N binary system, where the stoichiometric formulas of ε and δ phases are Ti_2N and TiNx (x≤1) [74].

I.6.1.2. Applications of tianium nitride

The application of titanium nitride is very wide due to its physical properties with high melting point, good chemical durability, and good conductivity compared to other materials, biocompatibility, and as well as excellent complementary metal-oxidesemiconductor (CMOS). Therefore, TiNcoating suitable for biomedical applications, CMOS-integrated devices, energy harvesting, optical devices, and as a protective coating in high temperature environments for applications as supersonic aircraft, and challenging mechanical applications such as grinding tool coating [20, 71].

I.6.1.3. Effects of deposition condition on the TiN proprieties

The structural physical and tribological properties of the sputter-deposited films were found to have strong correlations with the deposition parameters, in this part, we'll illustrate the effect of such parameter on the proprieties of the produced titanium nitride coatings.

Gas pressure

Concerning gas pressure, considerable investigations in the literature demonstrated its significant effect on the structural, morphological, physical, mechanical, and tribological proprieties on the obtained titanium nitride thin films: *E. Ajenifujaet al.* [77] deposited titanium nitride thin films on microscope glass using D.C reactive magnetron sputtering process in a 99.998% reactive nitrogen atmosphere, applying low (0.80 Pa), intermediate (3.40-5.33 Pa), and high (11.33 Pa) sputtering pressures,withkeeping the power constant at 200 W. The varying in the sputtering pressure was done to examine its effect on the as-deposited coating. It has been found that the lower sputtering pressure (0.80 Pa) prefers the appearance of oxygen-rich TiNx (Ti-Nx-Oy) films as noticeable from their color; where the dark blue colored oxygen-rich TiNx (TiNxOy) dense films were observed, while high sputtering pressure (3.40-11.33 Pa) enhances the formation of typical reflective golden yellow amorphous titanium nitride on glass at deposition time of 10 min.

In this case, we can conclude that the sputtering pressure has astrongimpact on the compositional characteristics and structural appearance of the films as experiential from their color. *S. Zhang et al.* [78] prepared TiN thin films on copper alloy (TL084) and Si(100) substrates by a closed field unbalanced magnetron sputtering system, using a high-purity (99.99%) titanium target with the dimension of 300×100×8 mm, in the process chamber with less than 150 °C. The whole sputtering gas flow is 16 sccm, which maintains the deposition pressure at 0.5 Pa. The various sputtering gas with the volume ratio of argon to nitrogen of 1:3, 1:2 and 1:1 is applied. Results showed that the rising in argon concentration in the gas mixture favors the growth of TiN nanocrystalline and decreases their surface roughness, friction coefficient, and wear rate. TiN films have a (200) preferred orientation at low argon flow rate, while the (111) preferred orientation dominates at high argon flow rate. TiN thin films fabricated with the ratio of argon to nitrogen of 1:1 has the most excellent tribological properties, which are the best sputtering condition as an ideal functional coating for synchronizer ring.

Nitrogen content

Generally, TMNs are synthesized by both physical and chemical methods utilizing the different N sources in the nitriding process, such as hydrazine, dicyanamide, urea, ammonia, and N_2. Magnetron sputtering technique uses the N_2 nitrogen gas as a source of nitrogene.

The insertion of nitrogen atoms (Since the size of the nitrogen atom is small (0.065 nm)) into the titanium lattice during deposition could be favour great changes in its structure, and allows the production of structures with desired nitrogen ratio from the stochiometric structure(x = N/TM) $TMN_{x=1}$ to the overstoichiometric coatings $TMN_{x>1}$ up to $TMN_{x=2}$,where the stoichiometry strongly influences the produced coatings properties [79]. *RD. Arnell et al.* [80] deposited with unbalanced magnetron sputtering on hard tool steel substrates TiNx layers with different nitrogen content. The film microhardness was found to have a maximum at ($x \approx 0.9$). For this value of (x), a maximum content of netrogen and the highest lattice distortion (especially for the (200) plane) was observed. The micro hardness, as well as intrinsic stress, developed due to lattice imperfections, and demonstrated a correlation to the chemical bonding between the film components.

By varying nitrogen flow rate between 0.25 and 1.75 sccm, *J.H. Hung et al.* [81] prepared nanocrystalline TiN thin films on Si(100) wafers using an unbalanced magnetron (UBM) sputtering system. The images of transmission electron microscopy (TEM), scanning electron microscopy (SEM) and atomic force microscopy (AFM) also presented a nanometer-size grain structure of the TiN thin filmswith a grain size less than 7 nm. The N/Ti ratio increased (N/Ti=0.4–1.1) while the deposition rate lowered with raising the nitrogen flow rate. The preferred orientation varied from (111) to (200), then back to (111) as the nitrogen flow rate increased. There was no important difference in the film hardness with nitrogen flow rate or preferred orientation. The highest film hardness was ranging from 23.4 to 27.6 GPa, even for the film thickness down to 140 nm. *L. Lu et al.* [82] varied the nitrogen flow rate from (1, 2, 4, to 20 sccm) to deposition of TiNx films on glass substrates by D.C reactive magnetron sputtering technique. TiN phase with a faced-centered cubic crystal structure was developed at 1, 2, and 4 sccm as indicated by XRD patterns. As the nitrogene flow rate rose from 1 to 4 sccm, the preferred orientation of the films altered from (111) to (200) plane. Upon further increased to 20 sccm, the XRD peaks were almost indiscernible. The analysis of XPS indicated that the TiNx films, titanium oxynitride, and TiO_2 phase formed in the films. With increasing nitrogen flow rates the N/Ti stoichiometry ratio improved from 0.69 to 0.98. In our previous work [83], we deposited the TiN coatings by magnetron sputtering using Ti target at various nitrogen content to investigate the influence of the nitrogen content on the mechanical characteristics and tribological performances of the TiN coatings were systematically examined usingnanoindentation and a bille-on-disk tribometer. Nanoindentation results confirm that the hardness and Young's modulus of the TiN coatings

improve with increasing N content in the coatings. Wear test results indicate that the wear rate and friction coefficient of the XC100 steel substrate was significantly reduced by deposition of the TiN coatings and the tribological behaviors of the TiN coatings are strongly dependent on the nitrogen content in the coatings.

Film thickness

It was demonstrated from experiments that film thiknessas significance a changes in the preferred orientation, grain size, grain boundary density, residual stress, that have a direct corolation with mechanical and tribological proprieties of titanium nitride thin films. *JH. Huang et al*. [84] deposited nanocrystalline TiN thin films on AISID2 steel substrates working unbalanced magnetron (UBM) sputtering method. The results showed that (111) was the principal preferred orientation in the TiN films. The roughness and grain size of the TiN films were only slightly reliant on the film thickness. The nanohardness of the films, ranging from 21–26 GPa, did not show a notable relationship with film thickness. All specimens comprised compressive residual stresses and reduced with growing TiN film thickness. An essential interlayer thickness, between 130 and 180 nm in the films with Ti interlayer, and in this case the residual stress in the TiN films could be substantially relieved.

To explain the influence of thickness on film properties, *H. Liang et al.* [85] prepared titanium nitride (TiN) thin films with direct current (D.C) reactive magnetron sputtering using a pure Ti target in an N_2 and Ar mixed atmosphere at 350 °C on Si (100) substrates. Results indicated that all the films were stoichiometric. In the initial stage, surface roughness decreased with increasing thickness related to the presence of particles diffusion and smoothing the underlying Si substrates. In the later growth process, the film surface was roughening with raising thickness due to the shadowing effect and change of surface morphologies with diverse orientations. Furthermore, film grain sizes and density monotonically increased with increasing film thickness, and preferred orientation also changed as a function of thickness. *V. I. Shapovalov et al.* [39] found that the titanium nitride films with the highest hardness (up to 30 GPa) and Young's modulus (up to 300 GPa) have the largest grains that was obtained at low nitrogen flow rate and at high discharge current density.

Substrate temperature

The substrate types could influence the adhesion between the thin deposited films and the substrate, but varying substrate temperature Ts demonstrated further powerful influence on the film's microstructural characteristics such as density, grain size, and orientation.*P. Patsalas et al.* [86] deposited TiNx films on n-type-Si(001) using D.C reactive magnetron sputtering with deferent substrate temperatures (Ts) to understand its impact on the mechanical properties and the microstructure of the TiNx films. It was found that the deposition at high Ts facilitates the growth of (002) oriented films with a density proximate to the bulk density of stoichiometric TiN, indicating the lack of voids and the growth of stoichiometric TiN. Both mechanical and microstructural properties of the film revealed a clear relationship between them. The denser and stoichiometric films grown along with the (002) exhibited the best mechanical performance. Films deposited with V_b= −100 V at T_d =400°C exhibit H=24 GPa, and E=320 GPa, respectively. *R. Bavadiet al.* [87] have studied the physical properties of titanium nitride thin film prepared by reactive D.C magnetron sputtering technique at different substrate temperature (300°C - 500 °C), respectively. AFM images show the creation of nanostructure thin films with increasing of surface roughness at high substrate temperature.

B. Subramanian et al. [88] prepared TiN thin films on mild steel (MS) by (PVD) method namely direct current reactive magnetron sputtering. A remarkable decrease in (111) plane peak intensity was detected for increased substrate temperature, whereas the intensity of the (200) plane showed an increasing trend. This means that the crystallographic orientation of the film changes from the presence of (111) to both (111) and (200) with the increase of Ts. Comparatively, one can observe that the sample prepared at Ts = 400°C shows good crystalline nature as observed from (111), (200), and (222) planes. It demonstrates the textured growth of the film with various planes to enhance its strength. The structural parameters calculated for both (111), and (200) planes were compared and both behave close to one another. The lattice parameter of the TiN sample prepared at 200 °C (Ts) was calculated to be 4.27 Å. When Ts increases the lattice parameter decreases, in accordance with the decrease of crystallographic volume.While increasing the Ts, grain size decreased, whereas strain and dislocation density were found to increase. The larger grain size of the film grown at 200 °C is also an evidence of its high compaction (decreasing the grain boundaries) confirmed by the highest intensity of the diffraction peak at this temperature. The grain size curve is highly influenced by the substrate temperature. At higher temperatures, desorption

process appears, because the adsorption energy is greater than the surface energy and the adatoms are desorbed leading to the reduction in grain size. *Ş. Ţălu et al.* [71] studied the influence of temperature on the 3-D surface morphology of titanium nitride (TiN) thin films synthesized by D.C reactive magnetron sputtering on a p-type silicon (100). The reactive sputter gas was a mixture of argon (99.999 %) and nitrogen (99.999 %) with the ratio Ar (97 %) and N_2 (3 %) by volume. In the vacuum chamber, the substrate was heated, then its temperature determined with a thermocouple. The deposition process was performed in 3 stages at different substrate temperatures (473 K, 573 K, 673 K, 773 K), respectively, and the deposition time for all samples was 120 min. Quantitative results of morphological transformations in the TiN thin films induced by substrate temperature variations.

I.6.2. Zirconium nitride

Zirconium

Zirconium was discovered by *Martin Klaproth* in 1789. But *Jons Berzelius* was the first to isolate it as a pure metal in 1824. It was only available in commercial amounts when the procedure for decomposing iodide was developed in 1925, and then in larger quantities after *Kroll* developed the reduction technique in 1947. Zirconium is a chemical element with the symbol Zr of a metallic appearance, and atomic weight of 91.22belongs to column IV-B of *the periodic Table*, with titanium and hafnium forms the second column transition components. Pure zirconium is soft, malleable, andductile, but even a percentage-point of impurities makes it hard and fragile. Although zirconium is the 18th most plentiful element in the Earth's crust, it is not widely dispersed. It is mainly acquired from two minerals: baddeleyite (ZrO_2) and zircon ($ZrSiO_4$ or $ZrOSiO_2$), with a colored gem that can be red, brown, yellow, green, or gray and can be transparent or opaque. Cubic zirconia crystals can grow to reach an inch in diameter or greater, notably in deposits from Canada and Australia. The United States, Australia, and Brazil are the primary sources of zirconium minerals, while considerable amounts may also be found in India, Malaysia, and Russia [89]. Because zirconium offers good corrosion-resistant properties against a wide range of substances, including saltwater, acids, and alkalis, it is frequently employed in the chemical industry. At low temperatures, zirconium is also a superconductor and may be utilized to generate superconductive magnets. Zirconium can be utilized as a medical implant material because of its features, which include being an extremely hard element similar to titanium [90].

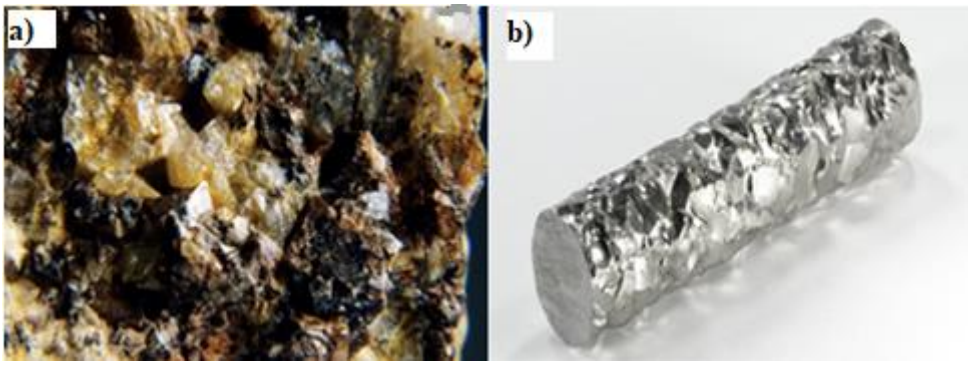

Figure I.19.a) Zirconium stone [91], **b)** Zirconium metal 99.8%of purity [92].

Zirconium has a temperature-induced polymorphism as well as another pressure induced. Zirconium is present in two structures allotropic: At atmospheric pressure and room temperature (25 °C), the Zirconium has the hexagonal compact structure α-zirconium. At atmospheric pressure and elevated temperatures exceeding 856 °C, the β-zirconium phase develops with a cubic centered (cc) structure, but also β-zirconium phase can exist at ambient temperature if the pressure is greater than 30 GPa.

At room temperature wit high pressures (between 2 and 8 GPa), zirconium forms new phase, known as omega zirconium (ω-Zr) which requires a hexagonal structure, with three atoms in the lattice (*Table I.5*). Furthermore, new study shows that the (**ω ↔ β**) transition can develop at extremely high pressure (30 - 60 GPa). According to numerousresearchers, the **α ↔ ω**transformation illustred a significant hysteresis and the phase **ω**, which has a superior density compared to α-Zr, can remain as a metastable phase at ambient conditions (persists after release pressure). It has been observed that the application of significant higher pressures phase ωdevelops phase **ω '**of centered cubic structure [93].

Table I.5. Allotropic forms of zirconium at atmospheric pressure (Variable: **pressure**) [93].

Phase	**Pressure regime(GPa)**	**Crystalline structure**
Alpha (*α*)	Until 2	Compact hexagonal (hc)
Omega (*ω*)	2-30	Hexagonal (h)
Omega (*ω′*)	>30	Centered Cubic (cc)

Table I. 6. Allotropic forms of zirconium at room temperature (Variable: **temperature**) [93].

Phase	Temperatureregime°C	Enthalpy of transformation KJ/mol	Crystalline structure
Alpha (*α*)	Until 866	4.103	compact Hexagonal (hc)
Beta (*β*)	866-1855		Cubic centered (cc)

Table I.7. Crystal structures and lattice parameters of the allotropic forms of zirconium [93].

phase	Structure		Meshparameter (laticeparameter)	Axial ratio
	Cristalline structure	Group of species		
α	Compacte hexagonal (hc)	P63/mmc	a=3.2316 c=5.1475	1.5929
β	Centredcubic	Im3̄m	a=3.6090	1.0
ω	Hexagonale	P6/mmm	a=5.036 c=3.109	0.617
ω′	Centredcubic	Im3̄m	-	-

Zirconium nitrides (ZrN)

Zirconium nitride is one of the important coatings today whether in hard and protective coating on mechanical tools as wear protective coatings, (such as cutting instruments, molds, dies), or abrasion and corrosion-resistant layers in aerospace, automotive, decorative coatings (that are used for scratch resistance and coloring in the jewelry industry) [94], diffusion barrier in the microelectronic industry or even in biomedical application [95]. ZrN possess excellent properties [96], where exhibits high hardness (~15 GPa), high melting point (2980 ± 50 °C), good thermal conductivity, low electrical resistivity, good abrasive resistance, and good corrosion resistance [97]. Magnetron sputtered ZrNthin films have a high deposition rate, uniform formation of film, low-temperature rises of substrate, and good bonding between the thin film and substrate, small damage to the film layer [41], and can change chemical compositions to obtain several structures of the deposited film such as ZrN, Zr_2N, Zr_3N_4, [98] and ZrN_2.

I.6.2.1. ZrN diagram phase

On the Zr-N diagram, the domain of the solid solution ZrNx ranges from 4 to 11.5% of nitrogen at 700 °C (*Fig. I.20*). This wide range of stoichiometry implies an evolution sensitive to the properties of nitride as a function of the N/Zr ratio. The solubility of nitrogen in the two phase's α-Zr and β-Zr is much higher by compared to that of carbon in zirconium; the nitrogen solubility limit in α-Zr is 3% by mass, while it is 0.8% in the β-Zr phase. The transformation temperature of α-Zr to β-Zr depends on the nitrogen content. The only stable intermediate compound in the Zr-N system is ZrN zirconium mononitride with a wide range of stoichiometry ranging from 9 to 13.5% by mass percentage of nitrogen. However, the metastable phases ZrN_2, Zr_3N_4 and ZrNx (x> 1) have been reported for ZrN thin films [89].

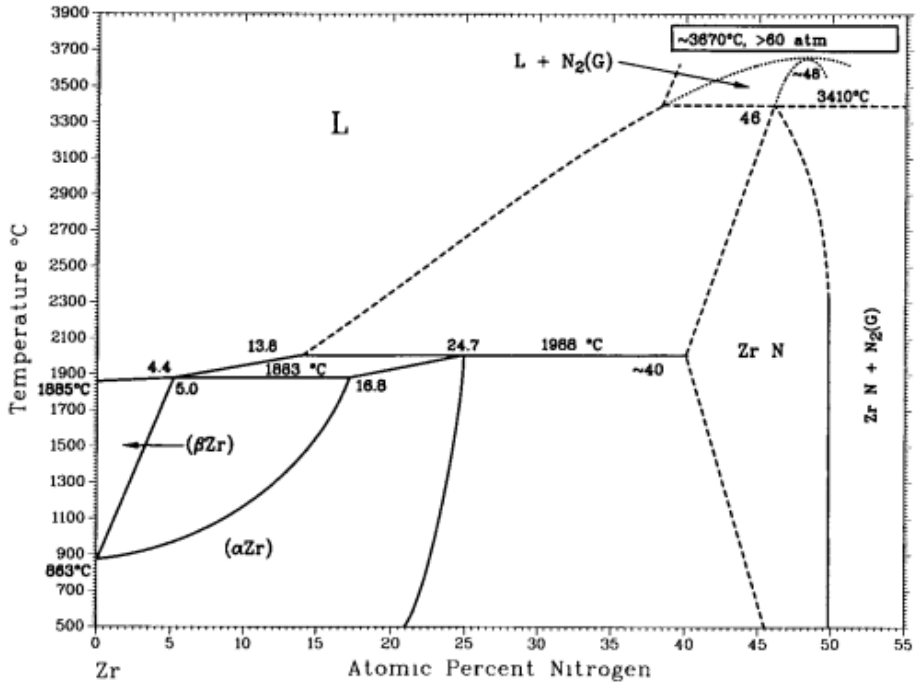

Figure I.20. Equilibrium diagram ZrN [93].

Table I.8. Crystal structures and lattice parameters of the system ZrN [89].

Phase	Compositin masse %.	Crystalline structure	Spaces group	Lattice parametre
αZr	0 to 24.7	Simple hexagonal	$P6_3/mmc$	a = 3.242 c = 5.169
βZr	0 to 5	Cubic centered	$Im\bar{3}m$	a = 3.609
ZrN	40 to 50	Cubic faces centred	$Fm\bar{3}m$	a = 4.63

Table I.9. Zirconium and zirconium nitride properties [89].

Component	**Zr**	**ZrN**
Diffusion temperature	1852	2982
Coefficient of thermal expansion ($10^{6-}/C^0$)	5.1	7.2
Volumic masse(g/cm^3)	6.439	7.042
Color	metallic	Golden
Specific heat(j/mol.K)	26.05	40.39
Heat of formation at25^0C(KJ)		-365.5
Thermal conductivity at 20^0C (W/m.K)	22.7	20.5
Electrical resistivity($\Omega.Cm$)	43	7 to 21
Hardness(GPa)	0.48	15.8
Yongue modulus	95	397

I.6.2.2. Effect of deposition condition on the ZrN properties

In this part, we presented some studies on the influences of synthesis parameters on the structure and quality of zirconium nitrides coatings deposited with magnetron sputtering starting with the effect of gas pressure, then, nitrogen content effect, and finally the substrate bias voltage effect.

- ***Gas pressure***

In a reactive sputtering process, the reactive gas pressure plays an essential role on the glow discharge characteristics and on the deposition rate *H.B. Bhuvaneswari et al.* [99] varied nitrogen partial pressure from $4x10^{-5}$ to $10x10^{-5}$ mbar in order to prepare zirconium nitride films on silicon substrates at room temperature by D.C reactive magnetron sputtering. Using

high purity of Nitrogen (99.99 %) and Argon (99.99 %) as reactive and sputtering gases, respectively. Results shwed that films formed at lower partial pressure (less than $5x10^{-5}$ mbar did not show the formation of ZrN but indicated only zirconium phase, whereas films formed beyond 6 $x10^{-5}$ mbar showed ZrN peaks corresponding to (121) and (111) phases.

Recently, *S. Lin et al.* [41] prepared five kinds of ZrN thin films in the range of sputtering pressures of 0.3 to 1.1 Pa by R.F magnetron sputtering system.ZrN coatings were deposited on zirconium alloy substrates at room temperature utilizing a ZrN target with a 99.5% purity, a diameter of 50.8 mm with 3 mm in thickness, the distance between substrates and target was 80 mm, ZrN target sputtering power was fixed to 100 W and the deposition time was 60 min. The results showed that the crystallinity of ZrN films increased first and then decreased with the increase of sputtering pressure. At 0.5 Pa ZrN film began to crystallize andthe best crystallization was obtained at 0.7 Pa,with surface roughness of 11.20 nm, and the best hardness and elastic modulus of about 16.022 GPa, and 193.518 GPa, and H/E and H^3 /E^2 were 0.11 and 0.083, respectively. More recently, *H. V. Patel et al.* [100] studied the effect of R.F sputtering power and working pressure on the properties of zirconium nitride coatings produced with magnetron sputtering. At 1 Pa of sputtering pressure a very high intensity (311) peak of Zr_3N_4 was observed, and the films showed excellent wettability with contact angle of 107° measured with water sample which was 980 this proves that the thin films deposited were hydrophobic.

Nitrogen content

Since the magnetron sputtered ZrN thin films produced witnitrogene N_2 gas that confirms the affectof nitrogen flow rateon the proprieties of ZrN thin films. From literatures, *P. Klumdoung et al.* [98] evaluate a color variation of the zirconium nitride thin film deposited in the range of 0.0 to 6.0 sccmN_2 flow rates, whereas the high Ar flow rate is fixed at 6 sccm. The XRD results reveal the structures changes of film system from αZr, α-$ZrN_{0.28}$, ZrN, Zr_3N_4 and finally amorphous with the increasing of N_2 flow rate. The average film thickness ranged from 85.8 nm to 276.0 nm. The colors of the deposited film were changed from silver, dark brown, brown and to blue. Indeed, no golden color zirconium nitride film was obtained under the interested conditions.

A. Singh et al. found [101] that Films deposited up to 1 sccm of nitrogen flow rate showed single phase fcc-ZrN, while for nitrogen flow rate >1 sccm and up to 6 sccm, the

deposited films revealed the growth of ZrN along with Zr_3N_4secondary phase. At 6 sccm a poor crystallinity was exhibited by the depositedfilms. XPS analysis of these films indicated the presence of Zr, ZrN, ZrO_2 and Zr_2N_2O phases. The effect of nitrogen flow rate on the nanomechnical properties exhibited an enhancement in hardness and elastic modulusas a result. More recently, *H. V.Patelet al.* [100] prepared Zirconium nitride (ZrN) films in the environment of argon as inert gas and nitrogen as reactive gas these the obtained thin films were hydrophobic; where an dxcellent wettability were achieved for the films deposited with 1Pa sputtering pressure.

- ***Substrate bias voltage***

D. Pilloud et al. [102] studied the substrate bias voltage effect on the properties of zirconium nitride films. The coatings are deposited on steel and silicon substrates by magnetron sputtering of a zirconium target in reactive Ar–N_2 mixture. Results show that when the bias voltage is applied to the substrateholder, the film texture changes into a (111). A porous films' surface with a decreased lattice parameter, were observed for negative bias voltage values higher than -110 V. The films present a maximum of hardness (39.5 GPa) at -100 V that surface roughness increases due to a sputtering phenomenon. Results show that the mechanical properties of the ZrN films are greatly influenced by the substrate bias and can be related closely to the microstructure evolution during sputtering. As negative bias is applied, the films tend to be denser with columnar grains, thus, the hardness and fracturetoughness can be largely enhanced. However the elastic modulus, on the other hand, is reduced, most likely owing to differences in preferred orientation.

M.A. Signore et al. [103] fond that the negative bias voltage applied to the substrate during thesputtering deposition, enable films to exhibit a highly (111) preferred orientation due to the minimization of the strain energy. Increasing the bias reduces lattice parameter; this outcome can be due to the nitrogen substitute by oxygen or the generation of nitrogen vacancies induced by the ion bombardment. *A. Kavitha et al.* [104] deposited ZrN thin films on SS substratesusing a mid-frequency reactive magnetron sputtering. The bias voltage increased from 100V to 300V and the preferred orientation changes from (111) to (200). When bias voltage increases, thickness also increases. When thickness increases crystallite size decreases, strain and dislocation density increases. Micro-hardness and surface roughness are found to increase as the bias voltage increases.

Effect of thickness

M. Valaiauksornlikit et al. [105] prepared ZrN thin films at different film thicknesses, the results indicated that all samples were cubic close-packed structure with the preferred-orientation (111) plane. However, at 300 nm, the (200) plane disappeared, eventually reducing the reflection and lightness of the samples.

I.6.3. TiZrN ternary nitride

Ternary transition metal nitrides have accumulated exceptional awareness to improve further the properties of the related binary compounds. Although the high proprieties that TiN exhibit whether it was mechanical, tribological, or electrical but, TiN limitations, are unstable by occurring oxidation resistance at high temperatures beyond 500 °C that can be reached during machining processes [106]. It has been reported that the effect of adding zirconium in to TiN structure to form TiZrN can present a better behaviorand cover demand for harder and tougher materials, the (Ti, Zr)N coating shows an enhanced hardness compared with the binary TiN and ZrN coatings deposited under the equivalent conditions [32, 107]. Ternary TiZrN films not only exhibit a golden color and low resistivity but also, better corrosion resistance and superior mechanical properties [108]. That could be explained by the formation of the stable oxide layers on the film, and the formation of solid solution strengthening, provides an energy barrier to the movement of dislocations throughout the crystals by distortion of the periodic lattice [109].

TiZrN crystallize in cubic densest sphere packing structure, which originally is the structure of both TiN and ZrN because, according to *Vegard's rule*, the lattice parameter of the other mixed phase is, in proportion to theamounts of the alloying components, between the lattice parameters of the single phases [108]. Many studies indicated that the addition of Zr into TiN or Ti into ZrN could enhance the fracture toughness of hard coatings [108]. *A. Hörling et al.* [110] show that the Ti_1xZr_xN thin films are promising candidates for cutting tools applications due to the retained high hardness even after post-deposition annealing above 1000 °C. Magnetron sputtering is one of the most important technique in Ti_1xZr_xN deposition and the expected or desired proprieties (crystal structure, surface morphology, microstructure or compositions element) are strongly dependent on the deposition parameters [106].

I.6.3.1. Ternary phase diagram of ternary TiZrN

Limited experimental information is available for Ti-Zr-Nsystem. *E. Etchessahar et al.* [111] found that 45 at.% N is the lower concentration limit for total miscibility in the ternary nitride region (named F_1) the phases resulting from the miscibility gap are $Ti_{0.13}Zr_{0.45}$ $N_{0.42}$ (named F_2) and $Ti_{0.49}Zr_{0.09}N_{0.42}$ (named F_3) the grain boundaries of the F_2 initial homogeneous ternary δ-nitride phase are the preferential sites for the nucleation and growth of the F1 and F3 phases. The partial $(Ti_{0.5}Zr_{0.5})$ N pseudo-binary phase diagram from 0 to 50 at. % illustrated the existence of three phases for temperature range (900–1520 °C) : δ-(Ti 0.5 Zr 0.5)–N and nitride and the two nitrogen solid solutions. The nitrogen dissolution in the β-$(Ti_{0.5}Zr_{0.5})$–N alloy is marked up to 5 at. % N in the 1300–1520 °C temperature range. The stabilization of theα-$(Ti_{0.5}$ $Zr_{0.5})$–N phase by nitrogen exists up to 1520 °C. Whatever the temperature is, the more elevated nitrogen solubility in this phase is approximately 16.5 at. %. Moreover, the nitrogen solubility threshold in thisα -phase depends on the temperature and rises up to 13 at. % when the temperature is higher than 1300 °C. Above 1300 °C α -phase domain is narrow (bounded by 13 and 16.5 at. % N).

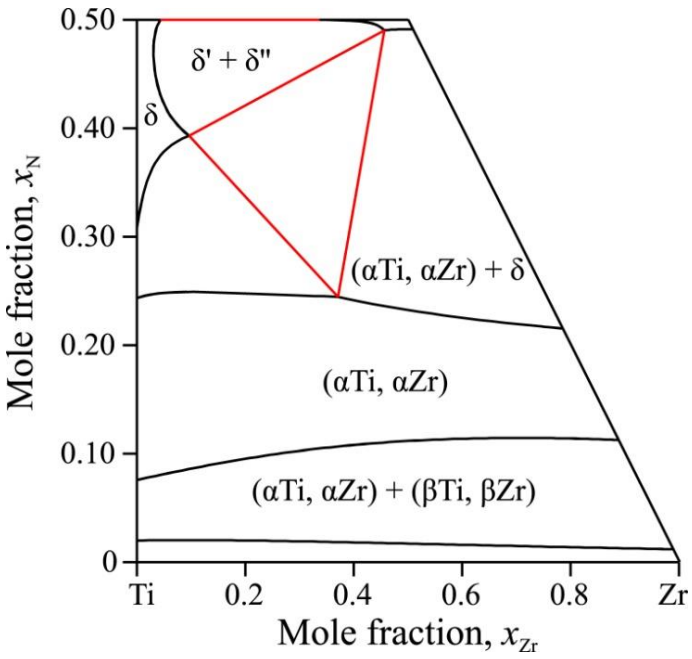

Figure I.21. Ternaryphase diagram of ternary TiZrN [112].

I.6.3.2. Effect of deposition condition on the TiZrN properties

Nitrogen flowrate

Y.W. Lin et al. [32] affirmed that it is feasible to produce the nanocomposite (Ti, Zr)N thin films at the lower nitrogen flow rateusing R.F magnetron sputtering system. For nitrogen flow rates of 2–7 sccm the single-phase solid solution of (Ti, Zr) N appeared, at the lower nitrogen flow rates of 1 sccm, phase of both (Ti, Zr) N and TiZr mixture appeared. The films grain size was less than 20 nm. The (Ti, Zr) N films show excellent hardness ranging from 35.5 to 37.5 GPa with exhibiting (111) preferred orientation.

Effect of bias voltage

The bias voltage of the substrate can significantly tailor the composition and microstructure of the films. At different substrate bias varying from −40 V to −120 V using D.C unbalanced magnetron sputtering with dual guns (Ti and Zr) targets *Y. W. Lin et al.* [108] deposited TiZrN thin films onto Si (100) substrates. At low substrate biases of −40 V and −45 V, a strong (111) texture was shown by all samples, with good roughness (0.5~0.6 nm). TiZrN films exhibited high hardness (33.4~37.8 GPa), low residual compressive stress (2.7 ~ 3.7 GPa), and a bright-golden color.

Deposition time

At different deposition times of (60, 120, 180 and 240 min) with reactive magnetron co-sputtering set-up using the OAD technique, *W. Phae-ngam et al.* [113] prepared nanocolumnar TiZrN films for self-cleaning applications, using (Ti with a 99.99 % purity) and (Zr with a 96.9 % purity) on the substrate of Si wafer (100). The result illustrated that the TiZrN films prepared at 60 min and 120 min, exhibited a broad reflection of the (111) peak, increasing the time to 240 min, the peaks shifted sharper and intense. All the prepared films showed a porous and well-separated, inclined nanocolumnar growth. The hardness and Yong's modulus reduced with increasing deposition time. The wettability was characterized by utilizing a water-contact-angle measurement. The results indicate that all the nanocolumnar films have a hydrophobic surface. At 60 min the water-contact angle for the nanocolumnar TiZrN films was 91°, and then lifted to 110° at 240 min due to the surface roughness increasing.

Plasma-processing power

F.M. ElHossary et al. [114] prepared the TiZrN thin film on AISI 316 substrates, using D.C-pulsed magnetron, the plasma-processing power was varied from 125 to 250 W. X-ray patterns revealed the formation of solid solution phase of TiZrN with diverse orientations. The results illustrated that the microhardness of TiZrN film improves with increasing the plasma-processing power to achieve the highest value of around 1050 HVat 200 W. When compared to the untreated sample, the tribological characteristics of AISI 316 coated with TiZrN were shown to be improved. The wear rate of the coated sample at 225 W has a value of nearly 0.0034 mm^3/Nm which is very low in comparison with AISI316 substrate that has a value of 0.137 mm^3/Nm.

Titanium content

Experiments confirmed that the structure, morphology and chemical composition of the films showed changes as function of Ti sputtering current. *S. Chinsakolthanakorn et al.* [115] studied TiZrN films fabricated on unheated Si (100) substrates by reactive D.C magnetron co-sputtering in flow rates of 8 and 4 sccm of Ar and N_2 sputtering gas and reactive gas, respectively. The Zr sputtering current was fixed at 0.6 A and Ti sputtering current varied from 0.6 to 1.2 A for 60 min. It was found that the all prepared films were (Ti, Zr) N solid solution. Increasing Ti sputtering current showed an increase in the crystallite size, roughness, and film thickness, but a decrease in lattice parameter.

Zirconium content

Only limited experimental information is available concerning the effect of Zr content on the proprieties of TiZrN ternary system; according to *W. Phae-ngam et al.* [116] during the deposition of the nanocolumnar TiZrN thin films on silicon wafer using magnetron co-sputtering with oblique angle deposition (OAD) at room temperature,the variation in sputtering power of Zr target from 100 to 300 W, shwed that withincreasing the Zr sputtering power, the length and diameter of the nanocolumnar TiZrN increased. Samples deposited at 150 to 300 W showed the diffraction (111) and (200) peaks. The hardness of all prepared samplesshowed low value in arrange between 1.44-2.87 GPa compared with dense TiZrN film; because of the porous structure resulting from the shadowing effect. As the sputtering powers of the Zr target rose from 100 to 300 W, the thickness, diameter, and length of the nanocolumnar TiZrN film increased (394-710) nm, (71-127) nm and (428-804) nm,

respectively. All nanocolumnar TiZrN films presented high surface roughness (RMS) values of 6.5-7.2 nm.

I.7. Conclusion

This chapter has been devoted to the presentation of the state-of-the-art, thin films description.Most common thin films application in the industry. Hard coatings, in particular, have been highlighted in order toillustrate their importance. The classification of hard coating is well discussed in this part. The synthesis of binary hard coating has been submitted and leads to conclude that the obtained binary transition metal nitride, oxides, boride, and carbides thin films deposited with magnetron sputtering demonstrated outstanding proprieties.

The bibliographical synthesis has shown that the characteristics of TiN and ZrN thin films are strongly dependent on the operating conditions of deposition. The crystallization in cubic (TiN, ZrN) or hexagonal (Ti_2N, Zr_2N) phases can determine its mechanical and tribological proprieties and as consequence the condition of adhesion to substrates. TiN films can change behavior when adding a third element as indicated by the state of the art. The Zirconium in particular has shown characteristics that depend on its content in the films. According to the above, further work remains to be done to improve the properties of coatings based on titanium nitride. Therefore, our study focused on this type of layer because of their industrial importance, in precise industrial applicatications.

Referances

[1] A. Jilani, M.S. Abdel-Wahab, A.H. Hammad, Advance deposition techniques for thin film and coating, Modern Technologies for Creating the Thin-film Systems and Coatings, 2 (2017) 137-149.

[2] Nouveau, C, Dépôts de revêtements durs (CrxNy) obtenus par méthode PVD: réalisation et caractérisations, Doctoral dissertation, Ph. D. thesis, Ecole Nationale des Arts et Métiers de Cluny, 2001.

[3] X. Shi, S. Liu, Y. Sun, J. Liang, Y. Chen, Lowering internal friction of 0D–1D–2D ternary nanocomposite-based strain sensor by fullerene to boost the sensing performance, Advanced Functional Materials, 28 (2018) 1800850.

[4] S. Farsinezhad, T. Shanavas, N. Mahdi, A.M. Askar, P. Kar, H. Sharma, K. Shankar, Core–shell titanium dioxide–titanium nitride nanotube arrays with near-infrared plasmon resonances, Nanotechnology, 29 (2018) 154006.

[5] P.M. Martin, L.C. Olsen, W.D. Bennett, C.H. Henager, Superlattice Coatings for Device, Structural and Protective Applications, Pacific Northwest National Lab.(PNNL), Richland, WA (United States), (2006) 1219-1229.

[6] M. Fleischauer, J. Li, M. Brett, Columnar thin films for three-dimensional microbatteries, Journal of the electrochemical society, 156 (2008) A33.

[7] M.L. García-Betancourt, S.I.R. Jiménez, A. González-Hodges, Z.E.N. Salazar, I.L. Escalante-García, J.R. Aparicio, Low Dimensional Nanostructures: Measurement and Remediation Technologies Applied to Trace Heavy Metals in Water, Trace Metals in the Environment-New Approaches and Recent Advances, IntechOpen, 2020.

[8] J.-C. Guillais, C. Leroux, Procédés électriques dans les traitements et revêtements de surface: enseignement de l'electrothermie, 1 (1989) 699 .

[9] Atkins, A. G., Westbrook, J. H., & Conrad, H.. The science of hardness testing and its research applications. ASM, Metal Park, OH, (1971) 223.

[10] S. Roy, Mesure de l'adhérence et des propriétés mécaniques de couches minces par des essais dérivés de la nanoindentation: application à la microélectronique et au biomédical, École Nationale Supérieure des Mines de Paris, 2008.

[11] J. Musil, J. Vlček, Magnetron sputtering of hard nanocomposite coatings and their properties, Surface and Coatings Technology, 142 (2001) 557-566.

[12]https://th.bing.com/th/id/OIP.C5nhmaJ6O8Jiz7K2pMK0twHaDt?pid=Api&w=800&h=400&rs=1.

[13] https://img.saurenergy.com/2016/12/Thin-Film-Solar-Cells-Market.jpg, DOI.

[14] https://pes.ee.ethz.ch/research/research-and-thesis-projects/dc-ac-converters/DC-AC-Converters-2/_jcr_content/par/fullwidthimage/image.imageformat, DOI.

[15] https://arci.res.in/programmes/1501751622_CAPVD%20Template_Programmes1.jpg, DOI.

[16] https://www.grandsmilesdental.com/wp-content/uploads/2015/12/Guyette-Single-Implant-Patient1a.jpg, DOI.

[17] D.M. Mattox, V. Mattox, Vacuum coating technology, Springer (2003) 1-7

[18] K. Mylvaganam, Y. Chen, W. Liu, M. Liu, L. Zhang, Hard thin films: Applications and challenges, Anti-Abrasive Nanocoatings, Elsevier, (2015) 543-567.

[19] J. Musil, J.J.S. Vlček, C. Technology, Magnetron sputtering of hard nanocomposite coatings and their properties, 142 (2001) 557-566.

[20] H. Caliskan, P. Panjan, C. Kurbanoglu, Hard Coatings on Cutting Tools and Surface Finish, Comprehensive Materials Finishing, 3 (2016) 230-242

[21] D. Luo, Selection of coatings for tribological applications, Doctoral dissertation, Ph. D. thesis, Ecully, Ecole centrale de Lyon, 2009.

[22] A. Voevodin, J. Schneider, C. Rebholz, A. Matthews, Multilayer composite ceramicmetal-DLC coatings for sliding wear applications, Tribology international, 29 (1996) 559-570.

[23] Z. Wan, T.F. Zhang, H.-B.-R. Lee, J.H. Yang, W.C. Choi, B. Han, K.H. Kim, S.-H. Kwon, Improved corrosion resistance and mechanical properties of CrN hard coatings with an atomic layer deposited Al_2O_3 interlayer, ACS Applied Materials & Interfaces, 7 (2015) 26716-26725.

[24] M. Kot, Ł. Major, J. Lackner, The tribological phenomena of a new type of TiN/aC: H multilayer coatings, Materials & Design, 51 (2013) 280-286.

[25] X. Xu, F. Su, Z. Li, Tribological properties of nanostructured TiAlN/W2N multilayer coating produced by PVD, Wear, 430 (2019) 67-75.

[26] S.-Y. Chun, Nanosize-controlled titanium nitride films in pulsed dc magnetron sputtering, Journal of Nanoscience and Nanotechnology, 13 (2013) 2021-2024.

[27] S. Ghasemi, A. Shanaghi, P.K. Chu, Corrosion behavior of reactive sputtered Ti/TiN nanostructured coating and effects of intermediate titanium layer on self-healing properties, Surface and Coatings Technology, 326 (2017) 156-164.

[28] S.A. Glatz, R. Hollerweger, P. Polcik, R. Rachbauer, J. Paulitsch, P. Mayrhofer, Thermal stability and mechanical properties of arc evaporated Ti–Al–Zr–N hard coatings, Surface and Coatings Technology, 266 (2015) 1-9.

[29] M.-L. Wu, Z. Yang, Y.-W. Chung, M.-S. Wong, W.D. Sproul, Synthesis of coatings with hardness exceeding 40 GPa by magnetron sputtering, Journal of Tribology, 2 (1998) 120–179.
[30] J. Musil, H. Polakova, Hard nanocomposite Zr–Y–N coatings, correlation between hardness and structure, Surface and Coatings Technology, 127 (2000) 99-106.
[31] S. Vepřiek, A. Niederhofer, K. Moto, P. Nesladek, H. Männling, T. Bolom, Nanocomposites nc-TiN/a-Si3N4/a-and nc-TiSi2 with hardness exceeding 100 GPa and high fracture toughness, MRS Online Proceedings Library (OPL), 581 (1999) 321-326.
[32] Y.-W. Lin, J.-H. Huang, G.-P. Yu, Effect of nitrogen flow rate on properties of nanostructured TiZrN thin films produced by radio frequency magnetron sputtering, Thin solid films, 518 (2010) 7308-7311.
[33] K. Khlifi, A.B.C. Larbi, Mechanical properties and adhesion of TiN monolayer and TiN/TiAlN nanolayer coatings, Journal of Adhesion Science and Technology, 28 (2014) 85-96.
[34] P. Mohamadian Samim, A. Fattah-Alhosseini, H. Elmkhah, O. Imantalab, Structure and corrosion behavior of ZrN/CrN nano-multilayer coating deposited on AISI 304 stainless steel by CAE-PVD technique, Journal of Asian Ceramic Societies, 8 (2020) 460-469.
[35] X.T. Zeng, TiN/NbN superlattice hard coatings deposited by unbalanced magnetron sputtering, Surface and Coatings Technology, 113 (1999) 75-79.
[36] S. Barnett, A. Madan, Superhard superlattices, Physics world, 11 (1998) 45.
[37] H. Holleck, Material selection for hard coatings, Journal of Vacuum Science & Technology A: Vacuum, Surfaces, and Films, 4 (1986) 2661-2669.
[38] H. Leiste, U. Dambacher, S. Ulrich, H. Holleck, Microstructure and properties of multilayer coatings with covalent bonded hard materials, Surface and Coatings Technology, 116 (1999) 313-320.
[39] R. Babinova, V. Smirnov, A. Useenov, K. Kravchuk, E. Gladkikh, V. Shapovalov, I. Mylnikov, Mechanical properties of titanium nitride films obtained by reactively sputtering with hot target, Journal of Physics: Conference Series, 872 (2017) 012035

[40] V. Merie, M. Pustan, G. Negrea, C. Bîrleanu, Research on titanium nitride thin films deposited by reactive magnetron sputtering for MEMS applications, Applied Surface Science, 358 (2015) 525-532.
[41] S. Lin, J. Zhang, R. Zhu, S. Fu, D. Yun, Effects of sputtering pressure on microstructure and mechanical properties of ZrN films deposited by magnetron sputtering, Materials Research Bulletin, 105 (2018) 231-236.

[42] C.-S. Chen, C.-P. Liu, C.Y.A. Tsao, H.-G. Yang, Study of mechanical properties of PVD ZrN films, deposited under positive and negative substrate bias conditions, Scripta Materialia, 51 (2004) 715-719.

[43] A. Fragiel, M. Staia, J. Muñoz-Saldaña, E. Puchi-Cabrera, C. Cortes-Escobedo, L. Cota, Influence of the N2 partial pressure on the mechanical properties and tribological behavior of zirconium nitride deposited by reactive magnetron sputtering, Surface and Coatings Technology, 202 (2008) 3653-3660.

[44] J.-W. Lee, S.-K. Tien, Y.-C. Kuo, C.-M. Chen, The mechanical properties evaluation of the CrN coatings deposited by the pulsed DC reactive magnetron sputtering, Surface and Coatings Technology, 200 (2006) 3330-3335.

[45] T. Elangovan, P. Kuppusami, R. Thirumurugesan, V. Ganesan, E. Mohandas, D. Mangalaraj, Nanostructured CrN thin films prepared by reactive pulsed DC magnetron sputtering, Materials Science and Engineering: B, 167 (2010) 17-25.

[46] J.-W. Lee, S.-K. Tien, Y.-C. Kuo, The effects of pulse frequency and substrate bias to the mechanical properties of CrN coatings deposited by pulsed DC magnetron sputtering, Thin Solid Films, 494 (2006) 161-167.

[47] E. Zalnezhad, A.M.S. Hamouda, G. Faraji, S. Shamshirband, TiO_2 nanotube coating on stainless steel 304 for biomedical applications, Ceramics International, 41 (2015) 2785-2793.

[48] D. Wojcieszak, M. Mazur, J. Indyka, A. Jurkowska, M. Kalisz, P. Domanowski, D. Kaczmarek, J. Domaradzki, Mechanical and structural properties of titanium dioxide deposited by innovative magnetron sputtering process, Materials Science-Poland, 33 (2015) 660-668.

[49] K. Koski, J. Hölsä, P. Juliet, Properties of zirconium oxide thin films deposited by pulsed reactive magnetron sputtering, Surface and Coatings Technology, 120-121 (1999) 303-312.

[50] X. Pang, K. Gao, A.A. Volinsky, Microstructure and mechanical properties of chromium oxide coatings, Journal of Materials Research, 22 (2007) 3531-3537.

[51] F.J. Silva, R. Casais, R. Martinho, A. Baptista, Mechanical and tribological characterization of TiB_2 thin films, Journal of nanoscience and nanotechnology, 12 (2012) 9187-9194.

[52] L. Tengdelius, E. Broitman, J. Lu, F. Eriksson, J. Birch, T. Nyberg, L. Hultman, H. Högberg, Hard and elastic epitaxial ZrB_2 thin films on Al_2O_3(0001) substrates deposited by magnetron sputtering from a ZrB_2 compound target, Acta Materialia, 111 (2016) 166-172.

[53] N. Nedfors, D. Primetzhofer, L. Wang, J. Lu, L. Hultman, U. Jansson, Characterization of magnetron sputtered Cr–B and Cr–B–C thin films for electrical contact applications, Surface and Coatings Technology, 266 (2015) 167-176.

[54] H. Wang, S. Zhang, Y. Li, D. Sun, Bias effect on microstructure and mechanical properties of magnetron sputtered nanocrystalline titanium carbide thin films, Thin Solid Films, 516 (2008) 5419-5423.

[55] C.-S. Chen, C.-P. Liu, C.Y.A. Tsao, Influence of growth temperature on microstructure and mechanical properties of nanocrystalline zirconium carbide films, Thin Solid Films, 479 (2005) 130-136.

[56] K. Nygren, M. Samuelsson, A. Flink, H. Ljungcrantz, Å. Kassman Rudolphi, U. Jansson, Growth and characterization of chromium carbide films deposited by high rate reactive magnetron sputtering for electrical contact applications, Surface and Coatings Technology, 260 (2014) 326-334.

[57] B. Navinsek, S. Seal, Transition metal nitride functional coatings, Jom, 53 (2001) 51-54.

[58] D.G. Sangiovanni, Transition metal nitrides: alloy design and surface transport properties using Ab-initio and classical computational methods, Doctoral dissertation, Ph. D. thesis, Linköping University Electronic Press, 2013.

[59] D. Holec, M. Friák, J. Neugebauer, P.H. Mayrhofer, Trends in the elastic response of binary early transition metal nitrides, Physical Review B, 85 (2012) 064101.

[60] H.A. Jehn, J.-H. Kim, S. Hofmann, Composition and properties of transition metal nitride thin films (ZrNx, NbNx, MoNx), Surface and Coatings Technology, 36 (1988) 715-727.

[61] L. Aissani, C. Nouveau, M.J. Walock, H. Djebaili, A.J.S.E. Djelloul, Influence of vanadium on structure, mechanical and tribological properties of CrN coatings, Surface Engineering, 31 (2015) 779-788.

[62] F. Ge, P. Zhu, F. Meng, Q. Xue, F. Huang, Achieving very low wear rates in binary transition-metal nitrides: The case of magnetron sputtered dense and highly oriented VN coatings, Surface and Coatings Technology, 248 (2014) 81-90.

[63] G. Matenoglou, L.E. Koutsokeras, C.E. Lekka, G. Abadias, C. Kosmidis, G.A. Evangelakis, P. Patsalas, Structure, stability and bonding of ternary transition metal nitrides, Surface and Coatings Technology, 204 (2009) 911-914.

[64] Q. Sun, Z.-W. Fu, Cr1− x Fe x N (0≦ x≦ 1) Ternary Transition-Metal Nitrides as Anode Materials for Lithium-Ion Batteries, Electrochemical and Solid-State Letters, 11 (2008) A233.

[65] D.H. Gregory, P.M. O'Meara, A.G. Gordon, D.J. Siddons, A.J. Blake, M.G. Barker, T.A. Hamor, P.P.J.J.o.a. Edwards, compounds, Layered ternary transition metal nitrides; synthesis, structure and physical properties, 317 (2001) 237-244.

[66] L. Aissani, M. Fellah, C. Nouveau, M. Abdul Samad, A. Montagne, A.J.S.e. Iost, Structural and mechanical properties of Cr–Zr–N coatings with different Zr content, Surface engineering, 36 (2020) 69-77.

[67] Q. Yang, D. Seo, L. Zhao, X. Zeng, Erosion resistance performance of magnetron sputtering deposited TiAlN coatings, Surface and Coatings Technology, 188 (2004) 168-173.

[68] https://www.scienceabc.com/wp-content/uploads/2019/02/titanium-raw-material-768x538.jpg, DOI.

[69] https://www.scienceabc.com/wp-content/uploads/2019/02/titanium.jpg, DOI.

[70] A.P. Mouritz, Introduction to aerospace materials, Elsevier (2012) 640.

[71] Ş. Ţălu, S. Stach, S. Valedbagi, S.M. Elahi, R.J.M.S.-P. Bavadi, Surface morphology of titanium nitride thin films synthesized by DC reactive magnetron sputtering, 33 (2015) 137-143.

[72] L. Lavisse, Elaboration, caractérisation physico-chimique et simultation thermo-cinétique de couches d'oxydes de titane sous faisceau laser Nd-YAG impulsionnel, Doctoral dissertation, Ph. D. thesis, Ecully, Ecole centrale de Lyon, 2002.

[73] H. Wriedt, J. Murray, The N-Ti (nitrogen-titanium) system, Bulletin of Alloy Phase Diagrams, 8 (1987) 378-388.

[74] L. Wang, Investigation of PVD and CVD Coatings for Manufacturing, Fuel Cell and Biomedical Applications, Doctoral dissertation, Ph. D. thesis, University of Windsor, 2010.

[75] A.J.M. de Oca-Valero, Elaboration du carbure et du nitrure de titane par ds procédés chimiques et physiques en phase vapeur: caractérisation de la microstructure, Doctoral dissertation, Ph. D. thesis, Université Sciences et Technologies-Bordeaux I, 2002.

[76] S. Yu, Q. Zeng, A.R. Oganov, G. Frapper, L. Zhang, Phase stability, chemical bonding and mechanical properties of titanium nitrides: a first-principles study, Physical Chemistry Chemical Physics, 17 (2015) 11763-11769.

[77] E. Ajenifuja, A. Yisau Fasasi, G. Ayo Osinkolu, Sputtering-pressure dependent optical and microstructural properties variations in DC reactive magnetron sputtered titanium nitride thin films, Transactions of the Indian Ceramic Society, 71 (2012) 181-188.

[78] S. Zhang, F. Yan, Y. Yang, M. Yan, Y. Zhang, J. Guo, H. Li, Effects of sputtering gas on microstructure and tribological properties of titanium nitride films, Applied Surface Science, 488 (2019) 61-69.

[79] J. Musil, Š. Kos, M. Jaroš, R. Čerstvý, S. Haviar, S. Zenkin, Z. Čiperová, Coating of overstoichiometric transition metal nitrides (TMNx (x > 1)) by magnetron sputtering, Japanese Journal of Applied Physics, 58 (2018) SAAD10.

[80] R. Arnell, J. Colligon, K. Minnebaev, V. Yurasova, The effect of nitrogen content on the structure and mechanical properties of TiN films produced by magnetron sputtering, Vacuum, 47 (1996) 425-431.

[81] J.-H. Huang, K.-W. Lau, G.-P. Yu, Effect of nitrogen flow rate on structure and properties of nanocrystalline TiN thin films produced by unbalanced magnetron sputtering, Surface and Coatings Technology, 191 (2005) 17-24.

[82] L. Lu, F. Luo, Z. Huang, W. Zhou, D. Zhu, Influence of the nitrogen flow rate on the infrared emissivity of TiNx films, Infrared Physics & Technology, 88 (2018) 144-148.

[83] A. Belgroune, L. Aissani, F. Salhi, C. Nouveau, A. Alhussein, Mechanical and Tribological Behaviors of Nanocomposite Titanium Nitrides Coatings, Defect and Diffusion Forum, Trans Tech Publ, 406 (2021) 312-318.

[84] J.-H. Huang, F.-Y. Ouyang, G.-P. Yu, Effect of film thickness and Ti interlayer on the structure and properties of nanocrystalline TiN thin films on AISI D2 steel, Surface and Coatings Technology, 201 (2007) 7043-7053.

[85] H. Liang, J. Xu, D. Zhou, X. Sun, S. Chu, Y. Bai, Thickness dependent microstructural and electrical properties of TiN thin films prepared by DC reactive magnetron sputtering, Ceramics International, 42 (2016) 2642-2647.

[86] P. Patsalas, C. Charitidis, S. Logothetidis, The effect of substrate temperature and biasing on the mechanical properties and structure of sputtered titanium nitride thin films, Surface and Coatings Technology, 125 (2000) 335-340.

[87] R. Bavadi, S. Valedbagi, Physical properties of titanium nitride thin film prepared by DC magnetron sputtering, Materials Physics and Mechanics, 15 (2012) 167-172.

[88] B. Subramanian, K. Ashok, M. Jayachandran, Effect of substrate temperature on the structural properties of magnetron sputtered titanium nitride thin films with brush plated nickel interlayer on mild steel, Applied Surface Science, 255 (2008) 2133-2138.

[89] K. Benouareth, A. Bouabellou, Etude de l'interaction entre le Zirconium en couche mince et un substrat en acier, Doctoral dissertation, Ph. D. thesis, Université Frères Mentouri - Constantin , 2018.

[90] J. Emsley, Nature's building blocks: an AZ guide to the elements, Oxford University Press (2011) 726.

[91] http://zirconiumzb.weebly.com/uploads/1/7/4/0/17401085/2220711_orig.jpg?274, DOI.

[92] https://chemcraft.su/sites/chemcraft.su/files/field/image/zr_yodidnyy_-d1a.jpg, DOI.

[93] L. Gribaudo, D. Arias, J. Abriata, The N-Zr (nitrogen-zirconium) system, Journal of phase equilibria, 15 (1994) 441–449.

[94] J. Ramana, S. Kumar, C. David, A. Ray, V. Raju, Characterisation of zirconium nitride coatings prepared by DC magnetron sputtering, Materials Letters, 43 (2000) 73-76.

[95] M. Azibi, N. Saoula, H. Aknouche, The influence of substrate bias voltage on the electrochemical properties of ZrN thin films deposited by radio-frequency magnetron sputtering: Biomedical application, Journal of Electrical Engineering, 70 (2019) 112-116.

[96] O. Maksakova, S. Simoẽs, A. Pogrebnjak, O. Bondar, Y. Kravchenko, V. Beresnev, N. Erdybaeva, The influence of deposition conditions and bilayer thickness on physical-mechanical properties of CA-PVD multilayer ZrN/CrN coatings, Materials Characterization, 140 (2018) 189-196.

[97] S. Zhao, J. Ma, R. Xu, X. Lin, X. Cheng, S. Hao, X. Zhao, C. Deng, B. Liu, Synthesis and characterization of Zirconium nitride nanopowders by internal Gelation and carbothermic nitridation, Scientific reports, 9 (2019) 1-9.

[98] P. Klumdoung, A. Buranawong, S. Chaiyakun, P. Limsuwan, Variation of color in Zirconium nitride thin films prepared at high Ar flow rates with reactive dc magnetron sputtering, Procedia Engineering, 32 (2012) 916-921.

[99] H. Bhuvaneswari, I. Nithiya Priya, R. Chandramani, V. Rajagopal Reddy, G. Mohan Rao, Studies on zirconium nitride films deposited by reactive magnetron sputtering, Crystal Research and Technology: Journal of Experimental and Industrial Crystallography, 38 (2003) 1047-1051.

[100] H.V. Patel, H.N. Patel, P.A. Soni, H.D. Parmar, N.P. Patel, K.V. Chauhan, Characterization of sputtered zirconium nitride thin films deposited at various RF power and sputtering pressure, AIP Conference Proceedings, (2019) 020093.

[101] A. Singh, P. Kuppusami, S. Khan, C. Sudha, R. Thirumurugesan, R. Ramaseshan, R. Divakar, E. Mohandas, S. Dash, Influence of nitrogen flow rate on microstructural and nanomechanical properties of Zr–N thin films prepared by pulsed DC magnetron sputtering, Applied Surface Science, 280 (2013) 117-123.

[102] D. Pilloud, A. Dehlinger, J. Pierson, A. Roman, L.J.S. Pichon, C. Technology, Reactively sputtered zirconium nitride coatings: structural, mechanical, optical and electrical characteristics, 174 (2003) 338-344.

[103] M. Signore, D. Valerini, A. Rizzo, L. Tapfer, L. Capodieci, A. Cappello, Investigation of the physical properties of ion assisted ZrN thin films deposited by RF magnetron sputtering, Journal of Physics D: Applied Physics, 43 (2010) 225401.

[104] A. Kavitha, R. Kannan, S. Loganathan, Effect of Substrate Bias Voltage on the Physical Properties of Zirconium Nitride (ZrN) Films Deposited by Mid Frequency Reactive Magnetron Sputtering, International Journal of Nanoscience, 13 (2014) 1450015.

[105] M. Valaiauksornlikit, W. Rakreungdet, M. Horprathum, P. Eiamchai, V. Patthanasettakul, P. Chindaudom, Effect of thickness on microstructure, electrical and optical properties of Zirconium Nitride thin film prepared by dc reactive magnetron sputtering at room temperature, Advanced Materials Research, Trans Tech Publ, 770 (2013) 217-220.

[106] S. Chinsakolthanakorn, A. Buranawong, N. Witit-Anun, S. Chaiyakun, P. Limsuwan, Characterization of nanostructured TiZrN thin films deposited by reactive DC magnetron co-sputtering, Procedia Engineering, 32 (2012) 571-576.

[107] W. Cui, J. Cheng, Z. Liu, Bio-tribocorrosion behavior of a nanocrystalline TiZrN coating on biomedical titanium alloy, Surface and Coatings Technology, 369 (2019) 79-86.

[108] Y.-W. Lin, H.-A. Chen, G.-P. Yu, J.-H. Huang, Effect of bias on the structure and properties of TiZrN thin films deposited by unbalanced magnetron sputtering, Thin Solid Films, 618 (2016) 13-20.

[109] Y.-W. Lin, J.-H. Huang, G.-P. Yu, C.-N. Hsiao, F.-Z. Chen, Influence of ion bombardment on structure and properties of TiZrN thin film, Applied Surface Science, 354 (2015) 155-160.

[110] A. Hörling, J. Sjölén, H. Willmann, T. Larsson, M. Odén, L. Hultman, Thermal stability, microstructure and mechanical properties of Ti1− xZrxN thin films, Thin Solid Films, 516 (2008) 6421-6431.

[111] E. Etchessahar, J.P. Bars, D. Ansel, The partial (Ti0.5Zr0.5)–N phase diagram from 0 to 50 at.%, Journal of Alloys and Compounds, 335 (2002) 126-131.

[112] S. Sridar, R. Kumar, K.H. Kumar, Thermodynamic modelling of Ti-Zr-N system, Calphad, 56 (2017) 102-107.

[113] W. Phae-ngam, C. Chananonnawathorn, T. Lertvanithphol, B. Samransuksamer, M. Horprathum, T. Chaiyakun, Effect of deposition time on nanocolumnar tizrn films grown by reactive magnetron co-sputtering with the OAD technique, Materials and Technology, 55 (2021) 65-70.

[114] F.M. El-Hossary, A.M.A. El-Rahman, M. Raaif, S. Qu, J. Zhao, M.F. Maitz, M.A. El-Kassem, Effect of DC-pulsed magnetron sputtering power on structural, tribological and biocompatibility of Ti–Zr–N thin film, Applied Physics A, 124 (2017) 42.

[115] S. Chinsakolthanakorn, A. Buranawong, S. Chiyakun, P. Limsuwan, Effects of Titanium Sputtering Current on Structure and Morphology of TiZrN Films Prepared by Reactive DC Magnetron Co-Sputtering, Materials Sciences and Applications, 04 (2013) 689-694.

[116] W. Phae-ngam, M. Horprathum, C. Chananonnawathorn, T. Lertvanithphol, B. Samransuksamer, P. Songsiriritthigul, H. Nakajima, S. Chaiyakun, Oblique angle deposition of nanocolumnar TiZrN films via reactive magnetron co-sputtering technique: The influence of the Zr target powers, Current Applied Physics, 19 (2019) 894-901.

Chapter II.

Elaboration and Caracterization techniques

II.1. Introduction

In this chapter, we presented the DFT software used for the simulation of the structural properties of TiN, and TiZrN systems. We assembled an overview of the most generally applied thin film preparation techniques. We'll discuss in more detail the sputtering process and magnetron sputtering techniques that we used for the preparation of TiN and TiZrN films in addition to the growth through sputtering technique. We also reviewed the most important techniques that are lead to determine the physicochemical characteristics, X ray diffraction (XRD), scanning electron microscopy (SEM), X-ray microanalysis (EDX, WDS), Atomic force microscopy (AFM), X-ray photoemission spectroscopy (XPS), and Raman spectroscopy. Wetting and surface energy of TiN and TiZrN coatings was estimated using contact angle measurement. Then we reviewed the used techniques to determine the mechanical and tribological properties of the obtained films, nanoindentation, and ball on disk tribometer (CSM, HIGH- TEMPERATURE TRIBOMETER).

II.2. The determination of TiN, TiZrN structures systems

In this thesis, the simulation is based on density functional theory (DFT), which has been shown to be one of the most accurate theories for calculating the electronic and structural properties of solids [1], with first principles calculations performed within the full potential linearized augmented plane wave (FP-LAPW) method [2] using the WIEN2k code [3]. The exchange and correlation potential was calculated using the generalized gradient approximation (GGA) parameterized by Perdew-Burke-Ernzerhof (PBE) [4]. The space is divided into two regions in the FP-LAPW method: the first is a non-overlapping muffin-tin (MT) spheres region, where the basis set within this region is described by radial solutions of the one-particle Schrodinger equation and their energy derivatives multiplied by spherical harmonics, and the second is an interstitial region (IR) Plane waves make up the basic set [5]. The convergence tests allow us to select the value Rmt*Kmax = 9, where Rmt denotes the smallest atomic sphere radius and Kmax denotes the plane wave cut-off [6]. The Gmax value was chosen to be 14 when Gmax is defined as the magnitude of the largest vector in the charge density Fourier expansion. Up to lmax=10, the MT sphere was considered. The Monkorst-Pack method was used with 1000 kpoints in the first Brillouin zone (IBZ). The charge convergence parameter was set at 10^{-4}.

II.3. Hard coatings deposition techniques

The three types of procedures used to apply hard coatings include gaseous state, solution state, molten, and semi-molten state processes. The thickness of the coatings that may be obtained (from 0.1 mm to 10 mm) and the deposition temperature (from room temperature to 1000 °C) are two important characteristic parameters for coating procedures. CVD and PVD are two common deposition methods used to provide hard coatings on cutting tools and machining steels (*Table II.1*) [7].

Table II.1. Thin film deposition method [8, 9].

Chemical deposition		**Physical deposition**
Wet Chemical Techniques	**Chemical vapour deposition (CVD)**	**Physical vapour deposition(PVD)**
1. Sol-gel spin-on techniques 2. Chemical Bath Deposition (CBD) 3. Spray pyrolysis 4. Electroplating	1. Atmospheric-pressure CVD (APCVD) 2. Law pressure (LPCVD) 3. Plasma enhanced PECVD 4. Atomic layer deposition (ALD) 5. Metal-organic CVD (MOCVD 6. Laser-induced CVD (LCVD)	1. Evaporation technique a. Vacuum thermal evaporation b. Electron beam evaporation c. Laser beam evaporation d. Arc evaporation e. Molecular beam epitaxy f. Ion Plating evaporation 2. Sputtering technique a. Direct current (D.C) sputtering b. Radiofrequency (R.F) sputtering

II.3.1. Sputtering

Sputtering was firstly experimental in a D.C gas discharge tube by Grove in 1852. He discovered that the discharge tube's cathode surface was sputtered by energetic ions in the gas discharge, and cathode materials were deposited on the discharge tube's inner wall. Sputtering was considered an undesirable phenomenon at the time since the cathode and grid in the gas discharge tube were damaged. However, sputtering is now widely utilized for surface cleaning and etching, thin film deposition, surface and surface layer analysis, and sputter ion sources, among other applications [10].

Sputtering is a thin film manufacturing technology that is widely utilized in sectors including semiconductor processing, surface treatment, and jewelry production. Metal deposition, as well as insulating materials, is the most common industrial use. Sputtering is the technique of speeding ionized atoms into a surface in order to eject atoms from that surface in their most basic form. The ejected atoms can then condense onto the sample, forming a thin layer of the substance ejected. Sputter deposition is the name for this procedure. The same physical mechanism may be used to remove undesired material from a sample, with the ejected atoms being gathered on the chamber shield in this situation. Sputter etching is the name for the latter method [11].

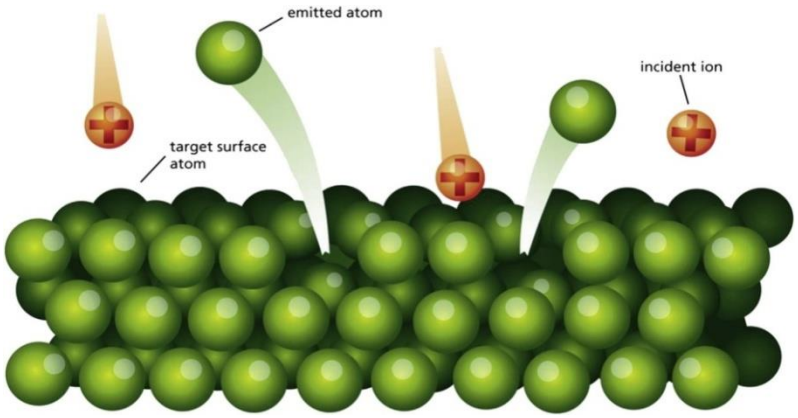

Figure II.1. The principle of sputtering [12].

Ion bombardment is accelerated into a substrate as a consequence of acceleration through an acceleration potential in the sputter chamber. Argon (Ar) is commonly utilized for bombardment in large-scale industrial applications in integrated circuit production, owing to its low cost and chemical inertness. Argon also has the benefit of having an atomic mass that is similar to that of several metals often employed in integrated circuits (IC), including as Ti, Al, and Cu manufacturing. In sputtering procedures, the accelerating energy of the ions bombardment is naturally delivered by the potential drop between the ionized plasma gas and the bombarded surface, which is referred to as the sputter target in typical deposition applications. Once the ion bombardment collides with the surface of the target, atoms from the target can be ejected to condense on a substrate surface to construct a thin film. A critical metric to represent the sputtering event is the sputter yield (Y) which measures the ejected atoms number from the target for each ion bombardment [11]:

$$Y = \frac{\text{Number of sputtered atoms ejected}}{\text{Number of sputtering atoms incident}} \qquad \text{(II. 1)}$$

Sputter yield is determined by the target species as well as the nature, energy, and angle of the incident bombardment species. When the mass of the bombarding particles is on equal with or more than that of the target atoms, the sputtering yield is highest. The target temperature has little effect on it. Furthermore, the sputter yield is independent of whether the bombarded species are ionized or not. The dependence of sputtering yield on incident ion energy exhibits a characteristic appearance as shown in *Figure II.2*. The surface binding energy, U_{sb}, (2–10 eV) of the atoms necessity is exceeded for the atom in order to escape from the solid by sputtering [7].

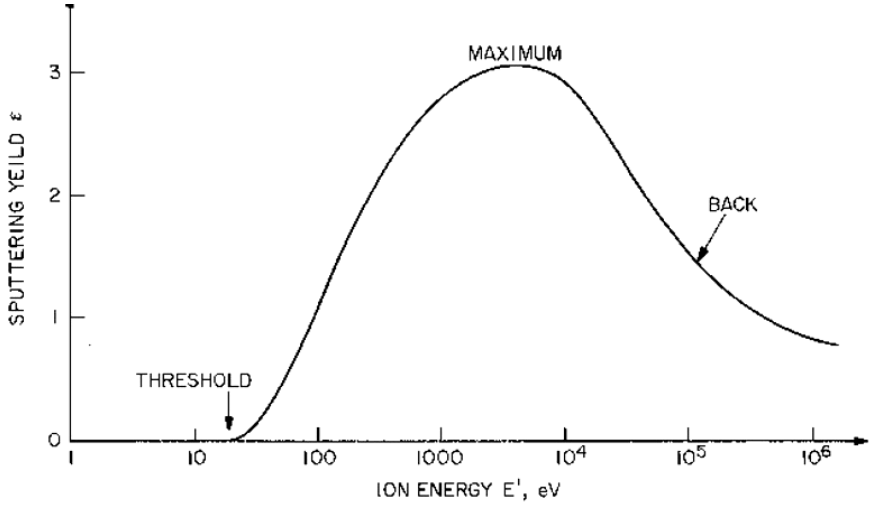

Figure II.2. Sputtering yield versus energy of the incident [13].

Above the threshold energy, the sputtering yield grows to reach a maximum. As the ions penetrate deeper into the surface solid at increasing energies, the sputtering yields rapidly drop. Concerning the energy range of 100–1000 eV, the sputtering yield is approximately linear in ion energies and separated of incident ion species [13].

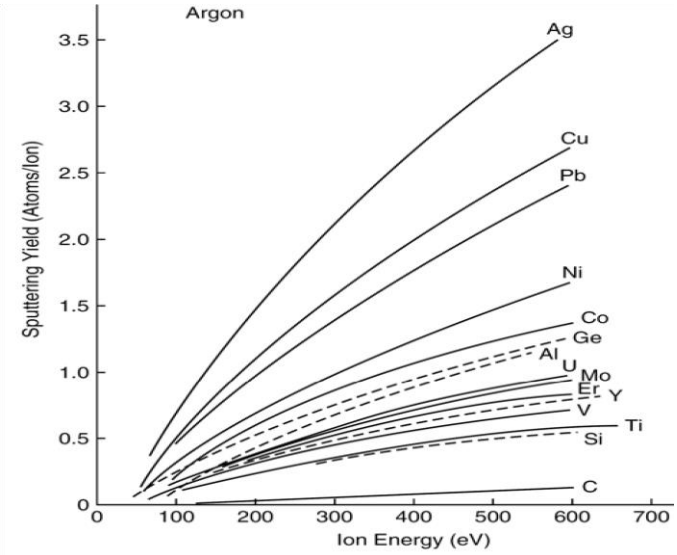

Figure II.3. Deposition rates for magnetron sputtering of different metals as function of power [13].

The sputtering yield grows to a maximum for off-normal bombardment, and then quickly drops as the bombarding particles are reflected from the surface, this phenomenon is known as the "*angle-of-incidence effect*". For argon, the highest sputtering yield occurs at roughly 70° degrees off normal, but this varies depending on the relative masses of the bombarding and target species. From normal incidence to maximum incidence, sputtering yield can rise by as much as 2 to 3 times [13].

II.3.1.1. Sputtering mechanisms

When an ion strikes the cathode, numerous interactions can appear on its surface as described in *Figure II.4*.These interactions comprise the liberation of neutral or ionized atoms, backscattering, X-ray emission, photon generation, secondary electron emission, and desorption of gas atoms from the surface of the target. Several additional operations can appear furthermore in the target, including the generation of collisional cascades, the creation of point defects, local heating, amorphization, implantation, and compound building [8].

In the sputtering process shown in *Figure II.4*, the impacted particle fractures bonds and dislodges atoms if it collides with the solid's surface with enough energy. Sputtered atoms are atoms that have been detached from a solid. Sputtering is classified into four energy categories, ranging from near the binding energy to several MeV. Extremely low energies: Although recent studies have shown that there is very little sputtering at incidence ion energies ranging from a few eV to 30–50 eV, and that the lowest ion energy for sputtering equals the binding energy of the most weakly bound surface atom, There is still widespread

agreement that a sputter threshold exists beyond which no sputtering occurs, as proposed in early publications (the 1960s). Reduced sputter yield measurements are challengeable, and are rarely mentioned in the literature [13].

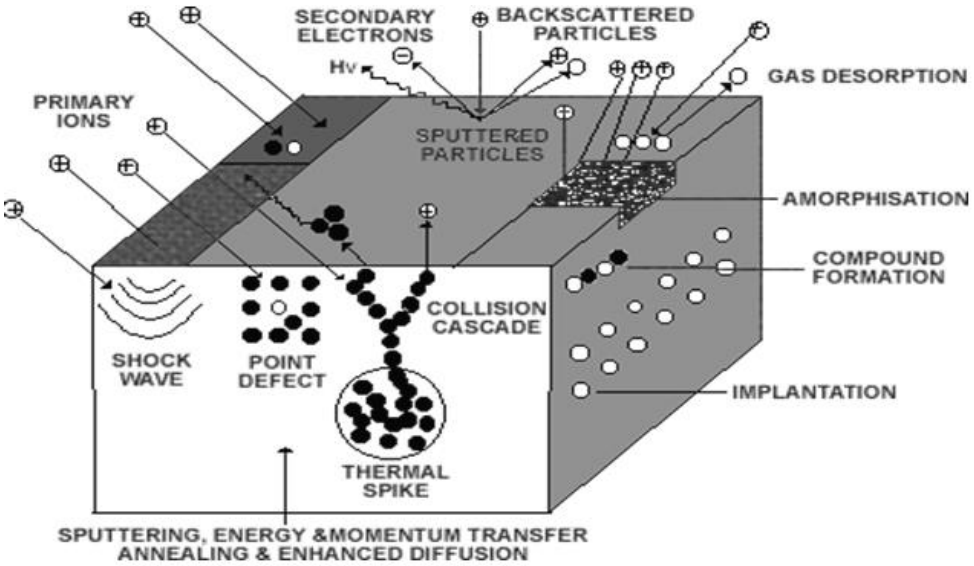

Figure II.4. The main physical process produced in sputtering technique (Weiss mantel, 1983) [14].

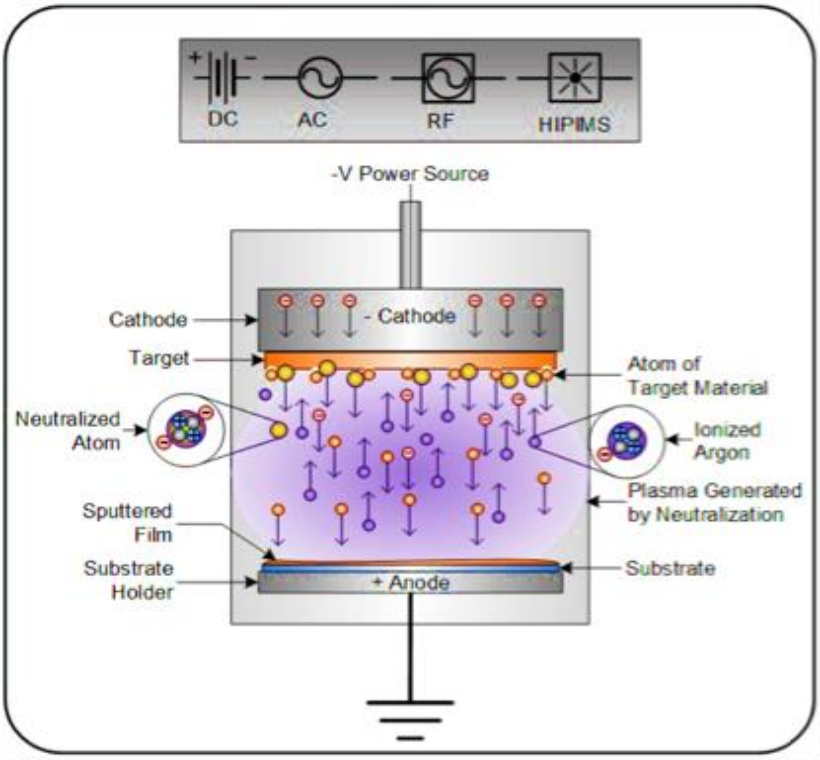

Figure II.5. Schematic presentation of sputtering and growth of thin films [15].

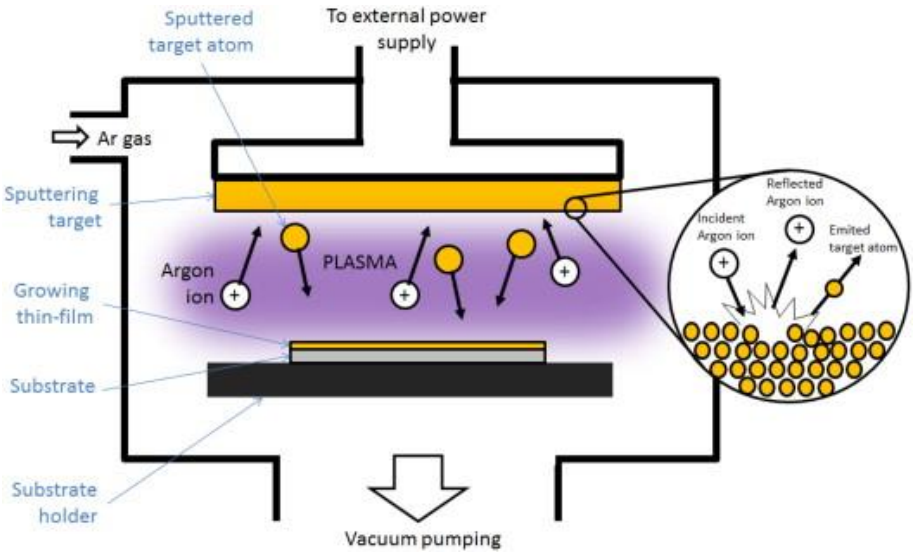

Figure II.6. Diagram-Sputtering-process [16].

II.3.1.2. Magnetron sputtering mechanism

Many applications have been recognized for sputtering. However, the poor deposition rate, low plasma ionization efficiency, and strong substrate heating effects restrict this technique. Due to variances in sputtering speed and high melting temperatures, alloys and refractory metals, in particular, present challenges. Moreover, under low working pressure, compounds can dissociate into their chemical constituents. The advance of magnetron sputtering has resolved these challenges. The conception behind this technology is to use a specifically tailored magnetic field on the cathode (target) to produce electron traps, affecting drift currents to adjacent in on themselves. The functional magnetic field develops the path length of primary and secondary electrons and impulsions them to trap in a localized area nearby to the cathode at inferior voltages than diode systems (500 - 600 V). These electrons have a significant role in maintaining the plasma and increasing the possibility of collision between ionized atoms and electrons. The increased ion current density supplied to the cathode as a result of the high ionization efficiency is related to the target erosion rate.

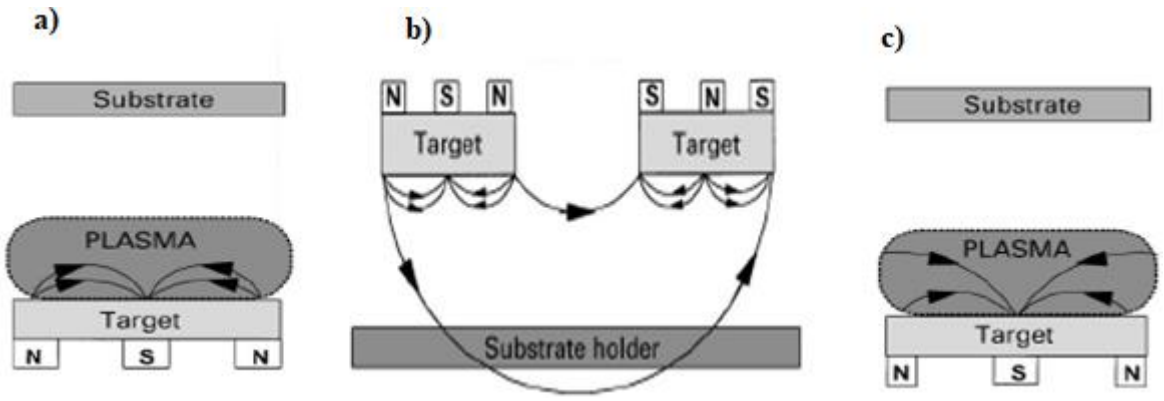

Figure II.7. Schematic view of**: a)** conventional magnetron sputtering, **b)** dual (co-planar) unbalanced magnetron sputtering, and **c)** unbalanced magnetron sputtering systems [17].

There are three principal types of magnetron design including D.C, R.F and reactive magnetron sputtering processes:

D.C (Direct Current) magnetron sputtering mechanism

The D.C (*Direct current*) magnetron is one of the simplest and the oldest application of sputtering process. Initially, the sputtering coatings were mainly concentrating on metallic films over a metallic substrate, so until 1960s this diode sputtering process was one of the most common sputtering techniques available in the market.

In the D.C mode the target is directly conducting electricity and may be operated up to power levels of perhaps 70 W/cm^2 averaged over the target. For a 100 mm circular magnetrons, power provides are qualified for delivering up to 5 kW into the plasma [18]. This will turn out deposition rates on static substrates of numerous micrometers per minute creating this appropriate for high-production-rate procedures. This can produce deposition rates on static substrates of several nanometers per minute making this very suitable for high-production-rate processes. The power required is dependent on target size such that large magnetrons may consume up to 50 kW. Consequently, D.C magnetron sputtering is used in different industrial areas including microelectronic circuits, electrical resistance films (Ni-Cr), magnetic films (Fe, Co-Pt, Co-Cr, Co-Ni), tapes and magnetic film heads, devices, corrosion-resistant films (Cr-Ni), glass fibers and gas sensors. However, the main disadvantages of the D.C magnetron sputtering would be the very low deposition rate (~ 10-20 nm/min), conductor materials can only be deposited, and the high pressure required to achieve plasma can degrade the film quality compared with the R.F magnetron sputtering process[18, 19].

R.F (Radio Frequency) magnetron sputtering mechanism

The D.C magnetron will not work if an insulating target is used, because no current can flow through it (*Fig.II.8.b*) [18]. This is done by applying a R.F potential to the target by using an alternating current at high frequency (typically 13.56 MHz) and the generated electrons move for a long distance during each half cycle, hence increasing the probability of further ionizing of the inert gas atoms (Ar^+) and generating stable high-density plasma that improves the efficiency of sputtering process. In addition, the increased ionization efficiency achieved in the R.F magnetron process leads to maintain the discharge at lower operating pressure (1-15 mTorr) and lower operating voltage (-500, -1012 V) than those in the basic sputtering mode [18, 20-22]

F.R magnetron sputtering can be used for different types of films such as polymers, ceramics or insulating compounds as well as ionic, covalent and metallic materials. Despite that R.F sputtering equipment (*power suppliers in particular*) is more expensive than the D.C magnetron, the R.F magnetron sputtering offers many advantages: the use of non-conductive targets, charge-up effects and reduced arching due to the use of alternating electric field. Passive and insulating films and electrical resistances are another industrial application for using them in microelectronic and strain gauges. For example, the SiO_2 films can separate the resistance element from the basic support, also the Ni-Cr films can be sputtered to form highly adherent strain-gauge elements [18]. In the R.F magnetron sputtering system, the ionized Ar atoms bombard the targets and their molecules/atoms consequently release to form thin layers on the substrates.

II.3.1.3. Reactive magnetron sputtering mechanism

Some dielectric materials can be sputtered by R.F or D.C magnetron sputtering in a reactive gas atmosphere. Reactive magnetron sputtering process is used to form films by co-deposition and reaction of the constituents or by the reaction of deposited species with the ambient gaseous or vapor environment [23]. Argon gas is injected inside the deposition chamber as a carrier gas in a mixture with small quantities of a second reactive gas. The reactive gas, typically nitrogen or oxygen, used during the sputtering process reacts with the target surface as well as the sputtered metal atoms and thus forms a thin film on the substrate surface as well as on the chamber walls receiving sputtered particles (*Fig.II.8*). These

reactions affect the whole procedure [24]. A film will only be formed if the product of the reacting species is nonvolatile. The co-deposition of reactive species does not necessarily guarantee the activation of chemical reaction [23]. Reactive sputter deposition may also occur if the sputtered particles react with adsorbed species already present on the substrate surface (e.g. contaminants). Generally, for deposing at low temperature, some of the reacting species should be condensable with the other gaseous ones [23].

Reactive sputtering can also be used for deposing films by chemical reaction between the target material and the gas introduced into the vacuum chamber where the compositions of these films can be controlled by adjusting the relative pressure of the mixture between Ar ions and reactive gases. The reactive magnetron sputtering can be used not only for sputtering of nitrides, oxides, carbides and other compounds, but also for the production of nanocomposite films with small grain size (1–20 nm) [24], which exhibit unique properties and enhance their performance and applications. Hard materials such as TiN are used for wear-resistant tools and decorative coatings of watchcases. The transparent conductor thin films of In-Sn oxide are also produced by reactive sputtering. These films are used for the electromagnetic interference, LCD displays, heated screens for vehicles and aircraft and in solar collector panels [23].When the reactive gas flow rate is maintained, the compound forms on the target surface in a sudden transition. The sputtering rate drops and the partial reactive gas pressure insuring even further target "*poisoning*" [18].

For example, the sputtering of an oxide covered target is generally not desirable because the sputtering rate of the oxide is much lower than that of the metal and the appearance of an insulating surface on the cathode causes arcs if D.C is used, and F.R power is required. This effect is particularly difficult to be solved for different oxides (e.g. aluminum and titanium oxides) because the deposition rate of oxides is unacceptably low. However, the oxides of materials such as indium, zinc and titanium can sputtered from a metal oxide target with D.C mode, without arcing, and largely have been used for coating of architectural glass. In order to decrease the influence of arcing effect, alternating voltages can be applied to prevent the building up of charges in the dielectric layer at the target surface [25].

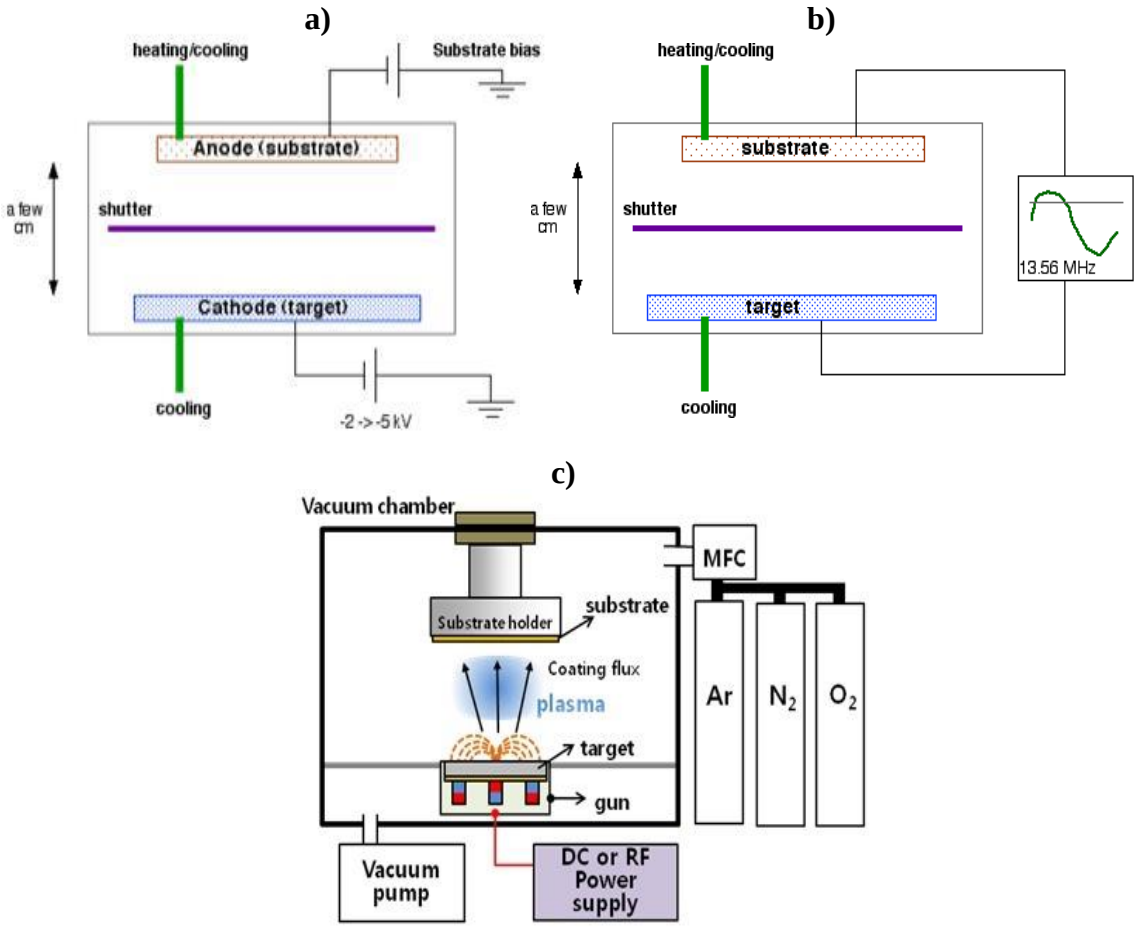

Figure II.8. Schematic view of**: a)** D.C, **b)** R.F, and **c)** reactive magnetron sputtering deposition systems [22, 24, 25].

The choice of this technique for the growth of our coatings has been established thanks to the numerous advantages of this technique, including:

- ✓ *The possibility of depositing nitrides, carbides, oxides, etc.,*
- ✓ *The ability of commanding the deposition parameters during the growth of the coating, which makes it possible to investigate the influence of every parameter on the overall features of the film obtained and to produce coatings at well-controlled deposition rates,*
- ✓ *The full cover of the surfaces coated,*
- ✓ *High purity of the product coatings.*

The magnetron sputtering deposition machine that we used in this research (DEPHIS, France) (*Fig.II.9*).

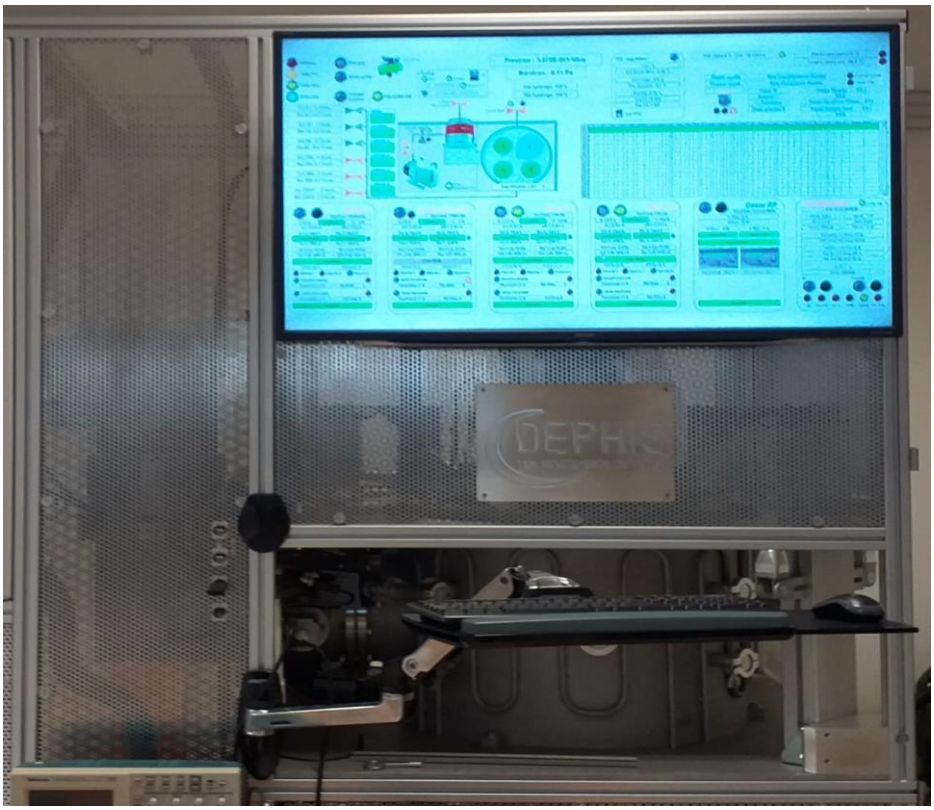

Figure II.9. The magnetron sputtering deposition machine (DEPHIS, France).

II.3.1.4.Thin Film Growth through Sputtering Technique

II.3.1.4.1.Nucleation and growth mode of sputtered thin films

The main physical mechanisms involved in the nucleation and crystallization of the films over the substrate. Studies done through X-Ray diffraction and mainly through electron diffraction have allowed establishing that there are three mechanisms of the nucleation and growth of thin films (*Fig.II.10*), which depend on the thermodynamic parameters of the deposit and the substrate surface interaction between the adatomes and the substrate material [14].

All the procedures of thin film growth from a vapor phase are obtained in three principals steps: firstly, creation of the appropriate species to be deposited on the substrates (ionic, atomic or molecular compounds) by the Ar^+ etching of the target surface. Then, transport of these species from the source (target) to the substrate surface with or without collisions between atoms and molecules. Finally, the condensation of these species by chemical or electrochemical reactions and forming the films [26].

❖ Nucleation

Sputtered adatoms reaching on the substrate lose their kinetic energy (physically diffused from the target surface). Thermodynamically, these species are not in equilibrium with the substrate and move over the entire surface. In this condition, these species interact with each other and form clusters. These are unstable and tend to be adsorbed. Under certain deposition conditions, they collide with other adsorbed species and start developing. After achieving a critical size, these clusters become thermodynamically stable and the nucleation barrier is over. The clusters grow in both size and number to reach a maximum density of nucleation; this is called the nucleation stage. The clusters size relies on many parameters such as sputtering rate, activation energy, thermal diffusion, and the type of the substrate. The film in form of an island can grow parallel or vertical by diffusion of the sputtered species to the substrate surface. In PVD processes, lateral growth in this stage is more important than perpendicular one.

❖ Coalescence

The islands grow largely and eventually meet to form a continuous layer. As soon as two islands are close enough to interact, they will begin restructuring to minimize their total surface and interface energy. The islands move from a discontinuous type to form grain boundaries leaving cannels and holes in the thin film deposited on the substrate [27]. Surface diffusion continues to change the grain shape until the new grain reaches its equilibrium shape. Size differences between the coalescing grains will lead to growth of the large grain at the expense of the smaller due to the larger curvature of the smaller grain. One of the consequences of island coalescence is that the areal fraction of the surface covered by deposited material decreases. These newly released surfaces are often large enough to allow for nucleation of a new generation of islands, known as secondary nuclei. There are three different initial growth modes of grain boundaries [24].

- ***Vollmer – Weber growth (3D-island growth) mode or mechanism of island growth mode***

The island mechanism growth happens when atoms in the film bind more with each other than with the substrate surface. In this case, three-dimensional islands are constructed and grow directly on the substrate surface. Small clusters of atoms directly nucleate on the

substrate and then extend in three dimensions in the form of islands. This happens when the deposited atoms are stronger bonded to each other than to the substrate (*Fig.II.10.a*).

- ***Frank–van der Merve (2D-layer growth) growth mode or layer by layer growth mechanism***

The layer-by-layer growth mechanism of *Frank-van der Merwe* occurs when the atoms of the thin film bind more to the substrate than to each other. The growth of the next layer does not start until the full formation of the previous layer, so obviously there is 2D growth (*Fig.II.10.b*).

- ***Stranski-Krastanov growth mode***

This mode is a combination of the two previous. It represents the situation in which two-dimensional (layered) development transforms into three-dimensional growth (island). The three-dimensional island formation happens once the two-dimensional layer growth is completed. The nature and thickness of the two-dimensional layer (often referred to as a *Stranski – Krystanov* layer)depends on the individual case (*Fig.II.10.c*) [28].

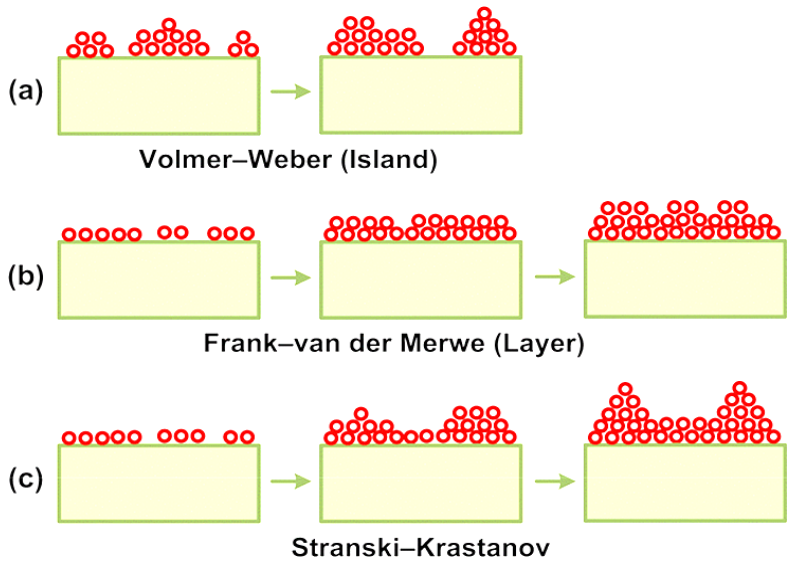

Figure II.10. Three different growth modes**: a)** Volmer–Weber island growth, **b)** Frank–Vander Merwe layer growth, and **c)** Stranski-Krastanov layer plus island growth [14] .

II.3.1.5. Physical models thin film microstructure growth through sputtering

The microstructure of thin films is related to the mobility of the adatoms during growth. The energy supply to the atoms is provided by the following mechanism:

- ✓ *Thermal effect,*
- ✓ *Ionic bombarding,*
- ✓ *Chemical reactions at the substrate.*

The effects that are produced by these mechanisms in the growth of thin films can be explained by the structure zone model (SZM).

II.3.1.5.1. Structure zone models SZM and microstructure

Regardless of the kind of material, the SZM model can predict the morphology and microstructure of films as a function of the adatomes. The temperature of the substrate, the ultimate working pressure, the bias voltage applied to the substrate, and the thermal properties of the target are the factors that the SZM model uses to determine the microstructure of the films [14]. Temperature and pressure are two of the most critical characteristics that impact its properties. Modern deposition processes, like as sputtering, may produce a wide range of coatings based on the mobility of the deposited atoms on the substrate surface, which can be improved by raising the deposition temperature. The increased mobility of the atoms allows the formation of thin films with significant crystallization. Low atom mobility, on the other hand, leads to the production of amorphous films [29]. To better understand the impact of deposition parameters on coating structure, Multiple structural zone models (SZM) have been proposed for describing thin film growth modes in response to temperature and operating pressure [29, 30]. Firstly, for thick evaporation films, *Movchan* and *Demchishin* proposed a three-zone model based on temperature variations [31]. The model was developed by *Thornton* and extended to include the effects of working pressure (P) and temperature ratio T_s/T_f, (T_s is the temperature of the substrate, and T_f the melting point of the sputter material).

A transition zone (T) Also considered between zones 1 and 2 as described in the following paragraphs. Now, with this extension, the model is called *Movchan-Demchishin*-Thornton (MDT) model [32].

A zone classification was developed by *Thorton* (*Thorton*, 1974) taking into account the final working pressure as it will affect neither the kinetic energy of ions reaching the substrate and the mean free paths of the particles, both of which can influence the degree of bombardment on the substrate surface, which controls adatoms mobility. In *Thorton's* model, there was a transitional zone called the T zone between the first and the second zone

discussed above. The T zone has been formed by grains defined by the limits of the low porosity. As compared to the two surfaces surrounding them, the surfaces of the T zone are denser with reduced roughness [14].

Zone 1: (Ts/T_f <0.3) composed of small and elongated grains with a porous morphology and weakly bound grains. The columnar structure is associated with a low diffusion rate, low mobility of atoms, as well as the atomic shadow effect, which are associated with varying velocity when the columns grow and various incidence angles at which the atoms strike the surface of the substrate [14].

Zone 2: ($0.3 < T_s/T_f <0.5$) is characterized by the growth of uniform crystalline columns continuously from the surface of the substrate. The grain size grows and may develop throughout the film thickness. The surface ends of the grains conduct to a faceted surface [30, 32].

Zone T: ($0.2 <T_s/T_f< 0.4$) Low gas pressure and similar low temperatures lead to transition morphology. It is characterized by exact low surface roughness and dense fibrous grains. These films are also amorphous or nanocrystalline and the grain boundary diffusion are strongly limited leading to competitive grain growth and resulting in V-shaped grains with a grain structure not homogenous through the film thickness. At higher temperature, bulk diffusion and recrystallization lead to dense films with large grains.

Zone 3: ($0.5<T_s/T_f< 0.75$) his structure distinguished by equiaxed (globular) three-dimensional grains, which is a educate indication that the crystal development has been blockaded periodically. These sorts of structure are commonly assigned to the elevated substrate temperature range. For $T_s/T_f\geq 0.75$crystallization and grain growth become essential [30, 32].

Recently, Anders published an expanded model (*Fig.II.11*) from the Thornton's model [31], which substituted the $\mathbf{T_s/T_f}$ ratio by the generalized temperature **T***, which incorporates the homologous temperature and the temperature shift forced by the potential energy of

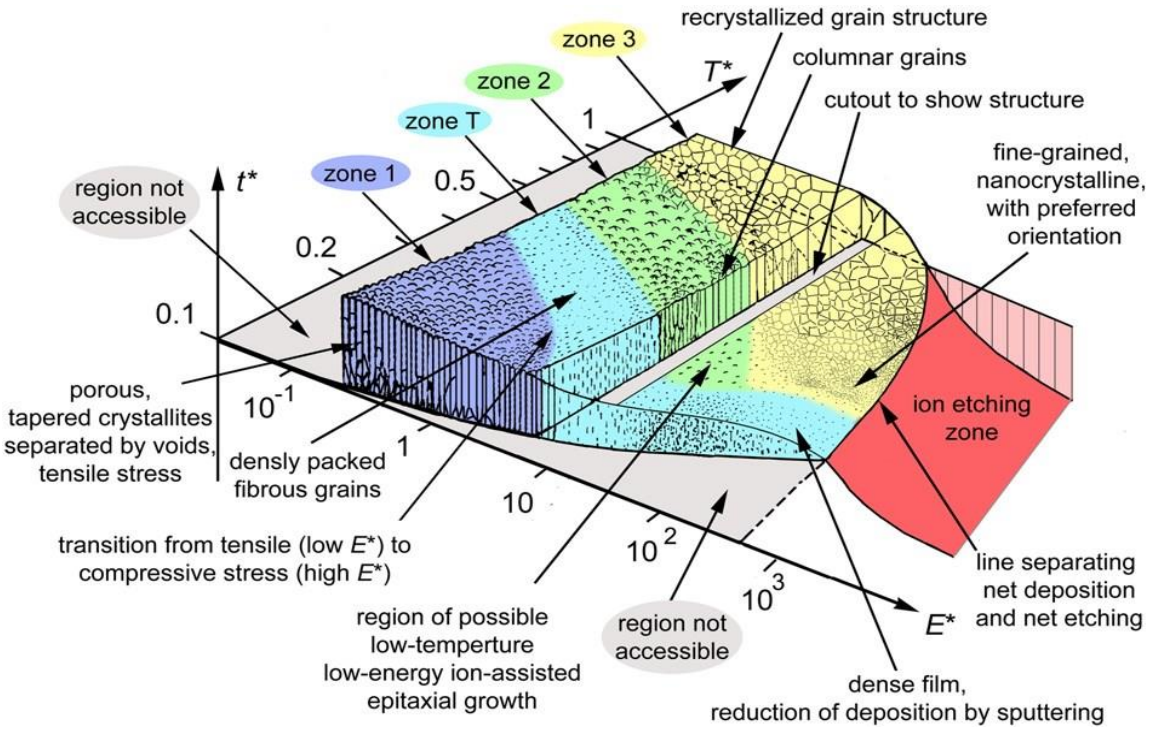

Figure II.11. Anders Structure zone diagramme [29].

particles reaching the surface. The linear pressure was also replaced by a logarithmic axis representing the normalized energy flux **E***, representing displacement and heating effects generated by the kinetic energy of bombarding particles. Finally, he replaced the z-axis with the net film thickness **t*** which can be negative in the case of ionic etching [31].

II.4. Thin films characterization techniques

Characterization is an important step in the development of better-quality of materials. We focused especially on the structural, mechanical, and tribological characterization techniques; owing to their significant role in the development of hard coating proprieties and also help the researcher better understand the corresponding domain of application according to the properties exhibited by thin films. In the first part, a variety of methods of Physico-chemical and structural characterization techniques, such as X-ray diffraction (XRD), Scanning electron microscopy (SEM), X-ray microanalysis EDS, and WDS, Atomic Force

Microscope (AFM), (XPS),and Raman spectroscopy have been adopted to investigate the structure, chemistry, and crystallography thin-film coatings.

Wetting and surface energy determined using the contact angle measurement. Nano indentation method is commonly used to evaluate the mechanical properties of thin films, also included. The film residual stresses were determined by using *Stoney's* formula [33].In addition, wear testing is briefly introduced. In the second part of this section, details of these characterization methods used in this thesis are summarized.

In this part, we introduce the used techniques available for the characterization of our coatings, consisting of phase analysis, structural elucidation, compositional characterization, surface, and microstructural analysis, which have a strong bearing on the properties of materials, and finally, mechanical and tribological characterization.

II.4.1. structural and physicochemical caracterization

II.4.1.1. X-ray diffraction

X-ray diffraction (XRD) is commonly applied for the analysis of material structure. This technique is popular as it is both non-destructive and can be applied to almost any solid sample without any special preparation techniques. The data delivered by XRD is interested with periodicity in a structure. Individually atom in a periodic structure functions as a point of scattering for waves. These scattered waves may interfere constructively to assemble sharp peaks in intensity. The conditions for constructive interference are illustrated by *Bragg's law*, as presented below in Equation (II. 1) with a simplified model given in *Figure II.12*.

Bragg's Law:

$$2\, d_{hkl} \sin\theta = n\lambda \qquad \text{(II.1)}$$

Where 'θ' is the incident angle, 'n' is the order of diffraction, 'λ' is the wavelength of beam, and 'd' is the spacing between diffracting planes. It demonstrates the relationship between scattering angle, the wavelength of radiation, and the spacing between the planes of atoms. Because the distances in between atomic planes are reliant on the atoms' size and distribution [34, 35].

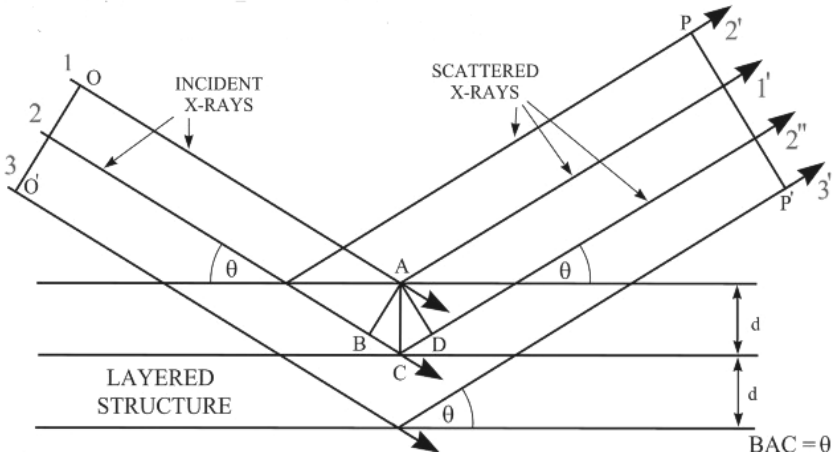

Figure II.12. Geometric principle of X ray-diffraction.

XRD provides information regarding crystal structure since periodicity and symmetry are components of ordered crystal structures. Distortions or alterations to the periodic structure can also be observed through distortions in the X-ray diffractogram, this provides information regarding grain size, epitaxial, texture, and even microstrain.

In our work, the crystalline structure was determined by X-ray diffraction analysis (*XRD, (XRD, BRUKER, Karlsuhe*, Germany, 40 kV/ 40 A, Cu–Kα radiation) over a 2θ range from 30 to 80°. All the reflections were equated with the standards gathered by the Joint Committee on Powder Diffraction and Standards (JCPDS, card #01-074-8388 for TiN, #00-004-0836 for Cu and #00-065-7723 for ZrN). The average crystallite size was determined by using the *Scherrer* equation.

Scherrer's formula evaluates the influence of crystallite size on the XRD peak broadening. Williamson–Hall method is a very comfortable and simplified one. According to this, total broadening of the XRD peak is due to the size and micro-strain of the nanocrystals and can be written as:

$$\beta_{total} = \beta_{size} + \beta_{strain} \qquad \text{(II.2)}$$

For a dense structure, we can calculate the average particle size by using the corrected physical broadening with the help of *Scherrer's* equation [22]:

$$D = \frac{0.9\lambda}{\beta\cos\theta} \qquad \text{(II.3)}$$

where, D is mean crystalline size, $\lambda$is X-ray wavelength (1.54 Å), $\beta$is the peak width and $\theta$is Bragg diffraction angle.

The lattice parameter could be calculated for fcc-crystal structure using the following equation:

$$a^2 = \left(\frac{\lambda^2}{4\sin^2\theta}\right)(h^2 + k^2 + l^2) \qquad \text{(II.4)}$$

The lattice distortion (ε) was calculated using the following equation:

$$\varepsilon = \left(1 - \frac{a}{a_0}\right) \qquad \text{(II.5)}$$

where, a is the lattice constant , produced in different, $a_0$is the lattice parameter of bulk structure.

II.4.1.2. Scanning Electron Microscopy (SEM)

Scanning electron microscopy (SEM) is a versatile technique used in many industrial labs, as well as for research and development. Due to its high lateral resolution, its great depth of focus and its facility for X-ray microanalysis, SEM is often used in materials science to elucidate the microscopic structure or to differentiate several phases from each other. In the SEM system, the electrons interact with the samples to produce secondary and backscattered electrons, which will be collected to generate scanning electron micrographs (*Fig.II.13*). Backscattered electrons were formed when an incident electron strikes the sample and is bounced back from the sample. The elements with higher atomic numbers absorb more incident electrons allowing fewer to be backscattered, leading to higher contrast to different elements. The secondary electrons will be generated when an incident electron strikes the sample. The electron from the sample with excess energy will be ejected by atoms near the sample's surface (10 nm) and will be strongly affected by the sample's topography [36].

In our work, the surface and film cross-section morphologies were examined using a field emission scanning electron microscope (*FE-SEM, Hitachi S3500 N, USA*).

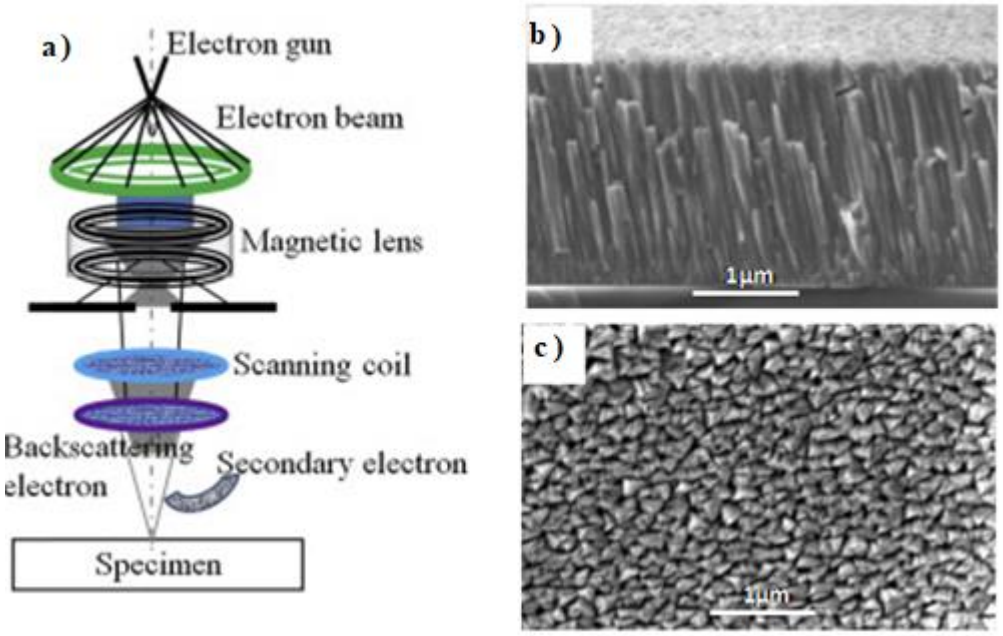

Figure II.13.a) Schematic diagram to show operational principle of SEM facility [37], **b)** cross section, **c)** surface morphology of thin films [38].

II.4.1.3. X-ray microanalysis (EDX, WDS)

The qualification and quantification of the chemical composition are carried out with gratitude to the EDS or WDS. Following their ionization by incident electrons, each atomic element emits on its return to equilibrium X-ray radiation having specific energy.

- ***Energy Dispersive Spectroscopy (EDS):*** The EDS detector consists of a diode (single silicon crystal doped with lithium) which receives the entire X-ray spectrum. A multi-channel analyzer classifies the number of occurrences (quantitative information) of each energy level received (qualitative information) and reconstructs the emission spectrum of the sample.
- ***Wavelength Dispersive Spectroscopy (WDS):*** In the WDS spectrometer, X-rays from the sample are collected on a crystal monochromator. Depending on the angle between the crystal and the sample, radiation will be diffracted. Knowledge of the diffraction angle makes it possible to calculate the wavelength of this radiation [39].

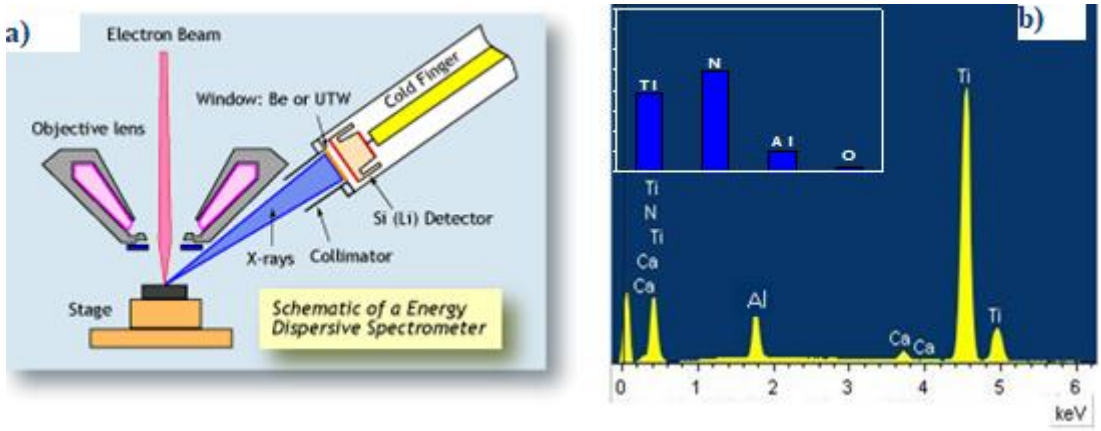

Figure II.14.a) Schematic energy dispersive Spectrometer [40], **b)** X-ray energy spectrum (WDS) KeV [41].

In our work, chemical compositions of thin films were analyzed with energy-dispersive X-ray spectroscopy (EDX, WDS, Oxford INCA x-act, 15 kV, USA) attached to the FESEM. The stoichiometric of TiN and ZrN phases was measured in two different points for every film and the precision is about 3 %.

II.4.1.4. Atomic Force Microscopy (AFM)

Atomic Force Microscopy (AFM) is a technique widely utilized to image the surface of a sample. It achieves very high-resolution levels that can reach the atomic level. We can therefore produce images of surfaces at extremely high resolution. The basic structure of an AFM microscope is shown schematically in *Figure II.15*. When the tip approaches the sample surface (at a distance of a few tenths of a nanometer), repulsive Van der Waals forces between the atoms of the point and those of the studied surface, which caused a deflection of the beam which depends on the distance which separates them.

A piezoelectric transducer is used to allow scanning of the sample surface and the deflection of the beam is usually measured by the reflection of a laser beam. The main mode of use of an AFM microscope is based on the use of a feedback loop to maintain a constant distance between the tip and the surface being analyzed through a piezoelectric actuator [42].

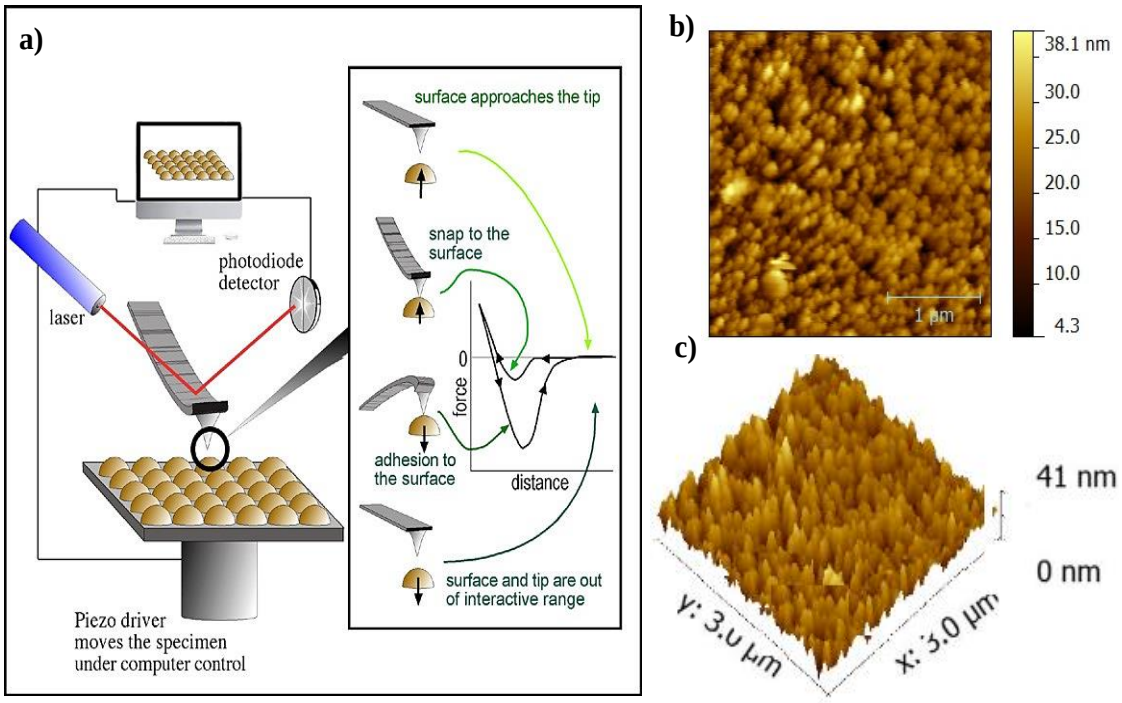

Figure II.15.a) Schematic diagram illustrating the principle of the atomic force microscope, **b)** 2D, **c)** 3D) AFM images of the thin films [43].

The roughness and surface topography of our deposited films were determined by an Atomic Force Microscopy (AFM, APE research) with a silicon nitride super tip. The AFM was operated in a contact mode and the scan zone was (3×3) μm^2.

II.4.1.5. X-ray Photoelectron Spectroscopy (XPS)

X-ray photoelectron spectroscopy (XPS) or electron spectroscopy for chemical analysis (ESCA) is a remarkably practical technology for analyzing thin surface layers. The technique is expressed by *Briggs and Seah*. In XPS, the substrate is bombarded with X-rays with well-defined energy. The X-rays interact with core electrons existing around the nucleus of the different atoms, and, if these electrons escape the sample, is emitted at a well-defined kinetic energy, Ek, given by:

$$E_k = h\nu - E_b - \varphi \qquad \text{(II.6)}$$

Where $h\nu$ is the X-ray photon energy, E_b is the electron binding energy, and φ the work function that is the energy needed for the electron to free itself from the surface.

It depends on the spectrometer and the substrate. The kinetic energy of the photoelectrons originating from various kinds of atoms and orbitals, and even the same type

of atom and orbital in diverse binding states, have different binding energies. Therefore, by isolating the electrons with different kinetic energy in an analyzer and indicating the results in a spectrum showing the photoelectron intensity as a function of kinetic energy, the types of atoms current in the surface layer and their abundance can be determined.

XPS is surface sensitive due to the short inelastic mean free path (λ), of electrons in condensed materials. Typical values are 1-2 nm for metals, (1.5-4 nm) for oxides and down to 3 nm for organic materials. This means that 63% of the signal emanates from a region that is at a distance less than (λ) from the surface. The ESCA results quantification can be carried out in diverse ways and to various degrees of complexity. The most typical way is to provide the data in atomic percent, in which the relative abundance of different types of atoms in the surface layer is determined by multiplying the photoelectron intensity for a specific element by the element's sensitivity factor. A more extensive investigation can be performed if the adsorbed layer contains an element that is not present in the substrate [44].

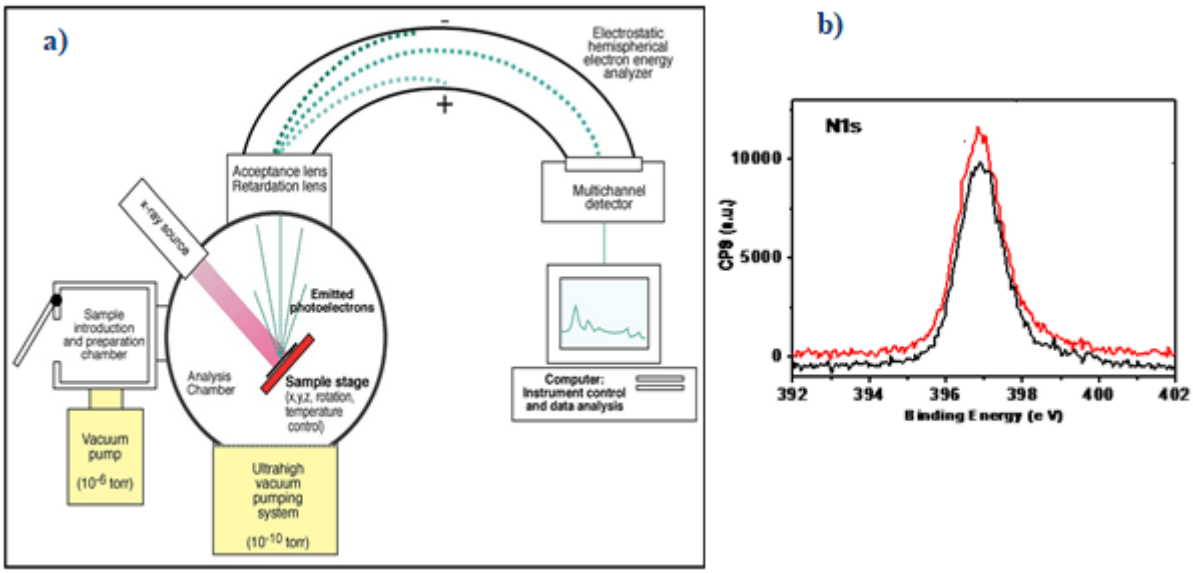

Figure II.4.a) Schematic diagram of a monochromatized ESCA instrument [44], **b)** N1s XPS binding energy of Titanium nitride films [45].

The elemental composition and chemical bonds of our films were characterized by X-ray Photoelectron Spectroscopy (XPS) with Al-Kα irradiation at energy of 1486.6 eV, after removing the surface contaminants by sputtering them with Ar^+ ions at a primary energy of 3

keV for 5 min. The spectra were calibrated by the C1s line (284.5 eV), then decomposed into peaks with Gaussian–Lorentzian line shapes by a non-linear least square fitting method.

II.4.1.6. Raman spectroscopy

Raman spectroscopy is an optical nondestructive technique sins the non-contact nature allowing the user to characterize a variety of materials while contact methods can deform thin films and bias the measurement [46]. Raman is based on the inelastic scattering of photons with elemental vibrational excitations in the material. The line shape and position of the Raman bands are determined by the crystalline structure and chemical composition of the measured samples, being sensitive to the presence of crystalline defects, impurities, and strain. The presence of peak characteristics of different phases also allows for the identification of secondary phases that are intensely bonded to the film growth and procedure conditions. All of these factors contribute to a great interest in Raman spectral analysis, which offers the perfect non-destructive analytical tool for assessing the structural and chemical properties of films [47].

Raman spectroscopy is based on the Raman Effect with inelastic light scattering. When a molecule is irradiated by an electromagnetic wave of frequency ν_0, a part of the light is absorbed and a part is diffused either with the same frequency, it is the diffusion elastic or Rayleigh, or with a different frequency ν it is Raman scattering.

If ν (diffused) $<\nu_0$ (incident) we have a Raman Stokes scattering: if ν (scattered) $> \nu_0$ (incident), we have a scattering Much weaker anti-Stokes Raman. A Raman spectrum is therefore a vibrational and rotational imprint of the analyzed compound at the molecular and/or crystalline level. It appears as a set of lines of changing intensity whose positions link to the frequencies of vibrations current in the molecule and whose observation is allowed by the selection rules of molecular symmetry [48].

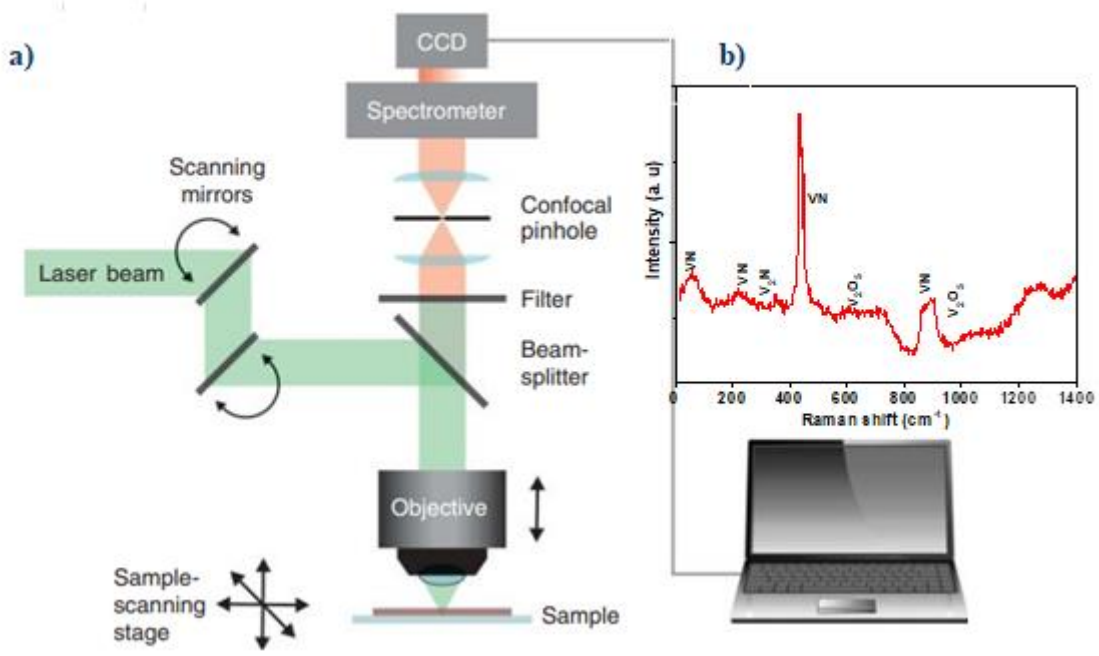

Figure II.5.a) Schematic setup of a Raman microscope [47], **b)** Raman spectra of VN films [49].

Raman spectroscopy with a *Bruker Senterra* spectrometer was applied in our study. Exciting laser radiation wavelength was 600 nm. This identification was supported by a reference Raman spectrum of obtained phases expected in V-N coatings.

II.4.2. Wetting behavior and hydrophobicity

Wetting surfaces have acquired increased awareness because water repellent materials have many promising features, such as self-cleaning, anti-icing, anti-bacterial, drag reduction, and adequate thermal transfer. Super hydrophobic surfaces may be applied to air-crafts, used as exterior coatings for buildings, automobiles, hospital equipment, wind turbines, etc. However, super hydrophobic surfaces have limited usage in high wear conditions due to their poor mechanical durability. Therefore, a water repellent material with good durability, good thermal stability, and good chemical stability is a requirement for more widespread use of these remarkable materials [50].

The surface wetting behavior can be categorized by measuring the water contact angle (CA) for a drop of liquid deposited on a surface, as shown in *Figure 1.18*. The contact angle θ is the angle between the baseline and the tangent to the liquid/gas interface at the point where the three phases overlap [51]. The CA is related to the three interfacial surface tensions through the Young's equation [51]:

$$\cos\theta_Y = (\gamma_{sg} - \gamma_{sl}) / \gamma_{lg} \qquad \text{(II.7)}$$

where θ_Y Young's equilibrium contact angle and γ_{ij} is the surface tension at the interface between the i and j phases with the subscripts s, l and g representing solid, liquid and gas, respectively. Surfaces with different wettability concerning water are conventionally referred to as either hydrophobic or hydrophilic as shown in *Table I1.2* according to the values of the CA.

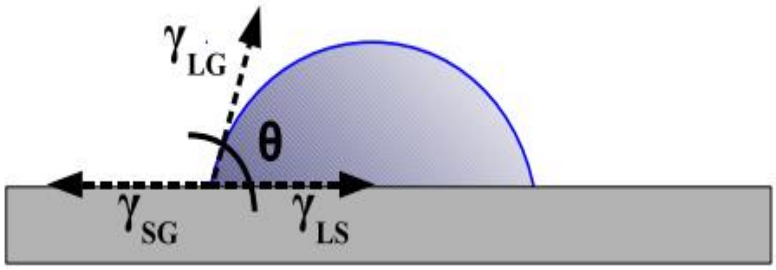

Figure II.6. Representation of the CA [51].

Table II.2. Relating hydrophobicity and the contact angle with water [51].

Surface	Contact angle	Figure
Superhydrophobic	>160	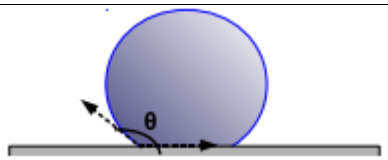
Hydrophobic	>90	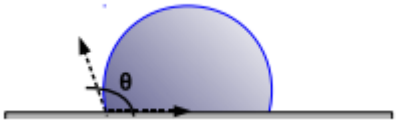
Hydrophilic	<90	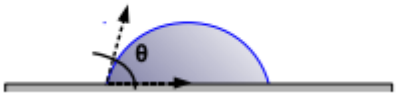
Superhydrophilic	~0	

Many parameters affect the water contact angle values, the surface energy, surface roughness, pressure, temperature, humidity, and surface contamination [50]. In this experimental investigation, the hydrophobicity of TiN, and TiZrN films' surface was

evaluated by the contact angle measurements . Water droplets (3 ml) were fallen down on the films and the contact angles were measured. The droplet profile was acquired using a camera (SCA Software for OCA and PCA Drpo6) aligned with the sample and a backlighting source.

II.4.3.Mechanical characterizations

Interest in mechanical-property effects in thin films has traditionally focused on two broad issues. The primary one has been the deleterious effects that stress cause in films. This has prompted much research to determine the type, magnitude, and origin of stress as well as means of minimizing or controlling stresses. A second central point regards improving the hardness and wears resistance of assorted coatings. Of the two issues, the first has historically generated the greatest scientific attention and is the one primarily addressed in this chapter.

On the other hand, the mechanical properties of metallurgical and protective coatings are important technologically and are the subject of an extensive literature. It is virtually always the case that stresses are current in coating. What must be appreciated is that stresses exist even though films are not externally loaded. Such residual or internal stresses directly affect a variety of phenomena including adhesion, generation of crystalline defects, perfection of epitaxial layers and formation of film surface growths such as hillocks and whiskers. Since they tend to increase with thickness, promoting film peeling, and stresses are a prime limitation to the growth of very thick films. Substrate deformation and distortion also necessarily arise from stresses in the overlying films [25].

II.4.3.1. Residual stress

Residual stresses can be described as the stresses, in the mechanical sense of the term, present within a material when it is not subjected to an action exterior mechanics. They are not specific to thin films or materials of a low thickness (< 10 μm). A massive material also presents, locally, stresses significant residuals. In a mechanically-welded structure, for example, stresses develop locally near welds. In the case of thin coatings, the residuals stress are represented in a preponderant way, sometimes involving the integrity of the microstructures [39]. In the case of hard coatings, the origin of the residual stresses (RS) is specifically connected to the coatings deposition process and the growth mechanism. The deformations and residual stresses existence can affect the properties of use (physical-chemical, mechanical, etc.) of the produced materials [42].

Residual stresses are classified according to three orders. The I order stresses presented the macroscopic stress. For a multiphase material, they affect several grains. Order II stresses are the residual stresses present at the grain scale, acquire from the difference in the grains constitution, their orientation, their size is at the origin of these constraints. Finally, the stresses of order III are the microscopic residual stresses. They can be due to the presence of interstitial elements, gaps, or other defects within the network crystalline. In the case of thin films, three types of residual stresses are considered: thermal stresses (negligible in our case), –intrinsic stress, –the structural stress. The thermal stress is originated principally from the difference in coefficient of thermal expansion between materials united, expressed by a deformation of the various elements during the cooling of the structure. These constraints can be categorized into the order I of residual stresses since they act globally on the structure. The intrinsic stresses existed during the elaboration process of the coatings and appear during the growth, resulting in residual stresses of order I, II, or III. In microsystems, each layer or multilayer presents intrinsic stress during its method of production and could originate from faults, defects, contamination, the problem of diffusion of oxygen towards the inside of the layer causing a volume expansion, the difference in the size of atoms of each component, oxidation of the surface, growth rate, dislocations of interfaces in single crystals, tension of area, etc. [39].

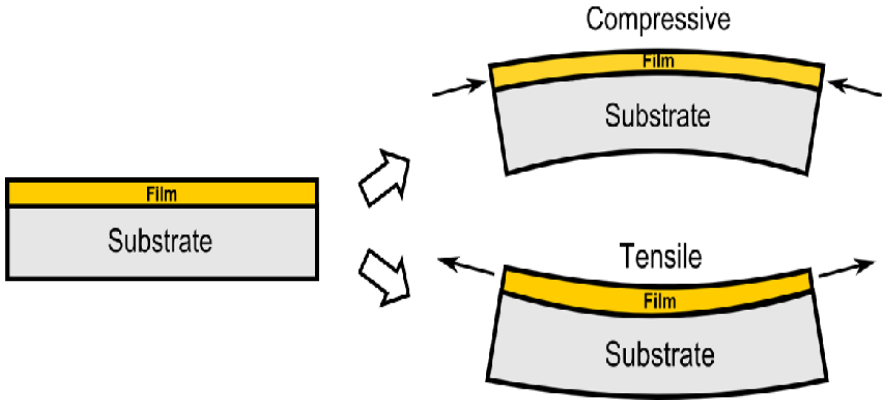

Figure II.7. Deformation of the film/substrate assembly according to the type of stress [52]**.**

The residual stresses generated in the films during the deposition procedure were calculated from the tensile steel substrate-curvature radii before and after deposition measured by an optical Profilometer (VEECO, Wyko-NT 1100), obtained by using *Stoney's* formula:

$$\sigma = \frac{Es}{6(1-\nu_s)} \frac{t_s^2}{t_f} \left(\frac{1}{R} - \frac{1}{R_0}\right) \qquad \text{(II. 8)}$$

Where E_s (181 GPa) and ν_s (0.28) are Young's modulus and Poisson's ratio of Si (100), respectively. t_s and t_f are the thickness of the Si(100) wafer and the deposited film, respectively, while R_0 and R are the curvature radius before and after deposition, respectively.

II.4.3.2. Nanoindentation

The indentation test is a simple and effective method for determining the mechanical behavior of materials that have been widely used in the 20th century. The mechanical characteristics of materials analyze by pressing an indenter into the material surface and then analyzing the impression. The indentation test was firstly utilized for the measure of hardness. A hard object with a specific form and size is operated as an indenter and indented into the tested material under specific force keeping for a period before being unloaded. Then the hardness of the tested material can be determined from the relationship between the total indentation load and displacement or area. There are many traditional methods of hardness testing based on the principle above, such as the Vickers hardness method (Vickers), Knoop hardness method (Knoop), and Rockwell hardness method (Rockwell).

The features of materials at nanoscales have become more essential with the advent of nanotechnology. At this point, the nanoindentation method occurs and takes the place of standard hardness measurements to satisfy the necessity of the examination of further materials. The nanoindentation method, which is furthermore known as the depth-sensing indentation technique, was firstly offered and developed by Oliver and his coworkers. This technology is founded on the theory of contact elasto-mechanics. In the nanoindentation test there are two indenter forms: Berkovich and cube corner. The Berkovich indenter is a three-sided pyramid with a face angle of 65.3 to the indentation vertical axis, and its area-to-depth operation is the exact as that of a Vickers indenter. The cube-corner is too a three-sided pyramid which is precisely the corner of a cube [53].

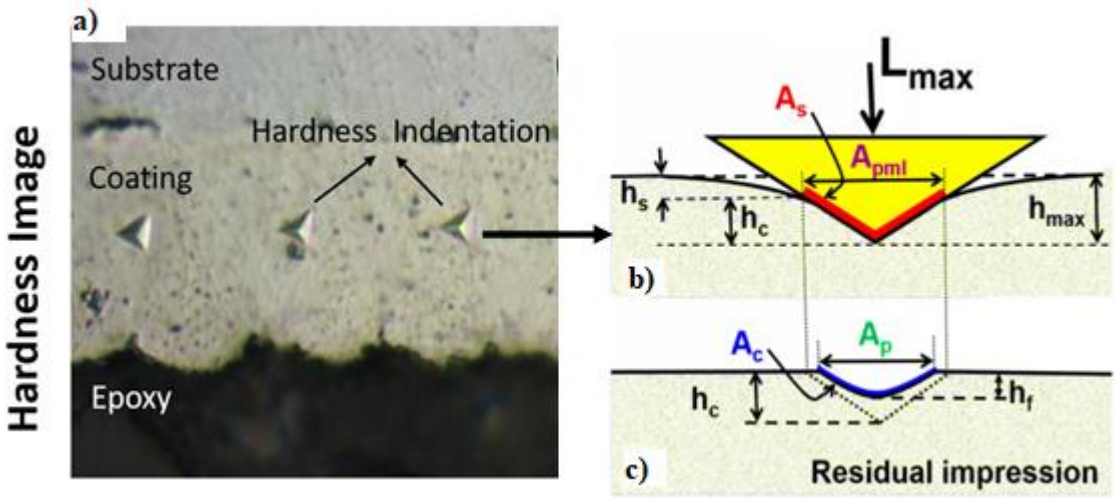

Figure II.8.a) Hardness indentation, **b)** Elasto-plastic deformation at the maximum applied load L_{max}, **c)** plastic deformation after releasing the load [54].

Through the analysis of the loading–unloading curve, not only hardness and elastic modulus can be obtained, but also information such as viscoelasticity, creeping, fracture toughness, strain-hardening effect, residual stress, phase transition, and dislocation movement. Recent years, with the development of nanoindentation technique, the investigation of the real contact area and pile-up of materials around the contact impression can be carried out by combining the application of atomic force microscopy. The finite element simulation technology has also been applied in nanoindentation tests, which makes the study of pile-up behavior much more convenient [55].

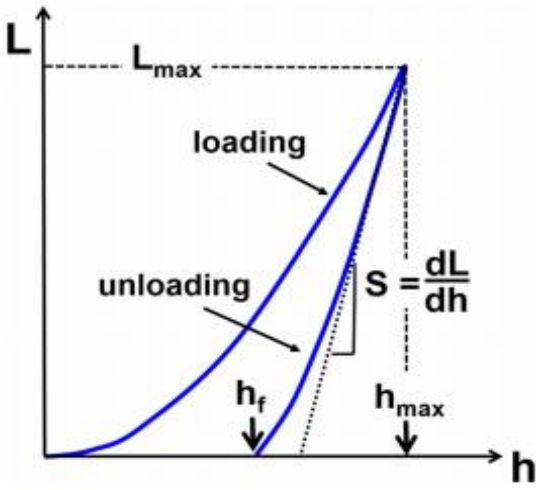

Figure II.21. Load–unload during nanoindentation [54].

II.4.4. Tribological characterization

The science and technology of interacting surfaces in relative motion and of related subjects and practices the tribology include the field of lubrication, friction and wear [56]. Wear is the result of friction, abrasion, etc. Friction occurs when two bodies are moved in connection with each other, as is the case for example in machining. Thus, wear is described as the progressive failure of matter from the surface of a body as a result of a relative movement to another body in contact. Indeed, the third body is formed of particles that are separated from the first two bodies [39]. Therefore appears that tribological behavior is not an intrinsic property of materials, but that it depends on the mechanical and structural characteristics of the two materials in contact and stress conditions [39].

In this study the tribological properties of the deposited TiN and TiZrN films were examined at room temperature and atmospheric conditions by a ball on disk tribometer (*CSM, HIGH-TEMPERATURE TRIBOMETER*). A 100Cr6 ball (diameter: 6 mm) was used as the upper specimen. The disc was rotated at a speed of 400 r/min (0.125 m/s), while the radius was 5 mm and the normal load was 2 N. The sliding distance was 400 m. After the test, the wear tracks were characterized using SEM for examining the wear mechanism. The wear rate was determined by using the wear volume values of the films in the related formula:

$$W = V/FxS \ (mm^3 \times Nm) \qquad (II.8)$$

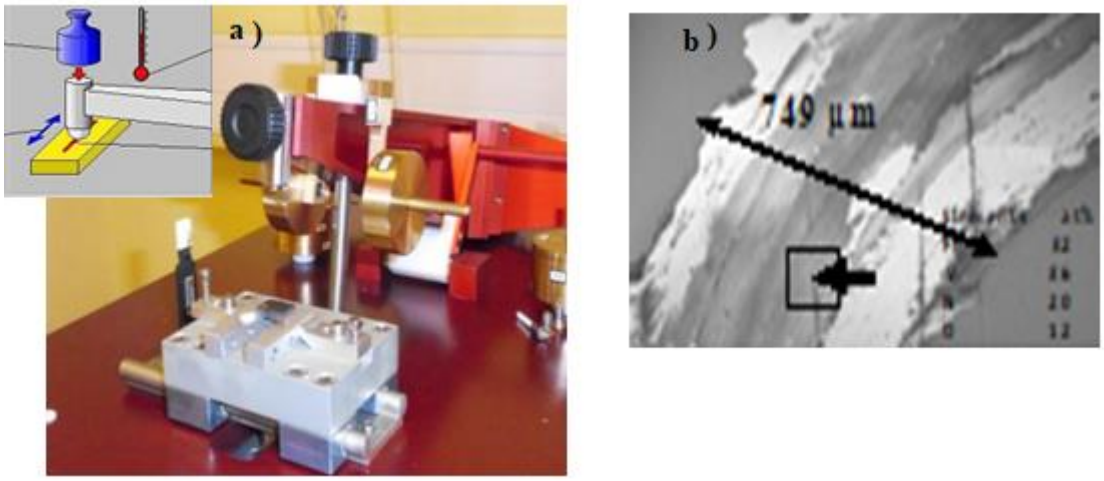

Figure II.22.a) Ball on disk tribometer (CSM, HIGH- TEMPERATURE TRIBOMETER), **b)**SEM image of wear track.

II.5. Conclusion

This chapter presents a review of deposition techniques in general, and the DC/RF magnetron sputtering in details since it used in our study of TiN, and TiZrN thin films, and the growth modes of the deposited thin coats, finally, the various experimental techniques for structural, morphological, mechanical, and tribological characterizations were presented. *Table II.3* summarizes the characterization techniques used during this study

Table II.3. Summary of the elaboration and characterization techniques used *in our work*

Propriety	**Technique**
Coatings	reactive R.F magnetron sputtering system
Structural	XRD
Morphology	SEM
Chemical Composition	EDS , WDS , XPS, RAMAN
Surface topography	AFM
Wetting and surface energy	Contact angle
Residual stress	Profilometer
Hardness and young s' modulus	Nanoindentation
Wear resistance	ball on disk tribometer (CSM, HIGH- TEMPERATURE TRIBOMETER)

References

[1] I. Ouadha, H. Rached, A. Azzouz-Rached, A. Reggad, D. Rached, Study of the structural, mechanical and thermodynamic properties of the new MAX phase compounds (Zr1-xTix) $_3AlC_2$, Computational Condensed Matter, 23 (2020) e00468.

[2] J.C. Slater, Atomic radii in crystals, The Journal of Chemical Physics, 41 (1964) 3199-3204.

[3] P. Blaha, K. Schwarz, G.K. Madsen, D. Kvasnicka, J. Luitz, wien2k, An augmented plane wave+ local orbitals program for calculating crystal properties, 60 (2001).

[4] J. Perdew, JP Perdew, K. Burke, and M. Ernzerhof, Phys. Rev. Lett, 78 (1997) 1396.

[5] S. Berri, D. Maouche, F. Zerarga, Y. Medkour, Ab initio study of the structural, electronic, elastic and magnetic properties of Cu_2GdIn, Ag_2GdIn and Au_2GdIn, Physica B: Condensed Matter, 407 (2012) 3328-3334.

[6] W.L. Bragg, The Crystalline State: The determination of crystal structures, by H. Lipson and W. Cochran, Cornell University Press, 3 (1876).

[7] H. Caliskan, P. Panjan, C. Kurbanoglu, 3.16 Hard Coatings on Cutting Tools and Surface Finish, in: M.S.J. Hashmi (Ed.) Comprehensive Materials Finishing, Elsevier, Oxford, 3 (2017) 230-242

[8] O.O. Abegunde, E.T. Akinlabi, O.P. Oladijo, S. Akinlabi, A.U. Ude, Overview of thin film deposition techniques, AIMS Materials Science, 6 (2019) 174-199.

[9] A. Jilani, M.S. Abdel-Wahab, A.H. Hammad, Advance deposition techniques for thin film and coating, Modern Technologies for Creating the Thin-film Systems and Coatings, 2 (2017) 137-149.

[10] K. Wasa, Sputtering phenomena, Handbook of Sputtering Technology, Elsevier, (2012) 41–75.

[11] A.H. Simon, Sputter processing, Handbook of thin film deposition, Elsevier (2018) 195-230.

[12] R. Bandorf, V. Sittinger, G. Bräuer, High power impulse magnetron sputtering-HIPIMS, Comprehensive materials processing (2014) 75-99.

[13] T. Tavsanoglu, Deposition and characterization of single and multilayered boron carbide and boron carbonitride thin films by different sputtering configurations, Doctoral dissertation, Ph. D Thesis, École Nationale Supérieure des Mines de Paris, 2009.

[14] E. Alfonso, J. Olaya, G. Cubillos, Thin film growth through sputtering technique and its applications, Crystallization-Science and technology, 23 (2012) 11-12.

[15] R. Pessoa, M. Fraga, L. Santos, N. Galvão, H. Maciel, M. Massi, Plasma-assisted techniques for growing hard nanostructured coatings: An overview, Anti-Abrasive Nanocoatings, (2015) 455-479.

[16] *http://www.semicore.com/images/photos/diagram-sputtering-process.png, DOI.*

[17] P.J. Kelly, R.D. Arnell, Magnetron sputtering: a review of recent developments and applications, Vacuum, 56 (2000) 159-172.

[18] S. Swann, Magnetron sputtering, Physics in technology, 19 (1988) 67.

[19] M.M. Waite, S.I. Shah, D.A. Glocker, Sputtering sources, SVC Bulletin, No. Spring, 2010 (2010) 42-50.

[20] I. Luciu, RF plasma synthesis and characterization of thin films for transparent conductors, Doctoral dissertation, Ph. D Thesis, University of Trento, 2012.

[21] M. Ohring, S. Zarrabian, A. Grogan, The materials science of thin films, Applied Optics, 31 (1992) 7162.

[22] L. Liljeholm, Reactive sputter deposition of functional thin films, Doctoral dissertation, Ph. D, Thesis, Acta Universitatis Upsaliensis, 2012.

[23] B.-S. Yau, C.-W. Chu, D. Lin, W. Lee, J.-G. Duh, C.-H. Lin, Tungsten doped chromium nitride coatings, Thin Solid Films, 516 (2008) 1877-1882.

[24] D. Magnfält, Fundamental processes in thin film growth: The origin of compressive stress and the dynamics of the early growth stages, Doctoral dissertation, Ph. D, Thesis, Linköping University Electronic Press, 2014.

[25] M. Ohring, Materials science of thin films, Elsevier 2001.

[26] R.F. Bunshah, C. Weissmantel, (Eds.), Handbook of hard coatings, Noyes publications Park Ridge, NJ, 3 (2001) 77-107.

[27] R. Aigner, Filter technologies for converged RF-frontend architectures: SAW, BAW and beyond, Topical Meeting on Silicon Monolithic Integrated Circuits in RF Systems (SiRF), IEEE, (2010) 136-139.

[28] P.H. Le, C.W. Luo, Thermoelectric and topological insulator bismuth chalcogenide thin films grown using pulsed laser deposition, Applications of Laser Ablation—Thin Film Deposition, Nanomaterial Synthesis and Surface Modification, (2016) 55-84.

[29] A. Anders, A structure zone diagram including plasma-based deposition and ion etching, Thin Solid Films, 518 (2010) 4087-4090.

[30] J.H. Cartwright, B. Escribano, C.I. Sainz-Díaz, Ice films follow structure zone model morphologies, Thin Solid Films, 518 (2010) 3422-3427.

[31] B.A. Movchan, A. Demchishin, Structure and properties of thick condensates of nickel, titanium, tungsten, aluminum oxides, and zirconium dioxide in vacuum, Fiz. Metal. Metalloved, 28 (1969) 653-660.

[32] J.A. Thornton, High rate thick film growth, Annual review of materials science, 7 (1977) 239-260.

[33] M.R. Ardigo, M. Ahmed, A. Besnard, Stoney formula: Investigation of curvature measurements by optical profilometer, Advanced Materials Research, Trans Tech Publ, 996 (2014) 361-366.

[34] J. Zhang, Z.-l. Wang, J. Liu, S. Chen, G.-y. Liu, Self-assembled nanostructures, Springer Science & Business Media, 2 (2003).

[35] C.R. Brundle, C.A. Evans, L. Wilson, S. Wilson, G. Wilson, Encyclopedia of materials characterization: surfaces, interfaces, thin films, Gulf Professional Publishing, 1992.

[36] G.H. Michler, Scanning electron microscopy (SEM), Springer, 2008.

[37] M. Joshi, A. Bhattacharyya, S.W. Ali, Characterization techniques for nanotechnology applications in textiles, 2008.

[38] J.L. Liu, S. Bashir, Advanced nanomaterials and their applications in renewable energy, 2015.

[39] A. Zairi, Elaboration et Caractérisation de revêtements à base de nitrure de chrome par pulvérisation cathodique magnétron en condition réactive: propriétés mécaniques et tribologiques, Doctoral dissertation, Ph. D, Thesis, Paris, ENSAM, 2013.

[40] *http://www.mcswiggen.com/graphics/TechNotes/WDSvsEDS/EDSschematic.gif*.

[41] J.A. Zapata Correa, J. Rodriguez-Viejo, Epitaxial thin film growth and study of charge and mass transport properties of mixed ionic electronic conducting $GdBaCo_2O_{5+\delta}$ (GBCO), Universitat Autònoma de Barcelona, 2016.

[42] I. Rahil, Élaboration et caractérisation de revêtements à base de nitrure de Chrome, carbonitrure et carbure de Titane élaborés par pulvérisation magnétron, Doctoral dissertation, Ph. D, Thesis, Paris, ENSAM, 2013.

[43] B.D. Ratner, D.G. Castner, Surface properties and surface characterization of biomaterials, Biomaterials science, Elsevier (2020) 53-75.

[44] I. Johansson, P. Somasundaran, P. (Eds.), Handbook for Cleaning/decontamination of Surfaces, Elsevier, 2007.

[45] L. Aissani, A. Alhussein, A. Abdelhak, C. Nouveau, E. Zgheib, A. Belgroune, M. Zaabat, R. Barille, Relationship between structure, surface topography and tribo-mechanical

behavior of Ti-N thin films elaborated at different N_2 flow rates, Thin Solid Films, 724 (2021) 138598.

[46] M.T. Riosbaas, K.J. Loh, G. O'Bryan, B.R. Loyola, In situ phase change characterization of PVDF thin films using Raman spectroscopy, Sensors and Smart Structures Technologies for Civil, Mechanical, and Aerospace Systems, International Society for Optics and Photonics, 9061 (2014) 235-245.

[47] J. Álvarez-García, V. Izquierdo-Roca, P. Pistor, T. Schmid, A. Pérez-Rodríguez, Raman spectroscopy on thin films for solar cells, Advanced Characterization Techniques for Thin Film Solar Cells, 2 (2016) 469-499.

[48] H. Manasevit, W. Simpson, The Use of Metal-Organics in the Preparation of Semiconductor Materials: II. II–VI Compounds, Journal of the Electrochemical Society, 118 (1971) 644.

[49] L. Aissani, A. Alhussein, C. Nouveau, L. Ghelani, M. Zaabat, Influence of film thickness and ArN2 plasma gas on the structure and performance of sputtered vanadium nitride coatings, Surface and Coatings Technology, 378 (2019) 124948.

[50] S.P. Fu, Investigation of the Wetting Behavior of Cerium Dioxide Coatings, Doctoral dissertation, Ph. D, Thesis, University of Illinois at Chicago, 2016.

[51] F. Rios, Hydrophobicity and its applications, New Mexico State University 2011.

[52] *https://th.bing.com/th/id/R.c27da8420fa369f3b278e0a2b511dda6?rik=NmIjdGB0UfOmRw&riu=http%3a%2f%2fwww.iue.tuwien.ac.at%2fphd%2fsingulani%2fimages%2fPicture37.png&ehk=9TD*lynH0brtLOSBSOAKXo3xAvHrAPDctKD4BP8zcdGs%3d&risl=&pid=ImgRaw&r=0.

[53] X. Huang, Mechanical characterization of thin film materials with nanoindentation measurement and finite element analysis, Rutgers The State University of New Jersey-New Brunswick, 2005.

[54] E. Broitman, Indentation hardness measurements at macro-, micro-, and nanoscale: a critical overview, Tribology Letters, 65 (2017) 1-18.

[55] H. Wang, L. Zhu, B. Xu, Principle and Methods of Nanoindentation Test, Residual Stresses and Nanoindentation Testing of Films and Coatings, Springer, (2018) 21-36.

[56] J. Halling, Principles of tribology, Macmillan International Higher Education, (1978) 401.

Chapter III.

Structure, surface topography and tribo-mechanical behavior of TiN thin films

III.1. Introduction

Titanium nitride (TiN) is the most basic transition-metal in the refractory materials group. The wide wholesome applications concern TiN coatings in industrial purpose, as wear-resistant coatings for cutting tools [1], automobile parts [2], in bio-implants [3], and also for the decorative uses [4], that can be attributed to their excellent mechanical proprieties especially high hardness, great toughness, and good elastic modulus [5]. Titanium nitride coatings also exhibited high wear, and corrosion resistance, biocompatibility [6], as well as the hydrophilic characteristics [7], besides the excellent chemical stability [8], and the golden color [9]. A wide variety of coating methods such as laser-assisted nitriding [10], plasma nitriding [11], chemical vapor deposition (CVD) [12], and physical vapor deposition (PVD) [9] have been used to deposit TiN coatings. Amongst PVD techniques, we cite the cathodic magnetron sputtering that has been used around the 1970s, vis-à-vis to other coating technologies.The method is prominent, compatible, and could enhance coating qualities, as well as it is effective, economic, and permit to provide various classes of coatings in a wide field of applications, and the most important is to create smooth coatings with defect-free [13].

In this chapter, we try to present the relationship between structure, surface topography, and tribo-mechanical behavior of TiN thin films elaborated at different nitrogen (N_2) flow rates in order to identify the effect of different nitrogen percentages on TiN thin films proprieties. We produced TiN nitride films using reactive magnetron sputtering of circular titanium target of 200 mm diameter and 6 mm thick (99.99 % purity)on Si (100) wafers, glasses, and Ti6Al4V substrates with a surface roughness of about (Ra ≈ 30 nm), measured by an optical Profilometer.

Our produced films deposited under different N_2 partial pressures and flow rates varied from 0 Pa (0 % N_2) to 0.12 Pa (corresponding to 30 % N_2 of mixture atmosphere).Firstly, we ultrasonically cleaned the substrates in acetone and ethanol, dried in air, and then fixed them on the substrate-holder. The distance between the Ti target and the substrates is about 100 mm. The evacuated deposition chamber down to 2×10^{-4} Pa, later a mixture of both Ar (99.99 % purity) and N_2 (99.98 % purity) gases were separately injected into the chamber. Before the film deposition, the Ti target was etched by Ar ions bombardment for 10 min. To increase the adhesion of TiN film on the substrate, Ti interlayer (≈ 60 nm of thickness) was firstly

deposited by applying 150 W to the Ti target in a pure Ar atmosphere of 50 sccm for 10 min. Then, TiN films were deposited at a fixed working pressure of 0.4 Pa by applying 550 W to the Ti target for 180 min. The rotation of the substrate-holder was set at 10 rpm. The deposition conditions were summarized in *Table III. 1*:

Table III.1. Deposition conditions for TiN films deposited with different nitrogen percentages.

Percentage (Ar, N_2)	(30 %, 70 %), (75 %, 25 %), (80 %, 20 %), (85 %, 15 %), (90 %, 10 %), (95 %, 5 %), (100 %, 0 %),
Applied Tension to Ti Target	-900 V
Distance Target-substrate	100 mm
Time	180 mn.
Pressure	0.4 Pa.
Etching (Si(100), glass, Ti6Al4V)	5 mn
Ti-interlayer	150 W, Ar (50 sccm), 10 min,0.4 Pa.

III.2. TiN structure presentation

Figure III.1 show the face-centred cubic crystal lattice of TiN (rocksalt-TiN) optimized from simulation. The atomic positions for Ti atoms are (0,0,0), (0,1/2,1/2), (1/2,0,1/2) and (1/2,1/2,0) while (1/2,1/2,1/2), (1/2,0,0), (0,1/2,0),) and (0,0,1/2) for N atoms. The lattice parameter obtained from DFT calculation is a= 4.255 Å. It is interesting to note that our calculated lattice constant is slightly higher than the previous calculated values (4.242 and 4.210 Å) by *S.Yu et al.* [14], and *G. Sai Gautamet al.* [15].

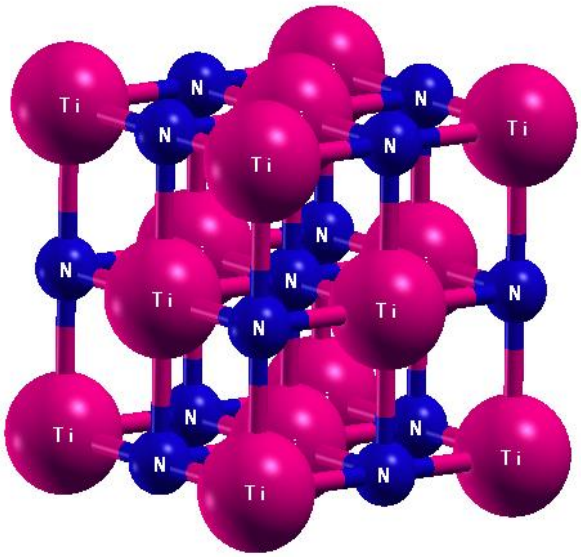

Figure III.1. Schematic view of the FCC-TiN atomic configuration.

III.3. Elemental chemical composition

(EDS, WDS) and XPS analyses were carried out on these coatings to specify their chemical composition. *Table III.2* shows the chemical composition of TiN films deposited under various nitrogen flow rates. We can see that the XPS chemical concentration is close to that obtained by (EDS, WDS).

A low N/Ti ratio of (0.17) corresponding to 5 % of N_2 , and we noticed the existence of higher concentration of Ti and a lower nitrogen content as obtained in previous work for TiN coatings [16]. The increase in the N_2 flow rate from 5 to 30 % , resulting a gradual increase in the nitrogen content from 14 to 54 at.% and a decrease of titanium content from 83 to 43 at.%. The decrease of titanium with the addition of nitrogen was earlier declared for TiN coatings in our previous work [17], and also for *S. Grosso et al.* [9] . The stoichiometric data for the TiN phase confirmed by the obtained N/Ti ratio that ranged between 0.98-1.04. *N. Arshi et al.* [18] showed that the N/Ti ratio in the TiN_X film initial increased and then decreased with increasing argon flow rate. The stoichiometry of the TiN films taken by (EDS; WDS) was found to be 0.2, 1, 0.98, and 0.7 at argon flow of 5, 10, 15, and 20 %, respectively. A lower amount of oxygen in the range of 2-5 at.% (*Table III.2*) was detected for all TiN thin films, because of the residual oxygen in the vacuum chamber and the affinity of Ti with oxygen (during deposition or post-deposition).

Table III.2. Chemical composition and structural properties of the TiN films

N_2 partial pressure Pa	N_2 gas flow	Chemical composition at.%				Film thickness µm	Lattice strain %	Grain size nm
		N	Ti	O	N/Ti			
0	0	0	97	3	0	1.80	0.0303	87
0.02	5	14	83	3	0.16	1.65	0.0252	80
0.04	10	21	74	5	0.28	1.54	0.8402	79
0.06	15	32	65	3	0.49	1.45	0.6369	77
0.08	20	48	49	3	0.98	1.26	0.7662	64
0.10	25	50	48	2	1.04	1.10	0.7920	75
0.12	30	54	43	2	1.26	0.97	0.5360	79

In order to verify the results acquired by EDS analysis of the chemical composition were carried out by XPS. Before the analysis, the argon etching was applied on whole samples to remove the surface oxide and superficial contaminant in films. *Figure III.2* shows typical XPS spectra Ti2p and N1s core levels of thin films prepared at different nitrogen flow rates. At 10 % N_2, the $Ti2p_{(3/2,\ 1/2)}$ corresponding to TiN is located at about 457.9and 459.43 eV [19] (*Fig. III.2.a*).

The N1s spectrum is located at a binding energy of 397.10 eV (*Fig. III.2.b*). Through Gaussian fitting analysis, peaks at 396.45 and 397.18 eV correspond to Ti-N bond [20]. At 20 % of N_2, we notice a significant decrease in the Ti2p and N1s spectra intensities and changes in the Ti area shape with a negative shift of Ti2p. These changes suggest that Ti-N bond exists in the films and the percentage of TiN phase increases with increasing N content. On the other hand, the N1s peak gradually increases, indicating that the number of Ti-N bonds increases gradually because of the large number of N atoms occupying the interstitial sites. Titanium is represented by a large area, which means three main states of Ti-N (456.18, 457.41 eV) and Ti-O (458.30 eV) [21] corresponding to TiN and TiO_2 (*Fig. III.2.c*). The N1s spectra, shown at 396.6 and 397.80 eV (*Fig. III.2.d*), can be assigned to Ti-N and Ti-O-N bonding energies of titanium nitride and oxide phases [22].

These results mean that titanium nitride and oxide coexist in the film. This indicates that the Ti-N binding is strongly formed in the Ti-N films with increasing of nitrogen content and

confirms the presence of titanium nitride phase in films deposited at high nitrogen flow rate. *Y.L. Jeyachandran et al.* [23] found that the XPS survey spectra of the films of thickness 42–153 nm prepared at the 0.5 % of N_2 concentration exhibited a characteristic Ti2p, O1s, and N1s peaks at 528.2, 456.5, and 396.2 eV, respectively.

Despite the very little content of oxygen, the Ti-O binding energy appeared in the XPS spectra. All Ti-N thin films contained a low amount of oxygen in the range of (2-5) at.%. At 10 % N_2, the high titanium concentration in the TiN film hides the appearance of the oxygen bond (Ti-O) in front of the titanium and nitrogen. However, with increasing the nitrogen flow rate, both titanium concentration and film density gradually decrease that facilitate the mobility of the oxygen atoms to take place of nitrogen during deposition and favourites the formation of Ti-O and Ti-O-N binding energies.

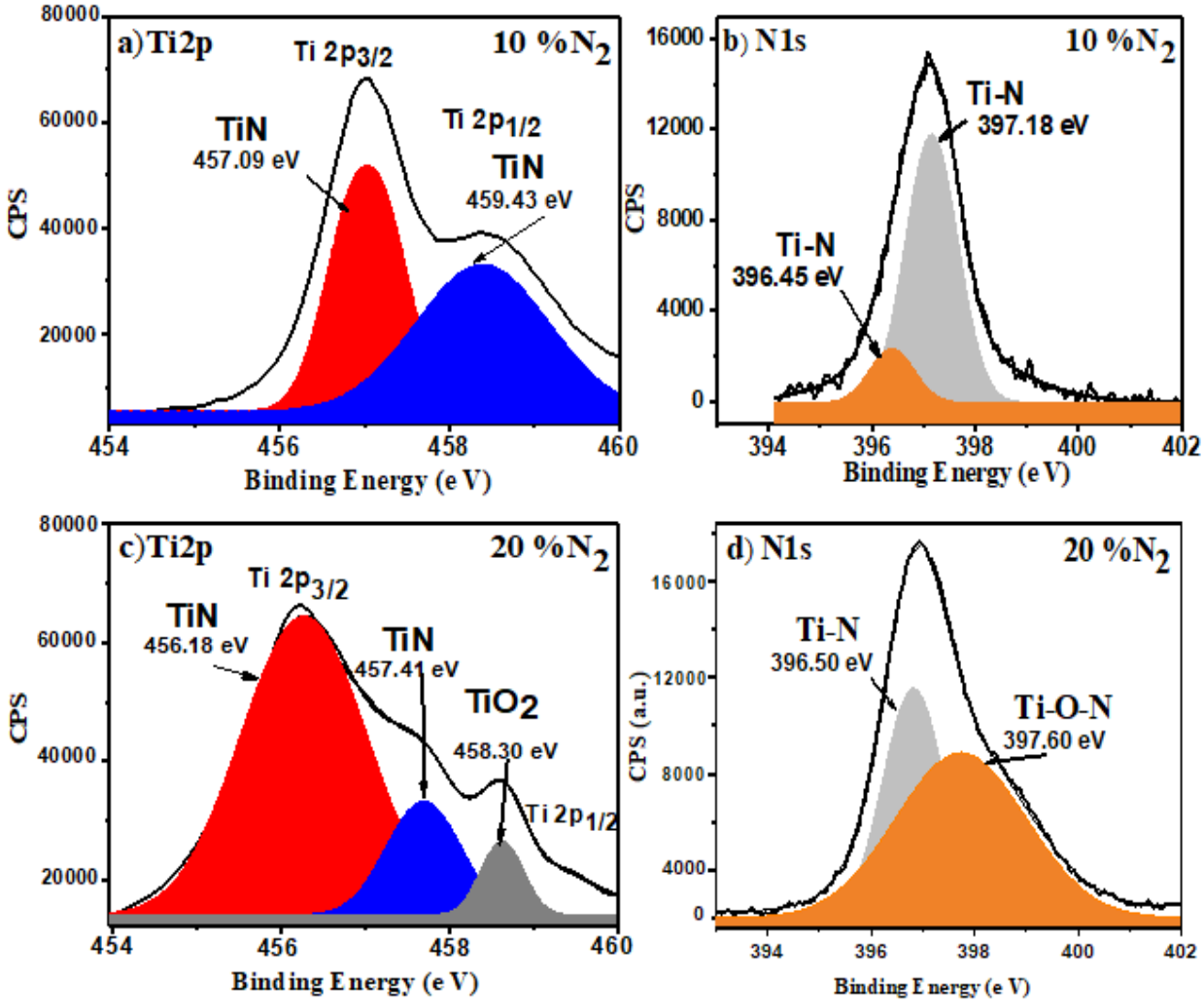

Figure III.2. XPS spectra of TiN films deposited at 10, and at 20 %N_2**: a)** Ti2p , **b)** N1s,**c)** Ti2p , **d)** N1s.

III.4. Crystalline structure

XRD analysis were performed on TiN films deposited on Si (100) in order to determine the crystal structure and deferent phases present in the titanium nitride thin films as function of nitrogen content as shown in *Figure III.3*. Very sharp diffraction peaks of *α*-(Ti+N) and Ti_2N at 40.8°, 43.1°, 44.7°, and 46.7°of TiN thin film deposited at a low nitrogen flow rate of 5 %, suggests that the film possessed a low strain (ε = 0.0252), and a slight decrease in the lattice parameter (a_{TiN}= 0.4205 nm). For the TiN films with a nitrogen content in the range of 21–32 at.% (corresponding to 10 and 15 % of N_2), X ray diffraction patterns present peaks at 36.85°, 42.19°, 61.88°, and 74.01° corresponding to (111), (200), (220) and (311) planes of the FCC-TiN phase. The peaks at 40.84°, 43.01°, and 78.80° correspond respectively to the (111), (200), and (220) planes of a tetragonal-Ti_2N phase. At 20 % N_2 (48 at.% of nitrogen), the TiN film exhibits (111) plane growth direction with a regular reduction of the (200) diffraction peak. It is known in reactive sputtering that the deposition rate commonly decreases drastically at a high adequately partial pressure level of the active gas to form a compound on the target surface identified as the poisoning of target phenomena [24], that could be justify the small diffraction peaks obtained for films deposited at significant N content (at 30 at.% of nitrogen) with a decrease in deposition rate, which is observed in other binary transition metal nitrides [25, 26].

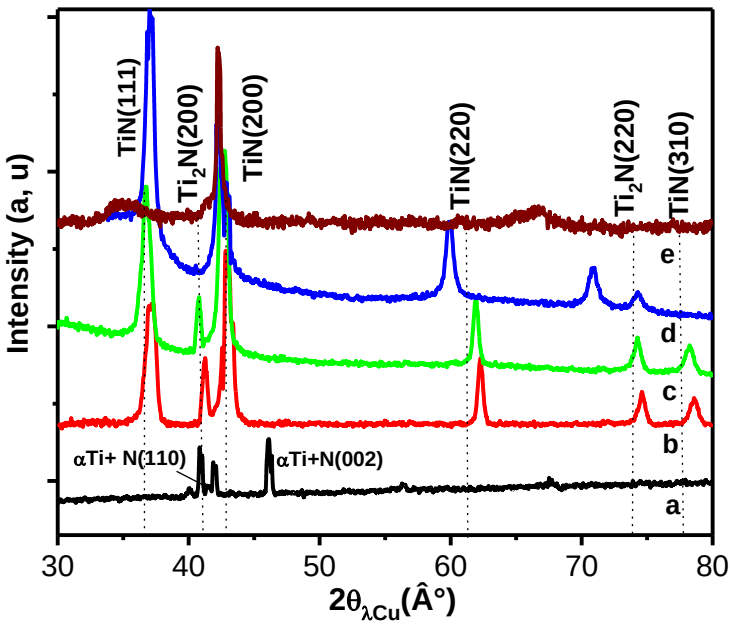

Figure III. 3. XRD patterns of the TiN films deposited at**: a)** 5 %N_2**, b)** 10 %N_2, **c)** 15 %N_2 , **d)** 20 %N_2 , and **e)** 30 %N_2

It has been noted that the intensity and the lattice strain of the predominant (111) plane increase by increasing nitrogen content. The lattice constant slightly increases when the N atoms can preferentially take the interstitial sites of TiN lattice [18, 27, 28]. *D. Munteanu et al*. [29] found that XRD diffraction patterns of the TiNx films, deposited by reactive D.C magnetron sputtering, on the polished (AISI M2) high-speed steel by varying nitrogen content from 0 and 55 at.%, exhibited the growth of the hexagonal α-TiN phase with strong (002) orientation for low nitrogen rate when the N atoms are distributed into octahedral sites. For nitrogen content ranged between 20 and 30 at.% they noticed the appearance of the ε-Ti_2N phase with (200) orientation. More raising the nitrogen content, the δ-TiN phase was obtained.

Other hind, TiNx films obtained by *Y.L. Jeyachandran et al.* [23] at a pressure of 0.5 Pa, showed the presence of mixture with oxynitride (TiOxNy), and oxide (TiO_2) phases at low nitrogen flow rate. The crystalline films presented reflections corresponding to the (111), (200), and (220) orientation of the Golden-colored stoichiometric of cubic-TiNat high nitrogen flow rate.

Using the FWHM, we can determine the average crystallite size of TiN phase with the help of Scherrer's equation [29-31]. *Figure III.4* illustrates the evolution of 1/β versus cosθ for the TiN phase. We noticed that the value of 1/β increases with the increasing cos θ values. As known as the Scherer plot, the average crystallite size can be calculated from the slope of the graph, which was found 80 nm in the film deposited at low nitrogen flow rate of 5%. Generally, we found that the average crystallite size of TiN phase was between 39.01 and 34.12 nm, which is in agreement with the results reported by *X. S. Wan et al*. [32] for the CrN coatings. According to *D. Munteanu, et al.* [33] at a moderate percentage of Nitrogen between 20 and 30 at.%, the diffraction peaks become broader indicating that small sizes grains and high micro strains are developed.

F. Eistner et al. [34] prepared Titanium nitride layers on silicon substrates by magnetron sputtering at a constant temperature of 200 °C and working nitrogen partial pressures (PN_2) varied from 0.001 to 0.36 Pa. The crystallite size reduced from 80 down to 64 nm when the amount of nitrogen increased from 14 to 48 at.%. In contrast crystallite size of TiN thin films reported by *A. Gelali et al*. [35] was found to increase rapidly from 25.66 to51.30 nm with increasing substrate temperature from 200 to 400°C.

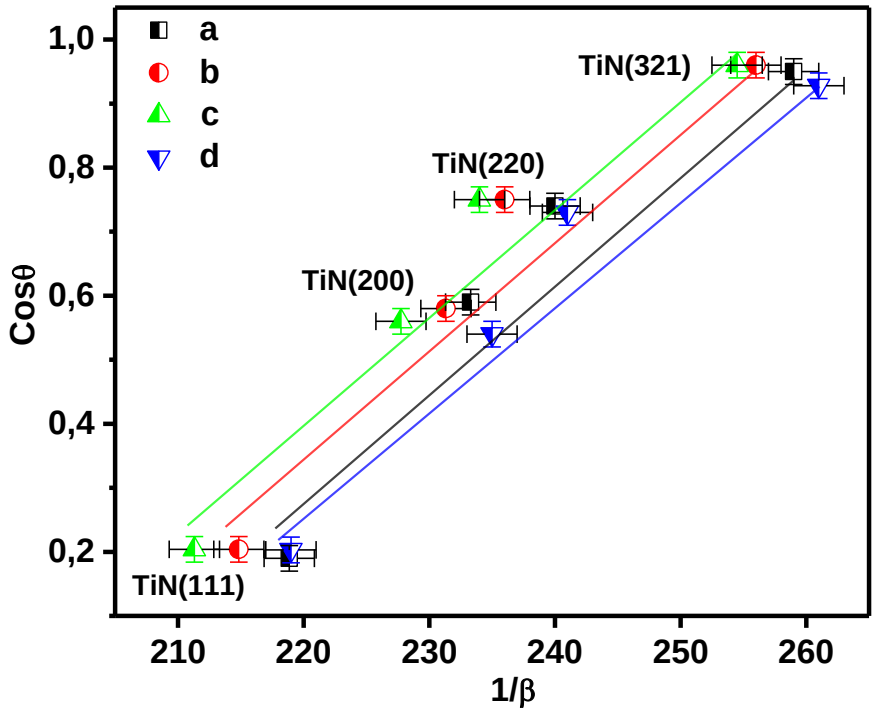

Figure III.4. Scherrer plot for TiN films deposited at**: a)** 5 %N_2,**b)** 10 %N_2, **c)** 15 %N_2, and **d)** 20 %N_2

III.5. Morphology

SEM and AFM are good complementary techniques used to determine the morphology and the roughness of hard thin films. *Figure III.5* shows the morphology of the TiN films deposited under 10, 15, 20 and 30 % of N_2. It can be seen that both Ti under layer and Ti-N film exhibited columnar structure. Approximately, the large columnar grains have about 100 nm of width in pure Ti layer, which is larger than that in the TiN.

A notable deference in surface roughness, typical surface, cross-section images and topography of the films deposited at different N_2. The main film's characteristics, such as thickness and crystallite size are arranged in *Table III.2*. The TiN film showed a columnar and packed structure consisting of well-separated grains with obviously a spherical form at 10 % of N_2. A rough and domed form (Ra = 12 nm) is related to the transition zone between T and I zones of Andres's structural zone model [36]. This is owing to the mutual interference of the intermediate Ti_2N and TiN phases. A reduction in surface roughness was detected (Ra = 5 nm.) with increasing nitrogen content in TiN film lead to a decrease in grain size due to the dense structure and the smooth surface. *K. Chakrabarti et al.* [37] found that the based TiN films fabricated at nitrogen flow rates of 10 and 20 sccm showed a decrease in the roughness from 2.3to 1.8 nm, respectively, due to the existence of more nuclei [38].

Besides, at high nitrogen flow rate, the deposited TiN thin films containing high Nitrogen showed a slight decrease in film thickness, this reduction accompanied with a decrease in the deposition rate generated by the less ionization and sputtering yield of N_2. Moreover, the target poisoning effect in reactive sputtering decreased the deposition rate [39].The same phenomena was noticed by *Y. W Lin et al.* [40] for (Ti,Zr)N film produced using R.F magnetron sputtering system, were films thickness reduced from 403 to 147 nm when N_2 ration increases from 1 to 7 sccm. *J.H. Huang et al.* [41] found that the nanocrystalline TiN films deposited on Si(100) wafers by means of unbalanced magnetron sputtering system, showed variation in film thickness as varying nitrogen flow rate ranging were thickness changed from 253 to 140 nm, for Nitrogen flow rate changed from 0.25 to 1.75 sccm. This decrease accompanied with significant reduce in deposition rate from 6.3 to 3.5 nm/min. *N. Arshiet al.* [18] found that the grain size along the sample surface showed a sharp decrease from 22 to 17 nm as the argon flow rate increased from 0 to 9 sccm.

Nevertheless, at elevated nitrogen flow rate (30 % N_2), the surface roughness increased to the average Ra = 11 nm with a columnar structure corresponds to the transition zone between T and I zones of Andres's structural zone model [36]. A columnar-type structure morphology for all films was reported by *D. Munteanu, et al.* [33], lying in the transition zone between T and I zones, as the N content increases the columns become thicker (in the columnar structure zone). The surface's roughness showed a decrease with the increase in the N content. The refinement in grain size illustrates the detected densification of the originally columnar coating structure as well as the smoothening of the surface.

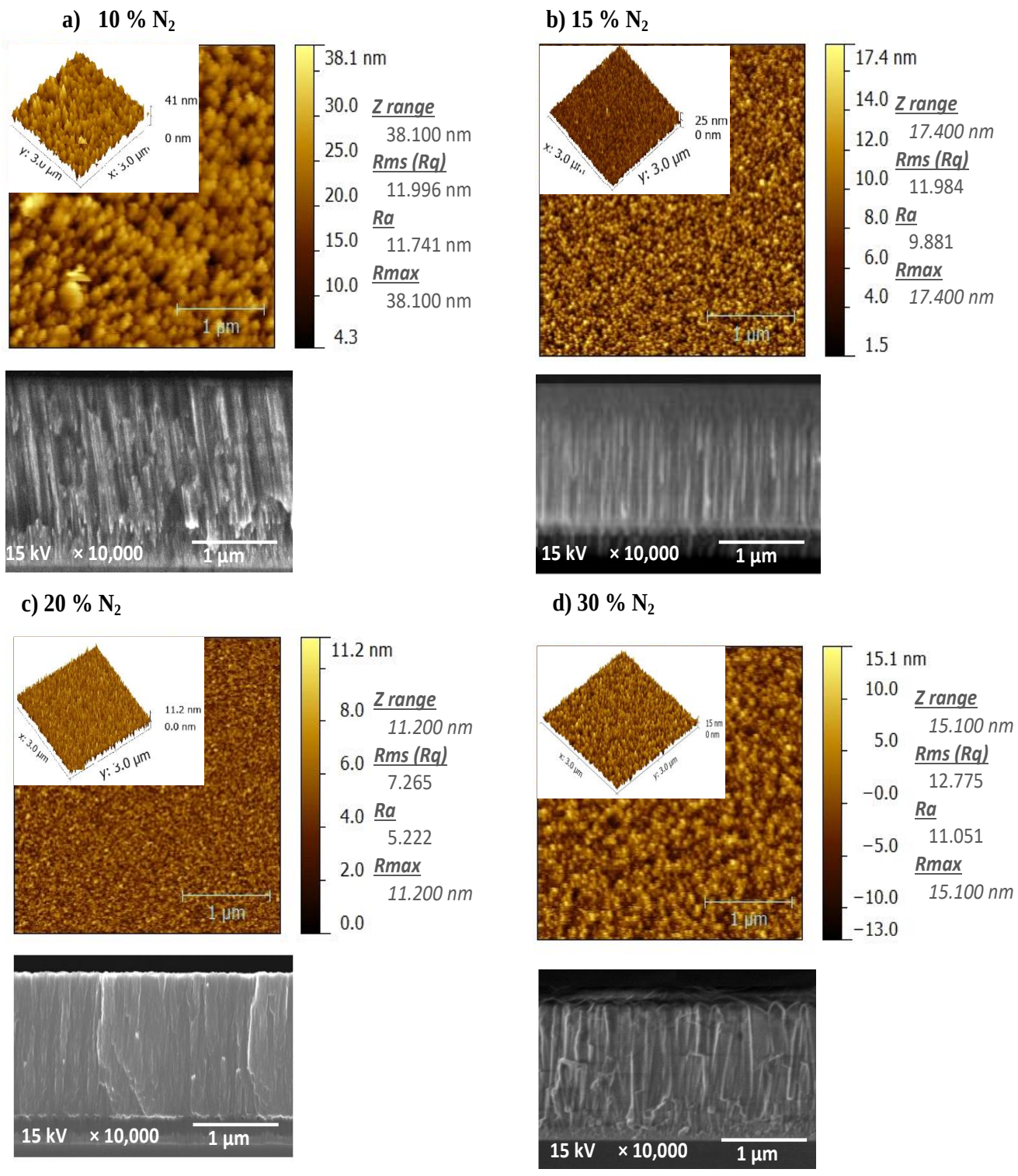

Figure III.5. (2D, 3D) AFM and cross section SEM images of the TiN films deposited at**: a)** 10 %N_2, **b)** 15 %N_2, **c)** 20 %N_2, and **d)** 30 %N_2

III.6. Wetting behavior and surface tension investigations of TiN films

The wetting of ceramics by liquids is an important aspect of many materials technologies. The wettability of solids by liquids is conventionally described by the equilibrium contact angle θ which encloses the liquid surface and solid-liquid interface. The angle θ is defined by the Young equation relating it to the characteristic interfacial energy of the system as mentioned in [42] *Chapter II* .

In this study, we adopted on the method of contact angle to estimate the interaction between droplet water and film surface. Samples were cleansed with ethanol in an ultrasonic bath for 10min. The contact angles of droplets water falling on the TiN films, deposited on glass substrates, were calculated at ambient temperature. *Figure III.5* shows the variation of the film hydrophobicity and wettability as a function of the nitrogen flow rates. As we see, the initial contact angles between water-droplets and film surfaces deposited at different N_2 flow rates of 0, 10, 15, 20 and 30 % were 57.6°, 86.4°, 94.6°,108.3°, and70.1°, respectively. All contact angles were about zero, after approximately one minute of exposure time. Those issues clearly demonstrated that the films deposited between 10 and 20 % N_2 showed a high degree of wettability and its hydrophobicity developed with the rise of the nitrogen content in the film.

We assume that increasing the nitrogen flow rate in plasma from 20 to 30 % led to a decrease in the contact angle from 108° to 70° corresponding to the surface tension change from 18.8mN/m to 11.2mN/m, due to the low surface roughness (*Fig. III.7*). The surface tension decreases when the growth mode changes from smooth to rough surface. Accordingly, the main plane is determined by the critical competition between the film growth and the surface tension, which could be interesting for certain applications. *S. C. Liao, et al.* [43] found that TiN (80 nm) deposited on medical grade Ti6Al4V substrate using a reactive HiPIMS technique with the electrode distance and the N_2/Ar flow 2/35, a contact angle of 73.2° ± 0.8.

V. Karagkiozaki et al. [44] confirms that the stoichiometric ratio and surface roughness of TiNx films have an effect on its wetting proprieties, indicating that the TiNx films grown by D.C reactive magnetron sputtering on Si (100) wafers were hydrophilic. Also, same behaviors was detected for other transition metal nitrides were *P. Pateletet al.* [45] declared that Zirconium nitride thin films deposited at (Ar:N_2) gas ratio of (20:20) sccm by magnetron sputtering showed a high contact angle of 99.5° which confirms that the produced film has a hydrophobic property.

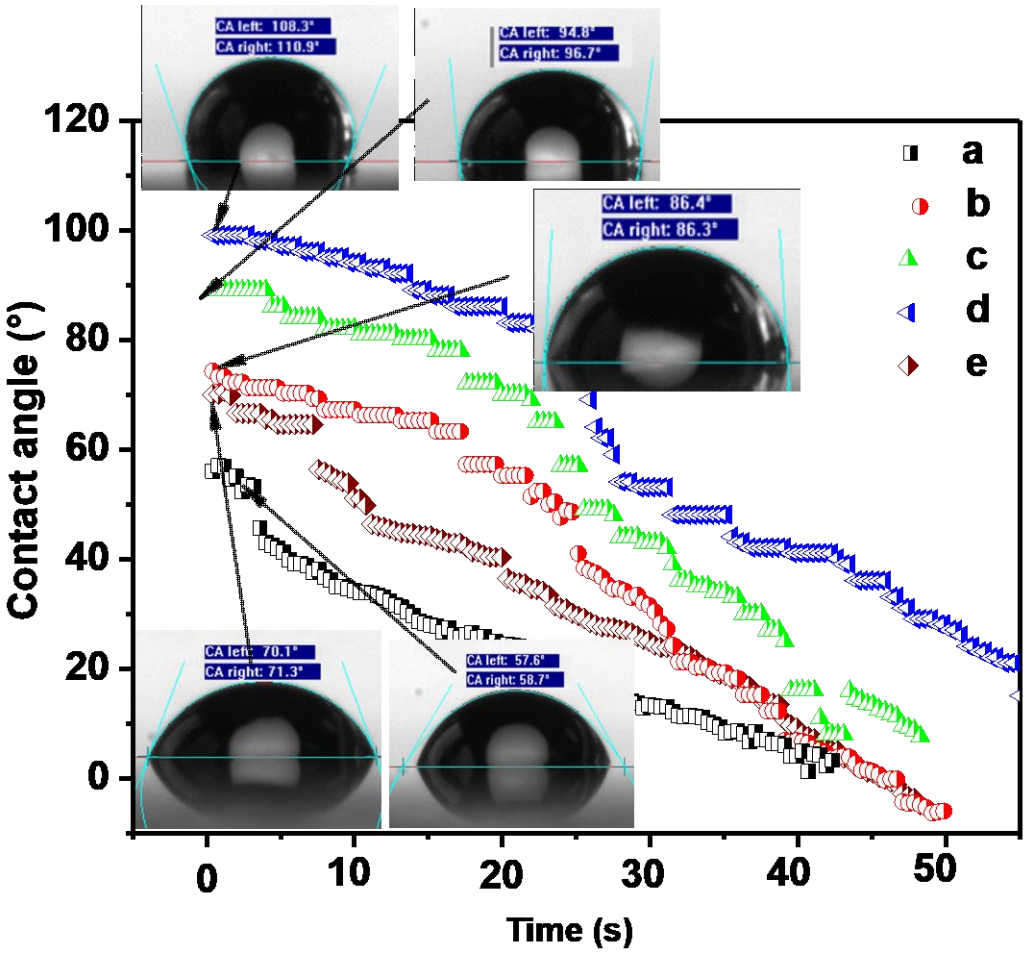

Figure III.6. Evolution of wetting proprieties of TiN films during the deposition at**: a)** 5 %N_2, **b)** 10 %N_2, **c)** 15 %N_2, **d)** 20 %N_2, and **e)** 30 %N_2.

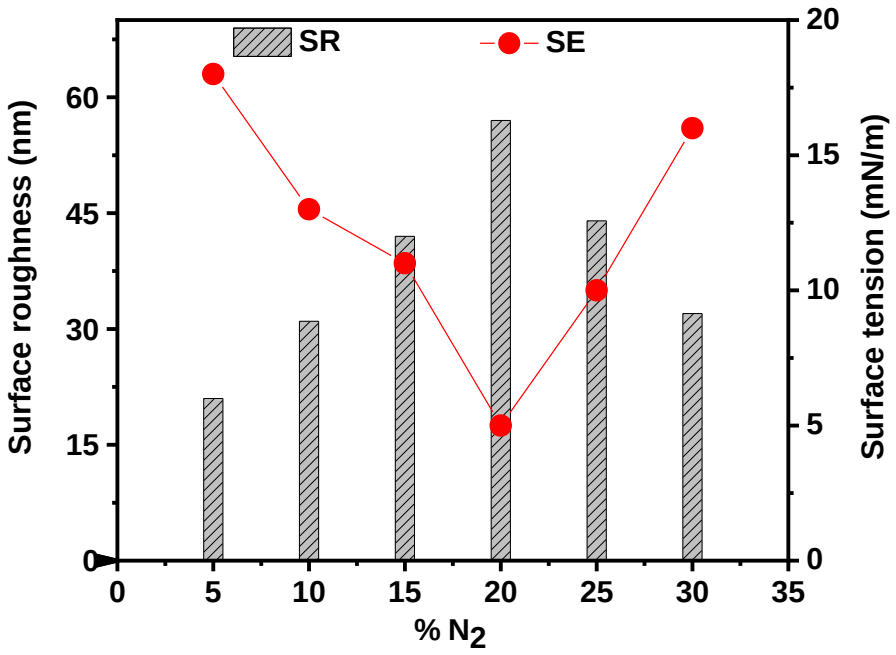

Figure III.7. Surface roughness and surface tension for water-droplets of TiN deposited at different N_2 flow rates.

III.7. Mechanical properties

III.7.1. Residual stress

The energy of the condensing species during a physical vapor deposition procedure is the most influential single parameter which specifies growth at thermal energies of smaller than 1 eV typically produces films under tensile stress, while deposition at energies of some tens of eV normally delivers films under compressive stress [46].

The residual stresses formed in the TiN films sputtered under various nitrogen flow rates, shown in *Figure III.8*. Tensile residual stress of 0.80 GPa was obtained for the pure titanium film. A raise in the compressive residual stress accompanied with increasing nitrogen flow rate from 5 to 30 % N_2. The change from tensile to compressive residual stress is associated with the growth mechanism and the microstructure. It can be seen from *Figure III.3* and *Table III.1*, the shifts in the predominant plan and the reduction of grain size play an important role in the evolution of residual stress. The decrease in grain with the increase of nitrogen content and (111) TiN became the predominant plane, which is the close-packed plane having the highest surface energy [30, 47]. The crystal densification impact and the influence of competitive grains growth with diverse orientations generated the change from tensile-to-compressive transition [30]. The dens films structure acquired from the ordinance

of atoms in the interstitial sites and annihilation of defects accompanied by the increase in nitrogen content. From the other side, the insertion of additional atoms in the film becomes more hard with small grains, thus tensile stress drops and slowly converts to compressive stress [48].

The films sputtered at 5 % N_2 showed compressive stress of -0.49 GPa, which increased continually to achieve the highest value of –2 GPa in the films sputtered in the range from 15 – 20 % of N_2 (*Fig. III.8*).The same phenomena were observed by *F. Vaz et al*. [49] for TiNx thin films prepared by D.C. reactive magnetron sputtering, the increase in nitrogen content from 30 to 55 at.% followed by lattice distortion and the formation of the **δ**-Ti phase offered an increase in residual stresses and thus a better stable and energetically favorable structure is expected. However, residual stress reduced down to -1.8 GPa with increasing nitrogen flow rate more than 20 %. This decrease is due to the increase in the grain size, which leads to the enhancement of the atom movement and the relaxation of the structure density [50, 51].
J.-H. Huang et al. [41] found that for all nitrogen flow rates, TiN thin films possess a high residual stress ranged from 8.1 to 10.1 GPa, showing that the increasing of residual stress is expected to ion bombard that affected lattice defects, the high residual stress, which indicates high defect density.

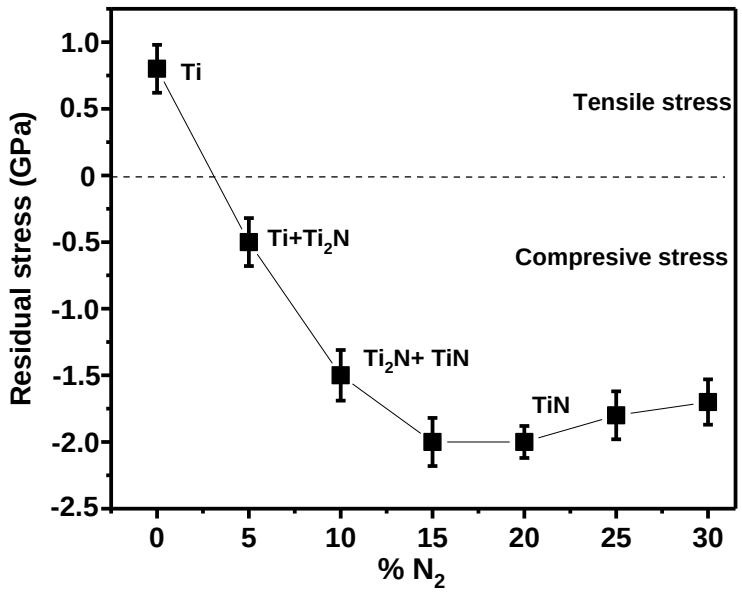

Figure III.8. Evolution of residual stress generated in the TiN films deposited at different N_2 flow rates.

III.7.2. Nanoindentation measurements

Nanoindentation tests were carried out on TiN films coatings deposited on glass substrates. Hardness (H), Young's modulus (E), (H/E), and (H^3/E^2) of TiN films as a function of the nitrogen flow rates are presented in *Figure III.9*. Thus, the hardness and Young's modulus of films, deposited at ≤ 5 % of N_2 are relatively low because of the low density of structure. Increasing the nitrogen content, H and E of TiN films increased significantly. Increasing nitrogen content, H and E of TiN films notably enhanced. At 20 % of N_2 films exhibited the highest hardness and Young's modulus of (27.78 ± 0.11) GPa and (304.8 ± 10.6) GPa, respectively, due to the fine grain size, lower roughness, and increased compressive residual stress which blocks the dislocation and thus strengthens the coatings, according to the *Hall-Petch* relation [52].

The large amount of the interstitial located nitrogen in the titanium matrix (about 48.5 at.%) led to form new hard compounds and solid solutions in the structure and generated high strain due to the lattice distortion [53] (*TableIII.1*). Nonetheless, the results showed clearly that the main hardening mechanism was related to the nitrogen concentration. However, when the nitrogen flow rate increased above 25 %, the decrease in the coating hardness was mostly caused by the reduction of film thickness (from 1.26 to 0.97 μm). The pollution of the Ti target during the deposition process could contribute to this softening behavior.

Moreover, the increase of the crystallite size (from 17 to 37 nm) and the stress relaxation (-1.8 GPa) seem to have a negative effect on the mechanical properties. *D. Munteanu et al.* [33] found that the increase in nitrogen content makes the films of TiNx samples deposited by reactive D.C magnetron sputtering, onto polished high-speed steel (AISI M2) and silicon substrates convert harder, where the hardness value ranges from about 8 GPa for pure titanium, up to 27 GPa for an optimal nitrogen content of 30 at.% (*Fig. III.9.a*).

Correlated that increase in hardness to lattice distortions affect the reduction in dislocations motion. The two harder samples are those that seem to reveal the presence of the ε-Ti_2N phase which play as a hardening factor, corresponding to 20 and 30 at.% N, where the initial hardening for the lowest N contents is the result of the distortion in the α-Ti lattice, due to N incorporation.

Y.-W. Lin et al. [40] reported that the hardness of spurted nanostructured based TiN thin films by radio frequency magnetron sputtering increase from 17.1 GPa at 1 sccm to a maximum value of 37.5 GPa at 4 sccm following the decrease in grain size from 19 to9nm then the hardness decrease to 24.4 GPa at 7 sccm with the increase of grain size to 12 nm. Assume that the improved hardness delivered by based TiN coatings is from the solid solution strengthening mechanism.

Other hind, the hardness is strongly related to the strength covalent (N-O) and ionic (Ti-N, Ti-O-N) binging energies that formed in the crystals. The hard materials films are influenced strongly by microstructure of nano-composites. The density of defects influences the texture and mechanical properties of the film. Hardness increases as the nitrogen flow rate is increased because it led to the generation of larger number of point defects. The high (111) textured film shows lower grain size, thus increasing the hardness. So, the high textured films may have dense structure, high residual stress, high activation energy and higher resistance to deformation when a load is applied suggesting that the hardness could increase with increasing the degree of texture in film [54]. Earlier studies reported that (111) is the hardest plane with TiN binding energy formed in the TiN film due to geometrical strengthening, hardness is supposed to increase as the (111) plane intensity increases [55].

The H and E values were used to determine H/E and H^3/E^2 ratios (*Fig. III.9.b*) [38, 40] that is useful to predict the wear behavior and toughness characteristics of coatings, respectively. The minimum values of H/E = 0.0213 and H^3/E^2 = 0.0028 GPa were obtained for the coating deposited at low nitrogen flow rate of 5%, indicating a low plasticity index and a poor resistance to plastic deformation, in agreement with other studies on TiN films [56, 57]

According to evolution of hardness and Young's modulus, the increase of nitrogen content led to an increase in the H/E and H^3/E^2 values. The TiN film deposited under 20% of N_2 flow rate presents the maximum values of H/E and H^3/E^2, 0.0888 and 0.2144 GPa, respectively. This is because of the high dense columnar coalescence, and the (111) predominate and the perfection of fiber texture of the densest packed plane. From *Figure III. 7*, we can see that there is a direct relation between the plastic strain and the film hardness. Then, films with higher (H^3/E^2) and (H/E) ratios are more resistant to deformation. However, at higher nitrogen flow rate, the lower degree of film texture led to a low crystallographic texture by the existence of (200) and (220) peaks in parallel with a predominate (111) peak

and a low number of grain boundaries the decrease in the deposition rate, the both ion bombardment and the formation energy.

D.D. Kumar et al. [58] found that the nanocrystalline titanium nitride (TiN) thin films deposited on Si (100) substrates with reactive DC magnetron sputtering presented a low H^3/E^2 value of 0.041 for 1 sccm. Further increase in nitrogen content led to an increase in the H/E and H^3/E^2 values. The TiN film deposited under 20 % of the N_2 flow rate displays the highest values of H/E and H^3/E^2 , 0.0888 and 0.2144 GPa, respectively, is expected to the high dense columnar coalescence, the (111) predominance, and the perfection of fiber texture of the densest packed plane.

The direct correlation between the plastic strain and the hardness of the film are shown in *Figure III.9*. So, films with elevated elastoplastic ratio (H^3/E^2 and H/E) are further resistant to deformation. On the other hand, at a higher nitrogen flow rate of 20 % N_2, the lower degree of film texture led to a low crystallographic texture by the existence of (200) and (220) planes in parallel with a predominate (111) plane and a base number of grain boundaries. The high amount of nitrogen injected in the deposition chamber led to a reduction in Ar ion bombardment energy and consequently the velocity of film growth (deposition rate) [59].

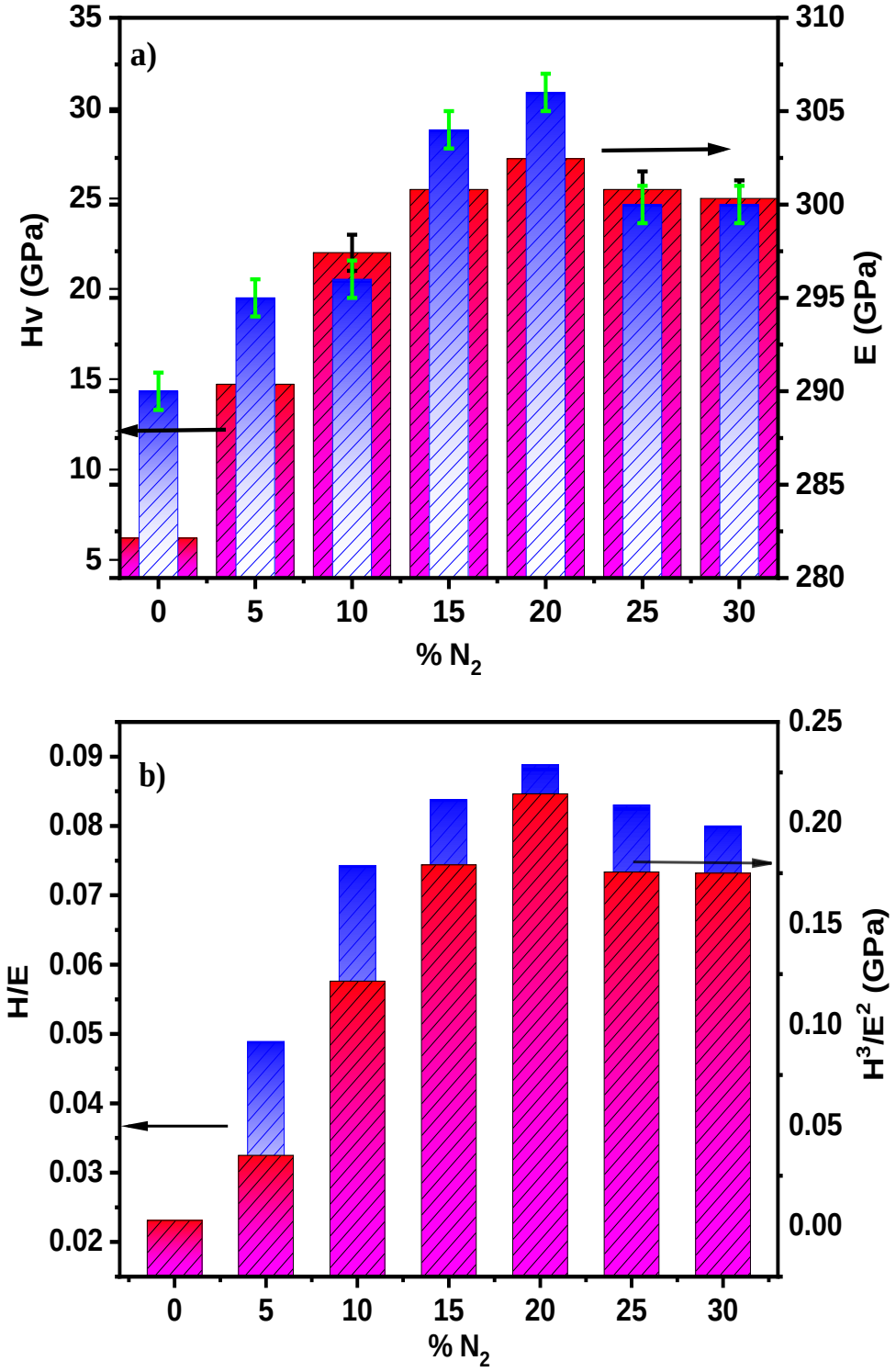

Figure III.9.a) Hardness and Young's modulus, b) (H/E) and (H^3/E^2) of TiN films as a function of the N_2 flow rates

III.8. Tribological properties

III.8.1. Friction coefficient

In recent decades, the use of hard anti-wear coatings received a growing interest in improving the functional properties of engineering materials, wear leads to degradation performance or damage to components. Separating the surfaces by the lubricant layer offer lower coefficients of friction delivers enhanced performance and service life while eliminating the need for wet lubricants in operating environments that demand resistance to heat, chemicals, or cleanroom requirements.

The evolution of the coefficient of friction (COF) and wear rate of the coatings deposited at deferent nitrogen flow rate are shown in *Figure III.10.* At a low nitrogen flow rate ≤ 5 %, the TiN film presented both highest friction coefficient (0.84 ± 0.06) and wear rate (8.5 $\times 10^{-5}$ mm^3/Nm) (*Fig. III.10.a.b*). The high COF is affected by the insufficient adhesion acting at the interface between the TiN coating and the substrate. We observe that films at nitrogen flow rate of 20 %, containing 48 at. % of nitrogen, revealed the lowest both friction coefficient of ~ 0.42 (± 0.06) and wear rate (2.7 $\times 10^{-5}$ mm^3/Nm) because of the good structural features; refinement in grain size a dense columnar structure .These arguments are confirmed by the XRD data, which revealed mainly TiN peaks that were broad with high intensity, suggesting an extremely small grain size. Another reason to suggest that the TiN film deposited at 20 sccm of nitrogen flow rate was predominantly hard ionic Ti-N binding energy.

The formation of oxides on the worn surfaces of the TiN coating that play a lubricant role between the two counterparts and controlled adhesion phenomena [60]. Furthermore, the existence of (111) TiN predominate plane in the film which reported to have high hardness. According to *A. Azushima et al.* [61] the friction coefficient of TiN coatings with (111) preferred grain orientation is lower than those of TiN coatings with (200) preferred grain orientation. *Y. Tanno et al.* [62] have studied the influence of the grain preferred orientations on the friction coefficient of titanium nitride-based coatings. The TiN films with (111) preferential plan presented a low friction coefficient value of ~ 0.2. In another study on the tribological properties of the TiN coatings deposited on high-speed steel at low temperature (150 °C), *M. Ali et al.* [63] have reported that the friction coefficient was 0.55. Comparing to

these previous works, the friction coefficient values were in the range of 0.36-0.84. In some cases, the friction coefficient is even lower than that of the conventional PVD TiN coatings [59, 63].

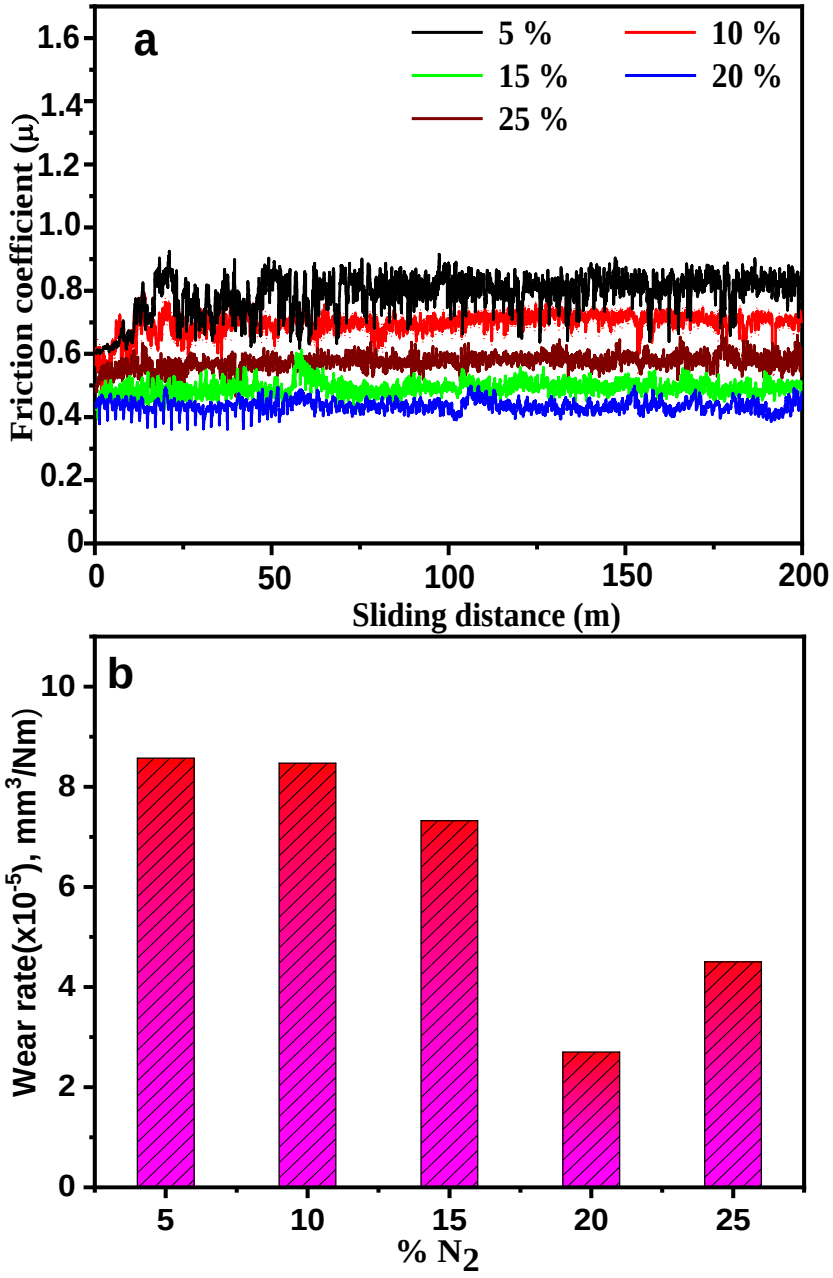

Figure III.10.a) Friction coefficients, and **b)** Wear rates of the TiN thin films deposited at different N_2 flow rates.

III.8.2. Adhesion

The film-to-substrate adhesion strength was estimated quantitatively utilizing a scratch tester and the wear tracks on the coatings were checked by an optical microscope as presented in *Figure III.11*. In the scratch test, critical loads (Lc_1 and Lc_2) could be used to measure the adhesion strength. Two critical loads are described: the cohesive failure critical load (Lc_1), the initiation of cracking in the coatings, and the adhesion failure critical load (Lc_2), which presents the adhesion strength of films.

It is clear from Figure *III.11* that the critical loads accompanied with an opposite trend as the friction coefficient. The TiN film with lowest nitrogen amount (14.3 at.%) wore out easily and delaminated from the substrate at the edges of the scratch track with a large amount of oxygen (12.5 at.%). This is the initial stage of the cohesive rupture of the film which is linked to its high friction coefficient (*Fig. III.11.a*). The cohesive failure occurred at a low value of 7 N; these kinds of cracks are associated with a soft coating and the lowest value of H/E ratio (0.074) that exhibited a poor wear resistance [64].

For the TiN films deposited between 10 and 15 % of nitrogen flow rate, their wear resistance is slightly improved and the wear pasts the middle of the track onto the edge of the coating at higher applied loads (27 ± 1 N and 38 N, respectively). The removal flakes appeared more complete at several areas of the substrate with a high content of nitrogen (39 at.%) (*Fig. III.11.b. c*). One can notice that the wear resistance of the hard TiN coatings was higher than that of the other relatively soft coatings. This feature was observed for the TiN coating deposited at 20 % of N_2 flow rate where the wear track did not reveal any cracks or delamination and the highest critical loads were Lc_1= 14 N and Lc_2 = 44 N (*Fig. III.11.d*). The best wear resistance of TiN film with high nitrogen content is directly related to the morphology and structure of TiN films [65].

A dense and smooth surface has less asperity as compared to porous coatings which result in better interlocking and adhesion. On the other hand, coating deposited at 20 % of nitrogen flow rate was found to achieve the desired combination of hardness (27.78 GPa) , low roughness (4.8 nm), and good wear resistance with higher H/E (0.0888) that show lower plasticity index and best resistance, in agreement with other previous [56, 66] studies. The TiN film deposited at 20 % N_2 having a low thickness presented the highest hardness and

critical loads and lowest friction coefficient. Consequently, it can be predicted that a film with a low thickness has a higher adhesion to the substrate and better resistance to failure. However, for the films deposited at a higher nitrogen flow rate (up to 25 %), there was larger debris on the edges of the track in the primary failure (Lc1 = 11N), while a full failure of the TiN films performed at higher critical load (32 N) due to the limited substrate-film cohesion (*Fig. III.11e*). These noticed failures might be originated from the small film thickness and the deference in mechanical properties between the deposited film and substrate [67]. The higher hardness correlated with the more diminutive grains increases the resistance to plastic deformation that results gave an enhancement in adhesion of TiN film. The failure of the film could be mainly affected by the high compressive stress. According to *S. Zhang et al*. [68] TiN thin films deposited at the ratio of 1:1 (Ar/N_2) gave a suitable COF (0.12) and the best wear resistance, which are the best coating TiN thin film condition; due to the dense columnar structure and low surface roughness.

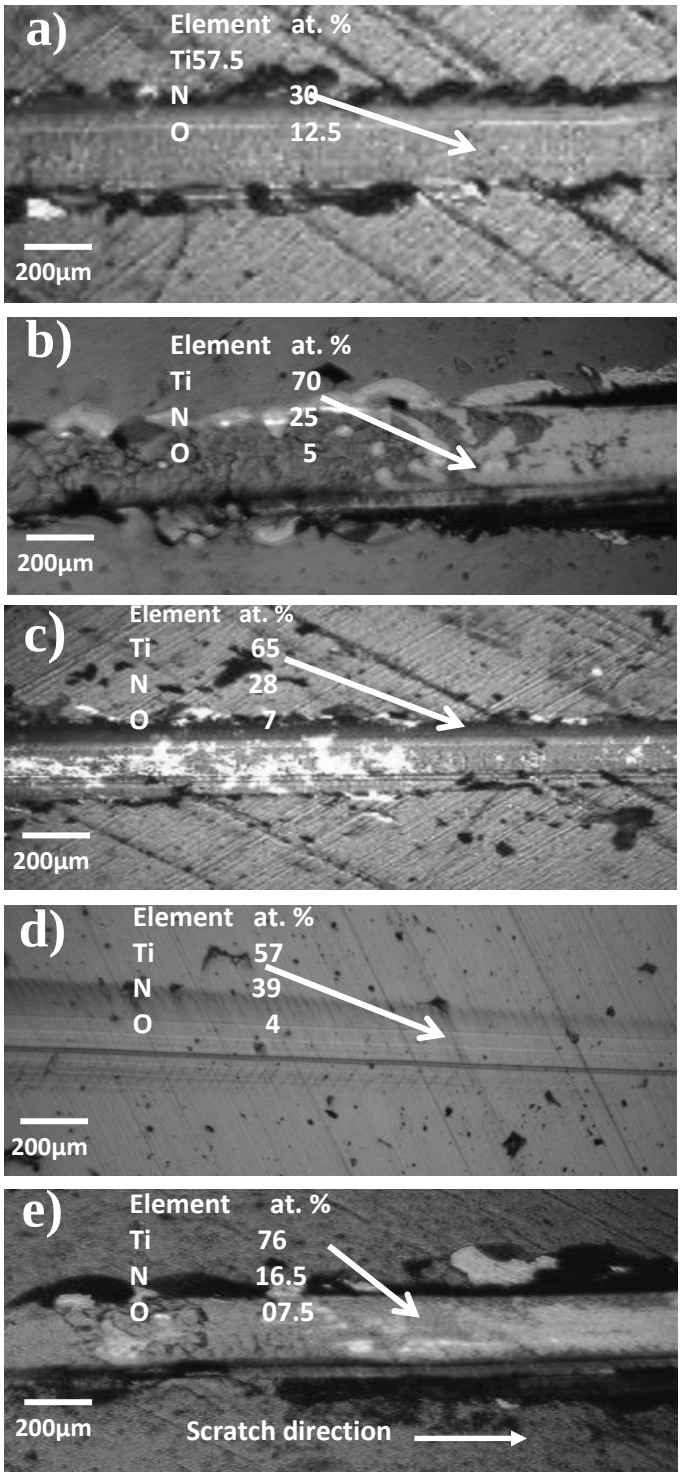

Figure III. 11. Micrographs of scratch tracks performed on the TiN coatings deposited at**: a)** 5%N_2, **b)** 10%N_2, **c)** 15%N_2, **d)** 20 %$N_2$and **e)** 25 %N_2.

III.9. Conclusion

In this chapter, structure, surface morphology and tribo-mechanical behavior of TiN thin films produced by reactive magnetron sputtering technique at various nitrogen flow rates have been investigated:

XRD analysis revealed that the film phases transformed from α(Ti+N) to Ti_2N and TiN with increasing nitrogen content.

The increase in the nitrogen content in the TiN films followed by the diffraction peaks shifted to lower 2θ angles with a (111) TiN preferential orientation indicating the existence of compressive residual stress, a reduction in the film thickness and grain refinement.

The measurements of contact angles between water-droplets and TiN film surfaces showed that all films had a high wettability and increasing the nitrogen content in film led to increase its surface hydrophobicity. This can be related to the enhancement of surface softness as mentioned by the AFM and SEM images.

Nanoindentation measurements showed that hardness and Young's modulus of the coatings exhibited an increase from (7.1 GPa, 195.2 GPa) to (27.78 GPa, 304.8 GPa) when nitrogen flow rate was varied from 5 to 20 %, respectively. Consequently, the both ratios increased H/E from 0.074 to 0.101 GPa and H^3/E^2 from 0.095 to 0.244 GPa. Increasing the nitrogen content up to 48.5 at.% in film led to enhance its hardness, elasticity modulus, resistance to plastic deformation and toughness.

The tribological tests showed that the lowest friction coefficient of ~ 0.36 and the best adhesion were obtained for the TiN coating deposited at 20 % of N_2 flow rate (film containing 48.5 at.% of nitrogen). This last configuration was confirmed as the best one and the addition of more nitrogen led to slightly decrease these properties.

References

[1] J. Bonse, S. Kirner, R. Koter, S. Pentzien, D. Spaltmann, J. Krüger, Femtosecond laser-induced periodic surface structures on titanium nitride coatings for tribological applications, Applied Surface Science, 418 (2017) 572-579.

[2] L. Mahesh, J.S. Reddy, P. Mukunda, Development and characterization of titanium nitride reinforced aluminium MMC's through powder metallurgy technique, Mechanics and Mechanical Engineering, 21 (2017) 29-36.

[3] C. Zeng, H. Wen, A.H. Ettefagh, B. Zhang, J. Gao, A. Haghshenas, J.R. Raush, S. Guo, Laser nitriding of titanium surfaces for biomedical applications, Surface and Coatings Technology, 385 (2020) 125397.

[4] P. Roquiny, F. Bodart, G. Terwagne, Colour control of titanium nitride coatings produced by reactive magnetron sputtering at temperature less than 100 C, Surface and Coatings Technology, 116 (1999) 278-283.

[5] S. Ranjan, B. Mukherjee, A. Islam, K.K. Pandey, R. Gupta, A.K. Keshri, Microstructure, mechanical and high temperature tribological behaviour of graphene nanoplatelets reinforced plasma sprayed titanium nitride coating, Journal of the European Ceramic Society, 40 (2020) 660-671.

[6] M. Łępicka, M. Grądzka-Dahlke, D. Pieniak, K. Pasierbiewicz, K. Kryńska, A. Niewczas, Tribological performance of titanium nitride coatings: A comparative study on TiN-coated stainless steel and titanium alloy, Wear, 422-423 (2019) 68-80.

[7] S. Datta, M. Das, V.K. Balla, S. Bodhak, V.K. Murugesan, Mechanical, wear, corrosion and biological properties of arc deposited titanium nitride coatings, Surface and Coatings Technology, 344 (2018) 214-222.

[8] C. Li, J. Shi, L. Zhu, Y. Zhao, J. Lu, L. Xu, Titanium nitride hollow nanospheres with strong lithium polysulfide chemisorption as sulfur hosts for advanced lithium-sulfur batteries, Nano Research, 11 (2018) 4302-4312.

[9] S. Grosso, L. Latu-Romain, G. Berthomé, G. Renou, T. Le Coz, M. Mantel, Titanium and titanium nitride thin films grown by dc reactive magnetron sputtering Physical Vapor Deposition in a continuous mode on stainless steel wires: Chemical, morphological and structural investigations, Surface and Coatings Technology, 324 (2017) 318-327.

[10] A. Lisiecki, Study of optical properties of surface layers produced by laser surface melting and laser surface nitriding of titanium alloy, Materials, 12 (2019) 3112.

[11] M. Bashir, M. Shafiq, M. Naeem, M. Zaka-ul-Islam, J. Díaz-Guillén, C. Lopez-Badillo, M. Zakaullah, Enhanced surface properties of aluminum by PVD-TiN coating combined with cathodic cage plasma nitriding, Surface and Coatings Technology, 327 (2017) 59-65.

[12] J. Su, R. Boichot, E. Blanquet, F. Mercier, M. Pons, Chemical vapor deposition of titanium nitride thin films: Kinetics and experiments, CrystEngComm, 21 (2019) 3974-3981.

[13] M. Braun, Magnetron sputtering technique, Handbook of Manufacturing Engineering and Technology, Springer, (2015) 2929-2957.

[14] S. Yu, Q. Zeng, A.R. Oganov, G. Frapper, L. Zhang, Phase stability, chemical bonding and mechanical properties of titanium nitrides: a first-principles study, Physical Chemistry Chemical Physics, 17 (2015) 11763-11769.

[15] G.S. Gautam, K.H. Kumar, Elastic, thermochemical and thermophysical properties of rock salt-type transition metal carbides and nitrides: a first principles study, Journal of alloys and compounds, 587 (2014) 380-386.

[16] M.F. Slim, A. Alhussein, E. Zgheib, M. François, Determination of single-crystal elasticity constants of the beta phase in a multiphase tungsten thin film using impulse excitation technique, X-ray diffraction and micro-mechanical modeling, Acta materialia, 175 (2019) 348-360.

[17] F. Salhi, L. Aissani, C. Nouveu, A. Alhussein, Influence of Nitrogen Partial Pressure on the Structural, and Mechanical Properties of Ti-N Thin Films, International Symposium on Materials and Sustainable Development, Springer, (2019) 187-195.

[18] N. Arshi, J. Lu, Y.K. Joo, C.G. Lee, J.H. Yoon, F. Ahmed, Study on structural, morphological and electrical properties of sputtered titanium nitride films under different argon gas flow, Materials Chemistry and Physics, 134 (2012) 839-844.

[19] Y. Liu, H. Liu, V. Pelenovich, Q. Wan, J. Guo, Y. Chen, J. Zhang, L. Xue, Z. Li, B. Yang, Influences of modulation period on structure and properties of AlTiSiN/AlCrSiN nanocomposite multilayer coatings, Vacuum, 193 (2021) 110516.

[20] Y. Chen, J. Xu, S. Jiang, Z.-H. Xie, P. Munroe, S. Kuai, Corrosion-resistant, electrically conductive TiCN coatings for direct methanol fuel cell, Surface and Coatings Technology, 422 (2021) 127562.

[21] Y. Li, Y. Zhou, C. Xu, Porous TiO2/rGO nanocomposites prepared by cold sintering as efficient electrocatalyst for nitrogen reduction reaction under ambient conditions, Journal of the European Ceramic Society, 42 (2022) 1548-1555.

[22] J. Marco, A. Agudelo, J. Gancedo, D. Hanžel, Corrosion resistance of single TiN layers, Ti/TiN bilayers and Ti/TiN/Ti/TiN multilayers on iron under a salt fog spray (phohesion) test: an evaluation by XPS, Surface and Interface Analysis: An International Journal devoted to the development and application of techniques for the analysis of surfaces, interfaces and thin films, 27 (1999) 71-75.

[23] Y.L. Jeyachandran, S.K. Narayandass, D. Mangalaraj, S. Areva, J.A. Mielczarski, Properties of titanium nitride films prepared by direct current magnetron sputtering, Materials Science and Engineering: A, 445-446 (2007) 223-236.

[24] S. Berg, T. Larsson, H.O. Blom, The use of nitrogen flow as a deposition rate control in reactive sputtering, Journal of Vacuum Science & Technology A: Vacuum, Surfaces, and Films, 4 (1986) 594-597.

[25] A. Singh, P. Kuppusami, S. Khan, C. Sudha, R. Thirumurugesan, R. Ramaseshan, R. Divakar, E. Mohandas, S. Dash, Influence of nitrogen flow rate on microstructural and nanomechanical properties of Zr–N thin films prepared by pulsed DC magnetron sputtering, Applied Surface Science, 280 (2013) 117-123.

[26] M. Signore, A. Sytchkova, D. Dimaio, A. Cappello, A. Rizzo, Deposition of silicon nitride thin films by RF magnetron sputtering: a material and growth process study, Optical materials, 34 (2012) 632-638.

[27] P. Prieto, R. Kirby, X-ray photoelectron spectroscopy study of the difference between reactively evaporated and direct sputter-deposited TiN films and their oxidation properties, Journal of Vacuum Science & Technology A: Vacuum, Surfaces, and Films, 13 (1995) 2819-2826.

[28] S. Groudeva-Zotova, R. Kaltofen, T. Sebald, DC reactive magnetron sputter deposition of (111) textured TiN films—influence of nitrogen flow and discharge power on the texture formation, Surface and Coatings Technology, 127 (2000) 144-154.

[29] D. Munteanu, F. Vaz, The influence of nitrogen content on the properties of TiN~ X thin films, Journal of Optoelectronics and Advanced Materials, 8 (2006) 720.

[30] Y. Xi, K. Gao, X. Pang, H. Yang, X. Xiong, H. Li, A.A. Volinsky, Film thickness effect on texture and residual stress sign transition in sputtered TiN thin films, Ceramics International, 43 (2017) 11992-11997.

[31] D. Constantin, D. Munteanu, The influence of nitrogen content on the mechanical properties of TiNx thin films prepared by reactive magnetron sputtering, Bulletin of the Transilvania University of Brasov. Engineering Sciences. Series I, 5 (2012) 59.

[32] X. Wan, S. Zhao, Y. Yang, J. Gong, C. Sun, Effects of nitrogen pressure and pulse bias voltage on the properties of Cr–N coatings deposited by arc ion plating, Surface and Coatings Technology, 204 (2010) 1800-1810.

[33] D. Munteanu, F.J.J.o.O. Vaz, A. Materials, The influence of nitrogen content on the properties of TiN~ X thin films, Journal of Optoelectronics and Advanced Materials, 8 (2006) 720.

[34] F. Elstner, A. Ehrlich, H. Giegengack, H. Kupfer, F. Richter, Structure and properties of titanium nitride thin films deposited at low temperatures using direct current magnetron sputtering, Journal of Vacuum Science & Technology A: Vacuum, Surfaces, and Films, 12 (1994) 476-483.

[35] A. Gelali, A. Ahmadpourian, R. Bavadi, M. Hantehzadeh, A. Ahmadpourian, Characterization of microroughness parameters in titanium nitride thin films grown by DC magnetron sputtering, Journal of fusion energy, 31 (2012) 586-590.

[36] A. Anders, A structure zone diagram including plasma-based deposition and ion etching, Thin Solid Films, 518 (2010) 4087-4090.

[37] K. Chakrabarti, J. Jeong, S. Hwang, Y. Yoo, C. Lee, Effects of nitrogen flow rates on the growth morphology of TiAlN films prepared by an rf-reactive sputtering technique, Thin Solid Films, 406 (2002) 159-163.

[38] W. Zhou, J. Liang, F. Zhang, J. Mu, H. Zhao, A comparative research on TiAlN coatings reactively sputtered from powder and from smelting TiAl targets at various nitrogen flow rates, Applied surface science, 313 (2014) 10-18.

[39] Y.-E. Ke, Y.-I. Chen, Effects of nitrogen flow ratio on structures, bonding characteristics, and mechanical properties of ZrNx films, Coatings, 10 (2020) 476.

[40] Y.-W. Lin, J.-H. Huang, G.-P. Yu, Effect of nitrogen flow rate on properties of nanostructured TiZrN thin films produced by radio frequency magnetron sputtering, Thin solid films, 518 (2010) 7308-7311.

[41] J.-H. Huang, K.-W. Lau, G.-P. Yu, Effect of nitrogen flow rate on structure and properties of nanocrystalline TiN thin films produced by unbalanced magnetron sputtering, Surface and Coatings Technology, 191 (2005) 17-24.

[42] P. Xiao, B. Derby, Wetting of titanium nitride and titanium carbide by liquid metals, Acta materialia, 44 (1996) 307-314.

[43] S.-C. Liao, C.-Y. Chen, Y.-H. Hsu, C.-T. Li, C.-C. Hsieh, M.-S. Tsai, M.-Y. Chan, C.-H. Lee, S.-H. Wang, S.-K. Ng, In vitro and in vivo biocompatibility study of surface modified

TiN deposited on Ti6Al4V using high-power impulse magnetron sputtering technique, Surface and Coatings Technology, 394 (2020) 125814.

[44] V. Karagkiozaki, S. Logothetidis, N. Kalfagiannis, S. Lousinian, G. Giannoglou, Atomic force microscopy probing platelet activation behavior on titanium nitride nanocoatings for biomedical applications, Nanomedicine: Nanotechnology, Biology and Medicine, 5 (2009) 64-72.

[45] N.P. Patel, K.V. Chauhan, J.M. Kapopara, N.N. Jariwala, S.K. Rawal, Characterization of sputtered zirconium nitride films deposited at various argon: nitrogen ratio, IOP Conference Series: Materials Science and Engineering, IOP Publishing, (2016) 012015.

[46] D. McKenzie, Y. Yin, W. McFall, N. Hoang, The orientation dependence of elastic strain energy in cubic crystals and its application to the preferred orientation in titanium nitride thin films, Journal of Physics: Condensed Matter, 8 (1996) 5883.

[47] S. Wu, H. Lin, P. Liu, An investigation of unbalanced-magnetron sputtered TiAlN films on SKH51 high-speed steel, Surface and Coatings Technology, 124 (2000) 97-103.

[48] L. Zhang, H. Yang, X. Pang, K. Gao, A.A. Volinsky, Microstructure, residual stress, and fracture of sputtered TiN films, Surface and Coatings Technology, 224 (2013) 120-125.

[49] F. Vaz, J. Ferreira, E. Ribeiro, L. Rebouta, S. Lanceros-Méndez, J. Mendes, E. Alves, P. Goudeau, J. Riviere, F. Ribeiro, Influence of nitrogen content on the structural, mechanical and electrical properties of TiN thin films, Surface and Coatings Technology, 191 (2005) 317-323.

[50] L.C. Hernández, L. Ponce, A. Fundora, E. López, E. Pérez, Nanohardness and residual stress in TiN coatings, Materials, 4 (2011) 929-940.

[51] J. Olaya, S. Rodil, S. Muhl, L. Huerta, Influence of the energy parameter on the microstructure of chromium nitride coatings, Surface and Coatings technology, 200 (2006) 5743-5750.

[52] J.-W. Lee, Y.-C. Kuo, C.-J. Wang, L.-C. Chang, K.-T. Liu, Effects of substrate bias frequencies on the characteristics of chromium nitride coatings deposited by pulsed DC reactive magnetron sputtering, Surface and Coatings Technology, 203 (2008) 721-725.

[53] K. Calamba, I. Schramm, M. Johansson Jõesaar, J. Ghanbaja, J. Pierson, F. Mücklich, M. Odén, Enhanced thermal stability and mechanical properties of nitrogen deficient titanium aluminum nitride (Ti0. 54Al0. 46Ny) thin films by tuning the applied negative bias voltage, Journal of Applied Physics, 122 (2017) 065301.

[54] C.T. Chen, Y.C. Song, G.P. Yu, J.H. Huang, Microstructure and hardness of hollow cathode discharge ion-plated titanium nitride film, Journal of Materials Engineering and Performance, 7 (1998) 324-328.

[55] W.-J. Chou, G.-P. Yu, J.-H. Huang, Mechanical properties of TiN thin film coatings on 304 stainless steel substrates, Surface and Coatings Technology, 149 (2002) 7-13.

[56] A.A.C. Recco, C. Viáfara, A. Sinatora, A.P. Tschiptschin, Energy dissipation in depth-sensing indentation as a characteristic of the nanoscratch behavior of coatings, Wear, 267 (2009) 1146-1152.

[57] H. Cao, F. Qi, X. Ouyang, N. Zhao, Y. Zhou, B. Li, W. Luo, B. Liao, J. Luo, Effect of Ti transition layer thickness on the structure, mechanical and adhesion properties of Ti-DLC coatings on aluminum alloys, Materials, 11 (2018) 1742.

[58] D.D. Kumar, N. Kumar, S. Kalaiselvam, S. Dash, R. Jayavel, Micro-tribo-mechanical properties of nanocrystalline TiN thin films for small scale device applications, Tribology International, 88 (2015) 25-30.

[59] H. Scheerer, E.M. Slomski, T. Troßmann, C. Berger, Characterization of CrN coatings concerning the potential to cover surface imperfections, Surface and Coatings Technology, 205 (2010) S47-S50.

[60] E. Santecchia, A. Hamouda, F. Musharavati, E. Zalnezhad, M. Cabibbo, S. Spigarelli, Wear resistance investigation of titanium nitride-based coatings, Ceramics International, 41 (2015) 10349-10379.

[61] A. Azushima, Y. Tanno, H. Iwata, K. Aoki, Coefficients of friction of TiN coatings with preferred grain orientations under dry condition, Wear, 265 (2008) 1017-1022.

[62] Y. Tanno, A. Azushima, Effect of counter materials on coefficients of friction of TiN coatings with preferred grain orientations, Wear, 266 (2009) 1178-1184.

[63] M. Ali, E. Hamzah, M. Radzi Toff, Friction coefficient and surface roughness of TiN-coated HSS deposited using cathodic arc evaporation PVD technique, Industrial Lubrication and Tribology, 60 (2008) 121-130.

[64] H. Van Swygenhoven, M. Spaczer, A. Caro, Role of low and high angle grain boundaries in the deformation mechanism of nanophase Ni: A molecular dynamics simulation study, Nanostructured materials, 10 (1998) 819-828.

[65] L. Aissani, M. Fellah, L. Radjehi, C. Nouveau, A. Montagne, A. Alhussein, Effect of annealing treatment on the microstructure, mechanical and tribological properties of chromium carbonitride coatings, Surface and Coatings Technology, 359 (2019) 403-413.

[66] B. Beake, V. Vishnyakov, A. Harris, Relationship between mechanical properties of thin nitride-based films and their behaviour in nano-scratch tests, Tribology International, 44 (2011) 468-475.

[67] L. Aissani, M. Fellah, C. Nouveau, M. Abdul Samad, A. Montagne, A.J.S.e. Iost, Structural and mechanical properties of Cr–Zr–N coatings with different Zr content, Surface engineering,36 (2020) 69-77.

[68] S. Zhang, F. Yan, Y. Yang, M. Yan, Y. Zhang, J. Guo, H. Li, Effects of sputtering gas on microstructure and tribological properties of titanium nitride films, Applied Surface Science, 488 (2019) 61-69.

Chapter IV

Effects of zirconium sputtering current on the structure, wetting mechanical and tribological properties of TiN Films

IV. 1. Introduction

Despite the outstanding proprieties of binary TiN films, much of the problems associated with this system, production has been the need to improve their properties by studying the effect of different parameters like voltage, pressure and temperatures. Recently, TiMN (M=B, Al, C, Si, Zr) [1-5] nanocomposite coatings with higher hardness, excellent tribo-mechanical properties, improved stabilization and higher oxidation resistance have been developed and investigated. Many researchers reported that the addition of specific elementsto TiN matrix could enhance the system properties [6, 7]. However, the effect of Zr on the structural and mechanical properties of TiN films was less researched compared with other elements, and it shows specific properties, like the high melting point, high refractoriness, biocompatibility with the human body, and good oxidation resistance.

Zr has a larger radius (0.158 nm) than Ti (0.147 nm), which may induce higher distortion in TiN crystal. Otherwise, the cooperation of Zr in the TiN film results in the super saturated solid solutions with a high hardness because it has high affinity with N element [8-11]. The (Ti,Zr)N coating shows an enhanced hardness compared with the binary TiN and ZrN coatings deposited under the equivalent conditions [12]. This increased hardness shown by (Ti,Zr)N coatings is due to a solid solution strengthening mechanism. Moreover, early studies on the effects of zirconium implantation on TiN coatings have shown improved wear resistance, but also high hardness and golden colour.

In this chapter, we are interested about the structure, wetting mechanical and tribological caracterization of TiZrN films deposited at different zirconium sputtering current. TiZrN films with various Zr contents were deposited onto Si (100) and XC100 steel substrates using a R.F reactive magnetron sputtering system (DEPHI Coating Limited) with tow high purity Ti (99.99 %, 103.2 mm diameter × 3.2 mm length) and Zr (99.99 %, 3.2 mm diameter× 3.2 mm length) targets in a mixture of (Ar + N_2) gases with 80 and 20 sccm, respectively, which ensured a constant work pressure of 0.4 Pa. Mixtures (Ar-N_2) were used as sputtering and reactive gases.

The films on Si (100) (20 mm × 20 mm) wafers were used in the XPS, EDS, SEM and wettability. While the films on XC100 steel substrates were deposited for XRD, nanoindentation and tribological tests. The substrates were ultrasonically cleaned in acetone,

dried and then mounted 100 mm above the target on a rotating (10 r/min) substrate holder in the deposition chamber, which was evacuated to a base pressure of 6 $\times 10^{-4}$ Pa.

Prior to deposition, the substrates were cleaned by Ar^+ bombardment at 0.1 Pa using a voltage of -700 V at a frequency of 250 kHz for 10 min. An additional, targets were sputter cleaned in Ar^+ using a current of 1 A for 10 min to removal the surface oxides and impurities. Prior deposition, a pure Ti layer for 10 min was deposited to enhance the film adhesion strength between the substrate and the film, and the Ti target current was kept at 2 A, while the Zr target current was varied from 0 to 2 A in order to acquire films with varied Zr concentrations. The deposit time was kept at 180 min. More detailed of deposition parameters are presented in *Table IV.1.*

TableIV.1. Detailed deposition parameters as-deposited of TiZrN films

Coatings	Current (A)		Voltage (V)		(Ar/N_2)Flow	Pressure	Deposition
	Ti	Zr	Ti	Zr	(sccm)	(Pa)	Time (min)
Etching	1	1	700	700	80/0	0.1	10
Ti layer	1	0	700	-	80/0	0.4	10
TiN	2	0	900	-	80/20	0.4	180
TiZrN	2	0.5-2	900	200-900	80/20	0.4	180

IV. 2. Structure, wettability, mechanical and tribological properties of TiZrN Films

IV.2.1. Effect of Zr content on Structure of TiZrN films

Figure IV.1 shows the face-centered cubic crystal lattice of TiN (fcc-rocksalt-TiN) optimized from WN2K simulation by using GGA-PBE approximation. The atomic positions for Ti atoms are (0,0,0), (0,1/2,1/2), (1/2,0,1/2) and (1/2,1/2,0), while, (1/2,0,0), (0,1/2,0), (0,0,1/2) and (1/2,1/2,1/2) for N atomes. The Zr atoms takes progressively the substututional position of the Ti in the TiN crystal lattice by increasing its concentration. The lattice parameter obtained from DFT calculation is a= 4.255 Å. It is interesting to note that our calculated lattice constant and the equilibrium energy increased with increasing the Zr content from (4.262Å, -24727.004 eV) of the pure TiN from to (4.454 Å, -62079.903 eV) $Ti_{0.5}Zr_{0.5}N$, which confirm the stability of the solid solution phase.

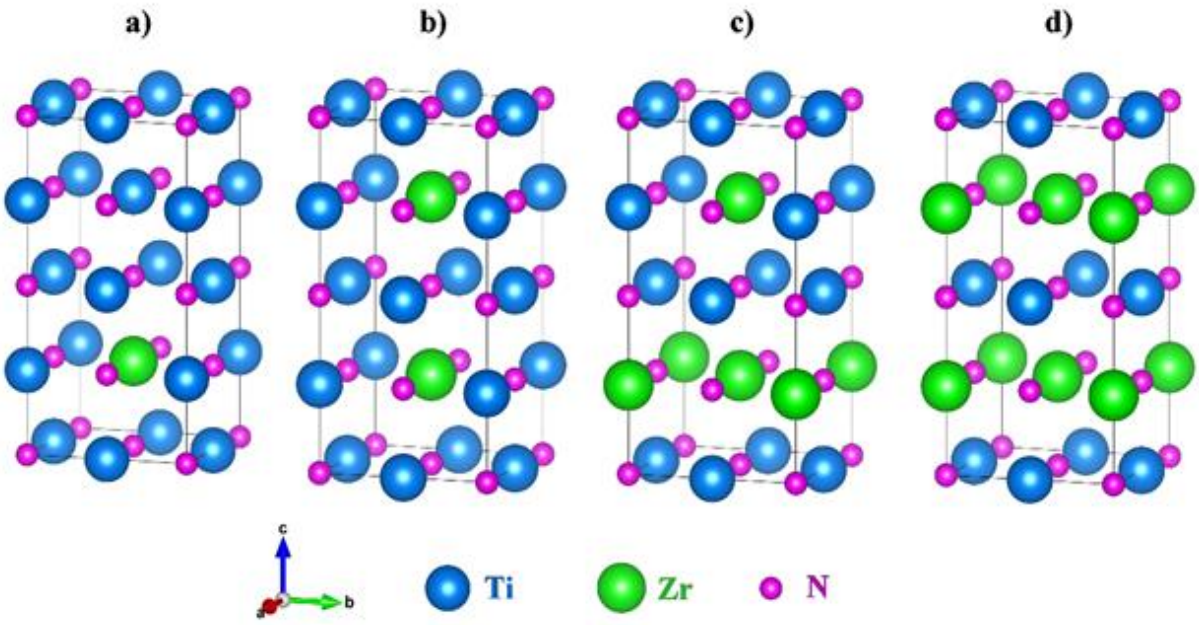

Figure IV.1. Schematic presentation of TiZN structure with different Zr content calculated by GGA-PBE approximation.

Table IV. 2. a) The lattice constant, and **b)** the Equilibrium energy as a function of Zr concentration calculated by GGA-PBE approximation.

(at. %)	Coatings	a (Å)	Equilibrium energy E_0 (eV)	Formation energy ΔE_f(eV/atom)
x=0 (0 %)	$Ti_{1-x}Zr_xN$	4.262	-24727.004	-18.357
x=0.125 (12.5 %)	$Ti_{0.875}Zr_{0.125}N$	4.320	-34065.213	-18.365
x=0.25 (25 %)	$Ti_{0.75}Zr_{0.25}N$	4.374	-43403.423	-18.374
x=0.375 (37.5 %)	$Ti_{0.625}Zr_{0.375}N$	4.401	-52741.649	-18.400
x=0.5(50 %)	$Ti_{0.5}Zr_{0.5}N$	4.454	-62079.903	-18.453

For our experimental part, the chemical composition analysis by EDS was carried out after each deposition to determine chemical elements of the deposited TiZrN films under different Zr content. The atomic compositions of TiN and TiZrN coatings, as a function of the Zr content, deposited on Si (100) wafers are listed in *Table IV.2.* The content of four elements (N, Ti, Zr, and O) determined by EDS are tested to confirm that the total content is 100 %. The N/Ti atomic ratio was used to determine a stoichiometric case of a binary TiN coating, while the N/(Ti+Zr) ratio was used to determine a stoichiometric case of ternary TiZrN coatings with nitrogen.

The EDS results show that the TiN layer (at 0 A on the Zr target) is stoichiometric (N/Ti ≈ 0.98), which is comparable to the chemical composition data of magnetron sputtering Tin coatings [13]. Keeping the voltage on the titanium target fixed (-900 V), and varied that of the Zr target. This variation leads to an increase in the Zr content in TiZrN coatings from 6.5 to 22.2 at. % with a concurrent decrease in Ti content, and an increase in the Zr/(Ti+Zr) ratio. The N content varied between 48.5 and 47.5, and the N/(Ti+Zr) ratio is close to 1; indicating that all films prepared in this work are stoichiometric.In addition, the oxygen impurities were found in the range of 2-4.4 at.%, which is possibly owing of the moderate vacuum degree during deposition process [14].

The same behaviours were observed in the work of *N. Witit-Anun et al.* [15] where the deposited TiCrN thin films with reactive D.C magnetron co-sputtering on Si substrates exhibited an increase in Ti content of the produced films from 3.5 at.% to 17.3 at.%, while the Cr and N contents decreased from (36.1 at.% to 27.3 at.%), and (60.5 at.% to 55.4 at.%), respectively, as Ti sputtering current increased. Suggesting that increasing of the Ti sputtering current increases the sputtering efficiency, which permitted to achieve additional Ti sputtered particles to form the TiCrN films. Also, in a previous work of reactive D.C Magnetron co-sputtering TiZrN thin films with different titanium sputtering currents (I_{Ti}) ranging from 0.6 to 1.2 realized by *S. Chinsakolthanakorn et al*. [16], showed that the atomic ratio of Ti to Zr elements and the N to (Ti+ Zr) ratio increased to 0.9 and 1.6, respectively, when Ti content increased insignificantly from 14.390 at. % to 18.125 at. % and the Zr content decreased significantly from 41.768 at. % to 20.026 at. %.

Table IV.2. The chemical composition, thicknesses, and surface roughness of as-deposited of TiZrN

Coatings	Chemical composition (at. %)						Thickness (nm)	Roughness Ra (nm)
	Ti	Zr	N	O	Zr/(Ti+Zr)	N/(Ti+Zr)		
Etching Ti layer							60	-
$Ti_{0.49}N_{0.48}$	49.5	0	48.5	2.0	-	0.98	1260	46
$Ti_{0.42}Zr_{0.06}N_{0.47}$	42.1	6.4	47.5	4.0	0.13	0.98	1280	37
$Ti_{0.36}Zr_{0.12}N_{0.47}$	36.0	12.1	47.5	4.4	0.25	0.99	1320	22
$Ti_{0.30}Zr_{0.18}N_{0.48}$	30.2	18.3	48	3.5	0.38	1.00	1550	17
$Ti_{0.26}Zr_{0.22}N_{0.48}$	26.2	22.2	47.8	3.8	0.46	0.99	1540	29

Figure IV.2.a) shows the XRD patterns of TiZrN films deposited at different Zr sputtering currents of 0, 0.5, 1, 1.5 and 2 A. Reference peaks of fcc-TiN, fcc-ZrN and t-ZrO_2 phase structure are marked according to the (JCPDS card No.65-2905), (JCPDS card No. 002-0536.) and (JCPDS card No. 79-1771) files, respectively. The increase in the applied current on the Zr target is followed by the insertion of zirconium into the TiN lattice and the formation of solid solution that observed on the XRD patterns. The diffraction pattern of pure TiN present (111), (200), (220), (331) and (222) planes corresponding to the fcc-TiN phase, which can be assigned to the formation of a solid solution structure with single phase [17]. Besides the fcc-TiN phase, the fcc-ZrN phase can be detected at high Zr content in the TiZrN films. This phase composition correlates with the results of *S. Chinsakolthanakorn et al.* [16] who reported that an applied current higher than 1 A leads to the formation of TiN and ZrN mixture in the TiZrN films.

The addition of Zr led to a gradual decrease of the (200) intensity compared to that of (111) plane, thus causing a decrease of T_C = I(111) /[I(111)+I(200)] ratio (*Fig. IV.2.b*). This change could be associated with the increase of Zr sputtering current and the high-energy ion bombardment, suggesting an increase in the inter-planar spacing. A similar behavior was observed by *W. Phae-Ngam et al.* [18] where the TiZrN coatings deposited at 200–300 W of Zr sputtering power, showed a (111) peak broadening due to the energy loss during the collision, which could decrease the adatoms mobility and diffusion on the columnar surface. In contrast, *S. Chinsakolthanakorn et al.* [16] confirmed that the high-energy ion bombardment

changed the preferred orientation of TiZrN from (111) to (200), with increasing Ti sputtering current resulting in an enhancement in the peaks intensity. This is due to an increase in the crystallinity and coating thickness.

The change in the growth direction from (111) towards (200) recently received in the research of *L. Aissani et al*. [19] for as deposited ZrON by reactive magnetron sputtering in a mixture of Ar (flow rate = 80 sccm), N_2 (flow rate = 20 sccm) and varied O_2 flow rate of 0 to 12 sccm, where the coatings changed the preferred orientation from (111) ZrN to (200) ZrN with growing O_2 flow rate.

The characteristic peaks gradually turn to a lower angle with improving the content of Zr due to the formation of substitution solid solutions and the formation of residual stress in the films [20]. The Zr atoms with a larger atomic radius (1.60 Å) are gradually incorporated in TiN and replaced Ti atoms with smaller atomic radius (1.47 Å), suggesting lattice parameters get bigger (4.42 Å), when compared to TiN JCPDS (*Fig. IV.3*) [17].

Similar results were reported in the as-deposited TiCrN films with deferent content of Ti, the crystal size decreased from 39.9 nm to 33.5 nm, while the lattice constants increased from 4.139 Å to 4.162 Å, with increasing of the Ti sputtering [15]. The (111) peak was enlarged with an increase of Zr content, which indicated a lattice distortion and grain refining [21]. As shown in *Figure IV.3*, the grain size of the TiZrN decreased with the increase of Zr content. Whereas, at 18.3 at. % of Zr, corresponding to 1.5 A of applied current, with the broadest (111) peak, showed the minimum grain size. However, at 22.3 at. % of Zr, the (111) peak with the lowest intensity presented weak crystalline with a large grain size.

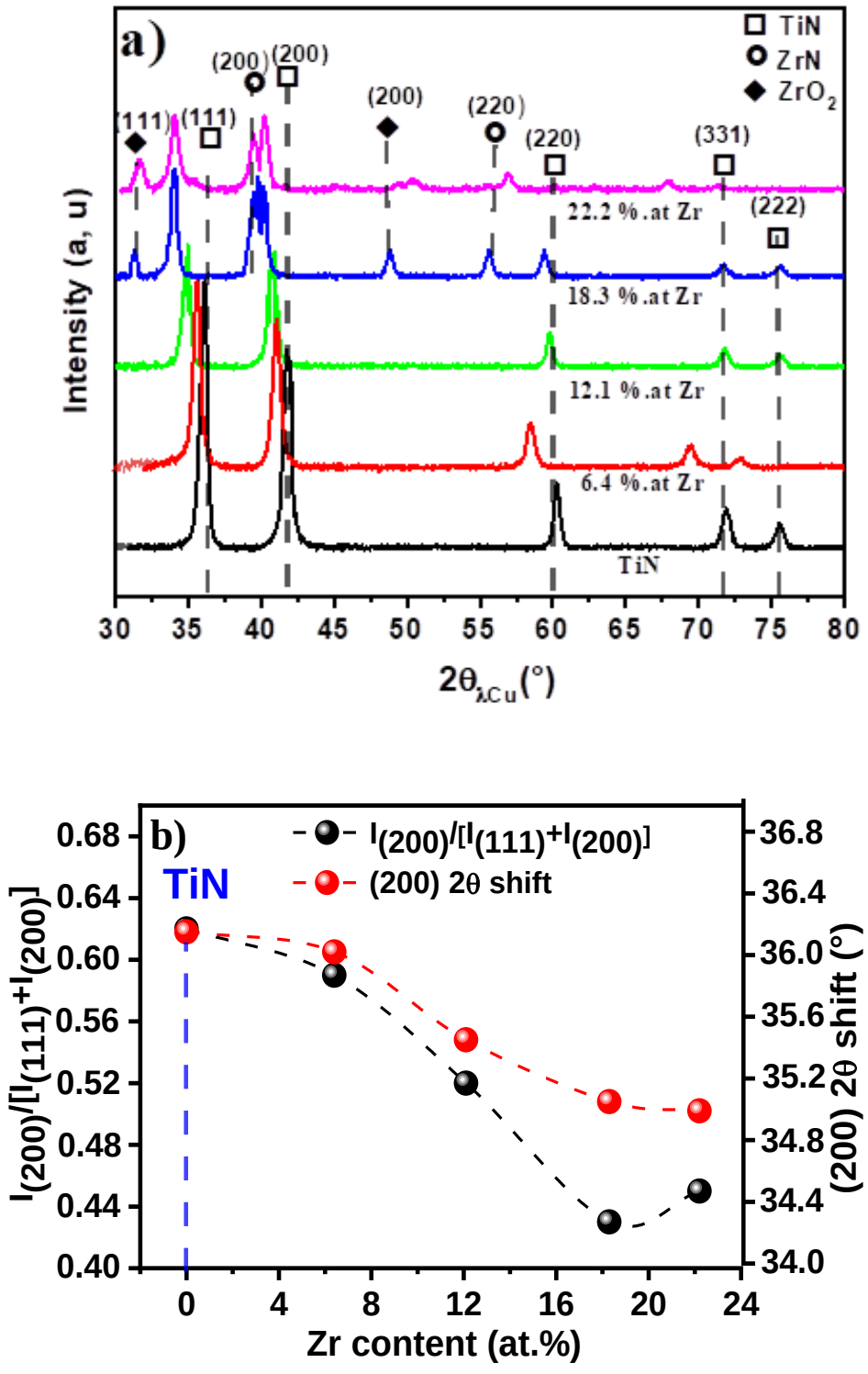

Figure IV. 2.a) XRD pattern of TiZrN films, **b)** peak intensity ratio and (111) 2θ shift as a function of Zr content.

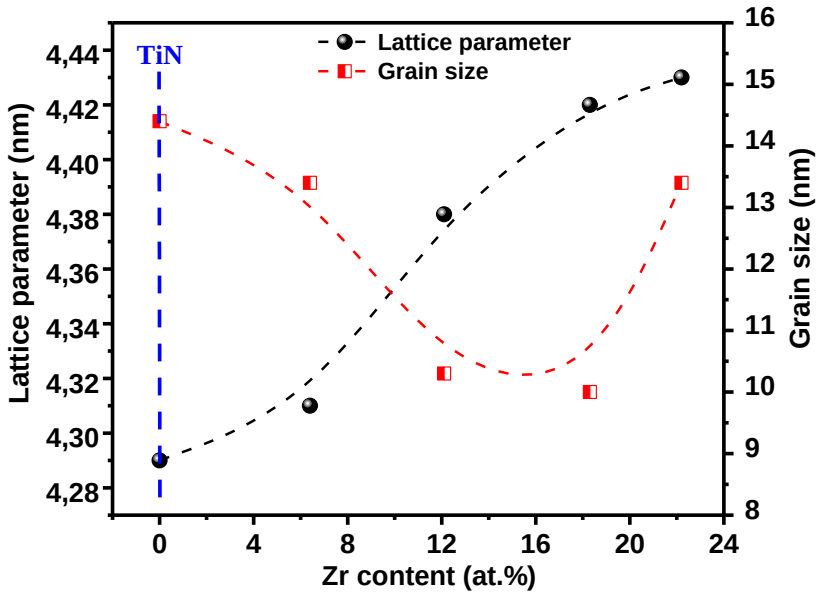

Figure IV.3. Lattice parameter and grain size for TiZrN films as a function of Zr content.

Figure IV.4 displays Raman spectra of TiN and TiZrN thin films. The spectrum of TiN coating shows two broad band's centered at 250 and 590 cm^{-1} of TiN layer spectrum, corresponding to (LA and TA) acoustic transition regions, and (LO and TO) optic mode regions that were primarily determined by the vibrations of the Ti and N bands [22].

The FWHM peaks gradually decrease as Zr content increases, and the peaks of TiZrN films become greatly narrower and incredibly stronger for films containing 18.3 at.% of Zr. Also, with increasing Zr content, the wavelength divergence is marked between the acoustic and optic regions from 250 and 618 cm^{-1} to 315 and 590 cm^{-1} respectively. The 215 and 668 cm^{-1} peak positions are proximate to the ZrN, which indicates more Ti atoms are replaced by the Zr atoms, and hence a stronger vibration of Zr-N bonds obtained during the deposition [23, 24].

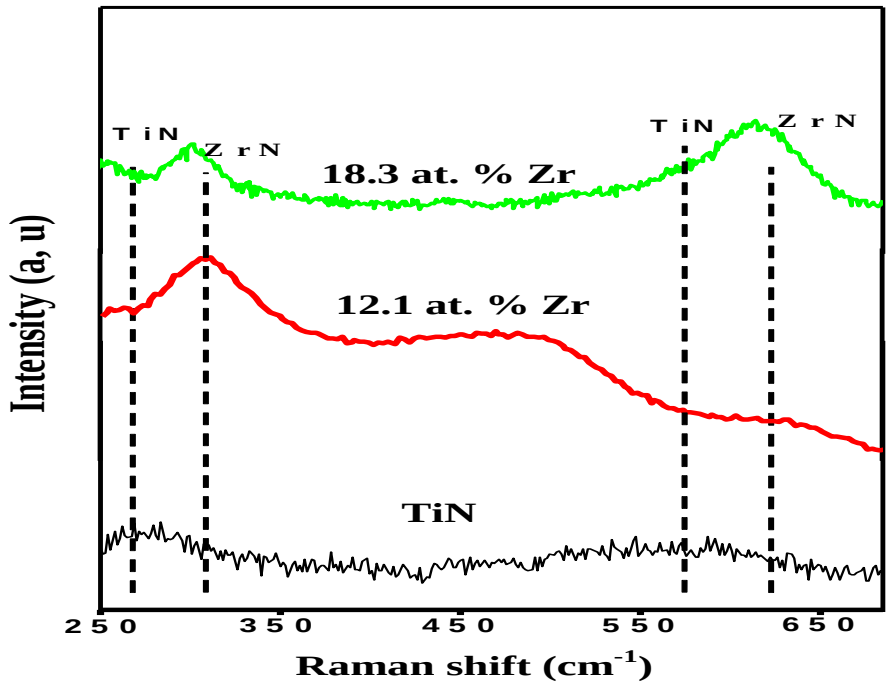

Figure IV.4. Raman spectrum of TiZrN films.

IV.2.2. Effect of Zr on the morphology of TiN thin films

To further clarify the effect of Zr content on the morphology of the TiN films, cross-sectional and surface FE-SEM of films were taken (*Figs. IV.5 and 6*). The film thickness varied from 1260 to 1550 nm, commonly in magnetron sputtering the columnar structure of the typical feature of the sputtered coatings, in this experiment, all our grown films with deferent Zr content have shown a columnar structure, which is a typical feature of the magnetron sputtered coatings.

For TiN film (containing no Zr), there exhibits a fibrous and columnar structure in addition to some droplets developed through the film (*Figs. IV.5.a, 6a*), leading to the creation of voids in-between the large globular grains. Regarding the morphology of TiZrN thin coatings with various Zr content, a remarkable change in growth structure from discontinuous columnar to continuous columnar and from globular to plane shape, is primarily attributed to hard metal of Zr. Here Zr with high atomic radius can hence the film densification and disrupt the columnar grain enlargement during deposition. For example, the TiZrN film demonstrates a continuous and refined columnar tilted to the normal's substrate corresponding to the

transition zone of Andres's structural zone model (*Fig. IV.5.d*) [16]. The surface morphology showed a fine plane grained structure with smaller crystallite size of about 10 nm as the Zr content is 18.3 at. % Zr, that is in accordance with (200) preferred orientation (*Fig. IV.6d*). This may be due to that the increase of high applied current could enhance the mobility of atoms by improving their energies, leading to film densification with a lowest roughness (Ra = 17 nm).

The grain refinement of the film structure has a significant influence on the TiZrN films proprieties, and at the same time, it can reduce the surface roughness of the film. The decrease in surface roughness was also observed in CrNiN coatings when I_{NiCr} increased from 0.75 A to 1.25 A, the surface roughness was found to decrease from 10.8 to 9.84 nm [25]. However at higher Zr content (22.2 at. % Zr) with applied higher current (2 A), corresponding to applied voltage of about - 900 V, to the two Ti and Zr targets, the dense columnar structure developed form the elongated columnar and porous surface with angular grains shape (*Figs. IV.5.e,6.e*). According to *H. Li et al*. [26] at higher applied power, the ions are repelled from the magnetron cathodes and this fact strongly weaken the plasma, which lead to the number and momentum of particles were reduced when reaching the substrate. Meanwhile, the increase of deposition rate is not significant and the thickness of TiZrN films shows little variation (1550 nm) with a rough surface (Ra = 18.7 nm) as the total applied powers reached maximum values (*Fig. IV.5.e*).

FE-SEM images of TiZrN thin films deposited at different Zr sputtering currents showed dense structure with much finer grain size at I_{Zr} of 0.6 A. As the sputtering current increased to 0.8 A, the films show small column across the surface and larger facet grain were shown at 1.0 A. The film deposited at I_{Zr} of 1.2 A exhibited porous columnar structure with highest porosity which corresponds to the zone T structure of of Andres's structural zone model [16].

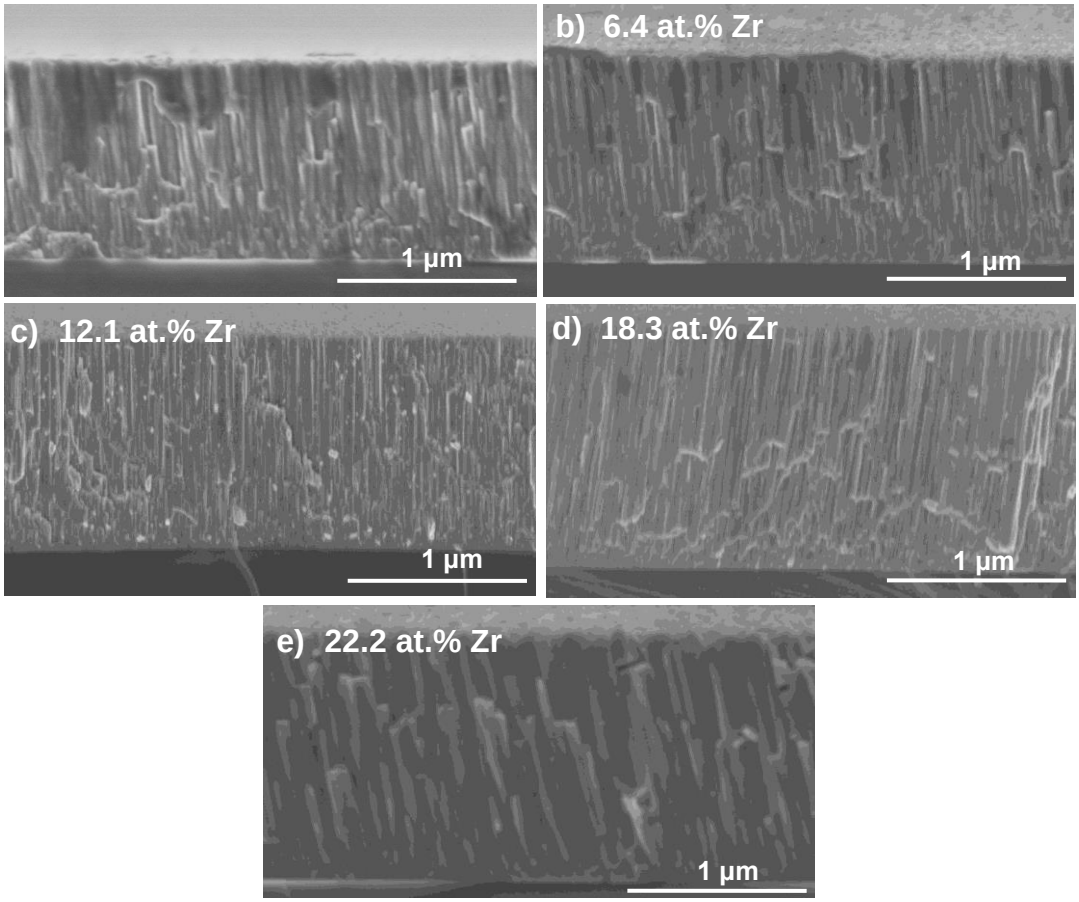

Figure IV.5. SEM image of cross-section for TiZrN films with different: **a)** 0 , b) 6.4, **c)** 12.1**, d)** 18.3 and **e)** 22.2 at. % of Zr.

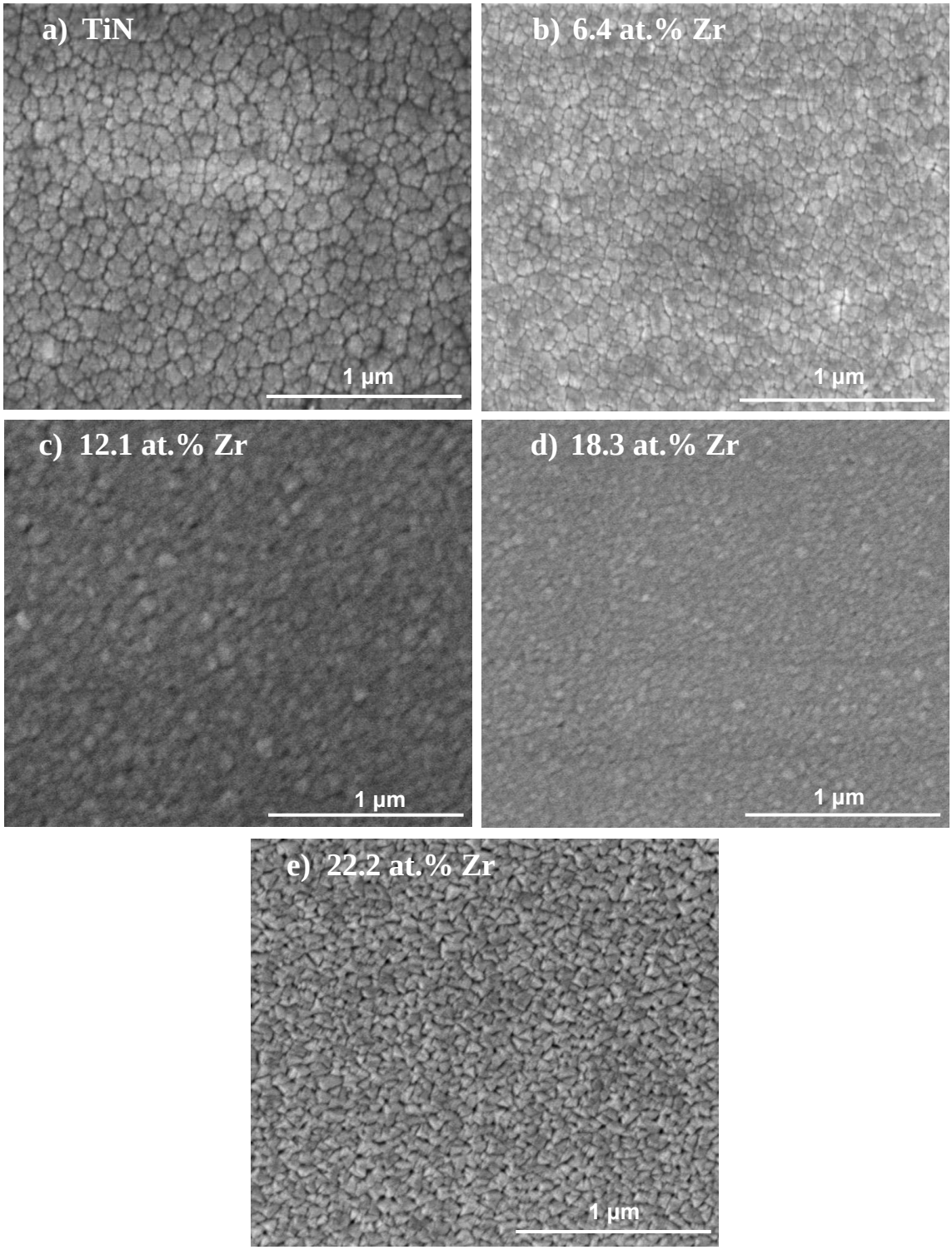

Figure IV.6. SEM image of surface for TiZrN films with different: **a)** 0 ,**b)** 6.4, **c)** 12.1, **d)** 18.3, and **e)** 22.2 at. % of Zr.

IV.2.3. Effect of Zr content on TiZrN films wettability and surface energy

The contact angle measurements were performed using three testing liquids (water, thiodiglycol and diidomethane) for each coating, and the total surface energy values of TiZrN films were calculated (*Figs. IV.7, 8*). The typical images of the apparent contact angles of water droplets on TiN, TiZrN films with different amount of zirconium are shown in *Figure IV.7*. Wettability is obtained by measuring the contact angle. A lower contact angle (≤ 90°) signifies greater wettability, whereas a higher contact angle (≥ 90°) infers lower wettability. TiN and TiZrN films containing 6.4, 12.1, 18.3, and 22.2 (at. %) of Zr delivered the following average contact angle values 123.0°, 113.2°, 111.4°, 76.0° and 96.4° , respectively. The lowest contact angle value of (76°) was provided by TiZrN coating containing 18.32 at. % of Zr as it is shown in *Figure IV.7*. This film demonstrates the highest wettability and a lower hydrophobicity as compared to the TiN coating (122.95°). According to the obtained results, we can assure that the addition of Zr to TiN coating drives its surface more hydrophilic and enhances its wettability. TiZrN system presented the highest contact angle as compared to that previous reported works (62°, 82.2°) [12, 27].

Wettability of the surface of the solid material is usually dependent on both the surface chemical status and the surface roughness. According to the SEM images of the coating containing 18.3 at. % of Zr, the surface becomes denser and smoother, with low surface roughness of 17 nm, which offered a higher wettability of TiZrN. With increasing the Zr content to 22.2 at.%, the contact angle increased as a result of an increase in the surface roughness.

This result is consistent with *F. Movassagh-Alanaghet al.* [28] work who reported a similar study on TiSiN films. They found that the TiSiN coating led to a decrease in the contact angle from 82.2°to 47.5° when Si content increased from 0 to 24.7 wt.%. Several parameters such as the morphology and the surface roughness play important role in the contact angle value [29]. The higher wettability of TiZrN coatings is attributed to the low surface roughness (17 nm for the coating containing 18.3 at. % of Zr). The contact angle increased with increasing the Zr content to 22.2 at.%, because of an increase in the surface roughness [30]. According to the SEM images of the coating containing 18.3 at. % of Zr, the

coating became denser with a smoother surface, which led to an improvement in the wettability of the coating.

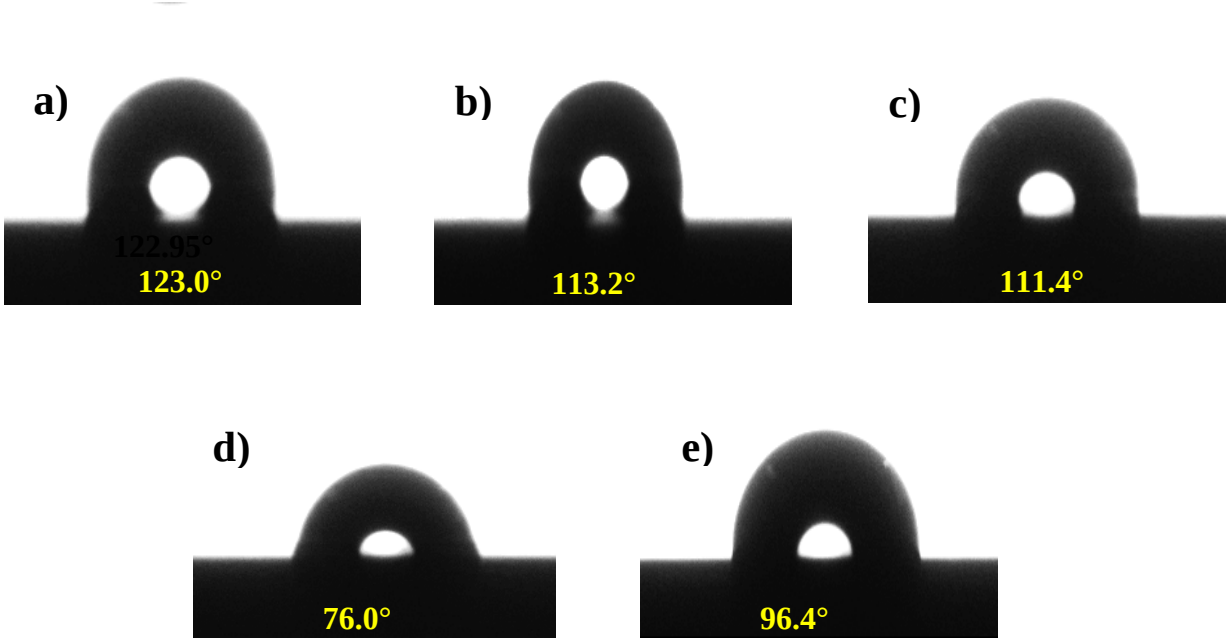

Figure IV.7. Photographs of water droplet contact angles on: **a)** TiN and TiZrN containing: **b)** 6.4, **c)** 12.1, **d)** 18.3 and **e)** 22.2 at. % of Zr.

The higher surface tension and the lower viscosity of water resulted in higher water contact angles for all TiZrN coatings than those obtained for thiodiglycol and diidomethane [31]. The total surface energy values for all TiZrN coatings were inferior to that of TiN coating (77.4 mN/m) (*Fig. IV.8*). Typically, it can be seen that increasing the Zr content provides a reduction in the total surface energy where the lowest value of 38.7 mN/m was obtained for the film 18.3 at. % of Zr. So in this case, we can say that the surface energy is inversely proportional to the wettability. The water contact angle is related to the hydrophilic property of the surface that affected by its free energy and roughness. Commonly, the higher surface free energy and/or surface roughness of a solid substrate compared to the surface tension of liquid results a better hydrophilicity and a smaller water contact angle [28]. However, many other factors affecting surface energy have been mentioned, such as phase structure, hardness or elasticity modulus [32]. According to *X. Pang et al.* [33], through film growth, the natural driving force reduce the surface energy, which controls the preferred orientation. The total surface energy reduction is caused by the decrease in (200) preferred orientation. Surface

energy of TiN coating with the (111) preferred orientation will be lower than that with the (200) orientation [33, 34], which is coherent with the results obtained in this study.

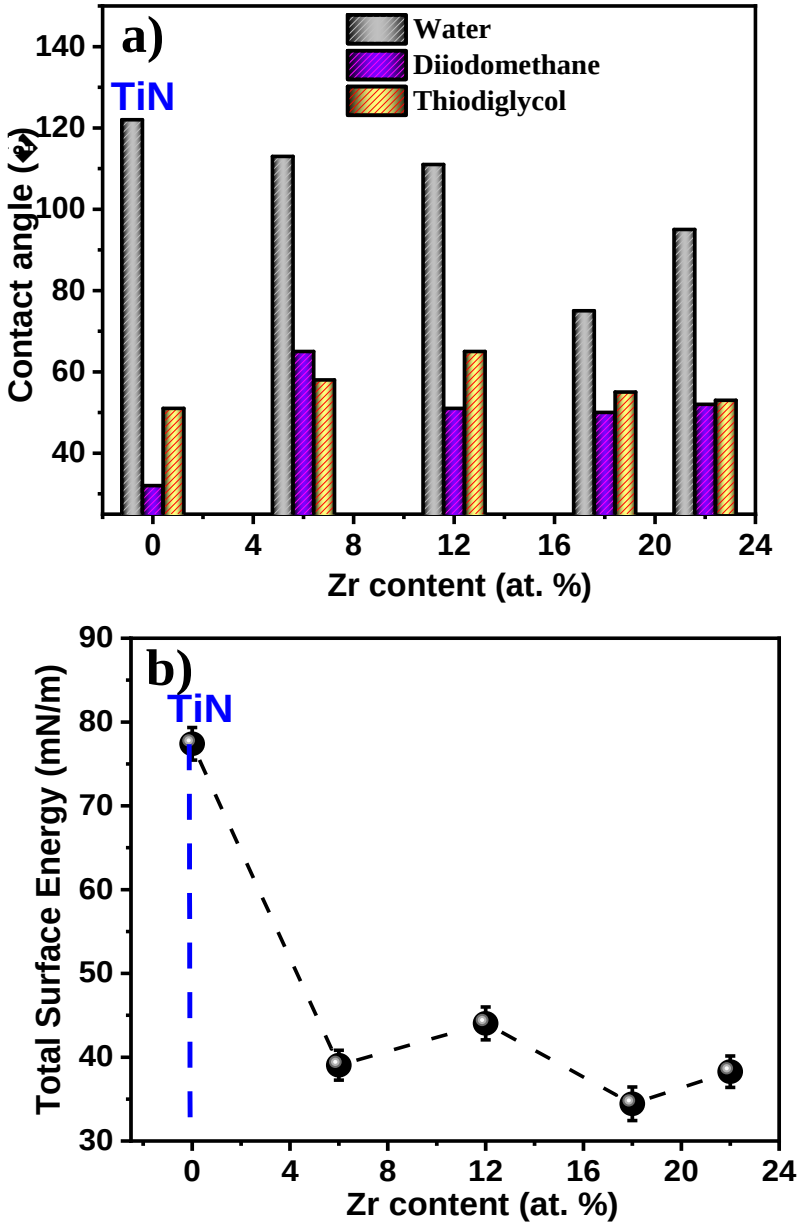

Figure IV.8.a) Contact angle measurements, and **b)** Total surface energy of TiN and TiZrN thin coatings as a function of Zr content.

IV.2.4. Effect of Zr on the mechanical properties of TiZrN films

Nanoindentation tests were performed on coated XC100 steel substrates in order to measure both the hardness (H) and Young's modulus (E) of TiZrN films with different concentrations of Zirconium (0, 6.4, 12.1, 18.3 and 22.2 at. % of Zr) according to Oliver-Pharr approach [35]. Moreover, to further elucidate the influence of Zr content on the mechanical properties of the films, H/E and H^3/E^2 were taken as effective quantitative parameters to analyze the elastic and plastic deformation resistance of hard TiZrN films [17].

Figure IV.9.a presents the variation of the hardness of TiZrN films as a function of Zr amount. At 0 at.% of Zr, TiN films exhibited hardness and Young's modulus values of (17.54 ± 0.11) GPa and (162.49 ± 4.6) GPa. The obtained values are lower than that in the case of TiN coatings obtained by other processes [36, 37] but higher than the other transition metal nitride coatings [38].

With increasing Zr applied current, the number of Zr atoms sputtered from the Zirconium target is expected to increase. The results showed a significant influence of the Zirconium content on the functional property of the TiZN nanostructured coatings. As the Zrcontent percentage increased from 0 to 18.3 at.%, the surface roughness decreased successfully refined from 46 nm to 17 nm. The coatings contained a densified structure achieved a high hardness value of (25.12 ± 0.11) and higher H/E (0.139) and H^3/E^2 (0.49 GPa). This is mainly attributed to the solid solution strengthening and the grain refinement [39]. In addition, the high strain and the lattice distortion induced by the incorporation of Zr atoms in TiN coating, as shown in *Figure IV.3*, also improves the coating hardness [40]. Furthermore, the coating growth through the packed (111) plane may also contribute to the hardness enhancement [17]. A similar decrease was reported by *Y.-W. Lin et al.* [41].

Further increasing the Zr content to 22.2 at. %, the hardness reduces to 18 GPa and therefore a drop in the H/E (0.11) H^3/E^2 (0.22 GPa) due to the increased disorder induced by weak crystallinity [38]. Similar behaviors obtained for CrWN ternary system grown on silicon substrates using a D.C magnetron reactive co-sputtering technique. The increases in W content delivered gradual increases in hardness from 20.3 GPa at 0 at. % W to the highest value of about 25.1 GPa for 24.0 at.%at of W content. Then, the micro-hardness decreases to 22.6 GPa as the W content increased to 40.5 at.% [32].

Also, *I. Asempah et al.* [42] found that the deferent concentration of Boron in TaBN nanocomposite films prepared by a reactive magnetron sputtering process, have an influence on the ternary system proprieties. The introduction of B into the films improved the hardness value from~27.9 GPa for TaN to the greatest value of ~33.3 GPa when the B concentration reched1.5 at.%. A further B concentration led to a continue reduction in hardness, due to both grain refinement and the augmentation in compressive residual stress.

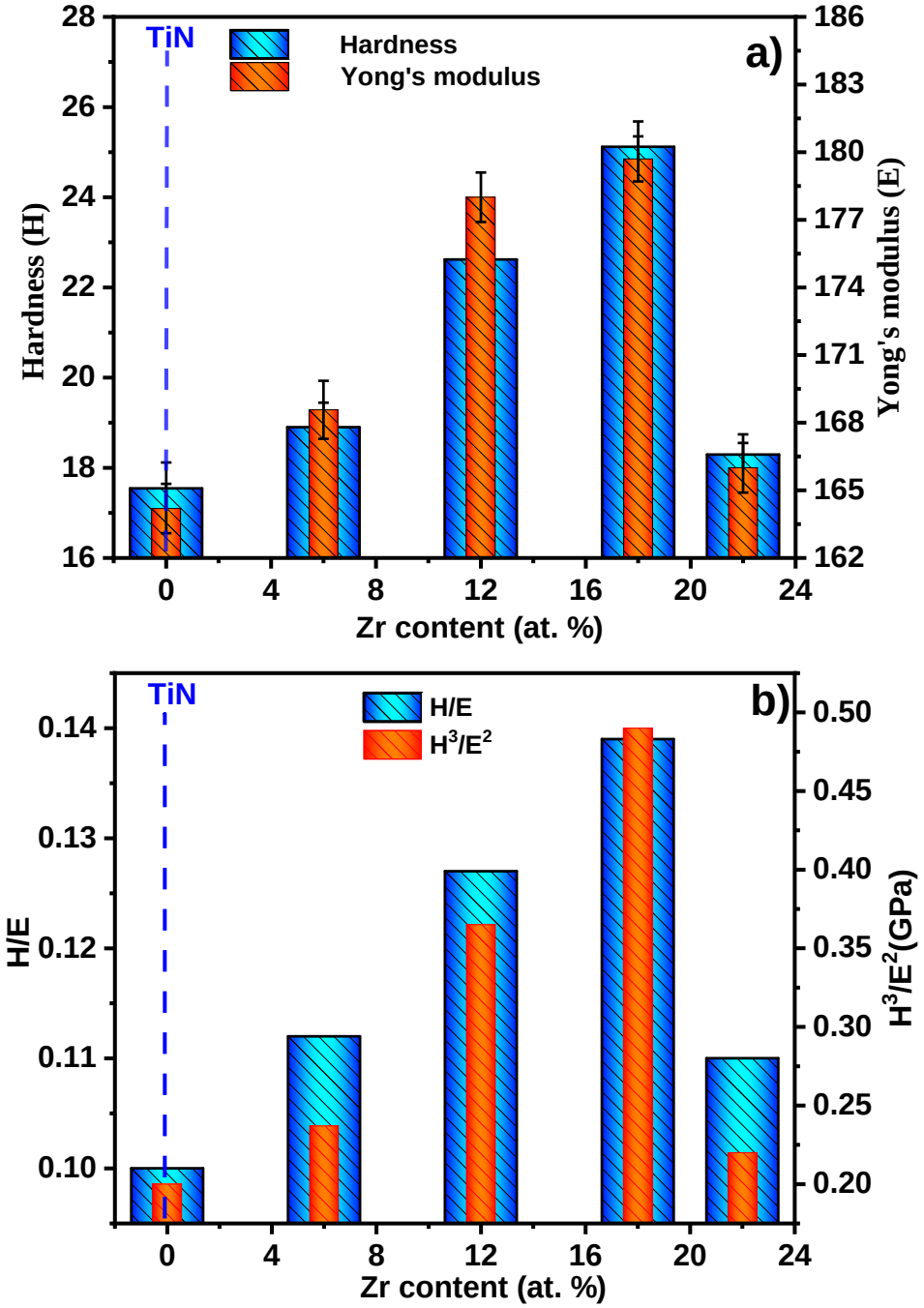

Figure IV.9.a) Hardness, Yong's modulus, and **b)** H/E and H^3/E^2 of TiZrN films as a function of Zr content.

IV.2.5. Effect of Zr content on friction and wear properties of TiZrN coatings

In order to investigate the tribological performance of TiZrN coatings, wear tests based on ball-on-disc configuration were performed. *Figure IV.10* displayed the results of the friction coefficient (CoF) and wear rate, reviewed from the tribological performance of TiZrN coatings with deferent Zr amounts.

At the beginning of the friction test, due to the low contact area and high contact pressure, sliding is difficult resulting in a higher CoF. In the later stage, the increased contact area leads to a reduction in the contact pressure and subsequently a reduction in the CoF as observed at the stable state [43].

The coefficient of friction of TiZrN films varied between 0.31 and 0.60. The maximum CoF value (0.60) and the highest wear rate (5.64×10^{-4} mm^3/Nm) were found for the TiN coating with the lowest hardness, higher roughness and higher TiN (200) intensity as compared to (111) intensity, which has a negative effect on the surface energy and provokes a higher friction coefficient [18]. The high CoF of TiN coating may also be attributed to the low TiN coating lower thickness as compared to the other coatings [44]. A relative reduction in the CoF and wear resistance of TiZrN coatings, accompanied by the incorporation of Zr, which indicates that the wear resistance of TiN is clearly improved by the cooperation of Zr *Figure IV.10*.

TiZrN coatings containing 6.4 and 12.2 at.% of Zr presented the following friction coefficient 0.56 and 0.50, respectively. TiZrN coating containing 18.3 at.% of Zr delivered the best tribological behavior and provided a lower value of CoF (0.31) and wear rate (6.65×10^{-5} mm^3/Nm). The improvement of anti-friction of TiN depends on many factors such as substrate characteristics, strain rate and contact pressure [45]. In our work, the decrease in the CoF and wear rate is attributed mainly to the solid solution's strengthening, originated by the big atomic radius of Zr, which increased with increasing Zr content. The morphology of our coating showed that surface roughness decreased and its density increased with increasing Zr content, and the highest hardness and H/E ratio of TiZrN coating containing 18.3 (at.%) [46]. At-ZrO_2 phase in TiZrN thin films at 18.3 at.% of Zr as shown in *Figure IV.10*, this phase has particularly high tenacity, increased hardness, elevated resistance to wear and corrosion, and is commonly considered as a perfect lubricant oxide so used as additives in lubricating tests [47,

48]. From the above, we assume that the decrease of friction coefficient to 0.31 mainly related to the existence of t-ZrO_2 as lubricant oxide phase protecting the surface with a soft layer. Regardless, TiZrN coating exhibited an increase in both friction coefficient and wear rate when Zr content raised to (22.2 at.%). Mainly provoked by the notable reduction in the coating hardness and H/E ratio.

The SEM observations and EDS analysis of worn surfaces of TiN and TiZrN coatings are shown in *Figure IV.11*. The surface morphology of the corresponding coatings was fond to exhibits elongated columnar and porous structure with angular grains shape with high surface roughness of 29 nm. Many studies have correlated the mechanical behavior and surface morphology with the wear performance. *H. Ju et al.* [41] declared that the increase in titanium content above 12.3 at.% in deposited WTiN films with reactive magnetron sputtering revealed the formation of the fcc-TiN phase. The wear rate (WR) was initially reduced and then increased after acquiring the lowest value of ~5.4×10^{-9} $mm^3/N\cdot m$mat 12.3 at.% of titanium. Wear rates was mainly influenced by the phase structure and some mechanical parameters such as H/E ratio, and hardness.

.

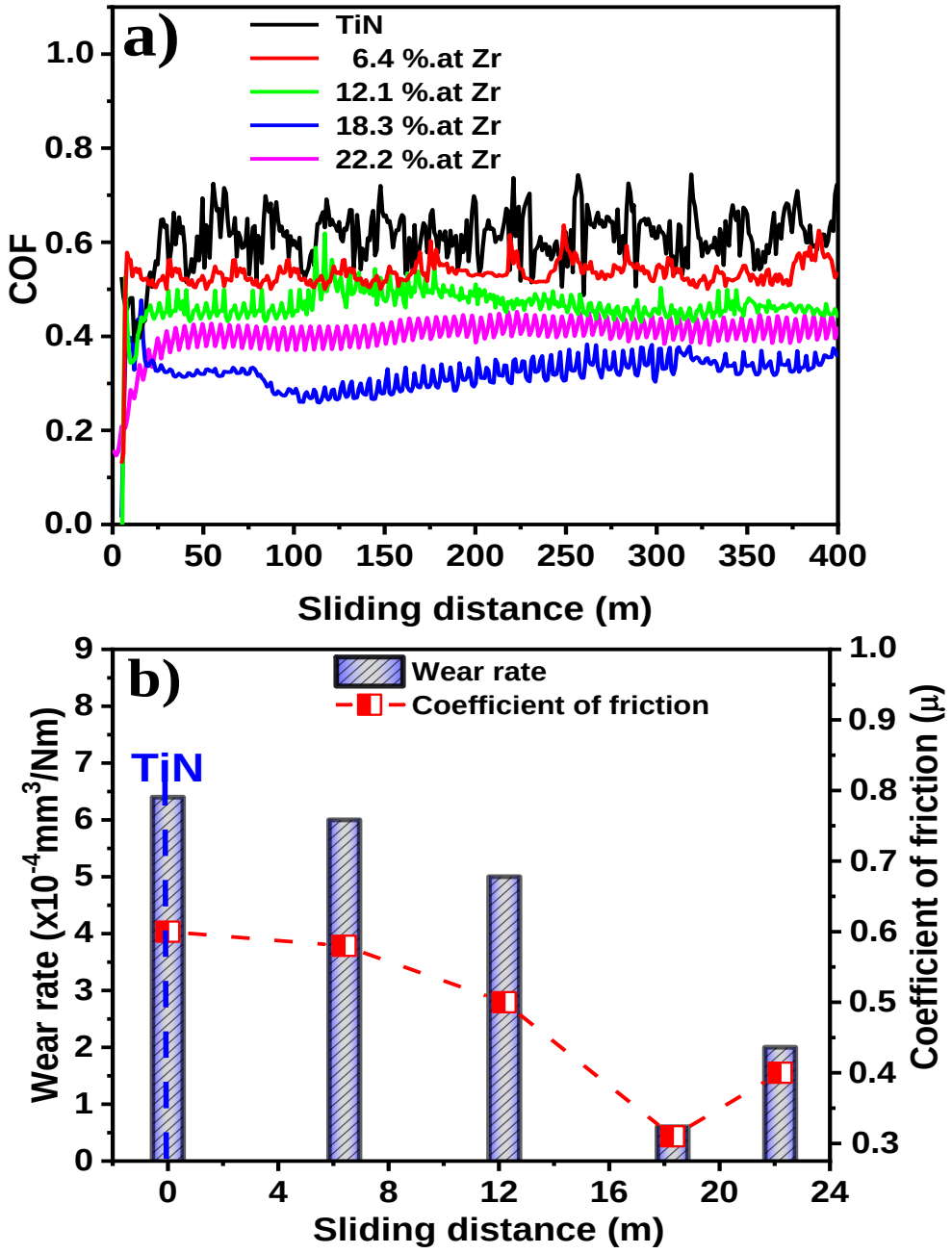

Figure IV.10.a) Friction coefficient Vs sliding distance, and **b)** wear rate and friction coefficient values of TiN and TiZrN thin coatings with different Zr content.

FigureIV.11 displays SEM observations and EDX examination of worn surfaces of TiN and TiZrN films. The worn track and undamaged zones in the coating were analyzed. EDX analyses demonstrated a difference in the elements that existed in both zones. Spalling and detachment were marked on the worn surfaces of TiN and TiZrN coating containing the most inferior Zr content (*Fig. IV.11.a, b*), which is expected to the bass mechanical proprieties where a low hardness value was detected for these coatings. The main wear mechanism of these coatings was found to be adhesive wear.

At 18.3 at. % of Zr, TiZrN coating demonstrated the lowest wear rate, friction coefficient, and roughness comparable to the other coatings with different zirconium content (*Fig. IV.10,* and *Table IV.2*). The lowest amount eliminated of the film experimented under a 2 N normal load for 400 m sliding distance was provided by this film indicating the best wear resistance attributed to its high structural and mechanical properties [49].

Figure IV.11 represents the elemental composition TiZiN thin films achieved by EDS analysis. There is an increase in the concentration of Ti, Zr, and N, and the existence of small amounts of O at the point where the wear track ends. At 18.3 at. % of Zr, the EDS analysis showed that the chemical composition of the wear debris in the middle of the track of the wear track region as following: Fe 40 %, Ti 35 %, N 14.5%, O 0.7 %, Zr 3.5 % that show a decrease in the concentration of Ti, Zr, and N, and the smallest concentration of Fe (correspond to the composition of substrate XC100) compared to other concentrations of Fe at 0, 6. 4, 12.1, and 22.2 at. % of Zr.

Figure IV.11 indicates good adhesion between TiZrN thin films and XC100 steel substrates. The lower wear rate exhibited by TiZrN coating is explained by its higher hydrophilicity as shown (*Fig. IV.7*), which leads to an increase in the number of atoms in contact with the surface. As we mentioned in section 3.4, the best mechanical properties were detected by the TiZrN coating containing 18.3 at.% of Zr, and the increase in film crystallinity improved the tribological behavior (low friction coefficient and wear rate) [50]. Similar results were obtained in our previous study, where friction coefficients and wear rates of CrZrN coatings were reduced with increasing Zr content [51]. However, at higher Zr content (22.2 % at.), there was more additional debris along the edges and the center of the track due to the insufficient substrate-film cohesion (*Fig. IV.11.e*).

These detected failures might develop from the large grain size and the differences in mechanical properties between the deposited film and substrate. The high Fe concentrations in TiN and TiZrN coatings display the inferior coating/substrate adhesion [52]. The smooth surface and the good coating adhesion decreased the friction coefficient and vice versa, roughness can therefore create an essential role in the coefficient of friction. Further, the hardness of the surfaces in contact is again so necessary: a hard, rough surface can retain a very low “real” contact area, whereas a soft, rough surface can have a higher “real” contact area than the “apparent” contact area, leading to an extremely high friction force [53].

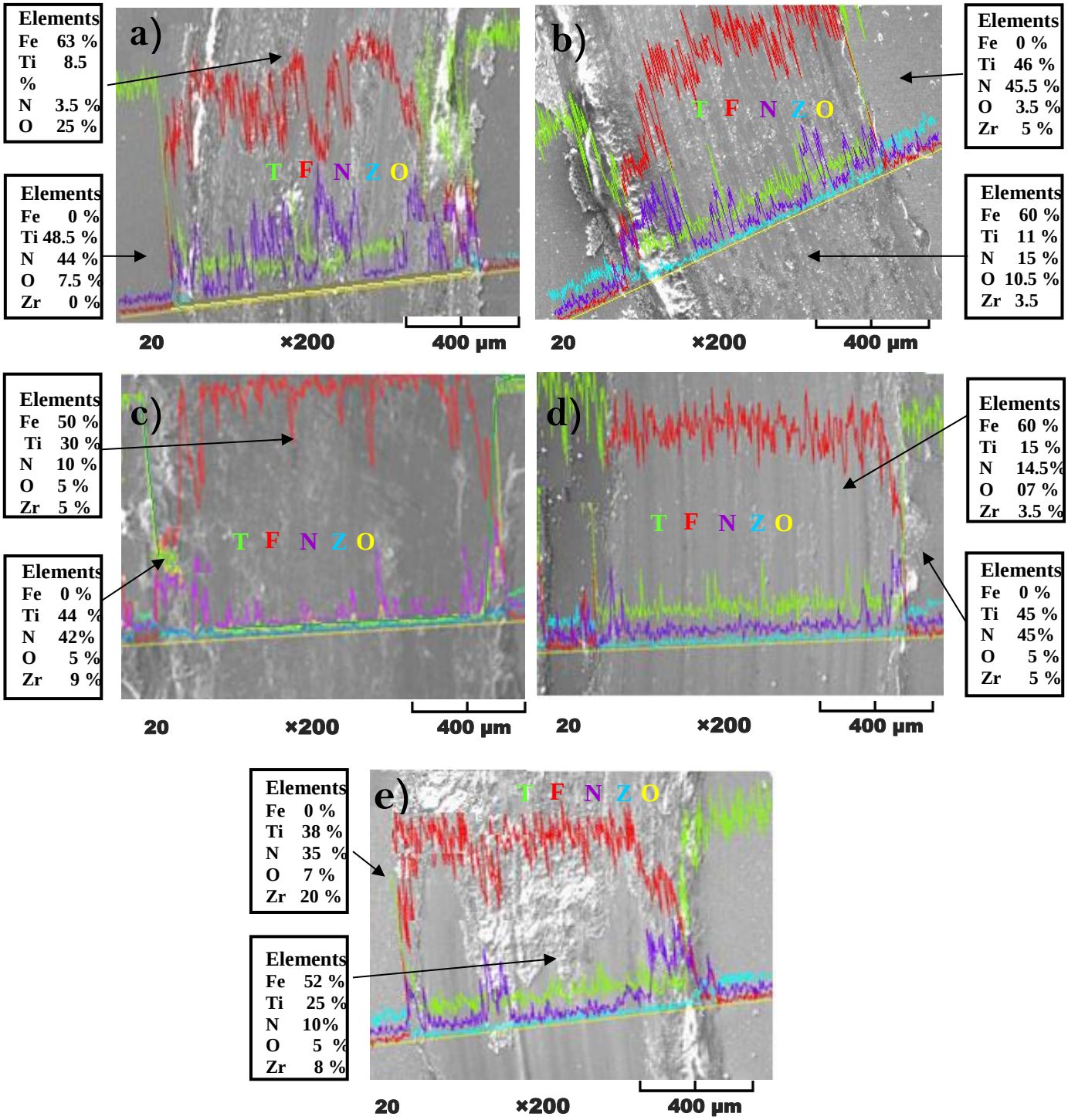

Figure IV.11. SEM images and EDX analysis of worn surfaces of **a)** TiN and TiZrN thin coating containing: **b)** 6.4, c) 12.1, **d)** 18.3 and **e)** 22.2 at.% of Zr.

IV. 3. Conclusion

In this chapter, we presented the effects of zirconium sputtering current on the structure, wetting, surface energy, mechanical and tribological properties of TiN films prepared by R.F reactive magnetron sputtering.

Firstly the examination of the effect of Zr on Structural proprieties of TiZrN films showed that TiZrN thin films displayed columnar structure, with changes in preferred orientation from (111) to (200) with increasing Zr content in the films. The grains get finer due to the in cooperation of the Zr atoms in the TiN.

Secondly, we studied the effect of Zr on the chemical composition of TiZrN films where the peak position shifted toward lower wavenumbers with increasing Zr to obtain 315 and 618 cm^{-1} close to ZrN nitride at higher Zr content, which indicate more Ti atoms are replaced by Zr atoms and a stronger vibration of Zr-N bonds are obtained during the deposition. The lowest contact angle value of (76°) was provided by TiZrN coating containing 18.32 at. % of Zr indicating good wettability provides lower surface energy.

In the end, the effect of Zr on the mechanical properties of TiZrN films demonstrated that TiZrN film with 18.3 at.% of Zr showed higher hardness and the lowest wear rate (1.033 $\times 10^{-6} mm^{-3}/N\ m$) and friction coefficient (0.39), which corresponds to the higher H/E and H^3/E^2.The tribological properties of TiN film are significantly enhanced by incorporating Zr due to solid solution strengthen and the increased H/E and H^3/E^2 are submitted to be the main motivation for the reduction of friction coefficient and wear rate.

References

[1] R. Chen, J. Tu, D. Liu, Y. Mai, C. Gu, Microstructure, mechanical and tribological properties of TiCN nanocomposite films deposited by DC magnetron sputtering, Surface and coatings technology, 205 (2011) 5228-5234.

[2] H.C. Barshilia, K. Yogesh, K. Rajam, Deposition of TiAlN coatings using reactive bipolar-pulsed direct current unbalanced magnetron sputtering, Vacuum, 83 (2008) 427-434.

[3] L. Chaleix, J. Machet, Study of the composition and of the mechanical properties of TiBN films obtained by DC magnetron sputtering, Surface and Coatings technology, 91 (1997) 74-82.

[4] F. Komarov, S. Konstantinov, V. Pilko, Formation of nanostructured TiAlN, TiCrN, and TiSiN coatings using reactive magnetron sputtering, Journal of Friction and Wear, 35 (2014) 215-223.

[5] Y.-W. Lin, J.-H. Huang, G.-P. Yu, Effect of nitrogen flow rate on properties of nanostructured TiZrN thin films produced by radio frequency magnetron sputtering, Thin solid films, 518 (2010) 7308-7311.

[6] N. Madaoui, N. Saoula, B. Zaid, D. Saidi, A.S. Ahmed, Structural, mechanical and electrochemical comparison of TiN and TiCN coatings on XC48 steel substrates in NaCl 3.5% water solution, Applied surface science, 312 (2014) 134-138.

[7] O. Maksakova, S. Simoẽs, A. Pogrebnjak, O. Bondar, Y. Kravchenko, V. Beresnev, N. Erdybaeva, The influence of deposition conditions and bilayer thickness on physical-mechanical properties of CA-PVD multilayer ZrN/CrN coatings, Materials Characterization, 140 (2018) 189-196.

[8] Y. Liu, G. Li, X. Wan, X. Zhang, Y. Shen, K. Wu, Toughness improvement by Zr addition in the simulated coarse-grained heat-affected zone of high-strength low-alloy steels, Ironmaking & Steelmaking, 46 (2019) 113-123.

[9] Z. Zhang, J. Jin, L. Liang, B. Peng, Y. Liu, S. Fu, M. Yan, High-performance Nd-Fe-B sintered magnets via co-doping high-melting-point Zr and low-melting-point Dy71. 5Fe28. 5, Journal of Magnetism and Magnetic Materials, 487 (2019) 165356.

[10] L. Chen, D. Holec, Y. Du, P.H. Mayrhofer, Influence of Zr on structure, mechanical and thermal properties of Ti–Al–N, Thin solid films, 519 (2011) 5503-5510.

[11] M. Aristizabal, P. Jamshidi, A. Saboori, S. Cox, M. Attallah, Laser powder bed fusion of a Zr-alloy: Tensile properties and biocompatibility, Materials Letters, 259 (2020) 126897.

[12] H.-L. Huang, Y.-Y. Chang, J.-X. Liu, M.-T. Tsai, C.-H. Lai, Antibacterial activity and cell compatibility of TiZrN, TiZrCN, and TiZr-amorphous carbon coatings, Thin Solid Films, 596 (2015) 111-117.

[13] G. Lu, L. Yu, H. Ju, B. Zuo, J.J.S.E. Xu, Influence of nitrogen content on the thermal diffusivity of TiN films prepared by magnetron sputtering, Surface Engineering, 36 (2020) 192-198.

[14] B. Xu, P. Guo, Z. Wang, R. Chen, Y. Ye, J. Shuai, A. Wang, P. Ke, Anti-wear Cr-VN coating via V solid solution: Microstructure, mechanical and tribological properties, Surface and Coatings Technology, 397 (2020) 126048.

[15] N. Witit-Anun, A. Teekhaboot, Effect of Ti sputtering current on structure of TiCrN thin films prepared by reactive DC magnetron co-sputtering, Key Engineering Materials, Trans Tech Publ, 675 (2016) 181-184.

[16] S. Chinsakolthanakorn, A. Buranawong, N. Witit-Anun, S. Chaiyakun, P. Limsuwan, Characterization of nanostructured TiZrN thin films deposited by reactive DC magnetron co-sputtering, Procedia Engineering, 32 (2012) 571-576.

[17] H. Li, Z. Liu, J. Li, J. Huang, J. Kong, Q. Wu, D.J.J.S. Xiong, C. Technology, Effects of Hf addition on the structure, mechanical and tribological properties of CrN film, Surface and Coatings Technology, 397 (2020) 126067.

[18] W. Phae-Ngam, M. Horprathum, C. Chananonnawathorn, T. Lertvanithphol, B. Samransuksamer, P. Songsiriritthigul, H. Nakajima, S.J.C.A.P. Chaiyakun, Oblique angle deposition of nanocolumnar TiZrN films via reactive magnetron co-sputtering technique: The influence of the Zr target powers, Current Applied Physics,19 (2019) 894-901.

[19] L. Aissani, M. Fellah, A. Belgroune, A. Obrosov, M.A. Samad, A. Alhussein, Effect of O2 flow rate on the structure, wettability and tribo-mechanical behaviour of Zr-ON thin films, Surfaces and Interfaces, 26 (2021) 101441.

[20] L. Aissani, M. Fellah, C. Nouveau, Structural Mechanical and Tribological Behavior of Reactive Sputtered Cr-N and Cr-VN Films, Diffusion Foundations, Trans Tech Publ, 18 (2018) 27-34.

[21] L. Duan, H. Wu, L. Guo, W. Xiu, X. Yu, The effect of phase on microstructure and mechanical performance in TiAlN and TiSiN films, Materials Research Express, 7 (2020) 066401.

[22] M. Franck, J.-P. Celis, J.J.J.o.m.r. Roos, Microprobe Raman spectroscopy of TiN coatings oxidized by solar beam heat treatment, Journal of materials research, 10 (1995) 119-125.

[23] R. Chowdhury, R. Vispute, K. Jagannadham, J.J.J.o.M.R. Narayan, Characteristics of titanium nitride films grown by pulsed laser deposition, Journal of Materials Research, 11 (1996) 1458-1469.

[24] B. Usmani, A.J.S.E. Dixit, Spectrally selective response of ZrOx/ZrC–ZrN/Zr absorber–reflector tandem structures on stainless steel and copper substrates for high temperature solar thermal applications, Solar Energy, 134 (2016) 353-365.

[25] R. Akhter, Z. Zhou, Z. Xie, P. Munroe, Harmonizing mechanical responses of nanostructured CrN coatings via Ni additions, Applied Surface Science, 538 (2021) 147987.

[26] H. Li, Z. Liu, J. Li, J. Huang, J. Kong, Q. Wu, D. Xiong, Effects of Hf addition on the structure, mechanical and tribological properties of CrN film, Surface and Coatings Technology, 397 (2020) 126067.

[27] Y.-W. Lin, P.-C. Chih, J.-H.J.S. Huang, C. Technology, Effect of Ti interlayer thickness on mechanical properties and wear resistance of TiZrN coatings on AISI D2 steel, Surface and Coatings Technology, 394 (2020) 125690.

[28] F. Movassagh-Alanagh, A. Abdollah-zadeh, M. Asgari, M.A. Ghaffari, Influence of Si content on the wettability and corrosion resistance of nanocomposite TiSiN films deposited by pulsed-DC PACVD, Journal of Alloys and Compounds, 739 (2018) 780-792.

[29] F. Madadi, A. Rezaeian, H. Edris, M. Zhiani, Influence of surface roughness and hydrophobicity of bipolar plates on PEM performance, Surface and Coatings Technology, 389 (2020) 125676.

[30] S.K. Rawal, A.K. Chawla, R. Jayaganthan, R.J.J.o.M.S. Chandra, Technology, Structural, wettability and optical investigation of titanium oxynitride coatings: effect of various sputtering parameters, Journal of Materials Science Technology, 28 (2012) 512-523.

[31] K.-Y. Law, Definitions for Hydrophilicity, Hydrophobicity, and Superhydrophobicity: Getting the Basics Right, The Journal of Physical Chemistry Letters, 5 (2014) 686-688.

[32] E. Lugscheider, K. Bobzin, M.J.T.S.F. Möller, The effect of PVD layer constitution on surface free energy, Thin Solid Films, 355 (1999) 367-373.

[33] X. Pang, L. Zhang, H. Yang, K. Gao, A.A. Volinsky, Residual Stress and Surface Energy of Sputtered TiN Films, Journal of Materials Engineering and Performance, 24 (2015) 1185-1191.

[34] C. Körber, J. Suffner, A. Klein, Surface Energy Controlled Preferential Orientation of Thin Films, Journal of Physics D: Applied Physics, 43 (2010) 055301.

[35] W.C. Oliver, G.M.J.J.o.m.r. Pharr, An improved technique for determining hardness and elastic modulus using load and displacement sensing indentation experiments, Journal of materials research, 7 (1992) 1564-1583.

[36] L.-J. Meng, M.J.S. Dos Santos, C. Technology, Characterization of titanium nitride films prepared by dc reactive magnetron sputtering at different nitrogen pressures, Surface and Coatings Technology, 90 (1997) 64-70.

[37] T. Reeswinkel, D.G. Sangiovanni, V. Chirita, L. Hultman, J.M.J.S. Schneider, C. Technology, Structure and mechanical properties of TiAlN–WNx thin films, Surface and Coatings Technology, 205 (2011) 4821-4827.

[38] B. Xu, P. Guo, Z. Wang, R. Chen, Y. Ye, J. Shuai, A. Wang, P.J.S. Ke, C. Technology, Anti-wear Cr-VN coating via V solid solution: Microstructure, mechanical and tribological properties, Surface and Coatings Technology, 397 (2020) 126048.

[39] L. Yu, H. Zhao, J.J.A.s.s. Xu, Mechanical, tribological and corrosion performance of WBN composite films deposited by reactive magnetron sputtering, Applied surface science, 315 (2014) 380-386.

[40] S. Tan, X. Zhang, X. Wu, F. Fang, J.J.A.s.s. Jiang, Effect of substrate bias and temperature on magnetron sputtered CrSiN films, Applied surface science, 257 (2011) 1850-1853.

[41] Y.-W. Lin, J.-H. Huang, G.-P.J.J.o.V.S. Yu, S. Technology A: Vacuum, Films, Microstructure and corrosion resistance of nanocrystalline TiZrN films on AISI 304 stainless steel substrate, Journal of Vacuum Science Technology A: Vacuum, Surfaces, 28 (2010) 774-778.

[42] I. Asempah, J. Xu, L. Yu, L. Wang, Effect of boron concentration on the mechanical, tribological and corrosion properties of Ta–B–N films by reactive magnetron sputtering, Ceramics International, 45 (2019) 19395-19403.

[43] F.X. Liu, F.Q. Yang, Y.F. Gao, W.H. Jiang, Y.F. Guan, P.D. Rack, O. Sergic, P.K. Liaw, Micro-scratch study of a magnetron-sputtered Zr-based metallic-glass film, Surface and Coatings Technology, 203 (2009) 3480-3484.

[44] O.P. Terleeva, A.I. Slonova, A.B. Rogov, A. Matthews, A.J.M. Yerokhin, Wear Resistant Coatings with a High Friction Coefficient Produced by Plasma Electrolytic Oxidation of Al Alloys in Electrolytes with Basalt Mineral Powder Additions, Materials, 12 (2019) 2738.

[45] E. Hornbogen, The role of fracture toughness in the wear of metals, Wear, 33 (1975) 251-259.

[46] X. Feng, K. Zhang, Y. Zheng, H. Zhou, Z.J.N.I. Wan, M.i.P.R.S.B.B.I.w. Materials, Atoms, Effect of Zr content on structure and mechanical properties of (CrTaNbMoV) Zrx high-entropy alloy films, Nuclear Instruments, 457 (2019) 56-62.

[47] S. Zheng, R. Guan, Q. Guo, D.J.S.R. Su, Letters, The design of surface modification of amorphous ZrO_2 nanoparticles as a lubricant additive, Surface Review and Letters, 14 (2007) 1047-1052.

[48] A. Hernández Battez, R. González, J.L. Viesca, J.E. Fernández, J.M. Díaz Fernández, A. Machado, R. Chou, J. Riba, CuO, ZrO2 and ZnO nanoparticles as antiwear additive in oil lubricants, Wear, 265 (2008) 422-428.

[49] K. Holmberg, A concept for friction mechanisms of coated surfaces, Surface and Coatings Technology, 56 (1992) 1-10.

[50] F. Song, Q. Wang, T. Wang, The effects of crystallinity on the mechanical properties and the limiting PV (pressure×velocity) value of PTFE, Tribology International, 93 (2016) 1-10.

[51] M. Fellah, L. Aissani, M. Abdul Samad, A. Purnama, H. Djebaili, A. Montagne, A. Iost, C.J.I.J.o.A.C.T. Nouveau, Effect of Zr content on friction and wear behavior of Cr-Zr-N coating system, International Journal of Applied Ceramic Technology, 15 (2018) 701-715.

[52] M. Łępicka, M. Grądzka-Dahlke, D. Pieniak, K. Pasierbiewicz, K. Kryńska, A. Niewczas, Tribological performance of titanium nitride coatings: A comparative study on TiN-coated stainless steel and titanium alloy, Wear, 422 (2019) 68-80.

[53] J.L. Hall, C.J. Bevas, S.J. Hinder, E.L. Kynaston, I. Lindsay, P. Gruber, J. Keddie, Environmental Effects on the Coefficient of Friction and Tack Adhesion of Formulated Waterborne Coatings, Frontiers of Mechanical Engineering, 7 (2022) 113.

GENERAL CONCLUSION

In conclusion

We carried out this investigation in: LASMIS laboratory, University of Technology (Troyes, France). Our purpose was to carry out experimentations on the improvement of structural mechanical, tribological, and wetting performance of the TiN binary system by the insertion of zirconium. The bibliographical study carried out made it possible to instruct our selection on this kind of coating. We were then particularly interested in the characterization of structured thin films of titanium nitride and titanium zirconium nitride. The main purpose of this thesis was to study and understand the effects of different amounts of zirconium Zr inserted into TiN lattice to obtain a strength solid solution and stoichiometric structure and well understand its effect on the surface and interface proprieties of the produced coatings.

These were produced by the technique of R.F magnetron sputtering in a reactive medium that delivers deposition efficiency and industrial adaptability. TiN films were deposited on Si (100) wafers, and XC100 steel substrates. The variation in nitrogen content from 0 and 30 % showed the appearance of various phases with different microstructures. XRD data showed that the film phases changed from Ti to Ti_2N and TiN with increasing nitrogen content. The diffraction peaks shifted to lower angles with a (111) TiN preferential plan indicating the presence of compressive residual stress. Increasing the nitrogen content in the TiN films led to increase the lattice strain in film crystals and decrease the film thickness and grain size.

The measurements of contact angles between water-droplets and TiN film surfaces showed that all films had a high wettability and increasing the nitrogen content in film led to increase its surface hydrophobicity. This can be related to the enhancement of surface softness as mentioned by the AFM and SEM images. Nanoindentation measurements showed that hardness and Young's modulus of the coatings exhibited an increase from (7.1 GPa, 195.2 GPa) to (27.78 GPa, 304.8 GPa) when nitrogen flow rate was varied from 5 to 20 %, respectively. Increasing the nitrogen content up to 48.5 at.% in film led to enhance its hardness, elasticity modulus, resistance to plastic deformation and toughness.

The tribological tests showed that the lowest friction coefficient of ~ 0.36 and the best adhesion were obtained for the TiN coating deposited at 20 % of N_2 flow rate (film containing 48.5 at.% of nitrogen). This last configuration was confirmed as the best one and the addition of more nitrogen led to slightly decrease these properties.

For the TiZrN films, the increase in Zr content, changed the preferred orientation from (200) to (111), and the maximum hardness value of (25GPa) was achieved and total surface energy of 38.7 mN/m for TiZrN coating with 18.3 at.% of Zr, corresponding to the grain refinement (17 nm) and the large lattice distortion due to the incorporation of Zr atoms in the TiN system.

The tribological performance of TiN coating was significantly improved by the incorporation of zirconium, and the solid solution strengthening managed the decrease of friction coefficient and wear rate.

Perspectives

- *The effect on the structure modulation using WIN2K for in the aim to determine the atoms' positions which will new data in the crystallography part.*
- *The preparations of other doped phases by other elements in the TiN crystal and study their structural, physical, and tribo-mechanical properties.*
- *Preparation and simulation of the physical properties of new hard ternary and quaternary systems.*
- *Trying to study the corrosion resistance and antibacterial activity with novel methods.*

Liste of our publication and cominications

Publications liste

Published research	Title	year
Article **Surfaces and Interfaces Volume 27, December 2021, 101519**	Experimental investigation of structural, wetting, mechanical and Tribological properties of TiZrN thin films deposited by magnetron sputtering. Faiza Salhi, Linda Aissani, Mamoun Fellah, Abdelhakim Chadlie, Abderrahmane Cheriet, Ahlam Belgroune, Corinne Nouveau, Aleksei Obrosov, Mohammed Abdul Samad, Akram Alhussein. https://doi.org/10.1016/j.surfin.2021.101519	2021
Article **J Mater Sci 56, 17319–17336 (2021).**	Investigating the effect of nitrogen on the structural and tribo-mechanical behavior of vanadium nitride thin films deposited using R.F. magnetron sputtering. Linda Aissani, Mamoun Fellah, Ablel Hakim Chadli, MohammedAbdul Samad, Abderrahmane Cheriet, Faiza Salhi, Corinne Nouveau, Sabine Weiß, Aleksei Obrosov & Akram Alhussein. https://doi.org/10.1007/s10853-021-06393-0	2021
Article **Algerian Journal of Engineering, Architecture and Urbanism** Vol. 5 Nr. 5 2021 ISSN: 2588-1760	Evolution of Structure and Mechanical properties of TiCrN Films. Linda AISSANI, Abdenour SAOUDI, Abderrahmane CHERIET, Faiza SALHI.	2021
Article **vol. 406, Trans Tech Publications, Ltd., Jan. 2021, pp. 312–318.**	Mechanical and Tribological Behaviors of Nanocomposite Titanium Nitrides Coatings. Ahlam Belgroune, Linda Aissani, Faiza Salhi, Corinne Nouveau, Akram Alhussein. https://doi.org/10.4028/www.scientific.net/DDF.406.312	2021
Chapter	Mechanical and Tribological Behaviors of Nanocomposite Titanium Nitrides Coatings. Ahlam Belgroune, Linda Aissani, Faiza Salhi, Corinne Nouveau, Akram Alhussein. https://doi.org/10.4028/www.scientific.net/DDF.406.312	2021
Chapter **Springer, Cham**	Influence of Nitrogen Partial Pressure on the Structural, and Mechanical Properties of Ti-N Thin Films. F. Salhi, L. Aissani, C. Nouveu, A. Alhussein DOI: 10.1007/978-3-030-43211-9_17	2020

Communication liste

Communication	Title	Date and Organization
Poster communication at th 5th international conferance on energy, materials, applied enegetics and pollution (ICEMAEP'19)	**Caracterization structurale et mécanique des nitrures de vanadium.**	**22nd.23th of october 2019 constantine, Algeria**

Oral cominication at the 4th international sympsium on material and sustainable develompment	**The study of mechanical proprieties of Ti-N on machines steel substrates**	**12-14 November , 2019, Boumerdes -Alegria**
Oral cominication at National Virtual Conference participation at The 1st National Virtual Conference on chemical Process and environnemental engineering**NVCCPEE2021.**	**Microstructural, taxture and micanical proprities of magnetron sutre CrN films deposited at defferent nitrogene flowrate**	**December 15-16, 2021At Biskra University**
Oral cominication at 1st National Conference on Applied Science and Advanced Materials, NCASAM-2021	**The influence of oxygen on structural, mechanical properties and wettability of sputtered Zr -ON coatings**	**December 20-22, 2021 – ENSET–Skikda**
Poster communication at Virtual conference the first International Conference on Sustainable Energy and Advanced Materials IC-SEAM	communication entitled: Elaboration and characterization of magnetron radio-frequency sputtered ZrC thin films	**21 April 21-22, 2021, Ouargla, ALGERIA,**

Surfaces and Interfaces 27 (2021) 101519

Contents lists available at ScienceDirect

Surfaces and Interfaces

journal homepage: www.sciencedirect.com/journal/surfaces-and-interfaces

Experimental investigation of structural, wetting, mechanical and Tribological properties of TiZrN thin films deposited by magnetron sputtering

Faiza Salhi [a], Linda Aissani [a,b,*], Mamoun Fellah [c,d,*], Abdelhakim Chadli [e], Abderrahmane Cheriet [f], Ahlam Belgroune [a], Corinne Nouveau [g], Aleksei Obrosov [h,i], Mohammed Abdul Samad [j,k], Akram Alhussein [l]

[a] Mater sciences Department, Abbes Laghrour-Khenchela University P.O 1252, 40004, Algeria.
[b] Active Components and Materials Laboratory, Larbi BEN M'HIDIUniversity, Oum El Bouaghi, 04000, Algeria
[c] Tribology, materials surface and interfaces group, laboratory of metallurgy and materials science, Annaba university BO, 12 CP 23000. Algeria
[d] Department of Mechanical Engineering, AbbesLaghrour- Khenchela University P.O 1252, 40004, Algeria
[e] Molecular Chemistry and Environment Laboratory, University of Biskra, Algeria
[f] Laboratory of studies and development of the Semiconducting and Dielectric Materials, Laghouat University, Algeria
[g] Arts et Metiers Institute of Technology, LABOMAP, HESAM Université, F-71250 Cluny, France
[h] Department of Physical Metallurgy and Materials Technology, Brandenburg University of Technology, 03044 Cottbus, Germany
[i] Laboratory of Medical Materials and Shape Memory Implants, National Research Tomsk State University, 634045, Tomsk, Russia
[j] Mechanical Engineering Department, King Fahd University of Petroleum and Minerals, Dhahran- 31261, KSA
[k] Interdisciplinary Research Centre for Advanced Materials, King Fahd University of Petroleum and Minerals, Dhahran- 31261, KSA
[l] LASMIS, University of Technology of Troyes, Technological Pole of South Champagne, 26 Lavoisier rd., 52800 Nogent, France.

ARTICLE INFO

Keywords:
TiZrN film
Magnetron sputtering
Structure
Surface wettability
Mechanical properties
Wear resistance

ABSTRACT

-TiZrN thin films were deposited on Si (100) wafers and XC100 steel substrates by reactive R.f. magnetron sputtering using titanium and zirconium targets in an Ar-N_2 mixture atmosphere to evaluate the effect of varying Zr content (0 to 22.2 at.%), on the film structure, surface wettability, hardness and wear resistance. The presence of different phases such as TiN, ZrN, and ZrO_2 were confirmed by XRD analysis. Results showed that, the lattice parameter and film thickness increased while the crystallite size and average roughness decreased with increasing Zr content. Total surface energy between the film surface and testing liquids decreased with the addition of Zr. TiZrN film containing 18.3 at.% of Zr showed the lowest surface energy of 38.7 mN/m, indicating its hydrophobicity. The nanoindentation measurements, friction and wear tests showed that the TiZrN thin film containing 18.3 at.% of Zr had the best tribo-mechanical performance. The TiZrN (18.3 at.% Zr) film exhibited the lowest friction coefficient (0.31), and the lowest wear rate (6.65×10^{-5} mm^3/Nm), which corresponds to the highest H/E ~ 0.139, and H^3/E^2 ~ 0.49 GPa ratios. The improvement in the tribo-mechanical properties is attributed to the solid solution strengthening due to the incorporation of Zr atoms in TiN system, which results in the highest hardness of 25 GPa for TiZrN (18.3 at.% Zr) film.

1. Introduction

In general, wear, friction and corrosion of components can be reduced by using advanced durable materials, which are very expensive. However, one of the more economical alternate routes available to improve the material performance against wear and corrosion are thin coatings, which is an effective surface treatment method in severe environments [1–8]. Hard thin coatings have found their way in a variety of applications, which are subjected to extreme tribological conditions such as high pressure, high temperature and corrosive environments.

Titanium nitride (TiN) is one of the most common transition metal nitride coatings used in many applications due to its outstanding proprieties, such as high corrosion resistance [8] and high hardness [9].

E-mail addresses: lindaaissani2004@yahoo.fr (L. Aissani), mamoun.fellah@yahoo.fr (M. Fellah).
* Corresponding authors.

https://doi.org/10.1016/j.surfin.2021.101519
Received 5 July 2021; Received in revised form 20 September 2021; Accepted 1 October 2021
Available online 20 October 2021

This nitride has also high chemical resistance [10,11], superconductivity [12], good biocompatibility [7] as well as a beautiful golden yellow color [13].

The TiN coatings have been found to be very effective in improving the performance of the components and in protecting them from wear and corrosion[2, 3]. Experimental data on potentiodynamic polarization show that the corrosion current densities of TiN-coated titanium were up to six times lower as compared to uncoated Ti [4]. Similar to gold, copper or silver, TiN thin films proved to be a better alternative plasmonic material for metamaterial fields in the visible and near-IR frequencies [5]. These coatings are also used in various other applications, such as decorative manufacturing or medical applications [6]. In contrast to other coatings, Hauer et al., confirmed that TiN-coated implants did not exhibit clinical benign results after long-term follow-up [13].

The in vivo wear resistance of cobalt-chromium femoral components coated with TiN showed damage caused by wear propagation at the implant, presence of stress and severe third-body wear resulting in the abrasion of the coating [14]. *Lapaj* et al. concluded that even though the TiN coating of knee prostheses forms a monolithic layer on the coated surfaces, caution must be administered in using these implants in patients, sensitive to metal because of the wear and degradation associated with third bodies and microscopic defects shown by TiN coating [15].

However, one of the major drawbacks of the TiN coatings is its lack of chemical stability and limited oxidation resistance at elevated temperatures [16]. Kumar et al. noted that TiN in the zone I microstructure includes a large amount of oxygen exhibiting an interdiffusion at 600 °C [17]. *Milošev et al.*, affirmed that at elevated temperatures TiN is oxidized due to the substitution of nitrogen by oxygen, resulting in the formation of TiO_2 layer at elevated temperatures leading to a phase separation between the nitride and oxide [18]. Thus, the interdiffusion of selective elements through the grain boundaries of the TiN film caused by annealing, at higher temperatures results in the reduction of its properties [19].

Recently, TiMN ($M = B$, Al, C, Si, Zr) nanocomposite coatings with higher hardness, excellent tribo-mechanical properties, improved stabilization and higher oxidation resistance have been developed and investigated. Many researchers reported that the addition of specific elements to TiN matrix could enhance the system properties [14–18]. *Lu et al.*, reported that the nanocomposite $TiB_{0.61}N_{1.04}$ thin coating exhibited a higher oxidation resistance at elevated temperatures as compared to TiN [16]. Implantation of Al-ions in a TiN film greatly improved thermal oxidation resistance at temperatures up to 973 K, and for periods up to 20 h in a pure oxygen atmosphere. The high thermal stability and the age-hardening effect are attributed to the coherent spinodal decomposition in the Ti-Al-N system [17,18]. Furthermore, addition of C to TiN resulted in enhanced hardness and resistance to uniform and pitting corrosion [19].

However, the effect of zirconium (Zr) on the structural, mechanical, and tribological properties of TiN coatings is less investigated in comparison to other elements. The TiZrN coatings show specific properties, such as excellent toughness [20], high melting point [21], biocompatibility with the human body [22], and good oxidation resistance [23]. When the film is mechanically damaged, it regenerates itself because of the formation of zirconium oxide on the surface [24]. Zr has a larger atomic radius (0.160 nm) than Ti (0.147 nm), which may cause higher distortion in TiN [25]. The incorporation of Zr in the TiN coating results in the supersaturated solid solution with high hardness. Under equivalent conditions, TiZrN coating shows enhanced hardness as compared to binary TiN and ZrN coatings [26]. Moreover, the TiZrN coating exhibits a higher contact angle (higher hydrophobicity) as compared to uncoated Ti plates or TiZrCN coating [27]. The TiZrN coating can be manufactured using different methods and techniques including plasma beam sputtering [28], arc ion plating [29], cathode arc deposition [30], and most commonly by RF/DC magnetron sputtering technique [31,32].

Lin et al. [33], produced nanocomposite (Ti, Zr) N thin coatings at low nitrogen flow rates by means of magnetron sputtering. The appearance of a (Ti, Zr) N single-phase solid solution was observed for the coating deposited at 2–7 sccm nitrogen flow rates. The coating presented (111) preferred orientation and an excellent hardness ranging from 35.5 to 37.5 GPa.

Ternary TiZrN coatings deposited by direct current unbalanced magnetron sputtering at different substrate biases ranging from −40 V to −120 V, exhibited low roughness, high hardness, low resistivity and a bright-golden color [34].

El-Hossary et al., [35] used DC-pulsed magnetron sputtering to produce TiZrN thin coatings on AISI 316 substrates. They reported an increase in the hardness of the TiZrN coating with increased plasma-processing power, which reached a maximum value of 1050 $HV_{0.015}$ at 200 W. The wear rate of the coating had a very low value of 0.0034 mm^3/Nm as compared to the AISI 316 bare substrate (0.137 mm^3/Nm). Recently, *Phae-ngam* et al., [36] deposited nano-columnar titanium zirconium nitride coatings on silicon wafer substrates via reactive magnetron co-sputtering with oblique angle deposition (OAD). Increasing the sputtering power of Zr target from 100 to 300 W led to an increase in the length and diameter of the nanocolumns in the TiZrN thin coating. However, the wear mechanisms of TiZrN coatings while protecting alloy surfaces remain largely unknown. Nevertheless, there have been few works on the tribological performance of TiZrN coatings [33–36]. Hence, the focus of this work is to improve the wear resistance and wettability of TiZrN thin coatings by creating a dense structure byusing the reactive R.F. magnetron sputtering technique. Moreoever, the effect of Zr content on the mechanical and tribological performance of TiZrN coatings is evaluated in detail.

2. Experimental procedure

2.1. Deposition process

TiN and TiZrN thin coatings were deposited on Si (100) wafers and XC100 steel substrates by a reactive radio-frequency magnetron sputtering technique using two high purity Ti (99.99%, 200 mm diameter × 6 mm length) and Zr (99.99%, 200 mm diameter × 6 mm length) targets. The deposition of the coatings was carried out in a mixture of (80 sccm Ar + 20 sccm N_2) gasses at a constant working pressure of 0.4 Pa. The coatings deposited on Si (100) wafers (20 × 20 mm^2) were used for RAMAN, EDX, SEM, contact angle and nanoindentation tests.

The coatings deposited on XC100 steel substrates were used for XRD and tribological tests. Prior to deposition, the substrates were ultrasonically cleaned with acetone and ethanol, then dried and placed at 100 mm above the targets on the substrate-holder. The deposition chamber was first evacuated to a pressure of 6×10^{-4} Pa. Initially, the substrates were cleaned by Ar^+ bombardment at 0.4 Pa at a voltage of −700 V for 10 min. In addition, the Ti and Zr targets were also sputtered and cleaned with Ar^+ bombardment for 10 min by applying a current of 1 A in order to remove the surface oxides and impurities.

Before the actual coating deposition, a pure Ti layer was deposited on the substrate for 10 min to improve the adhesion between the coating and the substrate. Subsequently, the Ti target current was kept constant at 2 A, while the Zr target current was varied from 0 to 2 A to fabricate TiZrN thin coatings with different Zr concentrations. For all thin coatings, deposition was performed for 180 min during which the substrate-holder rotation was set at 10 rpm in order to obtain a uniform coating thickness.. Table 1 presents the deposition parameters of these films.

2.2. Characterization techniques

The crystalline thin coating structure was characterized by X-ray diffraction (XRD, Bruker D8 Discover) with a Cu-Kαradiation (λ = 1.5418 Å) with 40 kV/30 mA X-Ray source. The coatings were scanned at a speed of 10°/min with a 0.02° step size in the 2θ range of 20 to 80° Texture coefficient (T_C) was defined as:

Table 1
Detailed deposition parameters of as-deposited TiN and TiZrN thin coatings.

Coatings	Current (A)		Voltage (V)		(Ar/N_2) Flow (sccm)	Pressure (Pa)	Time (min)
	Ti	Zr	Ti	Zr			
Etching	1	1	700	700	80/0	0.4	10
Ti layer	1	0	700	–	80/0	0.4	10
TiN	2	0	900	–	80/20	0.4	180
TiZrN	2	0.5–2	900	200–900	80/20	0.4	180

$$T_C = I(200)/I[(200)+(111)] \quad (1)$$

where I is the integrated intensity of the corresponding (200) and (111) diffraction peaks.

The full width at half maximum (FWHM) value was evaluated using X-ray diffraction (XRD) patterns to calculate the crystallites size of the coatings by using Scherrer formula:

$$D = \frac{0.9\lambda}{\beta\cos\theta} \quad (2)$$

where 0.9 is a dimensionless shape factor, λ the X-ray wavelength, β (in rad) the line broadening at half the maximum intensity (full width half maximum) and θ the Bragg's angle. The surface morphology and cross-sectional views were observed by a scanning electron microscope (Hitachi S3500 N SEM-FEG). The elemental composition of the coatings was evaluated by Energy-dispersive X-ray spectroscopy (EDX, Oxford INCA x-act, 15 kV).

In order to evaluate the interaction between the coating surface and a liquid, contact angles were measured using three testing liquids (water, thiodiglycol and diiodomethane) with a contact-angle optical goniometer (Data Physics Model ESr-N, Germany).The surface energy was calculated using Owens-Wendt-Rabel-Kälble (OWRK) method using the following formula [37]:

$$\gamma_L(1+\cos\theta) = 2\left(\sqrt{\gamma_S^D \gamma_L^D} + \sqrt{\gamma_S^P \gamma_L^P}\right) \quad (3)$$

where: $\gamma_L$is the total surface tension in (mN/m), θ is the contact angle in (deg), γ_S^D is the dispersive component of surface energy in (mJ/m^2), γ_L^D is the dispersive component of surface tension in (mN/m), γ_S^P is the polar component of surface energy in (mJ/m^2), and γ_L^P is the polar component of surface tension in (mN/m).The droplet volume placed on the coating surface was 2.0025 μl with a dosing rate of 1 μls^{-1}. This condition was appropriate to neglect the impact of the falling effect due to its weight [38,39].

The hardness (*H*) and elasticity modulus (*E*) of the thin coatings were measured using TI 980 triboindenter machine equipped with a *Berkovich* diamond indenter tip. For all measurements, five indentations were performed and the average value was calculated. The elasticity modulus of the thin coatings were calculated using the *Oliver-Pharr* method [40], where the Poisson's ratio of TiN ($\nu = 0.30$) was adopted as reported in the literature [41]. The tip penetration depth was limited to not exceed 10% of the coating thickness to avoid the influence of the substrate.

The tribological properties of the deposited coatings were investigated at room temperature by sliding wear tests using a tribometer (CSM Instruments, High-Temperature Tribometer) under a ball-on-disk configuration. The coatings were tested using 6 mm 100Cr6 balls (counterparts). The applied normal load and sliding speed were 2 N and 400 rpm (0.125 $m \bullet s^{-1}$), respectively. The tests were performed at 5 mm radius for 400 m sliding distance. The wear rates were calculated after the measurement of the worn track volumes with a profilometer using the following formula:

$$W = V/Fxd\left(mm^3 \times Nm\right) \quad (4)$$

where: V is the wear volume (mm^3), d is the sliding distance (m) and F is the normal load (N). The worn tracks and their elemental compositions were observed and determined using a SEM and EDX.

3. Results and discussions

3.1. Effect of Zr on TiZrN coating structure

The atomic compositions, thickness and average roughness of TiN and TiZrN coatings, as a function of the Zr content, deposited on Si (100) wafers are listed in Table 2. In the present work, the content of four elements (N, Ti, Zr, and O) are determined by EDX to confirm that the total content is 100%. The N/Ti atomic ratio was used to determine a stoichiometric case of a binary TiN coating, while the N/(Ti+Zr) ratio was used to determine a stoichiometric case of ternary TiZrN coatings with nitrogen.

The elemental composition confirmed that TiN coating (1260 nm thick) presented a N/Ti atomic ratio of about 0.98, which is comparable to the chemical composition data of magnetron sputtered TiN coatings [42]. Zr amount in the TiZrN films gradually increased from 6.4 to 22.2 at.%, with increasing sputtering current applied to the Zr target, balanced with the decrease of Ti content. The N content of about 48 at.% was constant in all the coatings and the N/(Ti+Zr) ratio close to 1 indicated that all the coatings prepared in this work were stoichiometric [43]. A similar result was reported in the literature [40,41]. In addition, oxygen impurities were found in the range of 2 to 4.4 at.%, which is probably due to the residual oxygen in the deposition chamber [44].

Fig. 1(a) shows the XRD patterns of TiN and TiZrN coatings deposited at different Zr target sputtering currents. Reference peaks of fcc-TiN, fcc-ZrN and t-ZrO_2 phases are marked according to the (JCPDS card No. 65–2905), (JCPDS card No. 002–0536.) and (JCPDS card No. 79–1771) files, respectively.

The diffraction pattern of pure TiN coating presents (111), (200), (220), (331) and (222) planes corresponding to the fcc-TiN phase, which can be assigned to the formation of a solid solution structure with single phase [45]. Besides the fcc-TiN phase, the fcc-ZrN phase can also be detected at high Zr content in the TiZrN coatings. This phase composition correlates with the results of *Somchai et al.* [43], who reported that an applied current higher than 1 A leads to the formation of TiN and ZrN mixture in the TiZrN coatings.

The addition of Zr led to a gradual decrease of the (200) intensity compared to that of (111) plane, thus causing a decrease of $T_C = I(200)/[I(111)+I(200)]$ ratio. This change could be associated with the increase of Zr sputtering current and the high-energy ion bombardment, suggesting an increase in the inter-planar spacing. A similar behavior was observed by *Phaengam et al.* [46], where the TiZrN coatings deposited at 200–300 W of Zr sputtering power, showed a (111) peak broadening due to the energy loss during the collision, which could decrease the adatoms mobility and diffusion on the columnar surface. In contrast, *Chinsakolthanakorn et al.*, [43] confirmed that the high-energy ion bombardment changed the preferred orientation of TiZrN from (111) to (200), with increasing Ti sputtering current resulting in an enhancement in the peaks intensity. This is due to an increase in the crystallinity and coating thickness.

The characteristic peaks were gradually shifted to lower angles with increasing Zr content. This is due to the formation of substituting solid solutions and the coating residual stress [47]. The Zr atoms with a larger atomic radius (1.60 Å) on being gradually incorporated in TiN, replaces the Ti atoms having smaller atomic radius (1.47 Å). This explains the increase of lattice parameter to (4.31 Å - 4.42 Å), for the TiZrN coatings as compared to the TiN coatings (~ 4.29 Å) (Fig. 2) [45]. The shift of peak position with Zr addition also explains the change in the lattice parameter [44].

Similar results were reported in other ternary transition metal nitrides like CrZrN [47] and ZrNiN [48] coatings. The (111) peak was slightly enlarged with increasing the Zr content, which implied a lattice distortion and grain refinement [49]. The crystallite size of the TiZrN

Table 2
Chemical composition, thicknesses, and surface roughness of TiN and TiZrN thin coatings.

Coatings	Chemical composition (at.%)						Thickness (nm)	Roughness Ra (nm)
	Ti	Zr	N	O	Zr/(Ti+Zr)	N/(Ti+Zr)		
Etching								
Ti layer							60	–
$Ti_{0.49}N_{0.48}$	49.5	0	48.5	2.0	–	0.98	1260	46
$Ti_{0.42}Zr_{0.06}N_{0.47}$	42.1	6.4	47.5	4.0	0.13	0.98	1280	37
$Ti_{0.36}Zr_{0.12}N_{0.47}$	36.0	12.1	47.5	4.4	0.25	0.99	1320	22
$Ti_{0.30}Zr_{0.18}N_{0.48}$	30.2	18.3	48	3.5	0.38	1.00	1550	17
$Ti_{0.26}Zr_{0.22}N_{0.48}$	26.2	22.2	47.8	3.8	0.46	0.99	1540	29

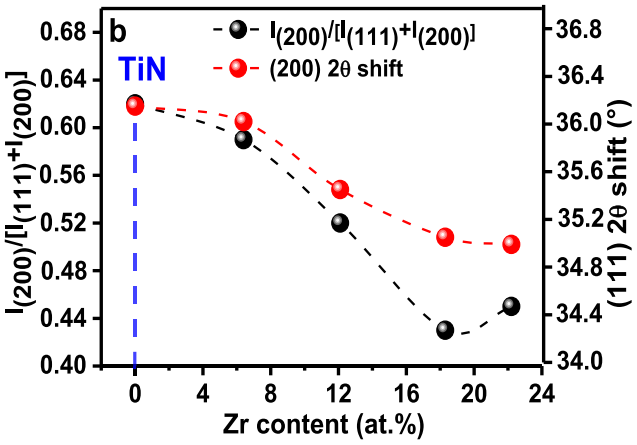

Fig. 1. a) XRD patterns of TiN and TiZrN thin coatings, and **b)** I(200) /[I (111)+*I*(200) and (111) 2θ shift as a function of Zr content.

coatings was decreased with increasing Zr content. The coating containing 18.3 at.% of Zr had the smallest crystallite size of about 10 nm. However, the coating containing 22.2 at.% of Zr revealed a weak (111) peak and presented a low crystallinity with a larger crystallite size.

3.2. TiZrN coating morphology

In order to evaluate the effect of Zr content on the morphology of the TiN coatings, SEM cross-sectional and surface images were obtained (Figs. 3 and 4). The coating thicknesses were measured to be in the range of 1.26 to1.55 μm. All coatings had a distinct columnar structure, which is a typical feature of the magnetron sputtered coatings [50]. TiN coating exhibited a fibrous and columnar structure in addition to some droplets developed through the coating (Figs. 3a, 4a), leading to the creation of pores between the large globular grains. This structure corresponds to the 2nd zone of Andres's structure zone model [33].

Regarding the morphology of TiZrN thin coatings, the structure growth presented remarkable changes from discontinuous columnar to continuous columnar and from globular to plane shape. This is primarily attributed to the Zr addition, where Zr with a high atomic radius can enhance the coating densification during deposition. The TiZrN coating shows continuous and fine columns tilted to the substrate normal corresponding to the transition zone of Andres's structural zone model (Fig. 3) [51].

The surface morphology showed a fine plane grained view related to the coating structure presenting smaller crystallite size and (111) preferred orientation (Fig. 4). The film containing 18.3 at.% of Zr presented the lowest roughness (Ra = 17 nm) (Fig. 4d, Table 2). This could be attributed to the increase in the applied current enhancing the adatom energies and mobility, leading to the coating densification.

The cohesion of the coating mainly depends on the shape, concentration, orientation, and distribution of the reinforced phases. In this study, the change of the preferential orientation from (200) to (111) can be explained in terms of the change in surface reactivity after the addition of Zr, which can also influence the surface energy [9]. Moreover, the increase of surface energy could be ascribed to the increase of

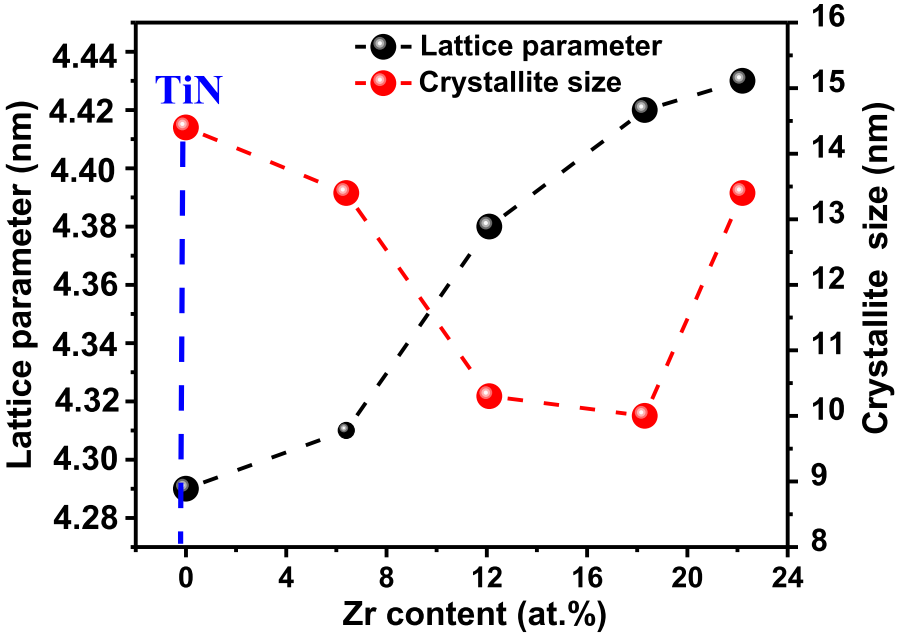

Fig. 2. Lattice parameter and crystallite size of TiZrN thin coatings as a function of Zr content.

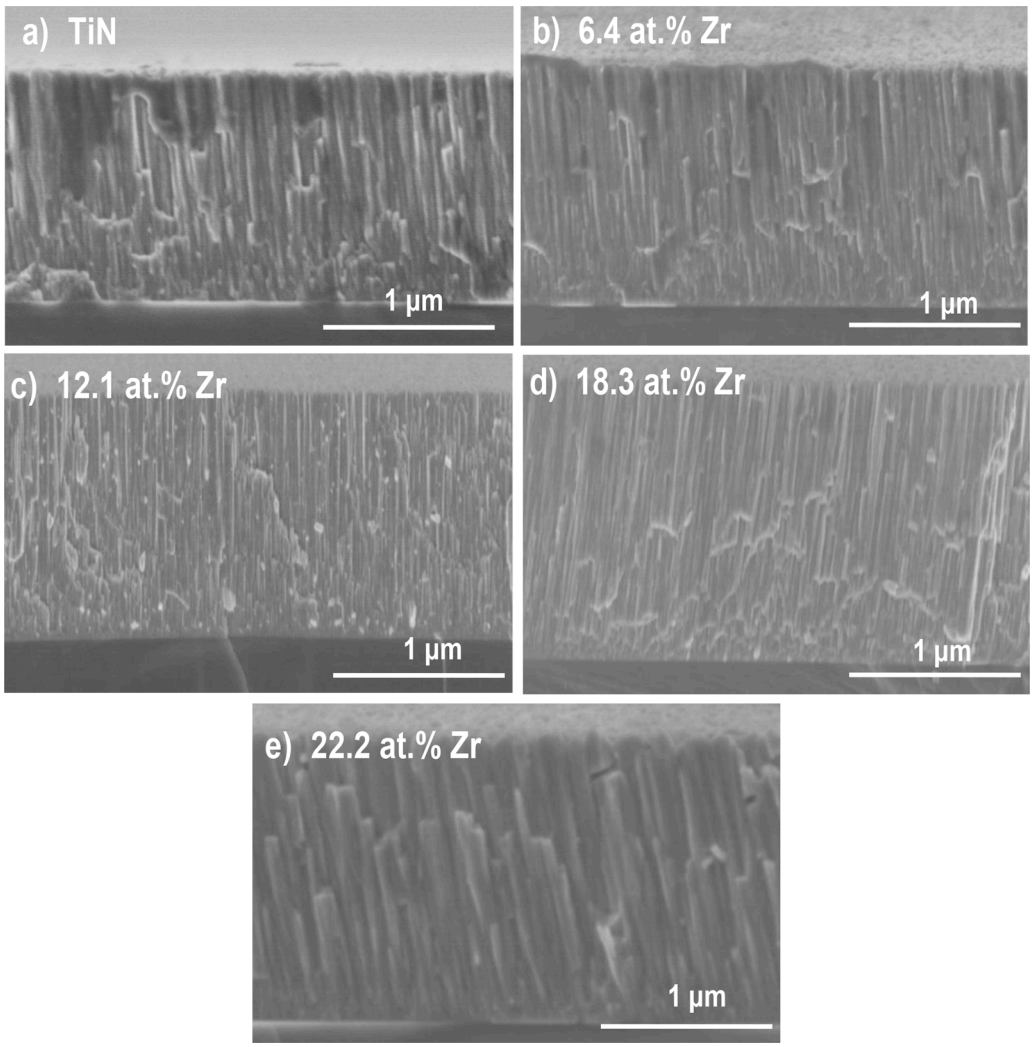

Fig. 3. Cross-sectional SEM images of a) TiN and TiZrN thin coatings containing: b) 6.4, c) 12.1, d) 18.3 and e) 22.2 at.% of Zr.

the lattice dislocations and distortions in the surface substrate caused by the addition of Zr, which subsequently refined the surface, and provided more nucleation sites [47]. A similar phenomenon was reported for CrZrN thin films deposited by magnetron sputtering with increasing Zr content. The dense structure and the high cohesiveness of the coating/substrate interfacial zone is explained by the fact that, the diffusion of nitrogen is faster in Zr than Ti ones and can easily move through interstitial sites of the zirconium lattice. Thus, the zirconium covers the surface of growing grains, serving as new nucleation sites and increases the cohesion between the coating and the substrate.

However, the coating containing the highest Zr content (22.2 at.% Zr), deposited at the highest applied current (2 A) (Figs. 3e, 4e), presented elongated columns and porous structure with angular grains corresponding to the 1st zone of Andres's structural zone model [33]. According to *Li* et al., [45] at higher applied power, the ions and electrons are repelled from the magnetron cathodes that strongly weaken the plasma, resulting in a corresponding reduction of number and momentum of particles reaching the substrate. The coating containing the highest Zr content (22.2 at.% Zr) was 1.54 µm thick and presented an average roughness of 29 nm (Fig. 4e and Table 2).

Raman spectra of TiN and TiZrN thin coatings are shown in Fig. 5. The spectrum of TiN coating shows two broad band's centered at 250 and 590 cm^{-1}, corresponding to (L_A and T_A) acoustic transition regions, and (LO and TO) optic mode regions that were primarily determined by the vibrations of the Ti and N bands [52–55]. With increasing the Zr content in TiZrN coatings, the FWHM peaks gradually decrease, and the peaks of TiZrN coating containing 18.3 at.% of Zr become much narrower, and remarkably stronger. Furthermore, a wavelength divergence is observed between the acoustic and optic regions from 250 to 618 cm^{-1} to 315 and 590 cm^{-1}, respectively, with increasing Zr content. The 215 and 668 cm^{-1} peak positions are close to the ZrN, which indicates that more Ti atoms are replaced by the Zr atoms, and hence a stronger vibration of Zr-N bond is obtained during the deposition [55,56].

3.3. *Effect of Zr content on the TiZrN coating surface energy and wettability*

Fig. 6 depicts the contact angles of water droplets on TiN and TiZrN thin coatings. The average contact angle values were 123.0°, 113.2°, 111.4°, 76.0° and 96.4° for TiN and TiZrN coatings containing 6.4, 12.1, 18.3 and 22.2 (at.%) of Zr, respectively. As shown in Fig. 6, TiZrN coating containing 18.32 at.% of Zr has the lowest contact angle (76°). This coating showed the highest wettability and a lower hydrophobicity as compared to the TiN coating (123.0°). Therefore, Zr addition to TiN coating makes its surface more hydrophilic and improves its wettability. TiZrN system in this study, presented the highest contact angle as compared to that previous reported works (62°, 82.2°) [27,57].

This result is consistent with *Movassagh et al.*, [58] work who reported a similar study on TiSiN films. They found that the TiSiN coating led to a decrease in the contact angle from 82.2° to 47.5° when Si

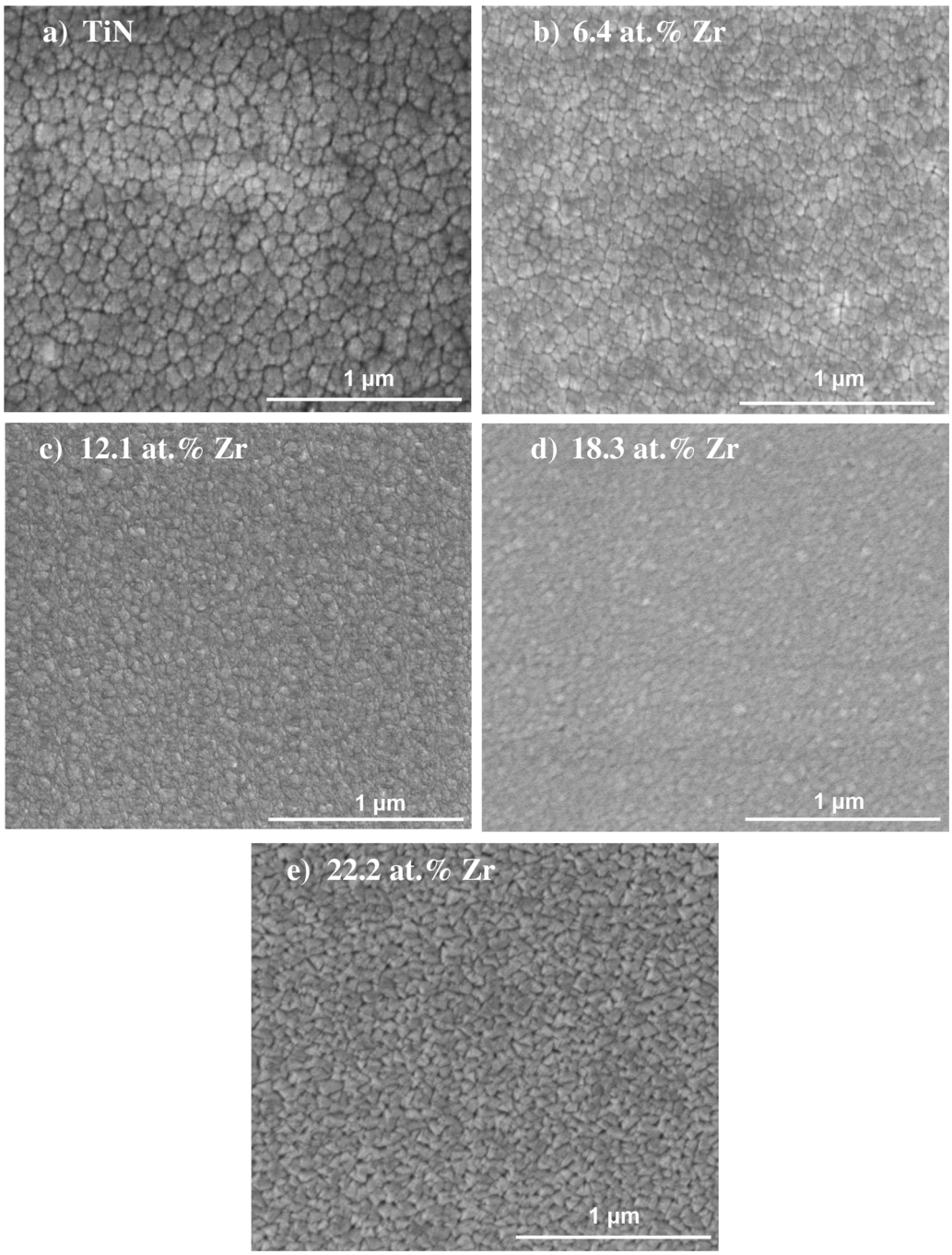

Fig. 4. SEM images of a) TiN and TiZrN coating surfaces containing: b) 6.4, c) 12.1, d) 18.3 and 22.2 at.% of Zr.

content increased from 0 to 24.7 wt.%. Several parameters such as the morphology and the surface roughness play important role in the contact angle value [59]. The higher wettability of TiZrN coatings is attributed to the low surface roughness (17 nm for the coating containing 18.3 at.% of Zr).

The contact angle increased with increasing the Zr content to 22.2 at.%, because of an increase in the surface roughness [60]. According to the SEM images of the coating containing 18.3 at.% of Zr, the coating became denser with a smoother surface, which led to an improvement in the wettability of the coating

The contact angle measurements were performed using three testing liquids (water, thiodiglycol and diiodomethane) for each coating, and the total surface energy values of TiZrN coatings were calculated (Fig. 7). The water contact angles were generally higher than that obtained for thiodiglycol and diiodomethane for all TiZrN coatings. This is due to the higher surface tension [61] and the lower viscosity of water as compared to thiodiglycol and diiodomethane. It was reported that wetting dynamics is changed according to fluid viscosity [62], and hence the variations in the wettability maybe because of the lower density and molecular weight of water as compared to thiodiglycol and diiodomethane [63]. The same results were obtained by *Navabpour* et al. [64], where water contact angles were always higher than that of ethyleneglycol and diiodomethane on various coating surfaces.

The total surface energy values for all TiZrN coatings were lower than that of TiN coating (77.4 mN/m) (Fig. 7). Generally, it can be seen that by increasing the Zr content, the total surface energy decreased, and the lowest value of 38.7 mN/m was obtained for the coating containing 18.3 at.% of Zr.

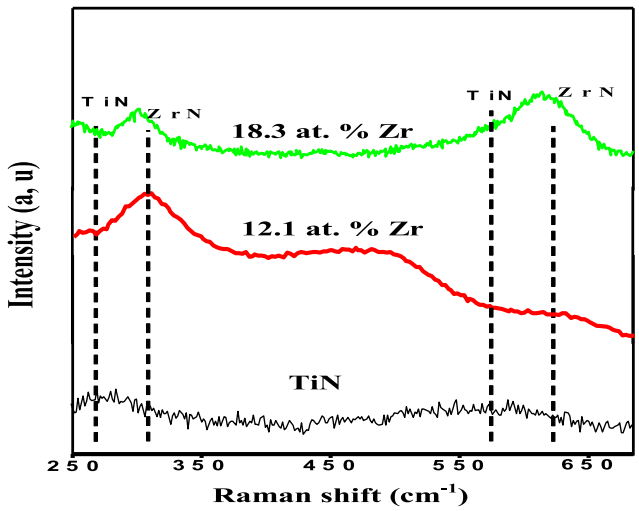

Fig. 5. Raman spectra of TiN and TiZrN thin coatings containing 12.1 and 18.3 at.% of Zr.

It is evident that surface roughness has a direct impact on the contact angle, and hence the surface energy. However, many other factors affecting surface energy have been mentioned, such as phase structure, hardness or elasticity modulus [65]. According to *Pang* et al. [66]., through film growth, the natural driving force reduces the surface energy, which controls the preferred orientation. The total surface energy reduction is caused by the decrease in (200) preferred orientation. Surface energy of TiN coating with the (111) preferred orientation will be lower than that with the (200) orientation [66,67], which is coherent with the results obtained in this study.

3.4. Effect of Zr content on the mechanical properties of TiZrN coatings

Hardness (*H*) and elasticity modulus (*E*) of TiN and TiZrN thin coatings were measured using nanoindentation tests according to Oliver-Pharr method [40]. In order to further investigate the effect of Zr content on the mechanical properties of the coatings, H/E and H^3/E^2 ratios were taken as effective quantitative parameters to analyze the elastic and plastic deformation resistance of these hard coatings [45,68]. Fig. 8 presents H, E and both ratios for TiN and TiZrN thin coatings.

The TiN coating hardness (17.5 ± 0.1 GPa) and elasticity modulus (164.9 ± 4.6 GPa) were lower than that in the case of TiN coatings obtained by other processes [69,70] but higher than the other transition metal nitride coatings [44,71]. According to *Hall-Petch* relation, from nanoindentation test, the low H and E values are mainly attributed to the high surface roughness and large grain size, which favors the dislocation displacement and the coating surface softening [38]. TiZrN thin coating with 18.3 at.% of Zr content showed the highest values of hardness (25.12 ± 0.11), and H/E (0.139) and H^3/E^2 (0.49 GPa) ratios (Fig. 8), which is mainly attributed to the solid solution strengthening and the grain refinement [53,73]. In addition, the high strain and the lattice distortion induced by the incorporation of Zr atoms in TiN coating, as shown in Fig. 2, also improves the coating hardness [72]. Furthermore, the coating growth through the packed (111) plane may also contribute to the hardness enhancement [45].

Similar result was reported by *He et al.* [73], where the addition of small amount of Cu led to a reductionin the TiN grain size from 25 to 5 nm, which enhanced the film hardness with a strong (111) orientation. Increasing the Zr content to 22.2 (at.%) led to a reduction in the hardness (18 GPa), the H/E (0.11) and H^3/E^2 (0.22 GPa) ratios. This is due to the disorder lattice caused by weak crystallinity [44]. A similar decrease was reported by *Lin* et al. [74],. Furthermore, the hardness reduction with increasing Zr (22.2 at.%) is mainly due to the incorporation of big Zr atoms that increases the grain size (Fig. 2) [75].

The enhancement of TiZrN thin coating hardness due to the grain size refinement is consistent with Hall-Petch relationship [76]. In this work, the lowest grain size was 10 nm, which is considered in literature as the lowest grain size leading to the highest hardness. Further grain size reduction leads to changes in intragranular processes (grain boundary sliding induced) resulting in a decrease in the hardness [77].

3.5. Effect of Zr content on friction and wear properties of TiZrN coatings

In order to investigate the tribological performance of TiZrN coatings, wear tests based on ball-on-disk configuration were performed. The friction coefficient (CoF) and wear rate results are presented in Fig. 9. At the beginning of the friction test, due to the low contact area and high contact pressure, sliding is difficult, resulting in a higher CoF. In the later stage, the increased contact area leads to a reduction in the contact pressure and subsequently a reduction in the CoF as observed at the stable state [78].

The maximum CoF value (0.60) and the highest wear rate (5.64×10^{-4} mm^3/Nm) were found for the TiN coating with the lowest hardness. The reason for this might be high surface roughness and higher TiN (200) intensity as compared by TiN (111) intensity, which has a negative effect on the surface energy and causes a higher friction coefficient [46,

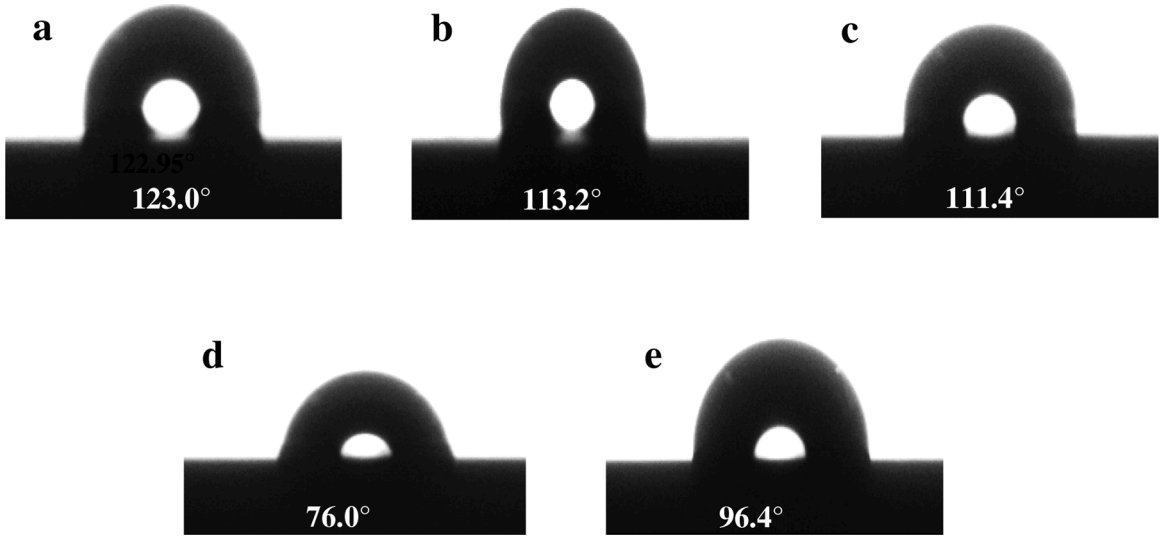

Fig. 6. Photographs of water droplet contact angles on: a) TiN and TiZrN thin coatings containing: b) 6.4, c) 12.1, d) 18.3 and e) 22.2 at.% of Zr.

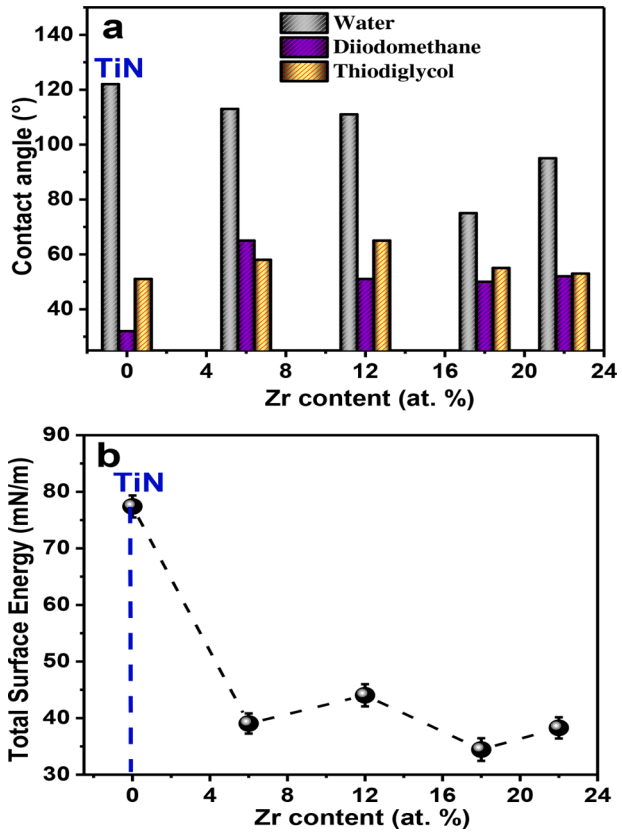

Fig. 7. a) Contact angle measurements, and b) Total surface energy of TiN and TiZrN thin coatings as a function of Zr content.

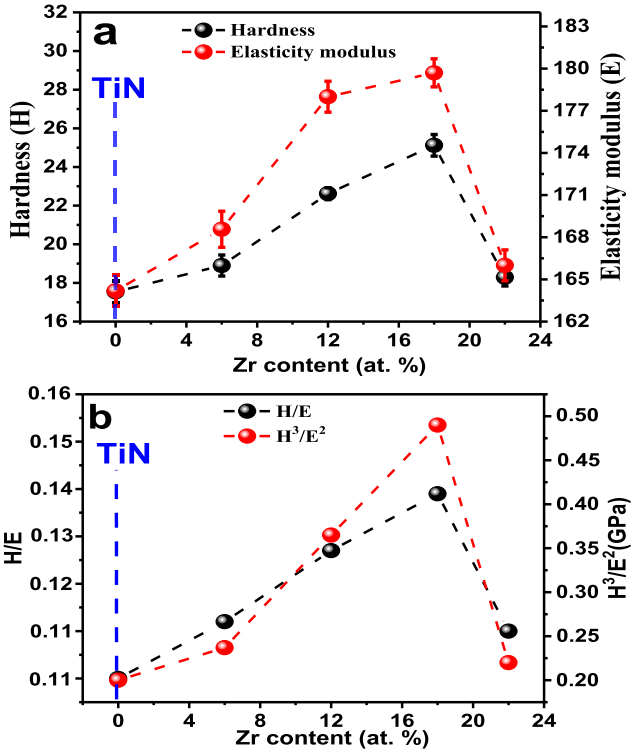

Fig. 8. a) Hardness and elasticity modulus, and b) H/E and H^3/E^2 ratios of TiN and TiZrN coatings as a function of Zr content.

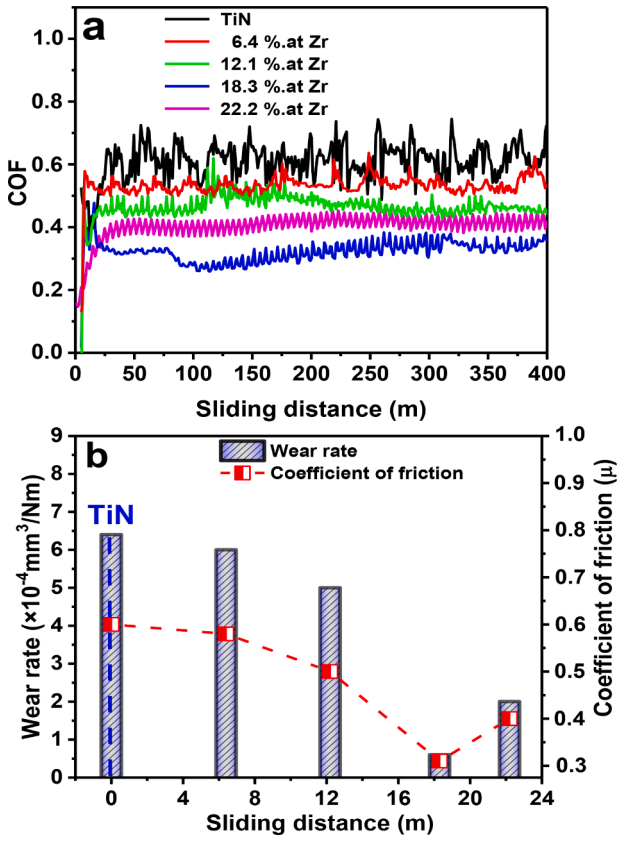

Fig. 9. a) Friction coefficient Vs sliding distance, and b) wear rate and friction coefficient values of TiN and TiZrN thin coatings with different Zr content.

64]. The high CoF of TiN coating may also be attributed to the lower thickness of TiN coating as compared to the other coatings [79].

From Fig. 9, we can notice that the addition of Zr led to a relative decrease in the CoF and wear resistance of TiZrN coatings, which indicates that the wear resistance of TiN is clearly improved by the cooperation of Zr.

The friction coefficient for TiZrN coatings containing 6.4 and 12.2 at. % of Zr were 0.56 and 0.50, respectively. The best tribological behavior was obtained for the TiZrN coating containing 18.3 at.% of Zr. It presented the lowest values of CoF (0.31) and wear rate (6.65×10^{-5} mm^3/Nm). The improvement of anti-friction of TiN depends on many factors such as substrate characteristics, strain rate and contact pressure [80]. In our case, the main reason for the decrease in the CoF and wear rate is the big atomic radius of Zr and an increase in the solid solution strengthening with increasing Zr content. In addition, coating surface roughness decreased, and its density increased with Zr content. All these factors may have contributed to the improvement of wear resistance. The highest hardness and H/E ratio of TiZrN coating containing 18.3 (at.%) of Zr can be effectively used to predict its tribological performance [81].

From Fig. 1, we can notice that TiZrN coating containing 18.3 at.% of Zr has a t-ZrO_2 phase. This phase has an extremely high tenacity, high hardness, high resistance to wear and corrosion. It is considered as an excellent lubricant oxide and utilized as additives in lubricating commercial oil [82,83]. In the present work, we can say that the existence of t-ZrO_2 as lubricant oxide phase covering the surface with a soft layer contributed to the reduction of friction coefficient to 0.31.

However, at a high Zr content (22.2 at.%), it is observed that the friction coefficient and wear rate of TiZrN coating increased. This could be explained by the significant decrease in the coating hardness and H/E ratio related to the large volume fraction of elongated columns and porous structure showing an angular grain shape (Fig. 3e) [84]

The SEM observations and EDX analysis of worn surfaces of TiN and

TiZrN coatings are shown in Fig. 10. Two zones corresponding to worn track and undamaged coating were analyzed. We can clearly notice the difference between the EDX elemental analyses of both zones. For TiN and TiZrN coating having the lowest Zr content (Fig. 10a, b), spalling and detachment were observed on the worn surfaces, which is due to the low hardness of these coatings. The main wear mechanism of these coatings was found to be adhesive wear.

The results indicated that the TiZrN thin coating with 18.3 at.% of Zr exhibited the lowest wear rate, friction coefficient and roughness as compared to the other coatings (Fig. 9, and Table 2). This coating presented the best wear resistance (lowest quantity removed of film tested under a 2 N normal load for 400 m sliding distance) owing to its high structural and mechanical properties [85].

A dense and smooth surface has less asperity or voids as compared to a rough surface which results in better adhesion. On the other hand, the TiZrN thin coating with 18.3 at.% of Zr was found to achieve the high hardness (25.12 ± 0.11 GPa), low roughness (17 nm) and higher elasto-plastic ratios ($H/E = 0.139$, $H^3/E^2 = 0.49$ GPa) that inhibit the plastic deformation effectively and decrease friction and wear. In addition, the presence of (111) TiN predominate plane in the TiZrN thin coating contributes to low friction coefficient [86].

Regarding the elemental compositions (Fig. 10), there is an increase in the concentration of Ti, Zr and N, and the presence of O in small amounts at the edges of the wear track. The EDX analysis of the worn track area (in the middle) showed that the chemical composition of the wear debris of the coating containing 18.3 at.% of Zr was 60% Fe, 15% Ti, 14.5% N, 7% Zr, and 3.5% O. It showed a decrease in the concentration of Ti, Zr and N, and the presence of Fe corresponding to the XC100 steel substrate.

The high iron (Fe) concentrations in TiN and TiZrN thin coatings indicate the low coating/substrate adhesion. The smooth surface and the good coating adhesion reduced the friction coefficient [87]. The reason for the lower wear rate of the TiZrN coating might be related to its higher hydrophilicity as well (Fig. 6), which leads to an increase in the number of atoms in contact with the surface. As we mentioned in Section 3.4, the best mechanical properties were exhibited by the TiZrN coating containing 18.3 at.% of Zr and the increase in film crystallinity enhanced the tribological behavior (low friction coefficient and wear rate) [88].

Similar results were obtained in our previous study, where friction coefficients and wear rates of CrZrN coatings were reduced with increasing Zr content [89]. However, the TiZrN coating containing a higher Zr percentage (22.2 at.%) showed more debris along the edges

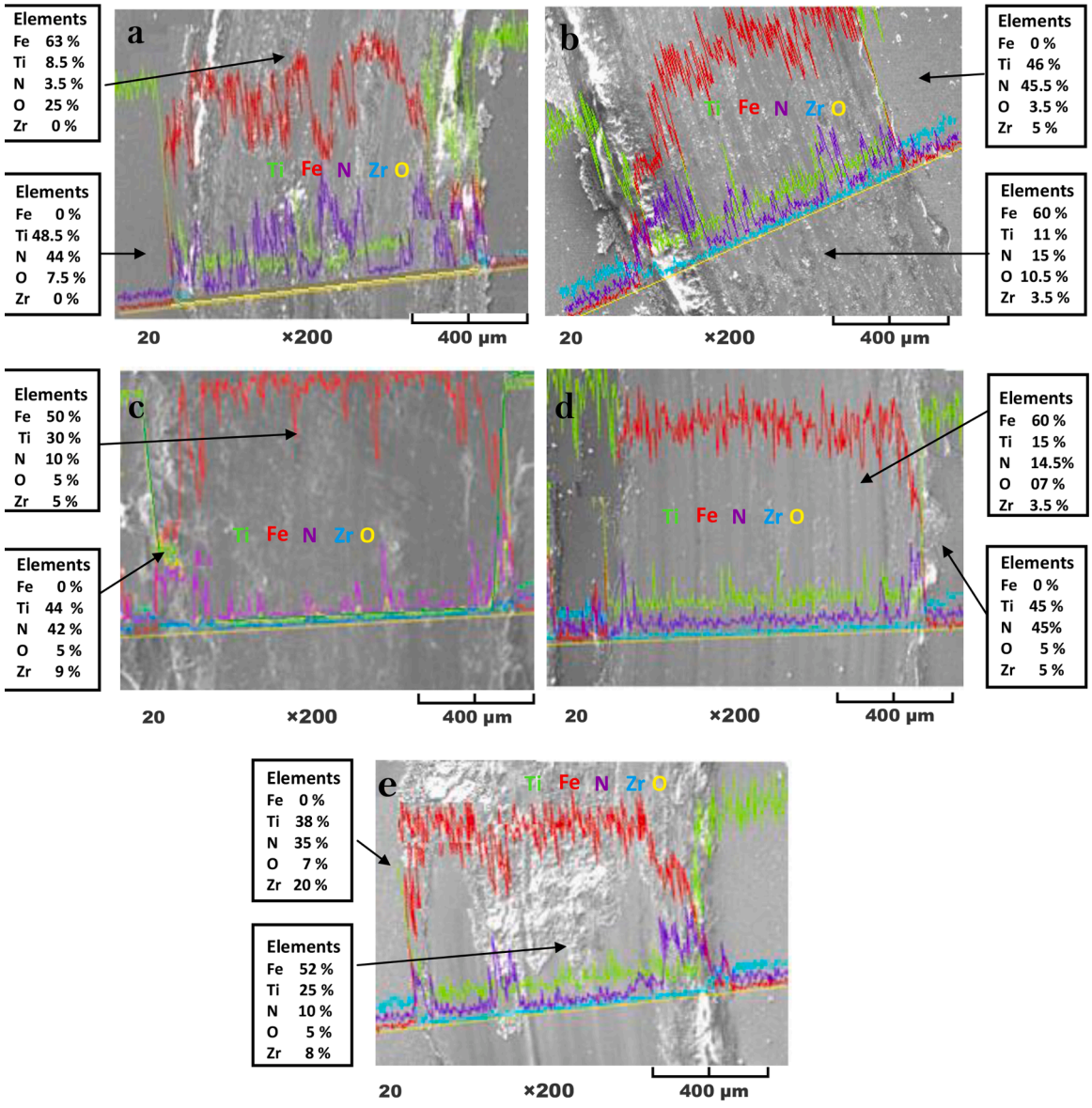

Fig. 10. SEM images and EDX analysis of worn surfaces of: a) TiN and TiZrN thin coating containing: b) 6.4, c) 12.1, d) 18.3 and e) 22.2 at.% of Zr.

and the middle of the track due to the weakness of substrate-coating adhesion (Fig. 10e). This abrasive failure might be originated from the large grain size and the differences in mechanical properties between the deposited coating and substrate [90].

4. Conclusions

TiN and TiZrN thin coatings with various Zr contents were deposited by r.f. reactive magnetron sputtering. The coating crystalline structure, elemental chemical composition, wettability, hardness and wear performance were investigated.

- The Zr content was varied up to 22.2 at.% and all the coatings presented a columnar growth.
- With increasing Zr content, the preferred orientation was changed from (200) to (111).
- The highest hardness value (25 GPa) was obtained for the TiZrN thin coating containing 18.3 at.% of Zr, which has the smallest crystallite size (17 nm) and the highest lattice distortion due to the incorporation of Zr atoms in the TiN system.
- In addition, this coating also presented a smooth surface and lowest total surface energy of 38.7 mN/m.
- The tribological properties of TiN thin coating were greatly enhanced by the incorporation of zirconium.
- The solid solution strengthening led to the reduction of friction coefficient and wear rate.
- TiZrN thin coating containing 18.3 at.% revealed the lowest wear rate (6.65×10^{-5} mm^3/Nm) and the lowest friction coefficient (0.31), which corresponds to the highest H/E (0.139) and H^3/E^2 (0.49 GPa) ratios.

CRediT authorship contribution statement

Faiza Salhi: Writing – original draft, Supervision, Writing – review & editing, Visualization, Resources. **Linda Aissani:** Data curation, Writing – original draft, Conceptualization, Methodology, Software. **Mamoun Fellah:** Conceptualization, Methodology, Data curation, Resources, Writing – original draft, Writing – review & editing, Project administration. **Abdelhakim Chadli:** Data curation. **Abderrahmane Cheriet:** Data curation. **Ahlam Belgroune:** Writing – review & editing. **Corinne Nouveau:** Resources. **Aleksei Obrosov:** Writing – review & editing. **Mohammed Abdul Samad:** Writing – review & editing. **Akram Alhussein:** Data curation, Writing – original draft, Conceptualization, Methodology, Software, Writing – review & editing.

Declaration of Competing Interest

The authors declare that they have no known competing financial interests or personal relationships that could have appeared to influence the work reported in this paper.

Acknowledgment

We would like to express our thanks and sincere appreciation to the LASMIS research unit for using their coating and characterization machines. The research was carried out with the support of a grant under the Decree of the Government of the Russian Federation No. 220 of 09 April 2010 (Agreement No. 075-15-2021-612 of 04 June 2021).

References

[1] B. Fotovvati, N. Namdari, A. Dehghanghadikolaei, On coating techniques for surface protection: a review, J. Manuf. Mater. Process. 3 (1) (2019) 28.
[2] K. Bobzin, Technology, High-performance coatings for cutting tools, J. Manuf. Sci. Technol. 18 (2017) 1–9.
[3] I. Pana, V. Braic, M. Dinu, E.S.M. Mouele, A.C. Parau, L.F. Petrik, M.J.C. Braic, In Vitro corrosion of titanium nitride and oxynitride-based biocompatible coatings deposited on stainless steel, Coatings 10 (2020) 710.
[4] K. Sarkar, P. Jaipan, J. Choi, T. Haywood, D. Tran, N.R. Mucha, S. Yarmolenko, O. Scott-Emuakpor, M. Sundaresan, R.K.J.S.A.S. Gupta, Enhancement in corrosion resistance and vibration damping performance in titanium by titanium nitride coating, SN Appl. Sci. 2 (2020) 1–14.
[5] G.V. Naik, J.L. Schroeder, X. Ni, A.V. Kildishev, T.D. Sands, A.J.O.M.E. Boltasseva, Titanium nitride as a plasmonic material for visible and near-infrared wavelengths, Opt. Mater. Express 2 (2012) 478–489.
[6] C. Zeng, H. Wen, A.H. Ettefagh, B. Zhang, J. Gao, A. Haghshenas, J.R. Raush, S.J. S. Guo, C. Technology, Laser nitriding of titanium surfaces for biomedical applications, Surf. Coat. Technol. 385 (2020), 125397.
[7] H. Wang, R. Zhang, Z. Yuan, X. Shu, E. Liu, Z.J.C.I. Han, A comparative study of the corrosion performance of titanium (Ti), titanium nitride (TiN), titanium dioxide (TiO_2) and nitrogen-doped titanium oxides (N–TiO_2), as coatings for biomedical applications, Ceram. Int. 41 (2015) 11844–11851.
[9] L. Wang, L. Li, G. Li, Q. Ma, Improved Adhesion of TiAlSiN Nanocomposite Coatings on Cemented Carbide Substrate by Pre-Implantation, Coatings 9 (3) (2009) 1–10.
[9] V.K. Prokudina, Titanium Nitride, Concise Encyclopedia of Self-Propagating High-Temperature Synthesis, Elsevier, 2017, pp. 398–401.
[10] L. Gao, J. Gstöttner, R. Emling, M. Balden, C. Linsmeier, A. Wiltner, W. Hansch, D. J.M.e. Schmitt-Landsiedel, Thermal stability of titanium nitride diffusion barrier films for advanced silver interconnects, Microelectron. Eng. 76 (2004) 76–81.
[11] A. Torgovkin, S. Chaudhuri, A. Ruhtinas, M. Lahtinen, T. Sajavaara, I.J.S. S. Maasilta, High quality superconducting titanium nitride thin film growth using infrared pulsed laser deposition, Supercond. Sci. Technol. 31 (2018), 055017.
[12] S. Borah, H. Bailung, J. Chutia, Decorative titanium nitride colored coatings on bell-metal by reactive cylindrical magnetron sputtering, Progress in color, colorants and coatings, 3 (2010) 74–80.
[13] G. Hauer, L. Leitner, M.C. Ackerl, S. Klim, I. Vielgut, R. Ehall, M. Glehr, A. Leithner, P.J.C. Sadoghi, Titanium-nitride coating does not result in a better clinical outcome compared to conventional cobalt-chromium total knee arthroplasty after a long-term follow-Up: a propensity score matching analysis, Coatings 10 (2020) 442.
[14] Z. Gao, Z. Zhang, X. Zhang, J. Kulczyk-Malecka, H. Liu, P. Kelly, P.J. Withers, P.J. A.M. Xiao, A conformable high temperature nitride coating for Ti alloys, Acta Mater. 189 (2020) 274–283.
[15] Y. Lu, Y. Shen, Z. Zhou, K. Li, Effects of nitrogen content on microstructure and oxidation behaviors of Ti–B–N nanocomposite thin films, J. Vacuum Sci. Technol. A: Vacuum, Surf. Films 24 (2006) 340–349.
[16] T. Akhadejdamrong, A. Mitsuo, C. Iwamoto, T. Yamamoto, Y. Ikuhara, T.J.M. T. Aizawa, Formation of protection layer during oxidation of Al-implanted TiN coating, Mater. Trans. 43 (2002) 1291–1297.
[17] F. Uny, E. Blanquet, F. Schuster, F. Sanchette, Ti-Al-N-Based Hard Coatings: Thermodynamical Background, CVD Deposition, and Properties. A Review, Coatin. Thin-Film Technol. (2018).
[18] N. Madaoui, N. Saoula, B. Zaid, D. Saidi, A.S.J.A.s.s Ahmed, Structural, mechanical and electrochemical comparison of TiN and TiCN coatings on XC48 steel substrates in NaCl 3.5% water solution, Appl. Surf. Sci. 312 (2014) 134–138.
[19] Y. Liu, G. Li, X. Wan, X. Zhang, Y. Shen, K. Wu, Toughness improvement by Zr addition in the simulated coarse-grained heat-affected zone of high-strength low-alloy steels, Ironmak. Steelmak. 46 (2019) 113–123.
[20] Z. Zhang, J. Jin, L. Liang, B. Peng, Y. Liu, S. Fu, M. Yan, High-performance Nd-Fe-B sintered magnets via co-doping high-melting-point Zr and low-melting-point Dy71.5Fe28.5, J. Magn. Magn. Mater. 487 (2019), 165356.
[21] M. Aristizabal, P. Jamshidi, A. Saboori, S. Cox, M.J.M.L. Attallah, Laser powder bed fusion of a Zr-alloy: tensile properties and biocompatibility, Mater. Lett. 259 (2020), 126897.
[22] L. Chen, D. Holec, Y. Du, P.H. Mayrhofer, Influence of Zr on structure, mechanical and thermal properties of Ti-Al-N, Thin Solid Films 519 (2011) 5503–5510.
[23] T.L. Yau, V.E. Annamalai, in: Corrosion of Zirconium and its Alloys, 2016. In book: Reference Module in Materials Science and Materials Engineering.
[24] Y. Huang, J. Shen, J. Sun, Formation, thermal stability and mechanical properties of Ti42.5Zr7.5Cu40Ni5Sn5 bulk metallic glass, Sci. China Ser. G: Phys., Mech. Astron. 51 (2008) 372–378.
[25] D.-Y. Wang, C.-L. Chang, C.-H. Hsu, H.-N.J.S. Lin, C. Technology, Synthesis of (Ti, Zr) N hard coatings by unbalanced magnetron sputtering, Surf. Coat. Technol. 130 (2000) 64–68.
[26] H.-L. Huang, Y.-Y. Chang, J.-X. Liu, M.-T. Tsai, C.-H. Lai, Antibacterial activity and cell compatibility of TiZrN, TiZrCN, and TiZr-amorphous carbon coatings, Thin Solid Films 596 (2015) 111–117.
[27] I. Milošev, H.H. Strehblow, B.J.S. Navinšek, I.A.A.I.J.d.t.t. development, i. application of techniques for the analysis of surfaces, t. films, Oxidation of ternary TiZrN hard coatings studied by XPS, Surf. Interface Anal. 26 (1998) 242–248.
[28] G. Du, D.C. Ba, Z. Tan, W. Sun, K. Liu, Q.J.S. Han, C. Technology, Vibration damping performance of ZrTiN coating deposited by arc ion plating on TC4 Titanium alloy, Surf. Coat. Technol. 229 (2013) 172–175.
[29] V. Beresnev, S. Lytovchenko, B. Mazilin, D. Horokh, V. Stolbovoy, D. Kolesnikov, I. Kolodiy, S. Zhanyssov, Adhesion Strength of TiZrN/TiSiN Nanocomposite Coatings on a Steel Substrate with Transition Layer, J. nano Electron. Phys. 12 (4) (2020) 04030, 1-6.
[30] S. Jeon, B. Kim, Y. Choi, I. Jo, H.J.C.I. Lee, Thermal shock behaviors of $Ti_{1-x}Zr_xN$ coatings by accelerated test based on pulsed laser ablation, Ceram. Int. 42 (2016) 2241–2249.

[31] E. Hong, H.J.S. Lee, C. Technology, Microstructure, bonding state and phase formation behavior of carbon-doped TiZrN coating by laser carburization, Surf. Coat. Technol. 385 (2020), 125373.

[32] Y.-.W. Lin, J.-.H. Huang, G.-P.J.T.s.f. Yu, Effect of nitrogen flow rate on properties of nanostructured TiZrN thin films produced by radio frequency magnetron sputtering, Thin Solid Films 518 (2010) 7308–7311.

[33] Y.-.W. Lin, H.-.A. Chen, G.-.P. Yu, J.-.H. Huang, Effect of bias on the structure and properties of TiZrN thin films deposited by unbalanced magnetron sputtering, Thin Solid Films 618 (2016) 13–20.

[34] F. El-Hossary, A. Abd El-Rahman, M. Raaif, S. Qu, J. Zhao, M.F. Maitz, M.A.J.A.P. A. El-Kassem, Effect of DC-pulsed magnetron sputtering power on structural, tribological and biocompatibility of Ti–Zr–N thin film, Appl. Phys. A 124 (2018) 42.

[35] W. Phae-ngam, M. Horprathum, C. Chananonnawathorn, T. Lertvanithphol, B. Samransuksamer, P. Songsiriritthigul, H. Nakajima, S. Chaiyakun, Oblique angle deposition of nanocolumnar TiZrN films via reactive magnetron co-sputtering technique: the influence of the Zr target powers, Curr. Appl Phys. 19 (2019) 894–901.

[36] D.K. Owens, R.J.J.o.a.p.s. Wendt, Estimation of the surface free energy of polymers, J. Appl. Polym. Sci. 13 (1969) 1741–1747.

[37] E. Lugscheider, K.J.S. Bobzin, C. technology, Wettability of PVD compound materials by lubricants, Surf. Coat. Technol. 165 (2003) 51–57.

[38] M. Kalin, M.J.T.I. Polajnar, The correlation between the surface energy, the contact angle and the spreading parameter, and their relevance for the wetting behaviour of DLC with lubricating oils, Tribol. Int. 66 (2013) 225–233.

[39] W.C. Oliver, G.M.J.J.o.m.r. Pharr, An improved technique for determining hardness and elastic modulus using load and displacement sensing indentation experiments, J. Mater. Res. 7 (1992) 1564–1583.

[40] A.J. Perry, A contribution to the study of poisson's ratios and elasticconstants of TiN, ZrN and HfN, Thin Solid Films 193-194 (1990) 463–471.

[41] G. Lu, L. Yu, H. Ju, B. Zuo, J.J.S.E. Xu, Influence of nitrogen content on the thermal diffusivity of TiN films prepared by magnetron sputtering, Surf. Eng. 36 (2020) 192–198.

[42] S. Chinsakolthanakorn, A. Buranawong, S. Chiyakun, P.J.M.S. Limsuwan, Applications, Effects of titanium sputtering current on structure and morphology of TiZrN films prepared by reactive DC magnetron co-sputtering, Mater. Sci. Appl. 04 (11) (2013) 689–694.

[43] B. Xu, P. Guo, Z. Wang, R. Chen, Y. Ye, J. Shuai, A. Wang, P.J.S. Ke, Anti-wear Cr-V-N coating via V solid solution: microstructure, mechanical and tribological properties, Surf. Coat. Technol. 397 (2020), 126048.

[44] H. Li, Z. Liu, J. Li, J. Huang, J. Kong, Q. Wu, D.J.J.S. Xiong, Effects of Hf addition on the structure, mechanical and tribological properties of CrN film, Surf. Coat. Technol. 397 (2020), 126067.

[45] L. Kara, D.D. Özkan, M.B. Yağci, E. Sulukan, Y. Sert, T.S. Sert, Friction and wear behaviors of TiN coatings under dry and vacuum conditions, Tribol Trans 62 (2019) 362–373.

[46] L. Aissani, M. Fellah, C. Nouveau, M. Abdul Samad, A. Montagne, A.J.S.e. Iost, Structural and mechanical properties of Cr–Zr–N coatings with different Zr content, Surf. Eng. 36 (2020) 69–77.

[47] J. Šůna, J. Musil, V. Ondok, J.G. Han, Enhanced hardness in sputtered Zr–Ni–N films, Surf. Coat. Technol. 200 (2006) 6293–6297.

[48] H. Mei, Q. Luo, X. Huang, J.C. Ding, T.F. Zhang, Q.J.S. Wang, Influence of lubricious oxides formation on the tribological behavior of Mo-V-Cu-N coatings deposited by HIPIMS, Surf. Coat. Technol. 358 (2019) 947–957.

[49] R. Surmenev, A. Vladescu, M. Surmeneva, A. Ivanova, M. Braic, I. Grubova, C. M. Cotrut, Radio frequency magnetron sputter deposition as a tool for surface modification of medical implants, Modern technologies for creating the thin-film systems and coatings, Intech (2017) 213–248.

[50] A.J.T.S.F. Anders, A structure zone diagram including plasma-based deposition and ion etching, Thin Solid Films 518 (2010) 4087–4090.

[51] M. Franck, J.-.P. Celis, J.J.J.o.m.r. Roos, Microprobe Raman spectroscopy of TiN coatings oxidized by solar beam heat treatment, J. Mater. Res. 10 (1995) 119–125.

[52] L. Yu, H. Zhao, J.J.A.s.s. Xu, Mechanical, tribological and corrosion performance of WBN composite films deposited by reactive magnetron sputtering, Appl. Surf. Sci. 315 (2014) 380–386.

[53] H.C. Barshilia, K.J.J.o.a.p. Rajam, A Raman-scattering study on the interface structure of nanolayered Ti Al N/ Ti N and Ti N/ Nb N multilayer thin films grown by reactive dc magnetron sputtering, J. Appl. Phys. 98 (2005), 014311.

[54] R. Chowdhury, R. Vispute, K. Jagannadham, J.J.J.o.M.R. Narayan, Characteristics of titanium nitride films grown by pulsed laser deposition, J. Mater. Res. 11 (1996) 1458–1469.

[55] B. Usmani, A.J.S.E. Dixit, Spectrally selective response of ZrOx/ZrC–ZrN/Zr absorber–reflector tandem structures on stainless steel and copper substrates for high temperature solar thermal applications, Sol. Energy 134 (2016) 353–365.

[56] Y.-.W. Lin, P.-.C. Chih, J.-H.J.S. Huang, C. Technology, Effect of Ti interlayer thickness on mechanical properties and wear resistance of TiZrN coatings on AISI D2 steel, Surf. Coat. Technol. 394 (2020), 125690.

[57] F. Movassagh-Alanagh, A. Abdollah-zadeh, M. Asgari, M.A. Ghaffari, Influence of Si content on the wettability and corrosion resistance of nanocomposite TiSiN films deposited by pulsed-DC PACVD, J. Alloys Compd. 739 (2018) 780–792.

[58] F. Madadi, A. Rezaeian, H. Edris, M. Zhiani, Influence of surface roughness and hydrophobicity of bipolar plates on PEM performance, Surf. Coat. Technol. 389 (2020), 125676.

[59] S.K. Rawal, A.K. Chawla, R. Jayaganthan, R.J.J.o.M.S. Chandra, Technology, Structural, wettability and optical investigation of titanium oxynitride coatings: effect of various sputtering parameters, J. Mater. Sci. Technol. 28 (2012) 512–523.

[60] K.-.Y. Law, Definitions for Hydrophilicity, Hydrophobicity, and Superhydrophobicity: getting the Basics Right, J. Phys. Chem. Lett. 5 (2014) 686–688.

[61] K.Y. Law, H. Zhao, Surface wetting: characterization, contact angle, and fundamentals, MRS Bull. 162 (2016).

[62] J.C. Moreira, N.R. Demarquette, Influence of temperature, molecular weight, and molecular weight dispersity on the surface tension of PS, PP, and PE. I. Experimental, J. Appl. Polym. Sci. 82 (2001) 1907–1920.

[63] P. Navabpour, D.G. Teer, D.J. Hitt, M. Gilbert, Evaluation of non-stick properties of magnetron-sputtered coatings for moulds used for the processing of polymers, Surf. Coat. Technol. 201 (2006) 3802–3809.

[64] E. Lugscheider, K. Bobzin, M.J.T.S.F. Möller, The effect of PVD layer constitution on surface free energy, Thin Solid Films 355 (1999) 367–373.

[65] X. Pang, L. Zhang, H. Yang, K. Gao, A.A. Volinsky, Residual Stress and Surface Energy of Sputtered TiN Films, J. Mater. Eng. Perform. 24 (2015) 1185–1191.

[66] C. Körber, J. Suffner, A. Klein, Surface Energy Controlled Preferential Orientation of Thin Films, J. Phys. D Appl. Phys. 43 (2010), 055301.

[67] X. Chen, Y. Du, Y.-W.J.T.S.F. Chung, Commentary on using H/E and H^3/E^2 as proxies for fracture toughness of hard coatings, Thin Solid Films 688 (2019), 137265.

[68] L.-.J. Meng, M.J.S. Dos Santos, C. Technology, Characterization of titanium nitride films prepared by dc reactive magnetron sputtering at different nitrogen pressures, Surf. Coat. Technol. 90 (1997) 64–70.

[69] T. Reeswinkel, D.G. Sangiovanni, V. Chirita, L. Hultman, J.M.J.S. Schneider, C. Technology, Structure and mechanical properties of TiAlN–WNx thin films, Surf. Coat. Technol. 205 (2011) 4821–4827.

[70] L. Aissani, C. Nouveau, M.J. Walock, H. Djebaili, A.J.S.E. Djelloul, Influence of vanadium on structure, mechanical and tribological properties of CrN coatings, Surf. Eng. 31 (2015) 779–788.

[71] S. Tan, X. Zhang, X. Wu, F. Fang, J.J.A.s.s. Jiang, Effect of substrate bias and temperature on magnetron sputtered CrSiN films, Appl. Surf. Sci. 257 (2011) 1850–1853.

[72] J. He, Y. Setsuhara, I. Shimizu, S.J.S. Miyake, Structure refinement and hardness enhancement of titanium nitride films by addition of copper, Surf. Coat. Technol. 137 (2001) 38–42.

[73] Y.-.W. Lin, J.-.H. Huang, G.-P.J.J.o.V.S. Yu, S. Technology, A: vacuum, Films, Microstructure and corrosion resistance of nanocrystalline TiZrN films on AISI 304 stainless steel substrate, J. Vacuum Sci. Technol. A: Vacuum, Surf. 28 (2010) 774–778.

[74] D.M. Devia, E. Restrepo-Parra, P.J. Arango, A.P. Tschiptschin, J.M. Velez, TiAlN coatings deposited by triode magnetron sputtering varying the bias voltage, Appl. Surf. Sci. 257 (2011) 6181–6185.

[75] E.J.P.o.t.P.S.S.B. Hall, The deformation and ageing of mild steel: III discussion of results, Proc. Phys. Soc. London Sect. B 64 (1951) 747.

[76] J.J.S. Musil, Hard nanocomposite coatings: thermal stability, oxidation resistance and toughness, Surf. Coat. Technol. 207 (2012) 50–65.

[77] F.X. Liu, F.Q. Yang, Y.F. Gao, W.H. Jiang, Y.F. Guan, P.D. Rack, O. Sergic, P. K. Liaw, Micro-scratch study of a magnetron-sputtered Zr-based metallic-glass film, Surf. Coat. Technol. 203 (2009) 3480–3484.

[78] O.P. Terleeva, A.I. Slonova, A.B. Rogov, A. Matthews, A.J.M. Yerokhin, Wear resistant coatings with a high friction coefficient produced by plasma electrolytic oxidation of Al alloys in electrolytes with basalt mineral powder additions, Materials (Basel) 12 (2019) 2738.

[79] E. Hornbogen, The role of fracture toughness in the wear of metals, Wear 33 (1975) 251–259.

[80] X. Feng, K. Zhang, Y. Zheng, H. Zhou, Z.J.N.I. Wan, M.i.P.R.S.B.B.I.w. Materials, Atoms, Effect of Zr content on structure and mechanical properties of (CrTaNbMoV) Zrx high-entropy alloy films, Nucl. Instrum. 457 (2019) 56–62.

[81] S. Zheng, R. Guan, Q. Guo, D.J.S.R. Su, Letters, The design of surface modification of amorphous ZrO 2 nanoparticles as a lubricant additive, Surf. Rev. Lett. 14 (2007) 1047–1052.

[82] A. Hernández Battez, R. González, J.L. Viesca, J.E. Fernández, J.M. Díaz Fernández, A. Machado, R. Chou, J. Riba, CuO, ZrO_2 and ZnO nanoparticles as antiwear additive in oil lubricants, Wear 265 (2008) 422–428.

[83] H. Choi, J. Jang, T. Zhang, J.-.H. Kim, I.-.W. Park, K.H. Kim, Effect of Si addition on the microstructure, mechanical properties and tribological properties of Zr–Si–N nanocomposite coatings deposited by a hybrid coating system, Surf. Coat. Technol. 259 (2014) 707–713.

[84] K. Holmberg, A concept for friction mechanisms of coated surfaces, Surf. Coat. Technol. 56 (1992) 1–10.

[85] L. Aissani, A. Alhussein, A. Ayad, C. Nouveau, E. Zgheib, A. Belgroune, M. Zaabat, R. Barille, Relationship between structure, surface topography and tribo-mechanical behavior of Ti-N thin films elaborated at different N_2 flow rates, Thin Solid Films 724 (2021), 138598.

[86] K.P. Purushotham, L.P. Ward, N. Brack, P.J. Pigram, P. Evans, H. Noorman, R. R. Manory, Tribological studies of Zr-implanted PVD TiN coatings deposited on stainless steel substrates, Wear 254 (2003) 589–596.

[87] F. Song, Q. Wang, T. Wang, The effects of crystallinity on the mechanical properties and the limiting PV (pressure×velocity) value of PTFE, Tribol. Int. 93 (2016) 1–10.

[88] M. Fellah, L. Aissani, M. Abdul Samad, A. Purnama, H. Djebaili, A. Montagne, A. Iost, C.J.I.J.o.A.C.T. Nouveau, Effect of Zr content on friction and wear behavior of Cr-Zr-N coating system, Int. J. Appl. Ceram. Technol. 15 (2018) 701–715.

[89] H. Ichimura, A. Rodrigo, The correlation of scratch adhesion with composite hardness for TiN coatings, Surf. Coat. Technol. 126 (2000) 152–158.

Elaboration and characterization of based titanium and zirconium nitrides coatings deposited by magnetron sputtering

Abstract

In order to enhance the performance of mechanical components subjected to aggressive applications, several investigations in the field of coatings are constantly carried out. In this thesis, we are interested in the development of hard coatings. A study on the Physico-chemical, mechanical and tribological properties of nanocrystalline coatings based on titanium nitrides obtained on XC100 steel substrates by the RF magnetron sputtering process under reactive atmosphere was carried out. The objective of our work is to demonstrate the opportunity of improving the mechanical properties and the tribological behavior of the TiN system by the addition of Zr according to an experimental study. The interest in examining these coatings is mainly related to the anti-wear properties of the TiN system. In addition, Zr is an important additional element allowing the hardening of metal alloys. Therefore, the association of this element can deliver advancement to a new TiZrN coating with better tribo-mechanical and hydrophobic properties. The results obtained showed a correlation between the microstructural and tribo-mechanical properties of the TiZrN coatings under the influence of the Zr concentration, which is confirmed by the variation of the mechanical properties by improving the wear resistance.

***Keywords**: Magnetron sputtering, TiZrN, Structure, Tribo-mechanical Properties, Hydrophobic Properties.*

Elaboration et caractérisation de revêtements à base de nitrure de titane et de zirconium par pulvérisation magnétron

Résumé

Afin d'améliorer les performances des pièces mécaniques soumises à des applications agressives, plusieurs investigations dans le domaine des revêtements sont constamment menées. Dans cette thèse, nous nous sommes intéressés au développement des revêtements durs. Une étude sur les propriétés physico-chimiques, mécaniques et tribologiques de revêtements nanocristallins à base de nitrures de titane obtenus sur des substrats en acier XC100 par le procédé de pulvérisation magnétron sous atmosphère réactive a été réalisée. L'objectif de notre travail est de démonter la possibilité d'améliorer les propriétés mécaniques et le comportement tribologique de système TiN par l'addition de Zr selon une étude expérimentale. L'intérêt d'étudier ces revêtements est principalement lié aux propriétés anti-usure du système TiN. De plus, Zr est élément d'addition important permettant le durcissement des alliages métalliques. Par conséquent, l'association des cet élément peut donner la naissance à un nouveau revêtement TiZrN présent des meilleures propriétés tribo-mécanique et hydrophobiques. Les résultats obtenus montrent une corrélation entre les propriétés microstructurales et tribo-mécaniques des revêtements de TiZrN sous l'influence de la concentration de Zr est confirmé par la variation des propriétés mécaniques en améliorant la résistance à l'usure.

Mots clés *: Pulvérisation Magnétron, TiZrN, Structure, Propriétés Tribo-mécaniques, Propriétés Hydrophobiques.*

إعداد وصف طلاءات نيتريدات التيتانيوم والزركونيوم الأساسية المترسبة عن طريق رش المغناطيسي

ملخص

من أجل تحسين أداء الأجزاء المعرضة لتطبيقات قاسية يتم إجراء العديد من الدراسات في مجال الشرائح الرقيقة باستمرار. في هذه الرسالة ، نحن مهتمون بتطوير الشرائح الرقيقة الصلبة ودراسة الخصائص الفيزيائية والكيميائية والميكانيكية والترايبولوجية على أساس نتريدات التيتانيوم التي تم الحصول عليها على مساند فولاذية من خلال عملية رش المغناطيسي تحت وسط التفاعلي. الهدف من عملنا هو إثبات إمكانية تحسين الخواص الميكانيكية والسلوك الترايبولوجي لنظام TiN بإضافة الزركونيوم وفقًا لدراسة تجريبية. يرتبط الاهتمام بدراسة هذه لشرائح الرقيقة بشكل أساسي بخصائص مقاومة التآكل لنظام TiN. بالإضافة إلى ذلك ، يعتبر الزركونيوم عنصرًا إضافيًا مهمًا يسمح بتصلب السبائك المعدنية. لذلك ، يمكن أن يؤدي ارتباط هذا العنصر إلى ظهور شرائح TiZrN جديد بخصائص تريبولوجية ميكانيكية وكارهة للماء. أظهرت النتائج التي تم الحصول عليها وجود علاقة بين الخواص البنيوية والميكانيكية الترابطية لشرائحTiZrN تحت تأثير تركيز الزركونيوم والتي تم تأكيدها من خلال تباين الخواص الميكانيكية عن طريق تحسين مقاومة التماسك مع مساند فولاذية.

الكلمات المفتاحية *: رش المغناطيسي ، TiZrN ، هيكل ، خواص تربوميكانيكية ، خواص كارهة للماء.*